ACOUSTIC CHARACTERISATION AND MODELLING OF MULTI-FIBROUS NONWOVENS

Neha Lalit Kumar Sharma

Ph.D. Thesis **2022**

Acoustic Characterisation and Modelling of Multi-Fibrous Nonwovens

A Thesis

Submitted for the Degree of

Doctor of Philosophy

in Acoustics Engineering

By

Neha Sharma

Supervised by

Dr. Olga Umnova

University of Salford MANCHESTER

Acoustics Research Centre, University of Salford, UK

September 2022

TABLE OF CONTENTS

LIST OF FIGURES

LIST OF TABLES

INDEX OF SYMBOLS

English Alphabets	Description
a	Normalised particle radius
a_{max}	Maximum inter fibre distance
A	Component of vector potential
$\vec{A}$	Velocity vector potential
A_{fib}	Fibre surface area
b_0	Constant
b^2	Mean spacing between fibres
b_n	Constant
b_n^c	Complimentary function
b_n^p	Particular solution
$B(r)$	Generic function
c	Constant pressure term
c_0	Speed of sound in air
C	Solidity
Cov	Coverage
$C_{1,2}$	Arbitrary constants
C_p	Molar heat capacity
d	Thickness of the material
d_{fib}	Fibre diameter/equivalent
D	Distance between two fibres
$D_{1,2}$	Arbitrary constants
$e_{x,y}$	Unit electric field
E	Scaled electric field
E_i	Incident sound energy
E_r	Reflected sound energy
E_t	Transmitted sound energy
E_α	Absorbed sound energy
f	Frequency of sound
$f(x)$	Generic function
F	External volume force

H_n	Hankel function of first kind
i	Imaginary unit $i = \sqrt{-1}$
$intop1$	Integral operator in COMSOL
J_n	Bessel function of first kind
k	Complex wave number
$k(\omega)$	Dynamic viscous permeability
$k'(\omega)$	Dynamic thermal permeability
k_0	Static viscous permeability
k_0'	Static thermal permeability
$\kappa_{1,2}$	Sub-cell permeabilities
$K_{1,2}$	Empirical Constants
K_N	Numerically calculated permeability
$K(\omega)$	Effective bulk modulus
L	Macroscopic scale
l	Microscopic scale
l_{fib}	Fibre length
m_{fab}	Fabric mass
m_{fib}	Fibre mass
n	Generic number or order
n_{fib}	Number of fibres
$Nor\ VP$	Normalised viscous permeability
p	Pressure
$pest$	P-estimate
$\tilde{p}$	Pressure point constraint
$p_{1,2}$	Pressure in sub-cell domain
P	External oscillatory pressure
P_0	Static pressure
P_{fib}	Fibre perimeter
$\vec{\nabla}p$	Pressure gradient
Δp	Pressure drop across the material
q	Fibre shape factor parameter
q_n	Constant
r	Radius of cylindrical fibre or pore
R_1	Infinitely long cylinder of radius
R_c	Reflection coefficient
s_n	Constant
S	Normalised surface area
S_c	Contact surface between the pores and the frame

S_{fib}	Fibre cross-section area
$S(\theta)$	Generic function
t_{fib}	Fibre fineness
u	Fluid velocity
v	Microscopic velocity of an inviscid fluid within pores
$\vec{v}$	Velocity of the fluid particles
$v_{1,2}$	Fluid velocity in sub-cell domain
v_{af}	Airflow rate passing through the material
$vest$	V-estimate
V	Homogeneous fluid volume
VP	Unnormalised viscous permeability
V_{fib}	Fibre volume
W	Generic function
$X_{1,2}$	Weighted average fractions of the fibre blend
Y_n	Bessel function of second kind
$zervor$	C-estimate
Z_c	Characteristic impedance
Z_n	Generic function
$\mathrm{Z_s}$	Surface impedance

Greek Alphabets	**Description**
α	Sound absorption coefficient
α_0	Static viscous tortuosity
α_0	Constant
α_0'	Static thermal tortuosity
α_∞	Tortuosity or high frequency limit of tortuosity
β_0	Constant
Γ_s	Fluid-solid interphase
ϵ	Volume fraction of the solid material
ε	Expansion parameter
η	Dynamic viscosity of air ($\sim 1.84 \times 10^{-5}$ $[N.s.m^{-2}]$)
θ	Angular orientation representation for the fibre
θ_i	Angular orientation representation for the external gradient
ϑ	Deviatoric part of an electric potential
κ	Thermal conduction coefficient
Λ	Viscous characteristic length
Λ'	Thermal characteristic length

ρ_0	Density of air
ρ_{fab}	Fabric density
ρ_{fib}	Fibre density
$\rho(\omega)$	Effective density
$\sigma^{\perp}$	Airflow resistivity for perpendicular flow conditions
$\sigma_{\parallel}$	Airflow resistivity for parallel flow conditions
σ_0	Static airflow resistivity
τ	Macroscopic excess temperature in fluid phase
ϕ	Porosity, open porosity fabric porosity
$\varphi_{1,2}$	Volumetric fractions contributed by sub-cells
Ω	Total volume of material
Ω_f	Fluid (non-solid) phase volume
ω	Angular frequency

Mathematical Symbols	**Description**
$\frac{\partial}{\partial x}$	Partial derivative with respect to space coordinate x
$\frac{\partial}{\partial t}$	Partial derivative with respect to space coordinate t
∂_r	Partial derivative with respect to cylindrical coordinate r
∂_θ	Partial derivative with respect to cylindrical coordinate θ
∂_z	Partial derivative with respect to cylindrical coordinate z
∂_{rr}	Partial double derivative with respect to cylindrical coordinate r
$\partial_{\theta\theta}$	Partial double derivative with respect to cylindrical coordinate θ
∂_{zz}	Partial double derivative with respect to cylindrical coordinate z
∇	Gradient operator
$\nabla \cdot$	Divergence operator
$\nabla \times$	Curl operator
$\nabla^2 = \Delta$	Laplacian operator
(r, θ, z)	Cylindrical coordinates
(x, y, z)	Cartesian coordinates
$\langle \cdot \rangle = \frac{1}{\Omega}\int_{\Omega_f} \cdot \, d\Omega$	Average over the REV

ABBREVIATIONS

4DG	4 Deep Groove
AFR-SCUR	Air Flow Resistivity – Single Component Uniform Radius
AFR-TCVR	Air Flow Resistivity – Two Component Varying Radius
ASTM	American Society for Testing and Materials
BH	Bies and Hansen
BS	British Standard
CEN	Comité Européen de Normalisation
DM	Direct Multiscale
DNS	Direct Numerical Simulation
EDANA	European Disposables and Nonwovens Association
HFL	High Frequency Limit
HM	Hybrid Multiscale
HPM	Homogenisation of Periodic Media
INDA	Association of the Nonwoven Fabrics Industry
ISO	International Organization for Standardization
JCAL	Johnson Champoux Allard Lafarge
JCALP	Johnson Champoux Allard Lafarge Pride
KC	Kozeny-Carman
LCM	Least Common Multiple
LFL	Low Frequency Limit

MEM	Membrane
MP-Th	Manning and Panneton -Thermal
NMR	New Resistivity Model
Nor VP	Normalised Viscous Permeability
NRC	Noise Reduction Coefficient
PES	Polyester
PET	polyethylene terephthalate
PUC	Periodic Unit Cell
REC	Recycled
REV	Representative Elementary Volume
SAA	Sound Absorption Average
SCM	Self-Consistent Method
SEM	Scanning Electron Microscope
SRSS	Square Root of the Sum of Squares
TCL	Thermal Characteristic Length
VCL	Viscous Characteristic Length
VIC	Viscose
VP	Viscous Permeability (Unnormalised)

"I often say that when you can measure
what you are speaking about,
and express it in numbers,
you know something about it;
but when you cannot measure it,
when you cannot express it in numbers,
your knowledge is of a meagre and unsatisfactory kind;
it may be the beginning of knowledge,
but you have scarcely in your thoughts
advanced to the state of Science,
whatever the matter may be."

– Lord Kelvin, 1883

ACKNOWLEDGEMENT

I have relied heavily, all through my studies on the professional judgement, encouragement and guidance of my Supervisor, Dr Olga Umnova, and constant support by Prof. Andy Moorhouse, Acoustics Research Centre, University of Salford. This has helped me immensely in carrying out this research work.

I gratefully acknowledge the library, software, and laboratory facilities at University of Salford, for carrying out the research work smoothly.

I am gratified to the Post Graduate Research, Academics teams of School of Science, Engineering and Environment, for encouraging me to pursue my studies.

I am highly indebted to the technical and manufacturing staff members at Cosmotec and Cha Technologies Group Ltd for not only providing me with the opportunity to take up my first Knowledge Transfer Project in collaboration with the University of Salford but also facilitating me with the essential training, resources and material samples needed to carry out this research.

I am thankful to the team at Fibre Innovation Technology (FIT), introduced by Cosmotec, for providing me with the inspiration to explore futuristic materials and techniques alongside my ongoing project work.

I would be failing in my duty if I do not acknowledge my sincere thanks to the faculty and laboratory technicians at the University of Leeds, the University of Bradford, and the University of Sheffield for the utilisation of their training resources and specialised laboratory facilities.

I would like to thank the team at Kimpton Energy Solutions and Acoustic Engineering, where I undertook my second Knowledge Transfer Project in collaboration with the University of Bradford, for their cooperation and guidance on application-oriented material characterisation.

I extend my heartfelt gratitude towards my talented consultancy team at Hoare Lea LLP, for exposing me to acoustic environmental pathways, helping me stay up to date with the relevant industry standards and regulations and encouraging me to carry out research with sustainable materials.

I would like to express my sincere gratitude towards my colleagues from this close-knit acoustic fraternity, zoning from the participating research groups at DENORMS to those presently working as subject experts across the industry, who have been around to guide me on various aspects of conducting my research work.

I have no words to express my thankfulness towards my family and my near and dear ones, who had been instrumental in providing me with all the moral support I needed.

I owe my accomplishments to my parents, who have been my greatest source of inspiration and have always patiently stood by me.

MISS NEHA LALIT KUMAR SHARMA

ABSTRACT

This thesis explores the theoretical, numerical, and experimental approaches for nonwoven materials with the intent of quantifying, testing, and characterising the acoustic performance of currently available products and to guide the development of a novel range of nonwovens. The literature review reveals that there is ample knowledge of technical textile driven functionality, but there is paucity in the understanding of nonwoven material interaction with sound waves. The acoustic response of nonwovens is an exigent research area, particularly for optimising the acoustic capability of technical textiles and sustainable materials.

The present work reviews existing theoretical and computational modelling approaches for fibrous materials and their limitations. Firstly, models for sound propagation around mono-disperse fibres were formed using three modelling approaches: regression based empirical models, theoretical methods adapting the analytical models for cylinders and numerical models. The current work extends the modelling capability to study bi-disperse fibres using two alignments: adjacent or tandem and staggered cases. Further work has been carried out to explore the interaction of poly-disperse fibres for symmetric and asymmetric arrangements.

Both dual and cluster fibre models have been assessed for realising the acoustic influence of three key parameters: anisotropy, inter-fibre spacing and blend ratio. Numerical models developed for single, dual and cluster fibre cases have been validated for the selected nonwoven samples and have generally shown good agreement with the experimental sound absorption measurements. Finally, the acoustic effect of some additional parameters of nonwovens arising due to textile enhancements and sustainable choices have been presented as practical applications. Key findings of nonwoven behaviour are reported in the thesis that demonstrate a realistic possibility of novel nonwoven product outcomes.

This work has been based on the author's contribution towards industrial research projects carried out as Knowledge Transfer Partnerships, funded by the Innovate UK.

Chapter 1

INTRODUCTION

Overview:

1.1. Research context

1.2. Objectives

1.3. Thesis outline

1.1. RESEARCH CONTEXT

In the present day, advancements in textile technology witness remarkable development of nonwoven based technical textile products that are inclusive of a well-balanced confluence of functionality and application specific aesthetics. The functionality trait has also gained significant focus owing to the ever-increasing stringency in the norms and regulations. Demand for high standards in overall performance from the transport, industrial and built-environment sectors has raised expectations from the existing textile product range. A sought-after solution for applications catering to controlling environmental noise pollution, the currently available nonwoven materials, are now being enhanced from a sustainable standpoint as well.

Unwanted sound, a form of pollution that is an outcome of rapid growth in urbanisation, conveyance modes and industrialisation, has gained attention from governing organisations, spanning from the local to the global level, who stress upon the environmental impact pertaining to noise related challenges. Research indicates that amongst the several textile-based materials, nonwoven materials have been reported to perform at par if not better as sound absorbing materials. Nonwoven fabrics, manufactured by mechanically, thermally, or chemically bonding fibres, introduce the desired attributes for noise control. Additionally, they can mimic various other

materials in terms of appeal and capability. These materials are usually accompanied with solutions that control noise.

The knowledge of acoustic functionality of typical nonwovens has been well comprehended. Owing to their nearly random and fundamentally complex make, these materials provide a highly tortuous and lengthy path for the sound waves to percolate through and thus retain most of the sound energy within the fabric. However, it has also been pointed out that there can be various other influencing factors that contribute to this noise controlling effect [1]. These specifically include the morphological features of constituting choice of fibres such as geometric shape, length, denier (linear density) and their types. Several studies on the impact of nature and orientation of these fibres within the fabric have substantiated their relevance [2]. Thus, not only macroscopic but also the microscopic traits of a fibre are known to have significant effect on the overall sound absorption characteristics. Yet another causative parameter is the controlled randomness introduced during the manufacturing, which can be beneficial to performance but challenging to quantify and replicate.

The nonwoven fabric is held together due to the binding treatment that its fibres undergo, wherein, the blend essentially comprises of at least two kinds of fibres; a staple fibre and a low melt fibre (generally referred to as the bicomponent fibre). Although both these fibre types may be of the same constituent polymer, but the secondary binding fibre is generally of a finer size than the staple type. Thus, the nonwoven material is recognised as a blend of at least two varieties of fibres or said to have a bi-modal fibre size distribution. As a result of the manufacturing process, the final product is based on the proportion of both these fibres, their individual fibre properties and the process adopted to bind them together. It is often cumbersome to characterise materials and understand the exact contribution of each fibre or additive in the mix to the overall acoustic performance of the bulk. A simple homogenous mix of fibres is apt for research purposes but when it comes to formulating practical applications, the general tendency is to make use of nonwoven fabrics having an inhomogeneous fibre combination [3]. In the process however, the interaction of such dual fibre blend nature of a nonwoven, with the sound waves still seeks an in-depth study.

Ultimately, the nonwoven material should be such that it reveals customer driven specification by being not only efficacious, ergonomic, and aesthetic but also in many cases, light weight and cost effective. It is with this understanding, that examination of the governing parameters of nonwoven

materials, investigation of the significance of bicomponent fibres within the dual fibre composition, development of an enhanced model accounting for the acoustically influential features, and finally, realisation of the commercial viability of these optimised nonwoven materials, frame the motivation of this doctoral research work.

1.2. OBJECTIVES

The primary objective of this doctoral research work is to test, characterise and optimise the acoustic performance of nonwovens. Having identified the limitations of existing modelling techniques, their assumptions and simplifications, the other aim of the project was to develop a robust model type that represents the essential features of a nonwoven material such as its dual fibre blend nature and provide a reasonable prediction of its acoustic properties. Ultimately, the motive of this thesis is to quantify acoustic properties of nonwovens to enable the development of a novel range of products. This will drive knowledge with an intent to bridge the gap between acoustic and textile approaches to optimise nonwoven materials.

The role of bicomponent fibres within the material mix has been investigated through this model. Focus has been given to the consideration of the ratio of blending and its impact along with the other key parameters that influence the overall acoustic performance of the nonwoven material. Finally, the model has been used to optimise and inform on the development of enhanced nonwovens based on their end application needs.

The methodology adopted to achieve the objectives of this thesis have initiated with understanding the nonwoven. To do so, sample materials have been characterised both acoustically and from textile perspective using various techniques. This information has been useful in defining the inputs needed for developing the framework or expectations from the models. The numerical models have then been validated with experimental test data such as sound absorption trends. Finally, studies have been conducted to combine acoustic and non-acoustic or textile parameters at fibre level or at bulk fabric level to explore various avenues of optimised nonwoven applications. Figure 1.1 provides a schematic flow diagram highlighting the initial thought process and rationale behind methods followed in this doctoral project work.

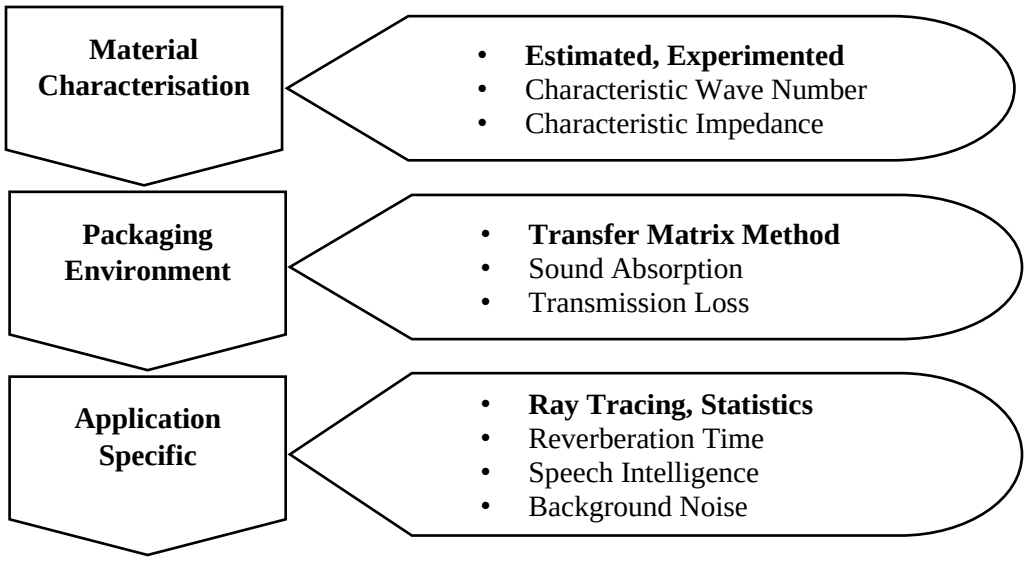

Figure 1.1.: Flow diagram showing material development approach.

1.3. THESIS OUTLINE

Chapter 1 provides the research context and motivation and presents the objectives of the work undertaken and the thesis outline.

Chapter 2 covers an in-depth literature review to help realise nonwovens as porous fibrous materials that can act as effective sound absorbers. This is followed by a review of the acoustic and non-acoustic properties of such materials and the associated models that have been developed over time to characterise them. Finally, it gives a summary of the bulk scale systems and techniques to better understand the acoustic approaches.

Chapter 3 details the research methods used throughout this thesis. The chapter starts with detailing the key test samples selected. This is followed by the methods to develop the acoustic models and techniques. Lastly, it provides a brief list of the various experimental techniques that have informed various aspects of the research work.

Chapter 4 aims to systematically elaborates the theoretical development behind the formulation of the governing wave equation problems. Dynamic case has been derived in cylindrical coordinates; however, the derivation has progressed with simplifications based on static case assumptions to arrive at solutions. From the simplified equation sets, various effective properties or the so-called transport parameters have been obtained.

Chapter 5 is divided into three sections based on three different modelling approaches that are popularly used to characterise fibrous materials. These sections delve deeper into the fundamental principles of using these models that claim to replicate a nonwoven fabric with the information of a single fibre. The model categories include empirical, theoretical, and computational modes.

Chapter 6 advances from the key learnings acquired in the chapter 5. In this chapter, computational models have been developed and compared to not only better replicate nonwoven structure but also to visualise its interaction with propagating sound waves at fibre level. The concept of nonwovens comprising of bi-disperse fibres has been tackled. This chapter has been divided into the exploration of the models and establishing the acoustic influence of obtainable parameters.

Chapter 7 builds on the limitations of the bi-disperse models cannot express conclusively. The factors like blending with is innate to a nonwoven has been the motivation to develop the fibre cluster models. These models aim to have the capability of accommodating the multi-fibre nature of a nonwoven but at the exact minimum proportion there should be in a representative unit of the material. This chapter concludes again with the acoustic influence of the relevant parameters specific to this model type.

Chapter 8 presents the application of the understanding gained on the acoustics of nonwovens from a holistic perspective. This includes investigating the impact of textile processing, bulk acoustic behaviour and finally provides a note on the optimisation for developing in-demand materials such as those classified as sustainable and eco-friendly.

Chapter 9 gives the concluding remarks for this doctoral thesis and indicates the possibilities of future investigations.

Chapter 2

LITERATURE REVIEW

Overview:

2.1. Introduction to nonwovens as sound absorbers

2.2. Review of properties and models for nonwovens

2.3. Acoustic studies for nonwovens at bulk-scale

Since the late 20th century, unwanted noise has been regarded much as an environmental concern than a mere nuisance. Until the present date, rise in noise levels has progressively contributed from being a factor disturbing the affability of the ambiance to being an agent rendering serious impact on human and animal health alike. Several local to global level organisations and governments have begun enforcing regulations on controlling noise pollution. Achieving the outcome of which, has been translated to the realisation of an “acoustically pleasing environment”.

Noise abatement techniques can be broadly classified based on one of the noise system elements:

a. Noise Source
b. Noise Path
c. Noise Receiver

While noise control at the source and the receiver might demand technological improvement at both the ends, noise propagation along the path seems easiest to tackle. The utilisation of suitable materials in between the source and receiver would ensure that the sound arriving at the receiving end would not be as distressing as generated at the source. Noise reducing materials are governed by their mode of transfer [4]:

a. Sound Isolation and/or Absorption
b. Vibration Isolation and/or Damping

In a similar parlance, from the viewpoint of sound wave propagation, materials would be termed as either Sound Barriers or Sound Absorbers. Sound barriers differ from structures that completely encapsulate either the source or the receiver. Barriers or screens could however be partial enclosures that stand on the path of propagation between the source and the receiver. To be able to obstruct elements of sound, barriers tend to be effective solutions when its overall dimensions are much larger than both source and receiver, have good sound absorption traits and are in the proximity to either the source or the receiver. Yet, barriers cannot comprise of sound absorbing materials alone. They should also possess components that block the transmission of sound. Examples of barriers include – fences, stand-alone walls, bunds, buildings, hedges, etc. Materials blocking the transmission of sound waves by reflecting back are classified as sound insulators.

Unlike the materials that reflect sound energy back into the space, sound absorbers dissipate this energy as heat. Hence, such materials target the reflected sound waves with an aim of reducing its further propagation in the space. Sound absorbing materials are defined as products that reduce the acoustic energy of a progressing acoustic wave by the phenomenon of absorption [5]. Absorption of sound using materials is governed primarily by the nature and composition of the material [6,7]. These materials are used to rectify the sonic ambience of spaces by controlling the amount and direction of reflections. Popular absorptive solutions include,

a. Porous Absorbers
b. Panel Absorbers
c. Resonance/ Cavity based Absorbers

Such materials and products find applications in diverse settings, from music studios and auditoriums to offices and home theatres, where they play a crucial role in improving sound quality, speech intelligibility, and overall acoustic comfort.

Each of these types target the sound control at various frequency ranges. To visualise this concept, reference can be made to the British Standard BS 8233:2014 document [8] which provides guidance and recommendations for addressing acoustic considerations in building design and construction.

The standard provides a plot as shown in Figure 2.1, which gives a comparison of sound absorption trends for the following sound controlling solutions labelled by number as:

1. Hard backing finish only
2. Sample porous absorber
3. Typical panel absorber (combination of hard backing, cavity, and porous material)
4. Perforated panel absorber (combination of perforated sheet and porous absorber)
5. Perforated ceiling tile (combination of gypsum ceiling tile, perforated sheet, and cavity)

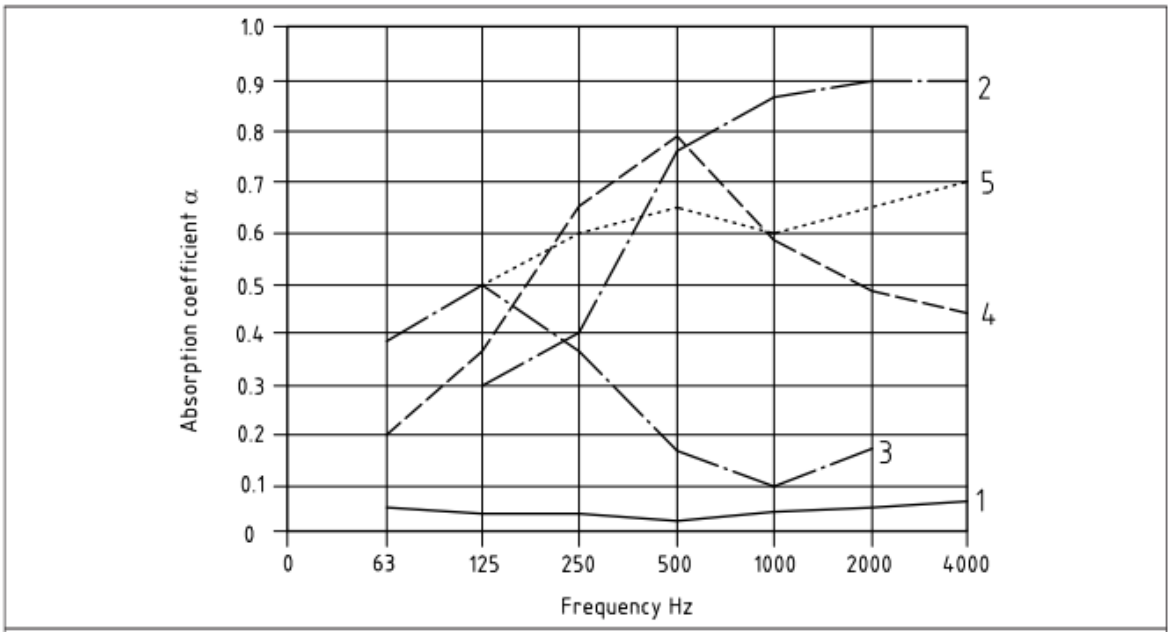

Figure 2.1.: Characteristics of sound absorbing materials [8]

Referring to porous absorbers, their absorptive character is determined by their structural and dimensional properties. As seen from the figure above, they are most effective in the mid-high frequency range. According to K. Attenborough and O. Umnova [9], these materials can be classified into three major categories, namely:

a. Fibrous – which include absorbers in the form of mats, boards, performed elements manufactured of glass, mineral, or organic fibres (natural or man-made), including the felts and felted textiles,
b. Cellular – which are polymer foams possessing varying rigidity,
c. Granular – such as the naturally occurring materials like sand, gravel, soil, and snow.

Fibrous textile materials, by far, have been opted for brilliant absorption response, also owing to them having an upper hand in terms of low production costs and overall density [10]. There are limitations of using some fibrous absorbers applied as certain treatments, as they can be deemed harmful to our health. For instance, using fibrous absorbing material with extremely fine loosely held fibres or particles as a lining for a ductwork where air passes at high velocities can shred blow out their minute fragments, thus posing harm to the occupants in areas where the duct terminates.

2.1. INTRODUCTION TO NONWOVENS AS SOUND ABSORBERS

In general, textile materials can be classified as woven, knitted and nonwoven [11]. According to Tascan and Vaughn [12], for the purpose of absorption of sound waves, a nonwoven material is most ideal due to,

a. High total surface area – surface area can be directly correlated to the fibre fineness and cross-section of the fibres, thus having high sound absorption capability
b. High packing density – high number of fibres packed per unit volume of material at same thickness of the fabric tends to absorb sound better

Nonwovens are engineered fabric materials that are manufactured by processes that are high-speed yet low-cost when compared to the woven and knitted fabrics. However, as a major disadvantage in certain applications, nonwovens, which are generally coated with a layer or covering, are not aesthetically as appealing as woven or knitted fabrics. This may sometimes affect the desired performance due to the presence of an additional skin, yet to keep up with the finishing effects, the final product could be compromised for. Nonwovens have been defined by several standards across the globe and although there is no unique definition, the most popular one is provided by the two leading nonwoven based associations –

a. EDANA [13] (The European Disposables and Nonwovens Association) has adopted the definition from the ISO 9092 or CEN 29092:

   "manufactured sheet, web or batt of directionally or randomly oriented fibers, bonded by friction, and/or cohesion and/or adhesion, excluding paper and products which are woven, knitted, tufted, stitch-bonded incorporating binding yarns or filaments or felted by wet-milling, whether or not additionally needled. The fibers may be of natural or man-made origin. They may be staple or continuous filaments or be formed in situ.

   To distinguish wet-laid nonwovens from wet-laid papers, a material shall be regarded as a nonwoven if

(a) more than 50 % by mass of its fibrous content is made up of fibers (excluding chemically digested vegetable fibers) with a length to diameter ratio greater than 300; or, if the conditions in a) do not apply, then

(b) If the following conditions are fulfilled:

more than 30 % by mass of its fibrous content is made up of fibers (excluding chemically digested vegetable fibers) with a length to diameter ratio greater than 300 and its density is less than 0.40 g/cm 3."

b. INDA [14] (The North America's Association of the Nonwoven Fabrics Industry) choose to define nonwovens as:

"Nonwoven fabrics are broadly defined as sheet or web structures bonded together by entangling fiber or filaments (and by perforating films) mechanically, thermally, or chemically. They are flat, porous sheets that are made directly from separate fibers or from molten plastic or plastic film. They are not made by weaving or knitting and do not require converting the fibers to yarn."

The manufacturing processes has two parts – web formation and web bonding. Details of which have been elaborated by Russell in the Handbook of Nonwovens and further in this chapter [15]. However, focus can be driven to certain web bonding techniques that have been studied in detail, as they tend to demonstrate significant impact on the sound absorption capability of nonwovens. Needle punching and needle punching with thermal bonding is a classical combination. Development of techniques such as spun bonding and more recently, melt blown have enabled the extraction of finer fibres that have good absorption [15]. Flame retarding, plasma treatments, and the likes that alter the surface finish of the nonwoven fibres have also been researched to improve sound absorption. Above all, since the last decade, nonwoven fabrics prepared with nano-fibres have been largely studied. Although limited by the high cost of the technique and the material, this field suggests great potential as sound absorbing materials.

Basic Characteristics of Nonwovens

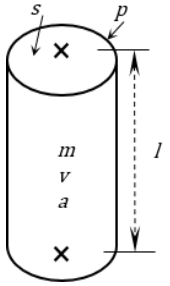

The structure of a nonwoven fabric visibly differs from the woven or the knitted textiles and can be described in terms of the packing and directional arrangement of the fibres. The geometry of the pores is also studied in some instances. A single nonwoven fibre structure is shown in the Figure 2.2, and the fibre and fabric characteristic relations are summarised as per the Table 2.1:

Figure 2.2.: Single nonwoven fibre

Table 2.1.: Fibre and fabric characteristics based on single fibre

Fibre/ Fabric Characteristic	Property relations	Units
Fabric mass	$m_{fab} = n_{fib} \cdot m_{fib}$	$[kg]$
Fibre fineness	$t_{fib} = \frac{m_{fib}}{l_{fib}}$	$[tex = \frac{1}{9} denier]$
Fibre cross-section area	$S_{fib} = V_{fib}/l_{fib}$	$[m^2]$
Fibre density	$\rho_{fib} = \frac{m_{fib}}{V_{fib}}$	$[kg/m^3]$
Fibre surface area	$A_{fib} = P_{fib} \cdot l_{fib}$	$[m^2]$
Fibre diameter/equivalent	$d_{fib} = \sqrt{\frac{4S_{fib}}{\pi}} = \sqrt{\frac{4t_{fib}}{\pi\rho_{fib}}}$	$[m]$
Fibre shape factor parameter	$q = \frac{P_{fib}}{\pi d_{fib}} - 1 \geq 0$	$[-]$
Coverage	$Cov = n_{fib} \cdot l_{fib} \cdot d_{fib}$	$[m^2]$

Notes on some key terms related to fibres:

a. Fibre fineness cannot be characterised purely by the geometry and so the classical definition fails to truly express the size of the fibre. Thus, the fibre size is well explained in terms of the cross-sectional area of the fibre. However, in most cases fibre fineness is resorted to as measuring the volume of a single fibre is impractical.

b. Fibre diameter is specified considering the cross-section of the fibre to be circular. In any other case the circular equivalent of the fibre diameter is calculated and used accordingly. When considering non-circular shapes of fibres [16], the perimeter is always greater than that of a circle. This introduces fibre shape factor parameter, q, which can be calculated using the perimeter and diameter values of fibres as shown in Table 2.1.

   Evidently, shape factor of a circular fibre is zero.

   The textile fraternity are presently researching upon the impact of non-circular shaped fibres on the absorption. With the progress in technological capability that allows manipulating with the fibre shapes of nonwovens, the industry is positively considering developing non-conventional solutions.

c. Fibre packing arrangement, also known as fibre volume fraction, is defined as the volume fraction occupied by solid phase. This can be characterised by the fibre packing density. This density is a ratio of the volume of all the fibres in the fabric to the volume of the fabric and its value ranges from $0 - 1$, such that values tending to 1 would mean tightest possible fibre packing within the arrangement.
d. Fibre direction arrangement or the fibre orientation is also a critical parameter as a typical single nonwoven fibre has a wide variation in curvature. When a group of fibres are considered, their orientation is accounted for in the 2D planar direction alone while along the fabric thickness is considered as insignificant.
e. Nonwoven fabrics consists of a multitude of fibres in combination with several resulting voids filled mostly by air. These air spaces are called pores. This aspect shall be dealt in greater detail later in this section. Projecting a fabric slice in 2D forms the elementary plane of the fabric. The plane is filled with fibres and the air-filled pores. Total projected area of the fibres per unit area of the plane is called coverage, Cov , refer Table 2.1 for its formula.

These fibre characteristics are used to study the effect of fibre parameters and their interaction with influencing properties. [15,17-18].

Structural parameters of acoustic significance

Nonwoven materials are well-known for their primary feature, absorbency, which is defined as the ability of a porous media to soak up and retain significant amounts of fluids such as air, water, and the likes under various conditions. This capability of a material is dependent on the following:

- bulk properties of solid - resistance to compression/ expansion, shear, and torsional distortion
- bulk properties of fluid - viscosity
- structure of solid - pore size, size distribution, shape, texture, and roughness of surfaces

Sound absorption properties of nonwoven materials can be affected by several parameters, and these have been presented as a flowchart by Puranik [2] in Figure 2.3:

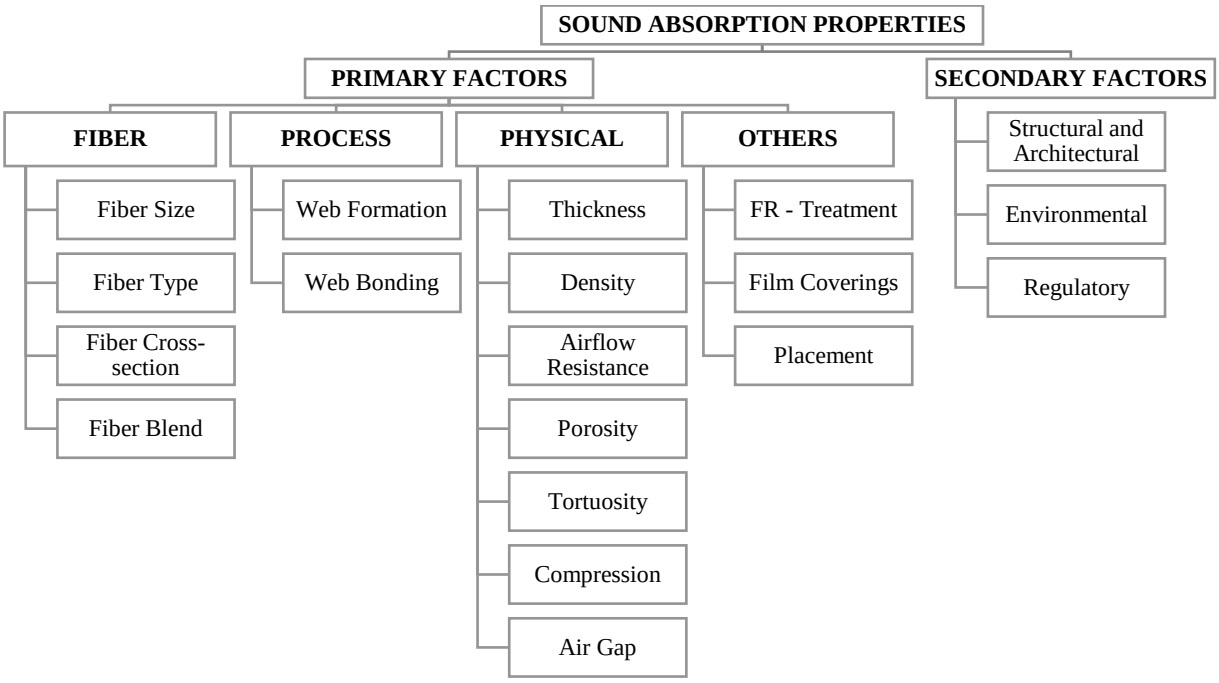

Figure 2.3.: Flow chart by Puranik [2] showing parameters affecting sound absorption.

The variations of certain prominent primary factors have been detailed as per [22] and can be thus summarised as per Table 2.2.

Table 2.2.: Summary of variation of primary factors in terms of sound absorption.

	Parameter	Variation with Sound Absorption	Comments
1.	Fibre		
a.	diameter	Inverse	Finer the denier better the absorption
b.	cross-section area/ shape	Direct	Higher surface area means higher friction so better absorption [19] (hollow, tri-lobal, penta-lobal, 4 -Deep Groove) > round
2.	Process		
a.	Web formation	Direct	Random web creates tortuous channels thus produces samples with small pores
b.	Web bonding	Weakly direct	Needle and needle with thermally bonded
3.	Physical		

a.	Thickness	Direct	• Effect visible at low frequency • Air space inside and behind material, peak absorption shifts from high to low • Effective absorption when thickness ~ $\frac{1}{10}$ wavelength of sound • Peak sound absorption at resonant frequency ~ ¼ wavelength
b.	Density	Inverse at low frequency Direct at medium-high frequencies	• Less dense, more open structure, low frequencies absorbed • Highly dense, high number of fibres per unit area, high surface friction, high energy loss, medium-high frequencies absorbed • High density implies high material cost
c.	Airflow resistance	Direct	• Airflow resistance related to characteristic impedance and propagation constant • Interlocking fibres are friction elements that resist acoustic waves that try to flow through the tortuous passages • Affects the height and width of the wavelength peaks
d.	Porosity	Direct	• Ratio of volume of the voids to the total material volume • High no of pores more amount of sound wave passes to get dampened • Porosity should increase along the propagation of wave • Affects the height and width of the wavelength peaks
e.	Tortuosity	Direct	• A measure of elongation of passage of way through the pores compared to the thickness

			• A measure of how far the pores deviate from normal • Affects the location of quarter wavelength peaks
f.	Compression	Inverse	• Compression decreases thickness, porosity, and thermal characteristic length • Compression increases tortuosity and airflow resistivity
g.	Air gap	Direct at medium-high frequency	• Air gap is present behind the layer
4.	Other		
a.	Flame retardant treatment	Direct	Flame treatment changes fibre structure by increasing voids on fibre to entrap more sound

Special note on fibre types

Effective utilisation of fibre-based textile materials has been a popular yet challenging science since ages owing to the changing trends in their production, properties, and processing. Historically, the development of fibre technology relied on trial-and-error methods, where the fibres were sourced from nature. Naturally occurring fibres have been derived from vegetables, animals and minerals and are termed as natural fibres (such as cotton, flax, jute, hemp, wool, silk). It was only towards the end of the 19^{th} century that man-made regenerated cellulosic fibres (viscose) were produced while it was only much recent, around $3^{rd} – 4^{th}$ decade of the 20^{th} century, that synthetic fibres such as nylon, polyester and the likes were produced. A popular Scanning Electron Microscope (SEM) image showing comparison between the various fibre types based on source and morphology is produced from online archives of National Geographic magazine [23].

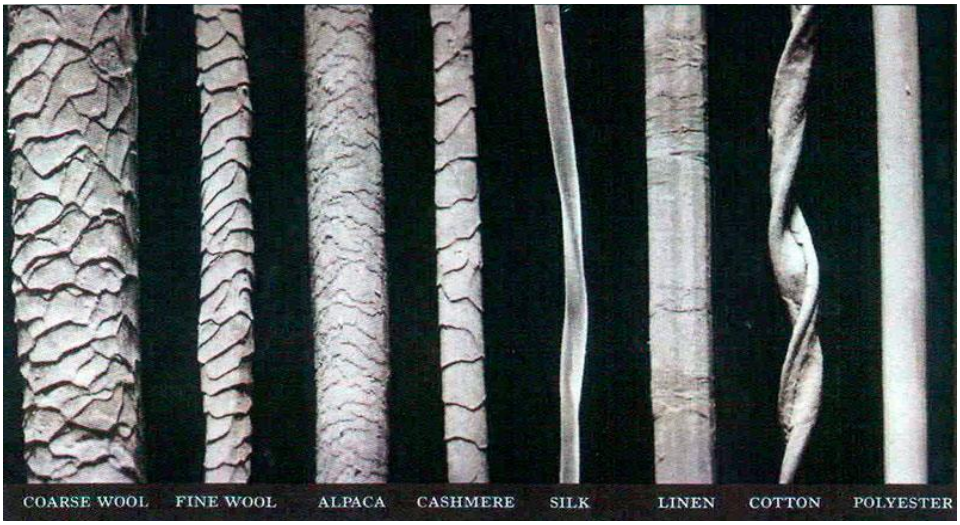

Figure 2.4.: SEM image of natural and synthetic fibre morphology [23].

As seen from the previous section, fibre composition, dimensions, local and bulk properties are particularly important when considering the overall performance of a material. Man-made and synthetic fibres are majorly incorporated as raw materials in the nonwoven industry and polyester is by far the most utilised. This is because of its compatibility for product applications and comparatively low cost. Various fibre types, grades and dimensions are blended to obtain a particular combination of expected physical properties or estimated cost effectiveness.

The polyester fibre [24]:

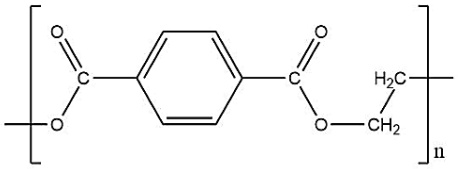

Figure 2.5.: Chemical structure of polyester [24].

Next in line to cotton fibres, polyester fibres have been the preferred based on their production tonnage. Polyester is defined as “a manufactured fibre in which the fibre-forming substance is any long-chain synthetic polymer composed of at least 85% by weight of an ester of a substituted aromatic carboxylic acid, including but not restricted to substituted terephthalate units or para-substituted hydroxybenzoate units”. Polyesters are made from petroleum from which the acid and

alcohol components are extracted. Long polymeric chains of polyethylene terephthalate (PET) are arranged in amorphous and crystalline regions. Its chemical structure is as shown in Figure 2.5. Due to the presence of aromatic rings in the polyester, this material does not crystallize easily, as these rings are bulky and do not allow alignment of molecules. Adaptability of polyester fibres owing to their receptiveness to heat treatment (setting and texturing) and the ease of their blending with other fibres such as cotton, wool and regenerated cellulosic, is of great significance.

The polyester fibres are manufactured in a variety of cross-sectional shapes [24] such as circular, trilobal, pentalobal, hollow, etc. Some of these are depicted in the Figure 2.6.

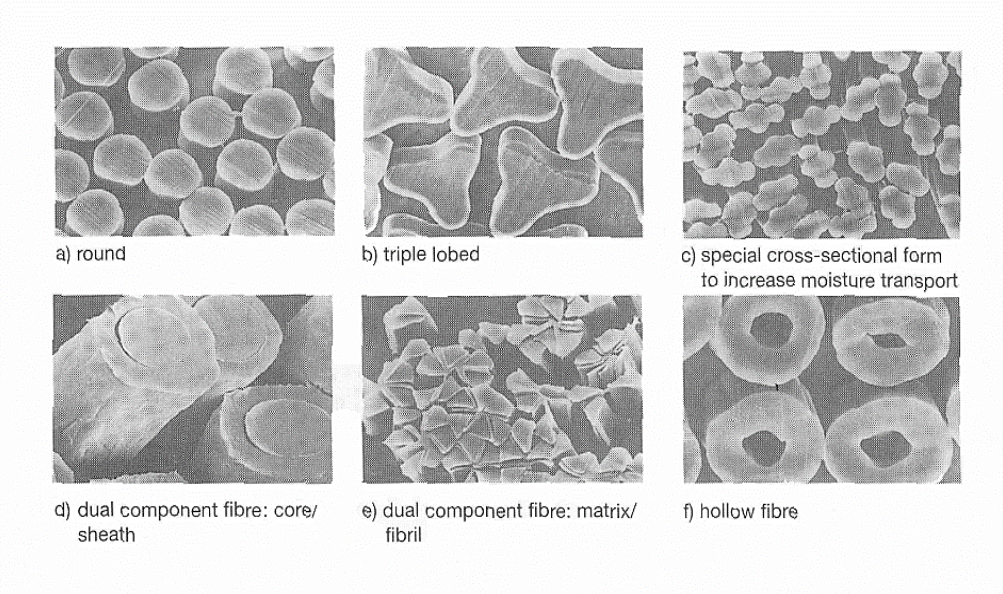

Figure 2.6.: Cross-sectional shapes of polyester fibres [24]

Review of bonding processes

There are three types of bonding process for a nonwoven material. These are mechanical, thermal, and chemical. The extent of bonding is an important factor in defining the mechanical properties of the fabric due to the resulting porosity, flexibility, bulk density, or thickness of the material. There is a possibility of using more than one bonding processes while manufacturing some fabrics depending on the need of the end application. Nonwoven product samples studied in this research work have been manufactured using needle punching and thermal bonding. Hence, only these relevant approaches have been reviewed in this section. Details for the other methods can be found in various reference books [15].

The mechanical bonding processes include methods such as needle punching, stitch bonding and hydroentanglement. Of these hydroentanglement has become popular in the recent years. Needle punching, also called is needle felting, the fibres are mechanically enmeshed to create a fabric by moving batt of fibres in a needle loom, through reciprocating fine barbed needles (felting needles). Figure 2.7 indicates this needle punching process. A localised view of a single needle working through a bunch of fibres is as depicted in this figure. Needle punched products can be produced using a variety of natural and synthetic fibres.

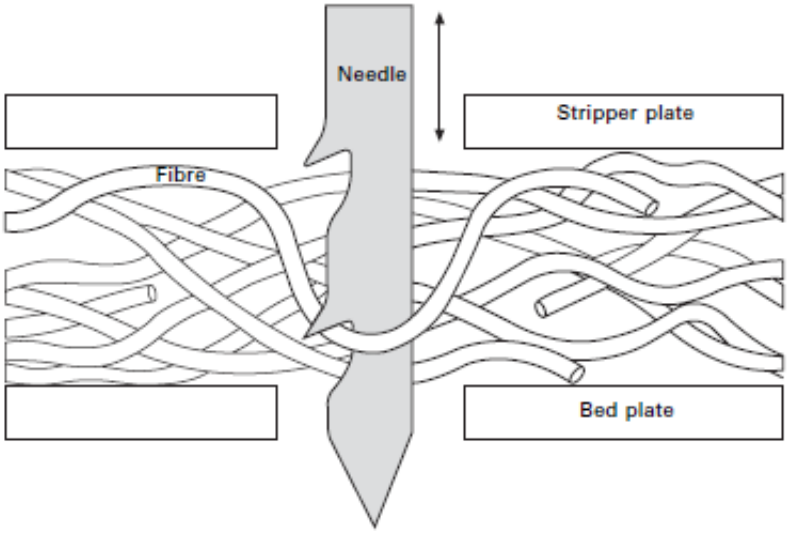

Figure 2.7.: Depiction of needle punching process [25]

Shahani *et. al.* [25] have studied the impact of needle punching process on the acoustic performance of such nonwoven materials. The observed that punch density was directly proportional to the noise reduction coefficient of the fabrics. Punch density up to a certain extent introduces effective fibre entanglement leading to increased tortuosity, smaller pore sizes and added fibre to fibre contact points. However, excessive punching can also lead to fibre breakage that has an impact on the fibre content and quality in the resulting fabric. Never-the-less, curated fibre breakage may lead to fibrillation, and this may be advantageous for certain applications where there is a need for introducing micro and nano size fibre components within the blend. Besides this parameter, they have also verified that greater the fibre fineness and fabric thickness, higher is the sound absorption coefficient of the nonwoven material. Finally, they even concluded that chemical bonding technique had an undesirable impact on the sound absorption characteristics of the nonwoven material.

Thermal bonding is an interesting technique that bonds a web made up of thermoplastic and non-thermoplastic fibres. On introduction to a suitable temperature sufficient to melt the thermoplastic fibre components, the softened polymer becomes viscous enough to flow by surface tension or capillary action towards the crossover spots created by the non-thermoplastic fibres, cools down and solidifies in the area to form the bonding regions. It is key to note that no chemical reaction takes place between the binding fibre and the base material, and the web is bonded and held together solely by thermal activity as detailed.

Majority of the research product samples have been formed using this technique, which is advantageous based on the following points:

- Depending on the choice of fibres to be blended, products can be soft and cloth-like
- Uniformity in bonding of high bulk products
- Fibre components are 100% recycled and eco-friendly.

As introduced in the fabrication process, there are two types of fibre components used in the thermal bonding technique. These are a non-binding kind that is usually called as the base or staple fibre and the thermoplastic variety that is the binder or bicomponent fibre. The proportion of these fibre types decides a lot about the outcome of the final blend fabric.

The staple or carrier fibre can be procured from various sources:

- Natural – cellulosic fibres, vegetation like cotton, animal protein like wool
- Synthetic – polyester, polypropylene, nylon, viscose
- Mineral – glasswool, rockwool, silica
- Metallic – aluminium, steel, alloys

The binder component is the thermoplastic component could be present in the fabric web as singular fibre webs, powders, films or as an outer sheath of a bicomponent fibre. These fibres are generally added about 10-50% by weight of the fibre. So, for instance, if the amount is at the lower end, say 10% of binder presence makes the fabric to be highly porous, flexible, and loosely bulky. On the other hand, if the portion is around 50% or higher, due to the high availability of melted plastic the viscous polymer will do more than just binding the bonding regions. In addition, it will start filling up the crevices in fibres and the pores created because of the well-bonded base fibre web. Once it solidifies and basically clogs the pores, the resulting fabric becomes stiffer and acts

like a toughened plastic rather than a limp fabric. The quality and portion of the binder fibres is also selected in such a way that it minimises energy costs.

The embodiment of a binder fibre plays a crucial role in its effective distribution over the web and this in turn has its influence on the overall fabric properties. The bicomponent (Bico-) type of binder fibres, is also called as conjugate fibres as they comprise of at least two different types of polymer components. In case of a bico- fibre, only a part of the fibre melts and leaving behind the thermoplastic component intact. This ensures that the web structure is maintained with minimum impact of thermal shrinkage and nonwoven material quality and strength is high [15]. The blend ratios are same for this variety of binder fibres as well lying in the range of 10-50% based on the application of the end-product. Table 2.3 provides a practical reference to resulting characteristics based on the proportion of the bico- material used.

Table 2.3.: Practical reference to nonwoven features based on bicomponent proportion.

Parameter	Nonwoven fabric handle		
	Soft	Medium	Harsh
Bicomponent fibre content (%)	10–20	15–30	>30
Bonding temperature (°C)	140–150	150–160	160–180
Fibre fineness (dtex)	1.7–3.3	3.3–6.7	>6.7

There are numerous approaches of a typical bico- fibre formation. Two popular types are the sheath/core, where the core of the fibre comprises of the base fibre material with an outer sheath of the low melting type or the side-by-side, where there are the non-thermoplastic and the thermoplastic components fused alongside to form a fibre strand. These can be depicted [16] as shown in Figure 2.8:

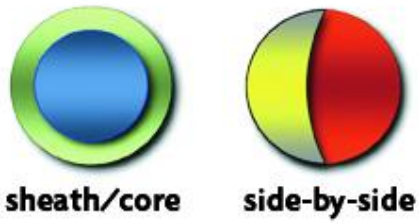

Figure 2.8.: Popular bicomponent polymer combinations [16]

The most common polymer combinations are:

- Polyester Core (250℃ melt point) and CoPolyester Sheath (melt points of 110℃ to 220℃)
- Polyester Core (250℃ melt point) and Polyethylene Sheath (130℃ melt point)
- Polypropylene Core (175℃ melt point) and Polyethylene Sheath (130℃ melt point)

There are several other ways of bico- formation, as presented in Figure 2.9, so much so that there is an incredible amount of research in developing just the bico- fibres.

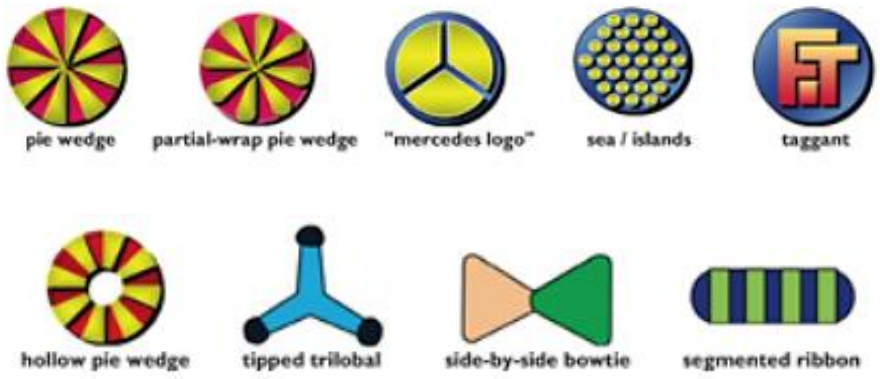

Figure 2.9.: Other variations of bicomponent polymer combinations [16]

Selecting the right polymer base and binder, ensuring the appropriate blend ratio and fibre cross-section size and shape, equally contributes to manufacturing thermal bonded nonwoven fabric structures that are not only highly functional but also efficacious and cost-effective.

A note on Size Distribution parameters

Nonwoven materials mainly comprise of the fibre or the solid phase and the pore volume that are essentially air-filled interstitial voids. Yet, a striking difference between the two is the focus on

the phase when analysing them for their performance of acoustic interaction. It is often considered that in the case of porous materials like foams, the pore phase is analysed while in the case of nonwoven materials the fibre phase takes the attention.

A. Modelling pore size and pore size distribution

In terms of the pore features, the prominent parameters of interest include fabric porosity or in terms of the pores, its volume, so also, pore geometry, its connectivity, size, and size distribution. Although these are majorly linked to foam like materials that have defined pore structures, it is found that an understanding of these parameters helps in effective characterisation of the fibrous materials as well. Porosity for a fabric material can be calculated based on its solid fibrous component. The weight of the volume occupied by solid fibres only is the fibre density and with the knowledge of the fabric bulk density, this leads to fabric porosity as per equation (2.1) below:

$$\phi(\%) = (1 - \epsilon) \times 100 \tag{2.1}$$

$$\epsilon = \frac{\rho_{fab}}{\rho_{fib}} \tag{2.2}$$

Where the volume fraction of the solid material is expressed in equation (2.2) and is defined as the ratio of the bulk fabric density to the fibre component density is the volume fraction of the solid material. Nonwoven fabrics usually have porosity values greater than 60% with highly porous and performing fabric materials with porosities above 80% with lofty nonwovens having low fibre density and porosities around 98%.

B. Modelling effective fibre size and fibre size distribution

For a nonwoven fabric material, understanding how best to consider the fibre components involved in the blend is of utmost importance. The parameters that are associated with fibres include fibre cross-section shape, its size and size distribution besides its density that has been covered in the calculation in the pore sub-section above. In this sub-section, a review of the how effective dimension of fibres have been previously considered is summarised.

For the case of simple cylindrical polydisperse fibre networks, Luu *et.al.* [26] have indicate that simply averaging the diameters may not be sufficient and that there is a need to deal with fibre diameter distribution differently from a unique fibre diameter. Their research then looks at various

approaches throughout literature that account for the calculation of an effective diameter. Using which, the acoustic properties of the material have been obtained and compared for each effective diameter approach. Table 2.4 summarises the various techniques reviewed in this work.

Table 2.4.: Summary of effective diameter calculation techniques

Effective Diameter calculation approach	**Researchers**
No effective diameter, model uses full range of fibre diameter distribution	Schladitz *et. al.* [27]
Nonwoven fibres follow log-normal distribution curve	Singha *et. al.* [28]
Fibres follow gamma distribution: model uses weighted averaged diameter of distribution	Peyrega *et. al.* [29]
Multiscale approach: REV model uses mean value instead of real fibre diameter normal distribution	Luu *et. al.* [30]
Polydisperse (gamma distribution around average diameter) Bi-disperse (two mixture proportional groups of constant fibres) Mono-disperse (weighted blending ratio based average diameter)	Luu *et. al.* [26]
Analytical model uses two component fibres with various radii	Xue *et. al.* [31]
Model uses single number equivalent fibre radius based on mean of the fibre radii (Weighted average was not suitable for the choice of fibres considered as individual fibre lengths are unknown)	Piegay *et. al.* [32,33]

The next basis for calculating effective diameter when the cross-sectional shape of the component fibres is not close to cylindrical. Generally, synthetic polymer-based fibres are selected for porous fibrous material characterisation research as they can have near cylindrical shape. As covered in the previous sections, many fibre materials have a variety of shapes such as triangular or trilobal as in the case of polypropylene fibres, cloud shaped viscose fibres or deep-grooved cross sections of polyesters. An interesting study looking at the inference of cross-sectional shape variation on the acoustic properties of polyesters was carried out by Das *et. al.* [34]. They concluded that circular fibres had higher air permeability than deep-grooved fibres. For the case of deep-grooved comparison with cylindrical fibres, they developed an expression to calculate weighted arithmetic mean of the shape factors of the individual fibre components. This diameter can be calculated from textile known parameters using the formula from Table 2.1.

Representing nonwovens as porous materials

Porous materials act as sound absorbers, transforming the propagating acoustic wave and dissipating it as heat energy. When these porous absorbing materials are not prepared to perform the function of blocking sound waves, they get differentiated from their variants that are utilised as sound barriers. However, at times they are modified to partially play the role of an absorbing barrier. This is done by either manipulating batches of material during its processing or by appending layers of materials serving these different purposes at a later stage of fabrication.

To visualise the mechanism of porous material-based absorption, the materials can be considered as dissipative fluids. This terminology shall be discussed in the phenomenological modelling approach in the next section. Despite their consideration in either consolidated or loose form, the acoustic wave motion through these materials is limited to the fluid within the pores. The acoustic pressure amplitude and phase get altered under the influence of the visco-thermal exchanges within the pores of the material [7].

In general, porous materials can be characterised by the solid frame response to acoustic wave excitations. Accordingly, materials can be as per Table 2.5. [35]

Table 2.5.: Porous material characterisation based on frame state and wave propagation.

Frame State:	Sound waves propagating in:	
	Fluid Phase	**Solid Phase**
Rigid	Longitudinal	Rigid
Limp	Longitudinal	Rigid
Elastic	Longitudinal	Longitudinal+ Transverse

Some important takeaways in relation to the tabulated information:

a. The longitudinal waves are also referred to as the compressional waves while the transverse are the shear waves.
b. Although the airborne and solid phase respond similar for the rigid and limp materials, what differ the two materials is that the solid frame is not entirely rigid; the frame shows

movement but is purely driven by the motion of the fluid. Sound waves do not directly have an influence on the solid fibrous material.

c. The nonwoven fabrics generally lie in the limp frame state [36].

With this basis, it is then convenient to classify the material based on the sound propagating through it. This can be done in any of the following three categories:

a. Diphasic model where the wave interacts with both the phases of the material,
b. Simplified equivalent fluid model where solid phase is motionless,
c. Simplified equivalent solid models where fluid phase is motionless.

The approaches followed to arrive at the appropriate model for representing a nonwoven material has been dealt in depth in the next section.

It is well established that nonwoven fabrics typically resemble porous fibrous materials [12]. A simplified understanding of the mechanism of sound absorption is that as the acoustic waves enter and propagate within the pores of the material, the wave speed slows down allowing a friction-based interaction with the fibres. This causes a fraction of the incident sound energy, E_i, to get dissipated as heat energy, while the rest could get either reflected, E_r, into the material and/or transmitted, E_t, out from the other side, based on the backing. The ratio of absorbed sound energy, E_α, to the total incident sound energy gives the acoustic absorption coefficient, α, which is simply stated in equation (2.3) as follows:

$$\alpha = \frac{E_\alpha}{E_i} = \frac{E_i - E_r - E_t}{E_i} \tag{2.3}$$

Highly porous nonwovens will tend to absorb more acoustic waves, but highly tortuous or randomly bonded fibres of the blend will grant an extended period of interaction for the wave, thus trapping in sound longer. Although the characterisation of a random mix is not realistic to describe accurately, for its behaviour, the introduction of a plurality of fibre types, be it in terms of their physical properties such as denier, shape, and length, as also material, will build up on the complexity. This implies that the material characterisation and optimisation is certainly still a challenge, particularly, by the study of acoustic-fibre interaction analytically and/ or numerically.

Understanding the acoustic behaviour of air-saturated fibrous materials plays a key role in quantifying the sound absorption and transmission capabilities. Applying fundamental principles

describing the physics of sound interaction, several theories have been postulated [37]. The theoretical techniques in combination with the material parameters as obtained using standard experiments, then lead to formulation of the predictive models. It is depending on complexity of blend and configuration of the material, that the models are thence chosen for further exploration.

2.2. REVIEW OF PROPERTIES AND MODELS FOR NONWOVENS

This section looks at a review of the essential modelling techniques that have been developed in the past to predict the acoustic behaviour of porous materials, particularly, fibrous nonwovens. These previous works that can be categorised into empirical and theoretical models, have been presented as a chronological summary. Further, an overview is provided for the literature pertinent to the context of this thesis. Topics of relevance are those of; multi-fibre component, bico- fibres and blending percentage These are explored as a confluence of both textile and acoustic perspectives.

Empirical models

The empirical studies have been created by fitting experimentally obtained data by the application of regression equations to various parameters such as the specific airflow resistivity and the characteristic impedance of the material. It is understood that each empirical model can be applied to only specific categories of fibrous materials having certain inherent traits as per Tang and Yan [38]. The models discussed here are segregated based on these parameters concerning the airflow resistivity and the characteristic impedance.

A. Airflow resistivity prediction models

Airflow resistivity has been considered as the most significant parameter to determine the acoustic performance of a fibrous material. It was Nichols Jr. [39] who first introduced an empirical model based on the airflow resistivity by obtaining an adjustable parameter whose value could be easily related to the fibre distribution within the material. Following suit, a simple model was presented by Bies and Hansen [40], owing to the experimental data collection. The model essentially considered the parametric influence of bulk material density and main fibre diameter to calculate the airflow resistivity of fibreglass material. Since the Bies and Hansen version, the past few decades have brought out several empirical model variations that have capabilities to account for

the various complexities that fibrous materials have been introduced with. Prominent instances are the works carried out by Narang [41], who has discussed the acoustic performance of polyester materials and has concluded that the existing models for mineral wools were not ideal for polyester materials. He indicated that model developed for the materials examined by Bies and Hansen assumed that the material comprised of a uniform fibre diameter with assigning negligible significance to the binder fibre component. This thought process was popular with the previous models including those by Nichols. Motivated by Narang's suggestion to prepare new models for polyesters, Garai and Pompoli [42], improvised the Bies and Hansen airflow resistivity model to be capable of studying the double fibre component of such nonwoven materials. In their study, they have looked at the impact of certain traits of polyester fibres such as the presence of bico-material and surface finish as a result of thermal treatment.

Acoustic properties of recycled or shoddy type fibrous material were studied by Manning and Panneton [43], who established three airflow resistivity based empirical models for each of the types of nonwoven manufacturing techniques, viz, mechanical, thermal, and chemical bonding. In a research paper [44], Tao Yang *et. al.*, have summarised the relevant empirical airflow resistivity-based models focusing on the multi-fibre component of typical polyester materials. These models explore the impact of fibre size distribution and its effect on the accurate predictions made by the recommended models. Through their work, they convey that there is still a gap in research dealing with models that help obtain effective acoustic and non-acoustic properties of multi-component fibrous materials such as nonwovens.

B. Acoustic impedance models

Once the airflow resistivity parameter has been modelled, the other parameter that leads to absorption property of the material, is acoustic impedance, which defines the impeding character of the material. The most popular empirical model known to obtain impedance value of a material is that of Delany and Bazley [45]. They presented a power-law relationship derived by best-fitting exhaustive experimental data. What also made this model predominant is the fact that it just needed an easy to access, non-acoustic parameter of the material, the airflow resistivity. In their work, Delany and Bazley have also provided a correlation between the airflow resistivity and the bulk density of fibrous materials. Further to their model, Miki [46] has provided a correction factor to account for low frequency range applicability. Based on the Delany-Bazley-Miki models [46] for

predicting the acoustic properties of materials, Komatsu [47] modified the model to include the characteristic impedance and propagation constant. Comparing experimentally obtained values for fibrous materials having finer fibre diameters, Voronina [48], has analytically formulated characteristic impedance and propagation constant leading to the acoustic properties of the fibrous material, by expressing them as a function of the fibre diameter and the porosity of the material. Fibre diameter and porosity together being governing factors have been derived to obtain the structural characteristic factor which an approximate expression to airflow resistivity. The empirical models that have been historically dominated may be used for conventional fibrous materials. However, there are limitations in adapting them for characterising the likes of sustainable materials with complex fibres from natural origins or treated technical textile-based fibres of varying features as per Piégay [33].

Theoretical models

There are several variations in the theoretical derivations of the influential parameters. A broad classification of these models is based on flow and temperature characteristics. Accordingly, models are either internal flow models, where flow through the pore features is considered, or external flow models, where the flow around solid inclusions such as fibres is considered [49]. To maintain the consistency from empirical models above, theoretical models have also been discussed based on airflow resistivity and impedance as primary parameters.

A. Airflow resistivity prediction models

Theoretically, airflow resistivity models have been developed with thought process of internal and external flow types just mentioned. The internal flow has been studied by capillary channel theory and the external flow have been based on the drag force theory. A summary of both these theory types has been presented by Tao Yang *et. al.* [44]. Here the inverse of flow resistivity or the permeability term gains significance during the formulation.

The capillary channel theory:

The Hagen-Poiseuille law [50] studied laminar flow through pipes of constant cross-section. Kozeny [51] established a relationship between pore characteristics and permeability, which was modified by Carman [52], later to be renown as Kozeny-Carman (KC) equation [53]. Works of this nature formed the basis of the capillary channel theory, where the equation modifications were

applied to examine the flow through porous materials. Further approximated equations were obtained by Davies, Lind-Nordgren and Göransson and the likes [54-56], known to be applicable for porosities up to about 0.7-0.8. Pelegrini *et. al.* [57] has provided a modification of the Kozeny-Carman equation to better predict the airflow resistivity of polyester fibres that normally have uniform diameter.

The drag force theory:

Whilst the capillary channel theory focused on the flow thorough the pores between the fibres, the drag force theory highlights the fibres and considers that they form the rigid structural frame that obstructs the flow of fluid through the material. Thus, the drag force theory as well as the unit cell models discussed later, give a relationship between the structure of the porous material and its permeability. A summation of the drags is equated to the airflow resistance provided by the fibrous material. The fibres are assumed to be aligned maintaining periodicity in one direction forming patterned arrays. Airflow resistivity is then obtained by Navier-Stokes equations within a unit cell having specific boundary conditions. It was Langmuir who perhaps expressed the dimensionless permeability for a fluid flow along the array of fibres. Popular works of Tarnow [58] have been rigorously referred for his approach to calculating airflow resistivity for fibres placed like Voronoi polygons. Tarnow has provided models that account for flows both parallel and perpendicular to the fibre orientation. Studies of much interest by Xue *et. al.* [31] have reviewed what they refer to as AFR-SCUR models (that stands for Air Flow Resistivity – Single Component Uniform Radius). Basing the formulation on Tarnow's perpendicular random version of this model, they developed AFR-TCVR models (Air Flow Resistivity – Two Component Varying Radius) that introduced the two-fibre component and fibre radius distributions. This version of the model claims to provide a correlation between the micro-macro links for fibrous materials.

B. Acoustic impedance models

Having established concepts around the flow resistance, theories have been elaborated to provide further insight into understanding the materials. Consequently, theoretical models could be further classified based on phenomenological approach and microstructural approach. The so-called phenomenological theory is based on the development of scaling functions that depend on autonomously measured macroscopic parameters. On the other hand, the microstructural approach

follows a micro-macro technique by firstly solving the governing equations at micro-scale and then estimates the macro-scale properties.

It has been realised that in comparison with the empirical models, the theoretical microstructure-based models could not only predict acoustic absorption coefficient with greater accuracy but also provide deeper know-how of the material functionality as per Tang and Yan [44].

Phenomenological approach:

Informed in the previous section, the conceptual understanding of a phenomenological approach lies in substituting a fluid-saturated porous solid material with an equivalent dissipative fluid. Along with Morse and Ingard [59], many researchers proposed model variations accepting this philosophy. Hamet [60], followed up by further considering viscous and thermal dissipation, thereby, proposing a three-parameter model to characterise materials having medium porosity values. Biot's theoretical research work [61] in development of models for the propagation of elastic waves in porous elastic framed solid medium saturated by fluid was a progressive step to characterise materials focusing on their mechanical traits. Many other researchers followed suit to derive analytical models for other types of porous materials. A typical limitation of the phenomenological models is that the structural non-acoustic parameters that serve as inputs need to be experimentally obtained by Garai and Pompoli [42]. Yet another drawback of the phenomenological approach is that the structural arrangements are based solely on the geometric information obtained and for volume fractions of the heterogeneous media.

Microstructural approach:

One of the most popular thought processes of developing theoretical models was using first principles to understand wave propagation within the pores at a micro-scale and then translate the outcome to the material's macroscopic characterisation. This fundamental thermodynamic approach also considers the structural factors as physical complexities of pores and the solid at the microscopic scale, and is thus, also referred to as semi-phenomenological models. The various complex non-acoustic parameters include, porosity, tortuosity, fibre density, viscous and thermal characteristic lengths and permeabilities. The definitions and formulae to obtain these parameters has been detailed in the next section.

Historically, the pores within the fibrous or granular medium were visualised as cylindrical tubes and thus theories associated with sound propagation in such tubes or pipes were used to approximate the acoustic behaviour at micro-macro scales. These concepts are said to have originated from the works by Kirchoff and Rayleigh [62]. Zwikker and Kosten [63] proposed theories for single cylindrical pores pertaining to the discrete treatment of the viscous and thermal losses. Accommodating features of porous structures including fibrous and granular materials, Attenborough [64] developed rigid-frame theoretical models dealing with pore complexities at the microscopic scale. These are models having five structural parameters that can be reduced to four by considering the frequency dependent pore shape factor ratio, along with porosity, airflow resistivity and tortuosity. Allard's work [65] combined the key parameters derived from Biot's theory and Zwikker and Kosten's expressions. Further, Johnson *et. al.* has introduced parameters linking to the viscous effects while Champoux, Allard, Lafarge and other researchers have developed parameters to account for the thermal effects for the pore sections [66-68].

The semi-phenomenological model JCALP is considered as the most detailed model to the present date comprising of 8 transport parameters. Variations on the relevance of complexities to be considered has brought down the number of parameters to be accounted for to 6 via the JCAL model and further down to 3 using the model by Kirill *et. al.* [69]. Their recent work provides a robust analytical model that involves the use of only three directly measurable properties of porous materials, viz., porosity, steady flow permeability and standard deviation of pore size distribution. Ideal for porous materials expressed with log-normal pore size distribution such as granular porous media, this model provides a relationship between the pore structure at the micro scale and the important acoustic properties of the bulk material. Several such models have been developed to provide an in-depth insight into the physical interaction with sound propagation and dissipation mechanisms. The key parameters have been explained in the next section.

However, acquiring experimental information about some of the structural parameters such as obtaining the characteristic lengths and thermal permeability have been known to be quite challenging. Also, these modelling techniques involve a general view of the pore network that may not correlate with the fibre and fabric specifications that are familiar with the textile fraternity. Focused mainly on pore-based modelling, it has been realised that to efficiently representing fibrous materials, it takes at least 5 transport parameters. Improvements to some models have been

proposed over time as a process of achieving higher accuracy of prediction of acoustic performance of porous and fibrous materials. For instance, Kino and Ueno [70], have improved upon the Johnson and Allard model by proposing a new model based on their experimental study on fibrous materials. Particularly, for polyester fibres their model provides a relationship between airflow resistivity, bulk density, and fibre diameter.

Homogenisation of Periodic Media:

The Homogenisation of Periodic Media (HPM) is a two-scale method that associates the properties of a heterogeneous material at the micro scale to those at the macro scale. This asymptotic method had been essentially developed for periodic structures but is equally applicable to any disordered media. It requires numerical analyses of governing equations involving the mass and momentum balancing of the macroscopic scale as also obtaining the effective properties of the porous media. Developed by Bensoussan *et. al.* [71] and Sanchez-Palencia [72], this method has been elaborated in the book by Auriault, *et. al*. [82]. As mentioned, the HPM method considers a dual scale approach where separation of scales process allows for addressing the problem at the micro and macro scales separately. As per the homogenisation theory, the fluid around the fibre is assumed incompressible, i.e., it has constant density throughout while the solid material is considered stationary. The porous fibrous material is studied at two scales, the macroscopic scale (L) corresponding to the scale of the fabric sample and microscopic scale (l), considered at the pore or inclusions. These two scales can be related to one another using an expansion parameter,

$$\varepsilon = \frac{l}{L} \tag{2.4}$$

The macroscopic length can be related to the complex sound wavelength λ as follows,

$$L = \frac{|\lambda|}{2\pi} \tag{2.5}$$

The microstructural aspects of the material are represented by either a periodic unit cell (PUC) or by a statistically Representative Elementary Volume (REV). The REV based approach has been used for the case of fibrous media by Peyrega [29] to simulate size variation and random distribution of fibres. Researchers have then developed numerical techniques to obtain transport parameters from the low and high frequency limits of sound propagation. By reconstructing the

random structures as REV or PUC, these idealistic numerical models help visualise the local micro-geometry of a porous fibrous material, generally such that $\varepsilon \ll 1$.

Locally governing linearised equations that describe the harmonic oscillations in the fluid phase of the REV can be obtained. From these equations, some dimensionless quantities can be obtained which leads to representing the local equations in a dimensionless format. Detailed derivations can be found in [82]. It is worth noting that the physical space variable X can be represented by two dimensionless independent space variables, as below.

$$y = \frac{X}{l} \tag{2.6}$$

$$x = \frac{X}{L} \tag{2.7}$$

Here, the variable y varies at microscopic scale while x is taken at the macroscopic scale. The macroscopic characteristic length is selected as a reference length for calculating the gradient and Laplace operators which can be applied in the form,

$$\nabla = \nabla_x + \varepsilon^{-1}\nabla_y \tag{2.8}$$

$$\Delta = \Delta_x + 2\varepsilon^{-1}\Delta_{xy} + \varepsilon^{-2}\Delta_y \tag{2.9}$$

This implies that in general, the physical quantities can be expressed in powers of ε as follows,

$$\Phi(x,y) = \sum_{i=0}^{\infty} \varepsilon^i \Phi^i(x,y) \tag{2.10}$$

where $\Phi^i(x,y) = \overrightarrow{u^i}, p^i, \rho^i, \tau^i$ being y- periodic. Further substitution and expansion derivations leading to the transport parameters can be obtained from references [82, 96].

The homogenisation method has also been used occasionally in combination with the JCAL model. Such combination is termed as the Hybrid Multiscale (HM) approach and generally solved using finite element methods [73]. An advantage of this method is that the REV being considered numerically is detailed enough to model the transport properties of the material efficiently. However, it does call for the use of numerical simulations to arrive at the properties that will have to be post-processed to link the micro-macro parameters. In comparison to the hybrid case, the Benchmarks paper [73] also elaborates two direct approaches, viz., Direct Numerical Simulation

(DNS) and the Direct Multiscale (DM) calculations. Extensive derivations for each of the three methods can be obtained from this paper.

A complementing variation to the homogenisation approach, the Self-Consistent Method (SCM) had been proposed by Berdichevsky and Cai [74] for fibrous materials. This method focuses on developing analytical cases by considering simplified features of the microstructure, unlike the extent of precision adopted for HPM simulations, and then correlating with actual material features. This correlation between the simplified representations and the equivalent medium is expressed by the energy consistency equation. Some authors, however, have assumed various other ways of correlating such as kinematic assumptions by Boutin [75] or conditions like the waning vorticity at cell boundary as per Umnova *et. al.* [76]. A key takeaway from the energy consistency condition is that it brings out two possibilities of consistency relating to the pressure and velocity approaches. Boutin terms them as the P-Estimate and the V-Estimate, while the zero-vorticity condition introduced previously by Umnova [49], is termed as the C-Estimate. Contributing to the understanding of the methods, Boutin [77] has indicated the SCM looks at the material from the macroscopic perspective and assumes that its microscopic properties will follow similar trends. In further works, Boutin has presented an approach of combining HPM and SCM methods.

Acoustic and non-acoustic properties

From the various models reviewed above, here is a compilation of the general terminologies for acoustic and non-acoustic properties that shall be rigorously mentioned all through this thesis. Thus, this section provides the reader with a ready reference to the properties and their formulae when time arises, say during the theoretical derivation process.

To begin with, a general review of the significant physical parameters having acoustic relevance has been carried out. These have then been shown to be progressively utilised in models, thereby building up on the complexities they treat materials with. Figure 2.10 expresses the various models that will be described in further detail in this section.

For an acoustic material, porosity ϕ, is defined similar to textile version defined in equation (2.1). In terms of volumes, as presented in equation (2.11), it is the ratio of the fluid (non-solid) phase volume Ω_f to the total volume of the material Ω, has been a prominent parameter that defined the preliminary empirical models.

$$\phi = \frac{\Omega_f}{\Omega} \tag{2.11}$$

For materials with known values of porosities nearing unity, by far can be conveniently characterised by the empirical model equations (2.12 a,b) by Delany and Bazley [45] and in certain cases by including the correction factor proposed by Miki [46] in the model equations (2.13 a,b) for low frequency range applicability. The empirical models are easy to use as they involve only a single parameter, yet they cannot account for the complexities in many instances and can thus be regarded as an approximate approach [42].

Note that the convention used throughout this thesis is based on the assumption of $(e^{-i\omega t})$.

$$Z_c = \rho_0 c_0 \left(1 + 9.08 \left(10^3 \frac{f}{\sigma_0}\right)^{-0.75} + i\, 11.9 \left(10^3 \frac{f}{\sigma_0}\right)^{-0.73}\right) \tag{2.12a}$$

$$k = \frac{\omega}{c_0}\left(1 + 10.8 \left(10^3 \frac{f}{\sigma_0}\right)^{-0.70} + i\, 10.3 \left(10^3 \frac{f}{\sigma_0}\right)^{-0.59}\right) \tag{2.12b}$$

Where, ρ_0 and c_0 are the density and speed of sound in air, $\omega = 2\,\pi f$ is the angular frequency and σ_0 is the static airflow resistivity. While with the correction from Miki [46],

$$Z_c = \rho_0 c_0 \left(1 + 5.50 \left(10^3 \frac{f}{\sigma_0}\right)^{-0.632} + i\, 8.43 \left(10^3 \frac{f}{\sigma_0}\right)^{-0.632}\right) \tag{2.13a}$$

$$k = \frac{\omega}{c_0}\left(1 + 7.81 \left(10^3 \frac{f}{\sigma_0}\right)^{-0.618} + i\, 11.41 \left(10^3 \frac{f}{\sigma_0}\right)^{-0.618}\right) \tag{2.13b}$$

Beyond this, using Z_c and k values of the characteristic impedance and the complex wave number are used to obtain the surface impedance, reflection coefficient and the sound absorption coefficient as follows:

$$Z_s = iZ_c \cot(kd) \tag{2.14a}$$

$$R_c = \frac{Z_s - \rho_0 c_0}{Z_s + \rho_0 c_0} \tag{2.14b}$$

$$\alpha = 1 - |R_c|^2 \tag{2.14c}$$

The semi-phenomenological models involve more than one parameter and are backed on several theories but particularly focus on the involvement of visco-inertial and thermal effects [78]. Wilson model [79] is a 4-parameter model catering to middle frequency range where the viscous and thermal boundary layers are typically of the order of the characteristic pore size. It was Zwikker and Kosten's contribution [63] on the propagation of sound assuming a motionless structure of cylindrical pores that have accounted for viscous and thermal interactions between the solid and fluid phases. M. A. Biot's model [61] considering the propagation of elastic waves through the medium and accounting for visco-inertial effects of materials performing in the low and high frequency ranges describes the diphasic model mentioned earlier.

Most of the multi-parameter semi-phenomenological models are based on the theories developed by Biot and being categorised into the equivalent models depending on the significance of the involvement of either of the phases. The models derived from the Biot's theory including the distinct or combined approaches by Johnson, Champoux, Allard, Lafarge [66-68]. As also, the Attenborough model [64] that introduces tortuosity and parameters that account for complex pore shapes at high frequencies. The correction given by Pride [80] to Johnson's model, accounts for the inertial effects at low frequencies for an equivalent fluid. These models usually involve 5 – 8 parameters, which can be independently measured or pre-defined at the time of manufacturing but might be slightly cumbersome to extract. There are eight parameters within the most popularly used model the Johnson-Champoux-Allard-Lafarge-Pride (JCALP) model.

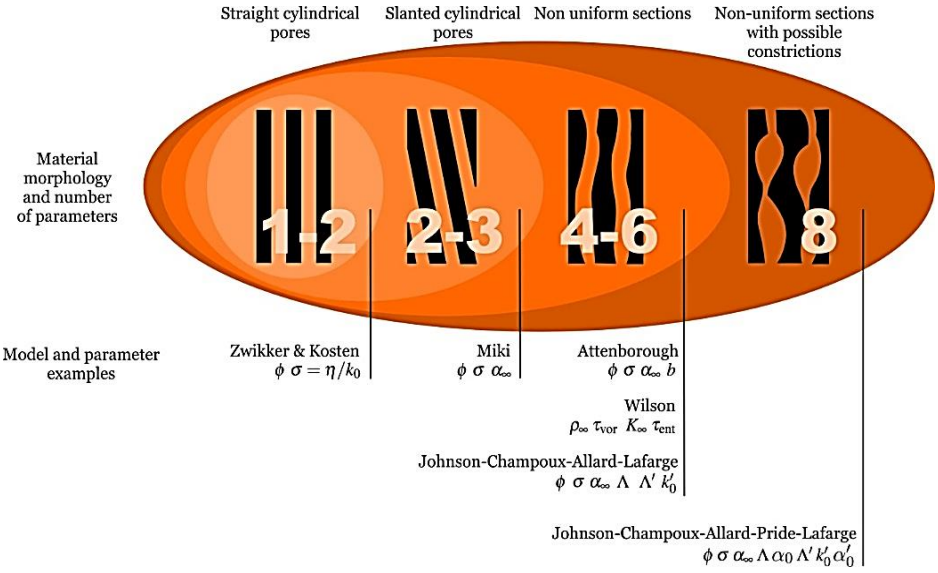

Figure 2.10.: Growing complexity of propagation models assuming motionless skeleton [81]

However, to describe the visco-inertial and thermal dissipative effects within a porous media as considered, the JCAL propagation model is widely used. In the JCAL equivalent fluid model, the effective quantities (effective density and effective bulk modulus) depend upon the following 6 macroscopic parameters:

1. Open porosity ϕ is a measure of the fractional amount of air volume in the interconnected pores within the tested material. The formula to calculate porosity is as per equation (2.11).
2. Airflow resistivity σ_0 is a measure of the resistance that airflow meets when passing through a material as expressed in equation (2.15), where, Δp is the pressure drop across the material, v_{af} is the airflow rate passing through and d is the thickness of the material.

$$\sigma_0 = \frac{\Delta p}{v_{af}\, d}\left[\frac{Ns}{m^4}\right] \tag{2.15}$$

3. Tortuosity α_∞ is also referred to as the high frequency limit of tortuosity and is a dimensionless quantity that considers the sinuous fluid paths through the porous material. In its equation (2.16), v is the microscopic velocity of an inviscid fluid within the pores and V is a homogeneous fluid volume.

$$\alpha_\infty = \frac{\frac{1}{V}\int_V v^2 dV}{\left|\frac{1}{V}\int_V \vec{v}\, dV\right|^2} \tag{2.16}$$

4. Viscous Characteristic Length (VCL) Λ are the viscous forces between the porous frame and its saturating fluid at high frequencies. It can be expressed as equation (2.17) where S is the contact surface between the pores and the frame

$$\Lambda = 2\frac{\int_V |v(r)|^2 dV}{\int_S |v(r)|^2 dS}\,[m] \tag{2.17}$$

5. Thermal characteristic Length (TCL) Λ' are the thermal exchanges between the porous frame and its saturating fluid at high frequencies and is calculated as shown in equation (2.18).

$$\Lambda' = 2\frac{\int_V dV}{\int_S dS}\,[m] \tag{2.18}$$

6. Static thermal permeability k_0' represents the low frequency limit of the thermal response function or $k'(\omega)$ the dynamic thermal permeability as expressed in equation (2.19 a,b) where, τ is the macroscopic excess temperature in fluid phase, p is the pressure and κ is the thermal conduction coefficient.

$$k_0' = \lim_{\omega \to 0} k'(\omega) \tag{2.19a}$$

$$\phi\tau = \frac{k'(\omega)}{\kappa}\frac{\partial p}{\partial t} \tag{2.19b}$$

Note also that similarly, static viscous permeability k_0 is defined as the ratio of $k(\omega)$, the dynamic viscosity of the air over the static airflow resistivity, as in equations (2.20 a,b), where $\vec{v}$ is the velocity of the fluid particles subjected to the pressure gradient $\vec{\nabla}p$ implying that $\phi\vec{v}$ is thus the fluid flow inside the porous material and η is the dynamic viscosity of air ($\sim 1.84 \times 10^{-5}$ $[N.s.m^{-2}]$) at ambient temperature and pressure conditions. Equation (2.20b) is the generalised Darcy's Law [82].

$$k_0 = \lim_{\omega \to 0} k(\omega) \tag{2.20a}$$

$$\phi\vec{v} = -\frac{k(\omega)}{\eta}\vec{\nabla}p \tag{2.20b}$$

According to JCAL model, the expressions for effective quantities of a porous material are as follows:

Effective density $\rho(\omega)$ is related to the existence of inertial and viscous forces is as per equation (2.21).

$$\rho(\omega) = \frac{\alpha_\infty \rho_0}{\phi} + \frac{\sigma_0}{i\omega}\sqrt{1 + \left(\frac{4i\alpha_\infty^2 \eta \rho_0 \omega}{\sigma_0^2 \Lambda^2 \phi^2}\right)} \tag{2.21}$$

Effective bulk modulus $K(\omega)$ accounts for the thermal exchanges between the frame and the saturating fluid is calculated as shown in equation (2.22). Here, C_p is molar heat capacity and P_0 is static pressure.

$$K(\omega) = \frac{\frac{\gamma P_0}{\phi}}{\gamma - (\gamma - 1)\left[1 - i\left(\frac{\phi\kappa}{k_0'\omega\rho_0 C_p}\right)\sqrt{1 + \left(\frac{4{k_0'}^2 \omega \rho_0 C_p}{\kappa {\Lambda'}^2 \phi^2}\right)}\right]^{-1}} \tag{2.22}$$

For a typical motionless material frame, the Figure 2.10 [81], suggests the progress in complexity for considering the best-suited propagation models. Basic level models that consider few bulk material properties are more suitable for the fabric level study than the fibre-based ones. However, the parameters are equally useful to characterise the material and derive meaningful connections with the complex models.

2.3. ACOUSTIC STUDIES FOR NONWOVENS AT BULK-SCALE

Sound absorption characteristics for materials in bulk can be improved by manipulating with the amount of material being used, either by increasing the density of the overall content by trying to compress a lot in a constrained space or by allowing high amount of content to occupy a thicker block. This approach is resorted to when the fibre dimensions of the material cannot be altered.

Layered Nonwovens

If there is scope of using different materials, then layering of these to achieve improved absorption is the first corrective instinct. A single layer of porous material does not always provide high internal attenuation along with having the desired impedance matching capability [83]. Several researchers over a period of time have shown that by adding porous materials in layers has had an impact on the overall absorption. The impact varies for different frequencies for different materials and layouts within the configuration. Gradation of material can be either obtained by skilful manipulation of the rate of material distribution during the fabric manufacturing or by alternatively fabricating layers with varying density or porosity. Rockwool®, a mineral wool manufacturer has recently introduced their dual density technology [84] which is based on layered materials for effective performance in terms of sound absorption.

Early works by Dunn and Davern [85] have suggested that due importance has been given to multi-layered configurations where theories have been validated against experimental data. The paper compares layered media with typical end terminations or hard backing and presence of an air cavity. In addition to this, the single layer has also been compared with multi-layer systems for their variation concerning the acoustic impedance and absorption capabilities. Similar studies have been carried out much recently that utilize the well-defined models that have been defined in the fibre level study previously [86]. Figure 2.11 shows the selected configurations and is a good visual descriptor of the systems based on their termination.

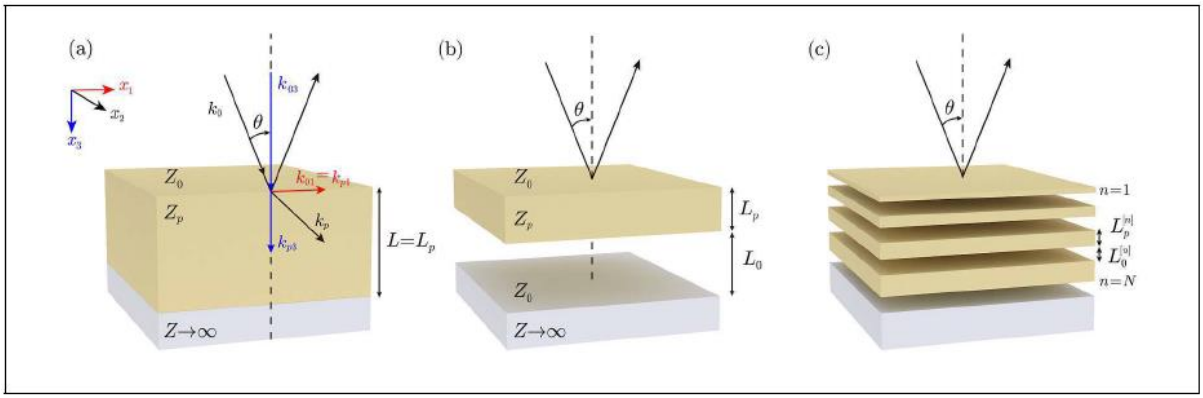

Figure 2.11.: Configurations [86] (a) rigidly backed, (b) air cavity backed, (c) multi-layered.

In the paper, Brouard *et. al.* [37] has presented a detailed analytical approach to handling layered media. The transfer matrix method has been heavily used by transforming the governing equations from first principles. To validate the theories defined, experimental examples have been covered where materials of different nature are layered and resolved for using their physical properties as inputs. The influence of such layers on the acoustic absorption and transmission characteristics has been reported. This information also forms the part of the multi-layer porous absorption characterisation in the book by Allard [35].

The trend to research and utilise multi-layer materials has gained prominence across the globe. Researchers at the College of Textiles, Donghua University, China conducted research on multi-layer textile materials for developing materials that strike a good balance between the noise reduction and production costs [87]. With the understanding of the acoustic capabilities of different materials, analytical, numerical and experimental work has been carried out on 'sandwich layers' of different material combinations. A key conclusion was that for common nonwoven fabrics, multi-layered structures have better absorption. The same group at the university then conducted a much extensive study on nonwovens alone [88]. This study was based on the impact of the construction of the layered composites. The layers were compared based on the experiments designed to study the effect of single layer, bi-layer and tri-layer combinations. Quite interestingly, the conclusions support their hypothesis of the importance of the layering sequence. The best performing material combination was that of the nonwoven-polyethylene-woven based set that had the highest acoustic absorption of them all.

Membranes and facings

While considering layered porous media, it is worth mentioning the contribution of upstream layers. These are either in the form of resistive screens or plates that primarily play the role of a decorative or protective covering over a bulky nonwoven wadding. These can also be termed as coverings, screens or membranes as their thickness is much greater than the thickness of layer that follows or in other cases is enclosed. An example in their book by Allard and Atalla [35], explains the effect of a facing fabric having very low thickness (1 mm or less). They say that the main effect is that around the mid-frequency ranges the real part of the impedance of the base layer is increased due to the membrane like layer on the top. The example has been verified by the experimental set of glass wool sheets on foams. The sound absorption curves show a comparison between the foam with and without facing. The trend generally suggests that the presence of the sheet on a high performing foam material contributes by improving its absorption values at the lower frequencies.

Chevillotte [89] has studied the sound absorption capability of facing layers. In this research, the formulae developed act as guidance to the designing of such multi-layered systems. It has been observed in this work that by adding such an upstream layer, enhanced absorption can be achieved in the low frequencies for an already good performing base material. As a caution, it has been highlighted that such layer can negatively influence the sound absorption capabilities at higher frequencies. Nonwoven textile materials tested during this study have had large perforation rate as a key parameter that have enabled in attaining good sound absorption over a wider frequency range. Similar observations have been discussed in great detail as a section in the reference book 'Acoustic Absorbers and Diffusers' [(section 6.3) 83].

Bulk characterisation techniques

The most prominent bulk property modelling techniques are categorised based on the material interaction with either the diffused field within the reverberation chamber or the plane wave propagation using the impedance tube methods. These approaches aid in obtaining the macroscopic characteristics such as the sound absorption, reflection, and the transmission coefficients. In addition to this, the airflow resistivity test setup is used to obtain the flow resistivity parameter that is useful in several model-based calculations. The reverberant room and the acoustic chamber method is defined by standard protocols as in BS EN ISO 354: 2003 [90] and while the

impedance tube method based on either the standing wave ratio or the transfer function method is as specified by parts 1 and 2 of BS EN ISO 10534: 2001 [91] respectively.

In comparison to the chamber method which requires large amounts of fabric material, the impedance tube utilizes very little sample (difference in surface areas being approximately of the order of 10 m2). The results from the reverberation room test are expressed as singular numerals or percentages termed as Noise Reduction Coefficient (NRC) or much recently Sound Absorption Average (SAA). The approach to calculate and present the information for the single number rating as used in buildings has been elaborated in BS EN ISO 11654: 1997 [92]. This British Standard also provides a uniform way of classifying sound absorbers that are intended for broad frequency band applications. Accordingly, the Figure 2.12 provides the various sound absorption classes that are bound by the reference curves. Further details in terms of parameters specified and calculation steps involved in classifying an absorber based on its actual trend can be obtained from standard.

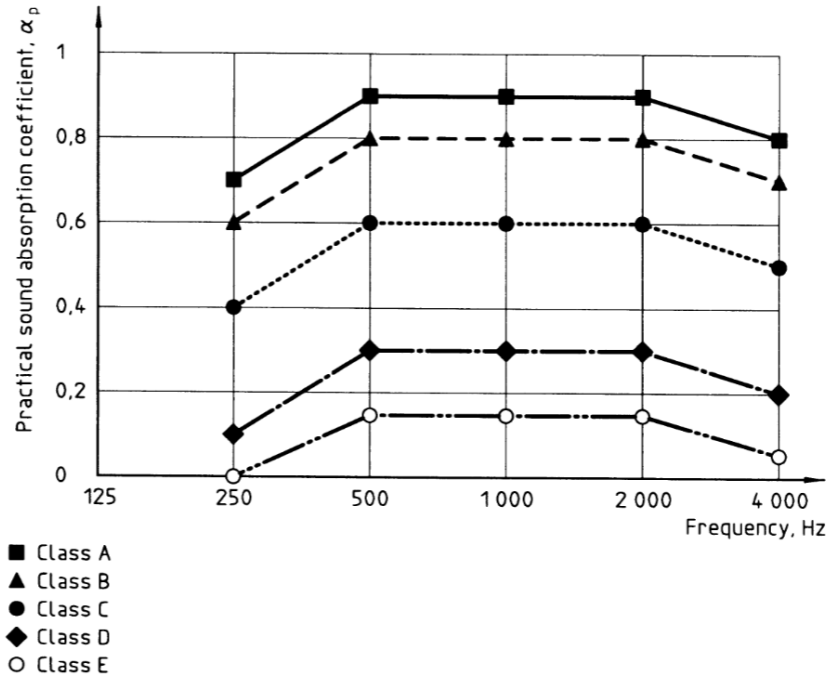

Figure 2.12.: Depiction of reference curves based on sound absorption classes [92].

The impedance tube provides quite a comprehensive result depending on the setup used. The setup primarily is selected based on the focus of the study based on low or medium to high frequency behaviour. Then depending on the application, the material to be used for would suggest the use of either the 2-microphone setup with rigid hard backing generating the absorption and reflection

coefficients or the 4-microphone setup that characterizes the material in the transmission regime and produces results that include the associated parameters. These being the standard tests, there are always certain limitations and distinctions based around them. Very few variations can be suggested for the reverberation room test, such as the consideration of the configurations in the mounting positions of the test materials and the sides of the material being exposed to the acoustic waves, most of which have been detailed in the standards. However, as the impedance tube can deliver a myriad of parameters owing to the complex calculations using the frequency response functions from the microphones that pass on into the processing software, several modifications can be accommodated. These include the 3-microphone method [93], the two terminations or the two cavity approaches [94] and the likes. A study of these is essential as the materials that are prepared for research purposes would be homogeneous while the practical applications often involve the use of quite a composite mix of fibres and may also be pseudo or anisotropic in nature.

Chapter 3

RESEARCH METHODOLOGY

Overview:

3.1. Selection of nonwoven material samples

3.2. Choice of acoustic models and modelling tools

3.3. Summary of experimental techniques

3.1. SELECTION OF NONWOVEN MATERIAL SAMPLES

Polyester based nonwoven materials have been selected for a major part of this study due to two obvious reasons. Firstly, because of the ease of sourcing of such materials from Cosmotec, a pioneering manufacturer [95], where the author was involved on a research project and secondly, as polyester fibres are mainly solid with a regular surface finish and have a cylindrical cross-section that reduces the parameters to be approximated during the modelling phase. Besides these composite materials made of viscose and cotton blended with polyester fibres have been used for comparative studies in the application section.

Sample Properties

The polyester fabrics manufactured for the present study have been developed considering a combination of physical parameters that are likely to influence the acoustic fibre interaction. Therefore, parameters such as the blend (% and dtex of each fibre component), overall fabric weights (g/m^2) and fabric thickness (mm) have been studied using the Design of Experiments

approach. The staple polyester fibres of 7 and 17 dtex have been blended with 20% of the low-melt polyester binder fibres of sheath/core (50/50). The fabric densities considered for test range from 20 to 60 kg/m³ for each blend in thicknesses 10, 20 and 30 mm.

Sample Preparation

The research samples have been manufactured at the industrial facility following standard techniques. The blended fibres have been carded, cross lapped, thermally bonded and calibrated to thickness. The test samples were die-cut to suit both large (diameter, 100 mm) and small (diameter, 29 mm) impedance tubes, ensuring sharp cuts to maintain the test accuracy. Nearly 10 m² of each sample with an aspect ratio from 0.7 to 1.0 has also been separately manufactured for the reverberation room tests.

Table 3.1.: Test sample selections and their properties

Sample	Blend Ratio	Main Fibre Radius	Sec Fibre Radius	Bico- Fibre Radius	Effective Radius
PES7	80-20	12.5 µm		10.2 µm	12.1 µm
PES17	80-20	20.0 µm		10.2 µm	18.5 µm
OPES	75-25	12.5 µm		10.2 µm	12.0 µm
SEN	66-34	20.0 µm		10.2 µm	17.3 µm
AEROZ	60-15-25	8.25 µm	12.5 µm	10.2 µm	9.50 µm

Image					
Sample	**PES7**	**PES17**	**OPES**	**SEN**	**AEROZ**

Figure 3.1.: Image references of selected test samples

3.2. CHOICE OF ACOUSTIC MODELS AND MODELLING TOOLS

Acoustic models

To progress with the most applicable acoustic model for a nonwoven fabric to be analysed, it is essential to first recognise the material under observation and then to associate the relevant model. In some situations, however, one or more models might be adopted depending upon the ease and availability of the required parameters, accuracy needs, scope of the study say in terms of the range of frequency. Finally, the expected analyses and outcome from the test material can be correlated to the best fitting models from amongst their sub-categories:

a. Empirical
b. Semi-phenomenological
c. Microstructural

These models are then used to correlate between the macro and micro properties of the material, essentially by obtaining the information from their microstructure and translating them to deduce meaningful macro scale performance.

The micro scale characterisation of the nonwoven sample would be attained from the microscopic images scanned or alternatively, if there is an understanding of the pore dimensions and interconnections then the micro characterisation is done by considering unit representative cell structures. However, the latter approach requires an understanding of the fundamental physics of the test sample. With the availability of well-defined micro properties, the macro properties can then be numerically computed using the semi-phenomenological models as suggested [35]. To be precise, the macro properties include the sound absorption coefficient with hard backing and/or anechoic termination as per the application of the test material and the transmission loss characteristics. For simple representative structures, approximated materials (such as the uniform shaped pores/ inclusions, etc.) can be solved for analytically.

However, as a generic case relating to the microstructural sub-category of models, the information from the microstructure is obtained using the linearised frequency dependent problems, which can be approached as described in steps by Venegas R. in his PhD thesis [96].

- The general problem statement is obtained in two parts:

1. To approach the visco-inertial consideration, the equations are:
    a. The conservation of momentum or typically the Navier Stokes equation
    b. The conservation of mass equation
    c. The no slip boundary condition
2. Thermal aspects are targeted using equations
    a. The conservation of energy, also termed as the heat equation
    b. The equation of state
    c. The isothermal or adiabatic boundary condition

- The general solution is in terms of the characteristic quantities of the material, viz. dynamic mass density and the dynamic bulk modulus.
- These dynamic properties are then used to obtain the characteristic impedance and the wave number, which ultimately lead to the major macroscopic absorption and transmission characteristics.
- The equation sets defined above can also be used to obtain other physical parameters such as the permeability, compressibility, and tortuosity.
- By solving the governing equations at the microscopic level, the effective properties of the test sample can be estimated.

In his works, Venegas [96] elaborates the various approaches to obtain properties from the governing wave equations using HPM method described in literature review section previously. These approaches leading to the acoustic performance properties of materials have been expressed in the flow diagram presented in Figure 3.2.

The direct approach can be related to the theoretical approach while the indirect approach corresponds much to the numerical and experimental methods of obtaining the required material properties. Starting from the governing equations, the process terminates with obtaining the characteristic wave number and impedance as mentioned above; using which the performance of the material in terms of the sound absorption characteristics and/or the associated transmission loss can thus be calculated using simple formulae or MATLAB codes.

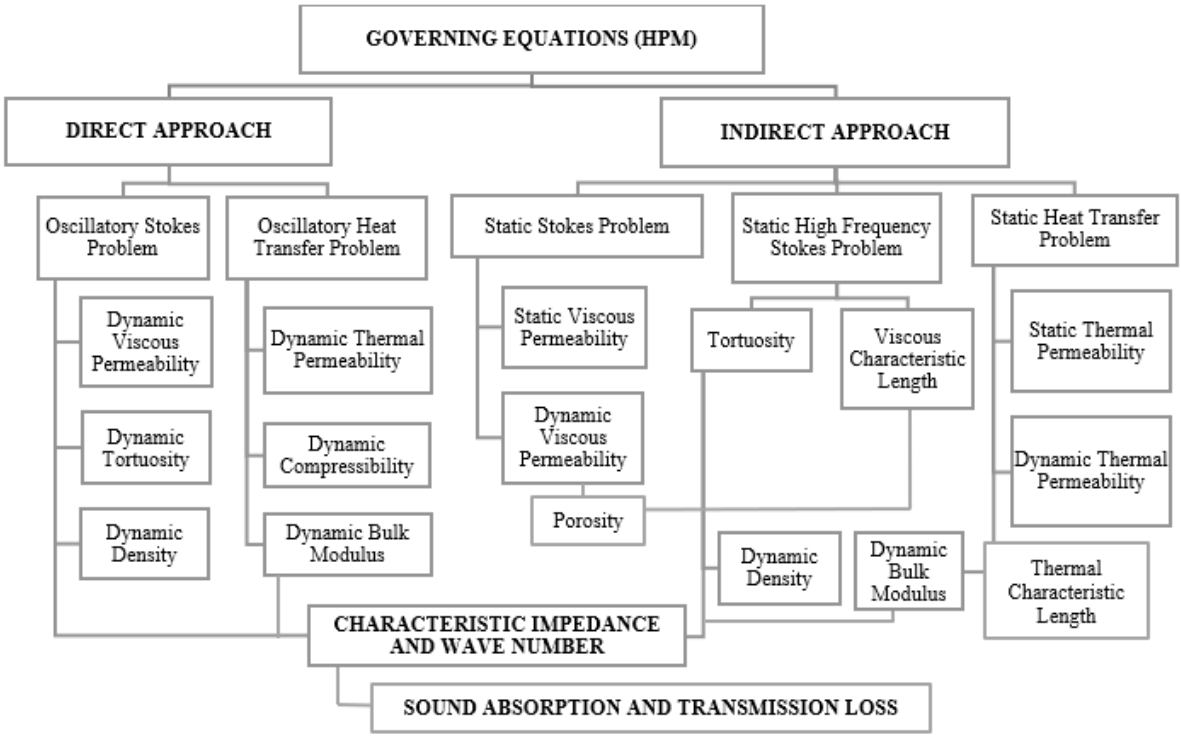

Figure 3.2.: Flow diagram for obtaining key properties from the governing wave equations.

Modelling tools

The models throughout this thesis have been studied with a variety of modelling tools, hence the need of this section of the chapter.

A major aspect of the numerical simulations has been conducted using COMSOL 5.5 software. This was carried out in association with MATLAB R2021b software for post-processing the data as well as analysing and corelating the information. Besides these other types of software that were used as a part of the application studies include FOAM-X software, ImageJ for SEM data analysis.

3.3. SUMMARY OF EXPERIMENTAL TECHNIQUES

Experimental techniques for characterising sound absorbing materials are essential for understanding and optimising their acoustic properties. This section details the various characterisation techniques that have been adopted at various stages of the research work. It gives details on how to process the data obtained and presents how the information has been used or may be applied beyond the experimental observations.

3.3.1. Microscopic tools and methods:

Microscopic methods play a pivotal role in the visual characterisation of sound absorbing materials. Both, Optical Microscopy and Scanning Electron Microscopy (SEM) are commonly employed techniques adopted to scrutinise the microstructure of such materials. Optical microscopy provides a broader view of the material's overall composition and can be used to measure pore sizes and distribution. SEM, on the other hand, allows researchers to delve into the intricate details of a material's surface, offering high-resolution images that reveal the morphology of fibres, pores, and other structural elements. These microscopic methods enable a researcher or an acoustician to gain valuable insights into the micro features of sound absorbing materials, thereby aiding in the design and optimisation of acoustic properties for various applications, from architectural soundproofing to automotive noise control.

A. Optical Microscopy

As introduced above, the optical microscopy method provides a visual characterisation of sound absorbing materials and focuses on the materials from a wider perspective where a bunch of fibres are picked and assessed. Optical microscopic tools include the optical lens and optical microscope, both of which have been used to examine fibre morphology.

a. Optical Lens

An optical lens is a transparent, curved piece of glass or other material that can bend and focus light rays. It plays a fundamental role in optics and imaging systems, including cameras, telescopes, eyeglasses, and microscopes. Lenses work based on the principles of refraction, where they cause light to change its direction as it passes through them. Convex lenses, which are thicker in the centre and thinner at the edges, converge light rays to a focal point, while concave lenses, which are thinner in the centre and thicker at the edges, diverge light rays. This property allows lenses to create real or virtual images, magnify or reduce objects, and correct vision problems. Optical lenses are essential components in optical instruments, including the optical microscope. These lenses can be used by themselves in the form of lens setups as shown in Figure 3.3. Such a setup was used to visually distinguish various fibrous material samples from each other.

Figure 3.3.: Optical lens setup

It is often found that textile researchers suggest optical lenses to be an indispensable component in the visual characterisation of fibrous materials. When dealing with fibrous specimens, lenses help in magnifying and focusing light onto the material, enabling their detailed observation. Depending on the specific requirements of analysis, different types of lenses, such as objective lenses and eyepieces, can be used to achieve various levels of magnification and clarity. The ability of optical lenses to manipulate light rays and form images is particularly useful when studying the microstructure of fibrous sound absorbing materials, allowing researchers to examine individual fibres, their alignment, and any structural defects. Optical lenses facilitate the precise measurement of fibre diameters, orientations, and distribution, contributing to a comprehensive understanding of the material's bulk and some micro properties.

b. Optical Microscope

An optical microscope, often referred to as a light microscope, is a scientific instrument that utilises optical lenses to magnify and observe tiny objects or specimens that are otherwise invisible to the naked eye. It consists of several key components, including an objective lens and an eyepiece or ocular lens. The objective lens collects and magnifies light passing through the specimen, while the eyepiece further magnifies the image for viewing. Illumination sources, such as light bulbs, provide illumination for the specimen. Figure 3.4a shows the optical microscope setup that was used for visual inspection of the fibre count and morphology. The setup shows the illumination provided at the base that assists in viewing thin strands of fibrous materials. Optical microscopes are valuable tools for acoustic research due to their ability to provide high-quality, three-dimensional images of material specimens without the need for complex sample preparation or harmful radiation. Modern optical microscopes can achieve impressive levels of magnification and resolution, making them essential for a wide range of scientific investigations.

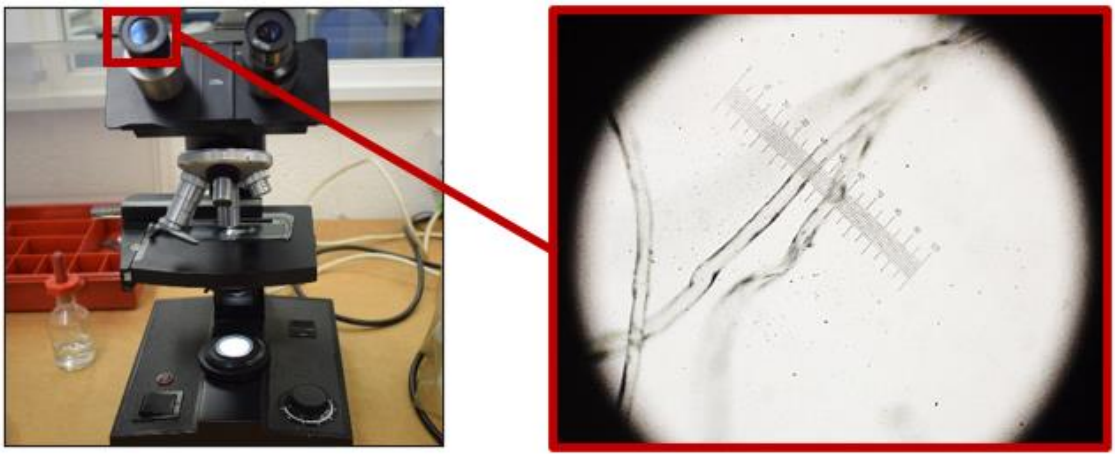

Figure 3.4.: a) Optical microscope b) Microscopic image of fibres with lens scale

Optical microscope is an invaluable tool for the visual characterisation of fibrous materials. In the context of fibrous materials, optical microscopes are utilised to examine their microstructure, such as the arrangement of fibres, their density, and any surface features or defects. By adjusting the microscope's settings, researchers can control factors like magnification, illumination, and contrast, allowing for the precise analysis of fibrous materials. Figure 3.4b illustrates a magnified and detailed image of polyester fibrous strands. With the provision of a lens scale, the diameter of fibre types can be easily measured. This information is essential for various applications, from textile manufacturing quality control to the development of sound absorbing materials. Optical microscopes are a cornerstone in the study and characterisation of fibrous materials due to their versatility, ease of use, and ability to provide valuable visual insights at the microscopic level.

Processing fibre data from optical microscopy using property calculation sheets:

Once fibres have been examined under an optical microscope, their types observed are compared using optical measurement data sheets that correlate the lens divisions to the fibre diameter for graticule calibration and to titre for measuring in decitex units (popularly used in textiles) based on the type of material identified.

As the fibre diameters are established, various bunches of such fibres are examined to manually establish the blend ratio of the staple and binding fibres. With inputs including fibre parameters (decitex, blend, density, cross-section, and cross-section factor) and fabric parameters (weight and thickness), material properties such as fibre surface area and fabric void volume are calculated.

B. Scanning Electron Microscope (SEM)

A Scanning Electron Microscope (SEM) is a powerful instrument used for imaging and analysing the surfaces of solid objects at high magnifications and resolutions. Unlike the optical microscopes covered above, SEMs employ a different principle of imaging known as electron microscopy.

Instead of using visible light, SEMs use a focused beam of electrons to illuminate the sample. These electrons are accelerated to high energies and directed onto the specimen's surface. A series of electromagnetic lenses within the SEM precisely focus the electron beam onto the sample, allowing for extremely fine detail and high-resolution imaging. SEMs operate by scanning the focused electron beam across the sample's surface in a raster pattern. This scanning process generates signals that provide information about the sample's topography and composition. Different detectors in SEMs capture various signals produced by the interaction of the electron beam with the sample. These signals help create images and provide compositional information. SEMs produce images based on variations in electron signals. Areas of the sample that emit more electrons will appear brighter in the resulting images.

For a fibrous sample, SEMs can provide detailed information about their microstructure and surface properties. Figure 3.5 shows the SEM setup along with highly magnified sample scans.

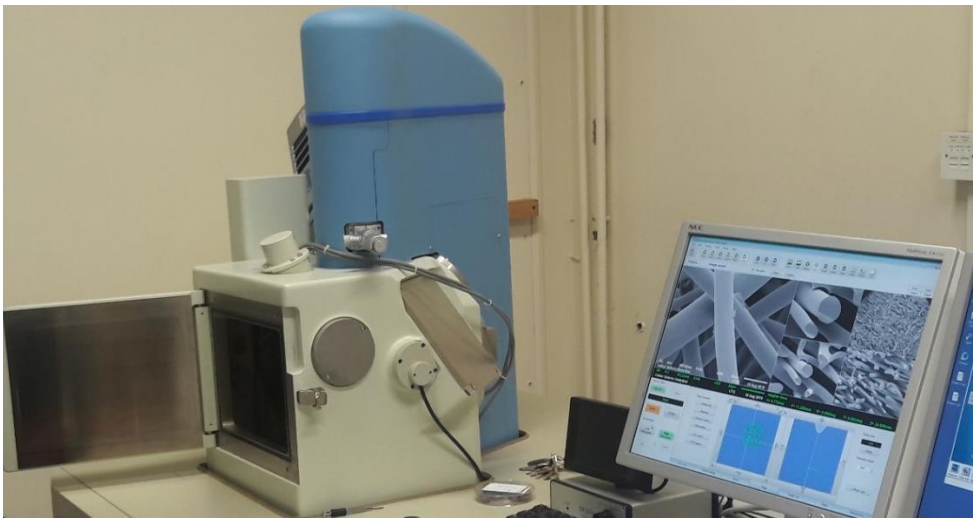

Figure 3.5.: SEM setup at University of Leeds test facility

There are many advantages provided by SEMs when characterising fibrous sound absorbing materials; particularly, offering much higher resolution than optical microscopes, making them suitable for observing micro and nanoscale features and providing detailed 3D images of the sample's surface topography, helping visualize surface structures and textures.

SEM image processing:

Images obtained from SEM need further processing to extract meaningful data. DiameterJ, a plugin for ImageJ [97], is an open-source image processing and analysis software that is widely used for this purpose. It is specifically developed to measure fibre properties from SEM images. The software provides training manuals that can be accessed online that offer the methodology for processing the SEM image. The key steps include, image cropping and segmentation, manual segmentation and unit conversion, fibre diameter analysis and fibre diameter metric analysis.

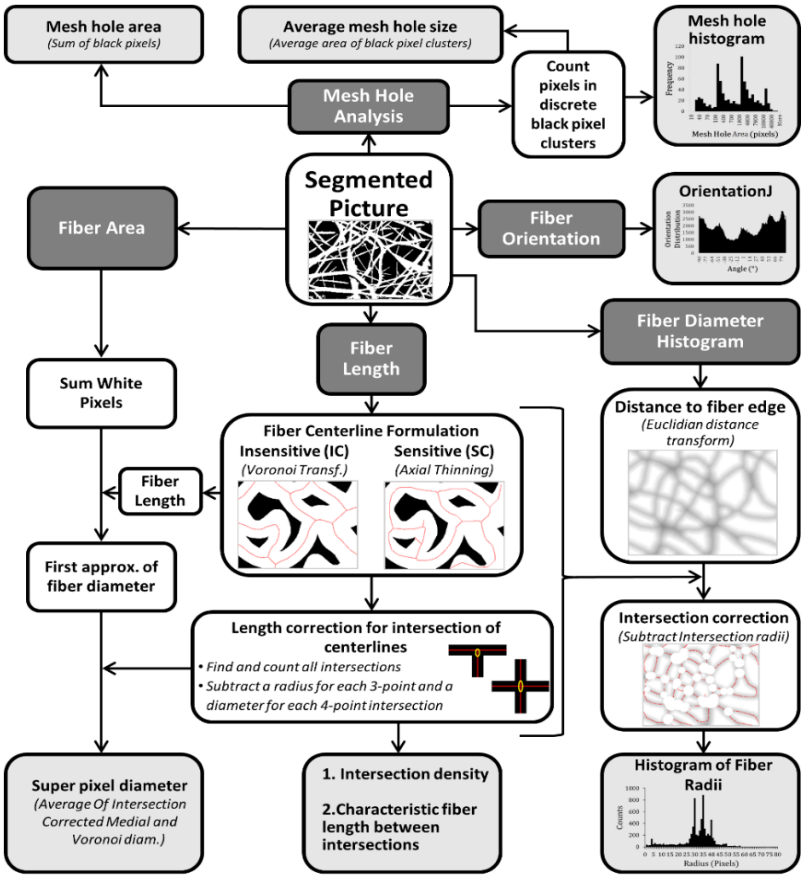

Figure 3.6.: Process diagram [97] for SEM data extraction and analysis using DiameterJ software.

A process flow diagram of the various capabilities that DiameterJ software provides as an extension to what ImageJ can deliver has been illustrated in Figure 3.6. The workflow of using DiameterJ within ImageJ typically involves opening an image, calibrating it to define measurement units, using DiameterJ's measurement tool to mark and measure object diameters, and exporting the data for further analysis or visualisation. DiameterJ streamlines the process of calibrating images, measuring diameters accurately, and exporting the data for further analysis.

3.3.2. Physical and acoustic characterisation methods:

Physical and acoustic characterisation of sound absorbing materials can tailor them to meet specific acoustic requirements for a variety of applications and contribute to improved acoustic comfort and noise control in built environments. Physically, these materials are evaluated for their density, porosity, thickness, and air permeability, as these properties directly impact their ability to attenuate sound. Acoustic characterisation involves measuring parameters like sound absorption coefficient, sound transmission loss, and impedance, which help quantify the material's effectiveness in absorbing and dissipating sound energy. Laboratory tests such as the airflow resistivity test, impedance tube method, and reverberation chamber tests are commonly employed to gather data on the acoustic behaviour of these materials. These methods have been extensively used for experimentation purposes throughout the research and have been elaborated below.

A. Airflow resistivity rig

The airflow resistivity test rig is a useful tool used to assess the acoustic performance of fibrous materials. This test measures the material's airflow resistivity, which is a crucial parameter in understanding its sound absorbing capabilities. By passing air through a sample of the fibrous material and measuring the pressure drop across it, the rig calculates the airflow resistivity, which is typically expressed in Rayls per square meter (Rayl/m^2). This tool enables the selection of materials with specific airflow resistivity values to achieve desired acoustic performance.

The airflow resistivity rig shown in Figure 3.7 was modified for the Acoustics Research Centre at the University of Salford as a part of this research work to ensure that the sensitivity of the setup is accurate. The test setup comprises of two transparent tubes, sample holders along with a pressure transmitter and differential pressure transmitter. The flow through the tubes is controlled by a needle valve. The tubes of the rig can measure samples with two different diameters (29 mm and

100 mm) that correspond to small and large B&K impedance tubes used for acoustic property measurements. A calibrator sample is used to calibrate before use.

Figure 3.7.: Airflow resistivity test setup at University of Salford laboratory

B. Impedance Tubes

Impedance tubes are essential in the characterisation of fibrous materials for their acoustic properties. These tubes are designed to measure the complex acoustic impedance of a material, which comprises its resistance and reactance to sound waves at different frequencies. By analysing the impedance spectrum, the absorption coefficient and sound transmission loss of sound absorbing materials can be obtained. There are various types of impedance tubes that provide acoustic characteristics of materials based on the type of samples available for testing. Figure 3.8 provides a flow diagram that classifies the known variants that have been referred and/or used at various stages of this research to obtain experimental data. At the Acoustic Research Centre of the University of Salford, impedance tubes developed by Brüel & Kjær (B&K) have been set up and modifications have been made in-house for accommodating different sample studies.

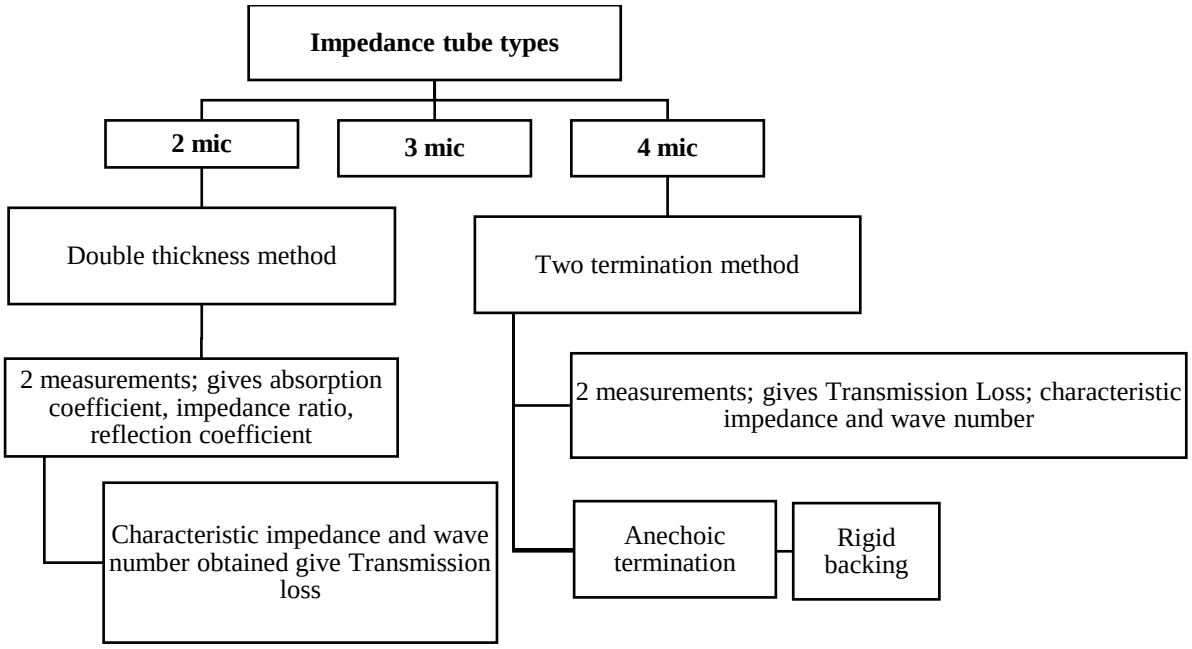

Figure 3.8.: Types of setups and outcomes using Impedance tubes.

Broadly, there are three categories of impedance tubes based on the number of microphones involved in the measurement tube. Acoustic property measurements can then be obtained from these tube setups by various standard and modified methods. Besides the standard approach as detailed in BS EN ISO 10534-2-2001 [98] or ASTM E1050-19 [99], two further modifications have been researched [100]; these include two cavity method and double thickness method. A further improvement in the method of testing involves the introduction of a third microphone. This method is suitable for homogeneous materials. The techniques developed for a 3-mic setup have been elaborated in the references [93,101]. Figure 3.9 illustrates the 2- and 3- mic setups [93].

The four-microphone impedance tube method is also a standard test based on ASTM E2611-17 [102]. The general procedure and properties that can be obtained from this method have been detailed in B&K's technical review [103]. Figure 3.10 shows the4-mic impedance tube setup [102]. This complete setup is used to provide detailed information about a material sample covering properties such as Sound Absorption Coefficients, Reflection Factor, Transmission Loss Characteristics and Frequency Response Functions.

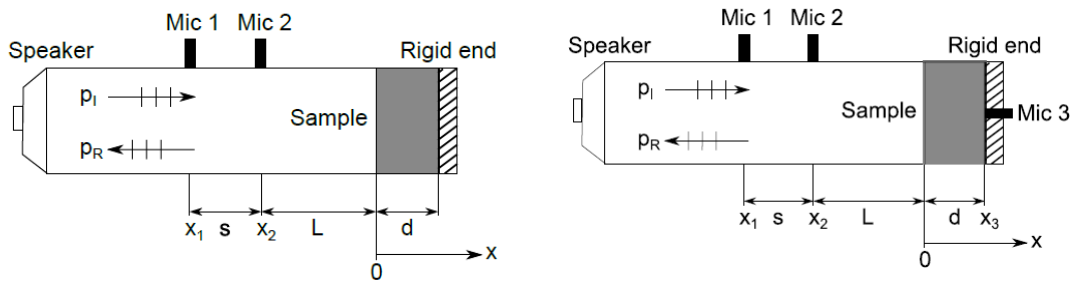

Figure 3.9.: Impedance tubes with 2- and 3- microphone setups [93].

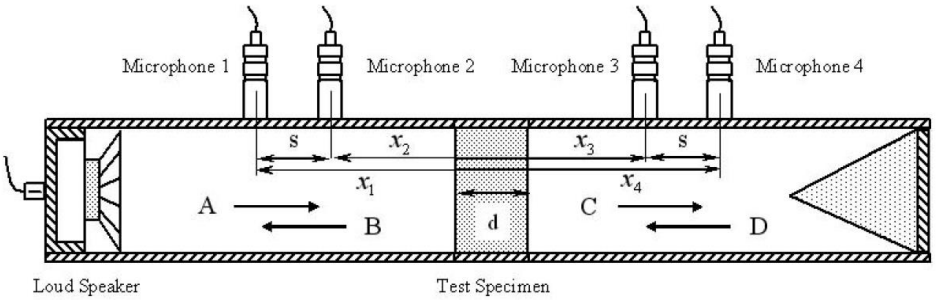

Figure 3.10.: Impedance tubes with 4- microphone setup [102].

C. Reverberation room

In the reverberation room technique, a test specimen is placed inside a specially designed room with highly reflective surfaces. Sound is emitted into the room, creating a diffuse sound field with no direct sound path between the source and the material. By measuring the change in sound pressure levels before and after introducing the fibrous material, acousticians determine its sound absorption coefficient. This coefficient provides essential information about the ability of the material to absorb and dissipate sound energy across a range of frequencies. This method is valuable for characterising fibrous materials used in architectural acoustics, such as wall panels and ceiling tiles, helping engineers and designers make informed choices to optimise acoustic comfort in various environments. Materials have been tested for their sound absorption characteristics at the Acoustic Transmission suite which is a full commercial scale reverberation room test facility at the University of Salford research laboratory shown in Figure 3.11a. The methods are based on standards BS EN ISO 354:2003 [104] and BS EN ISO 11654:1997 [105]

and a performance report based on the format can be prepared with the information obtained from the tests conducted, a template of which is shown in Figure 3.11b. From the reverberation time values obtained from the test, sound absorption can be evaluated and plotted.

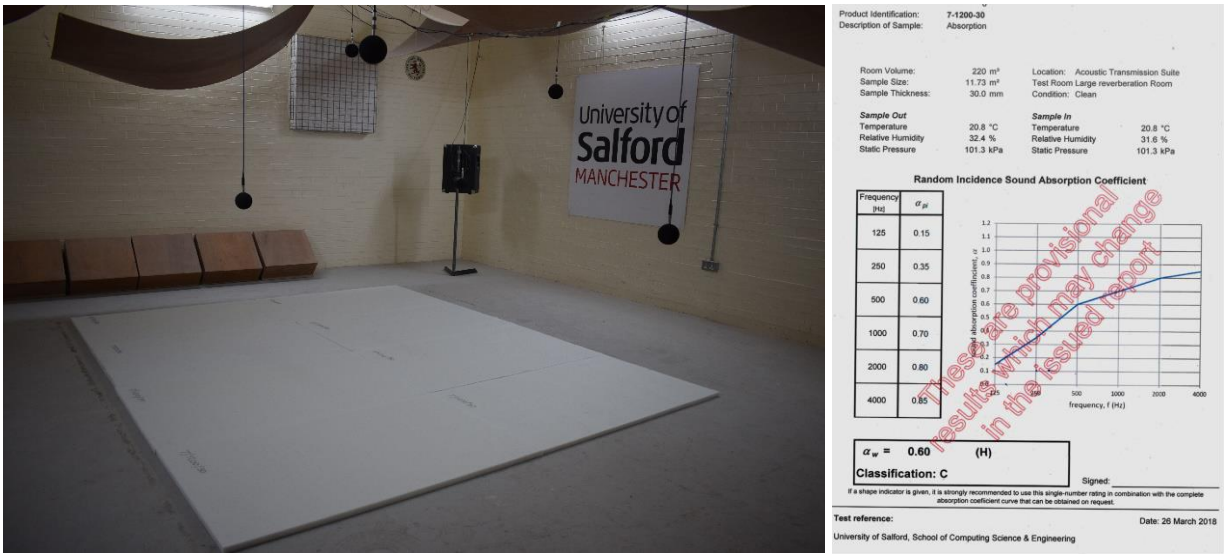

Figure 3.11.: a) Reverberation room at University of Salford b) Standard performance report format.

For a sample studied in this research, the sound absorption characteristics obtained from the reverberation room has been compared with the standard 2- and 4- mic impedance tube methods. The data shown in Figure 3.12 suggests that as the sound field encountered by the sample material is diffused in the case of a reverberation room, the low frequency performance is higher than that obtained from the impedance tubes. Both the impedance tubes show comparable trends.

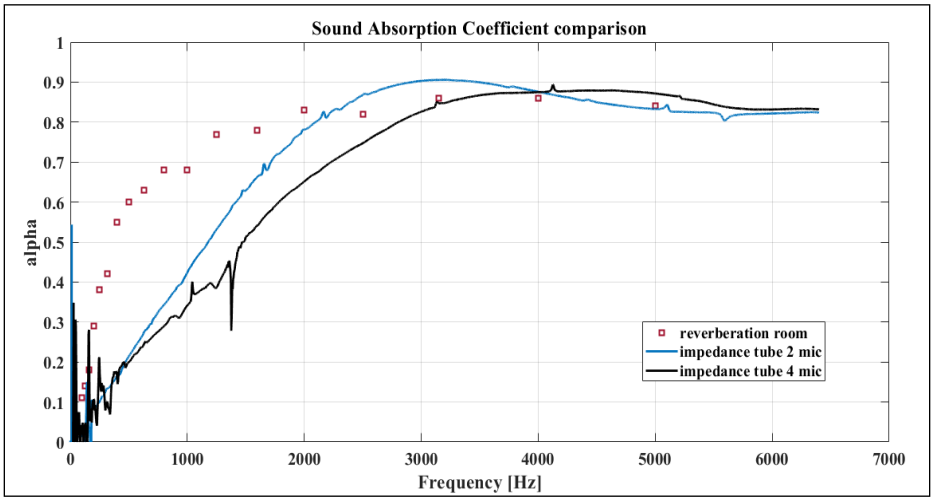

Figure 3.12.: Sound absorption data comparison between reverberation room and impedance tubes.

Chapter 4

THEORETICAL MODEL DERIVATIONS

Overview:

4.1. General wave equations for fibrous absorbers
4.2. Static case for single fibre

As discussed in the literature review, the steps to model the sound wave interaction with a single fibre were derived using the first principles. This chapter is divided into two sections. The first part derives the general wave equations for a viscous incompressible fluid in cylindrical coordinates. This dynamic problem can be solved only up to a stage where general solutions for velocity and pressure are obtained. The next section covers the static version of these cylindrical equation forms that simplify the problem and attempts to solve by applying appropriate boundary conditions. In this part a concentric single fibre in a unit cell is considered. The expression for the static flow resistivity is derived for this case.

4.1.GENERAL WAVE EQUATIONS FOR FIBROUS ABSORBERS

The case of a representative single fibre enveloped by a cylindrical fluid domain, is resolved in cylindrical coordinate system. The geometry of this problem is illustrated in Figure 4.1. The solid cylinder represents an infinitely long fibre while the concentric dotted line cylinder represents the fluid domain. An external pressure gradient applied on the system of fibre and fluid is shown by the arrow to the left of the system.

As per this figure, this gradient is externally applied and has the potential to influence at an angle. Thus, for representing the directions better, cartesian coordinates have been selected to depict the pressure gradient.

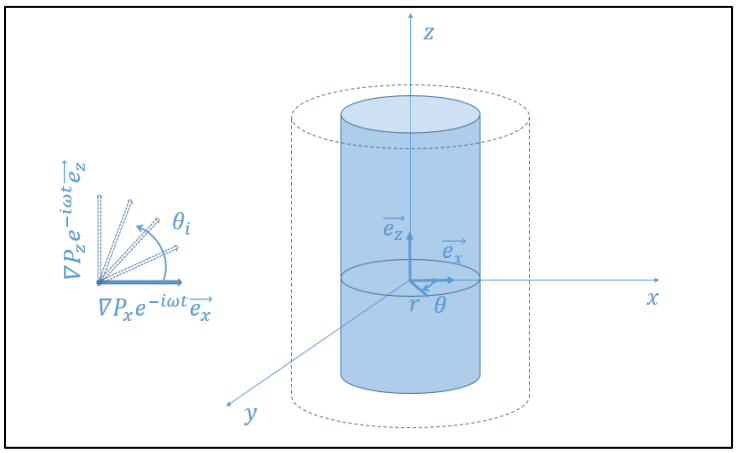

Figure 4.1.: Shows representative single fibre enveloped by a cylindrical fluid domain, adapted from [49].

For such a system, Umnova *et. al.* [49] have discussed the analytical formulation of equation of wave motion for a single fibre under the influence of a parallel and perpendicular pressure gradient. Owing to the symmetric nature of the problem, this derivation was attempted in cylindrical coordinate system. The single fibre system was then impinged with an oblique pressure gradient. The oblique orientation of pressure gradient is a general case suggesting the random orientation, typically observed in nonwoven fibres.

As expressed earlier, a time dependence of $e^{-i\omega t}$ is assumed for the derivation and used throughout this thesis. Under the influence of an oblique oscillatory pressure gradient $\nabla P(x,z)\ e^{-i\omega t}\overrightarrow{e(x,z)}$, the motion of fluid around an infinitely long cylinder of radius R_1, is governed by the set of equations as derived in the cylindrical coordinate system [96]:

Dynamic Navier-Stokes Equation (within the volume of the fluid)

The three components of Navier-Stokes equation under the impact of external pressure gradient:

$$-i\omega\rho_0 u_r = -\partial_r p + \eta(\Delta u_r) - (\nabla P)_r \tag{4.1a}$$

$$-i\omega\rho_0 u_\theta = -\frac{1}{r}\partial_\theta p + \eta(\Delta u_\theta) - (\nabla P)_\theta \tag{4.1b}$$

$$-i\omega\rho_0 u_z = -\partial_z p + \eta(\Delta u_z) - (\nabla P)_z \tag{4.1c}$$

where,

$$\Delta\vec{u} = \frac{1}{r}\partial_r(r\partial_r u) + \frac{1}{r}\partial_{\theta\theta} u + \partial_{zz} u \tag{4.1d}$$

while,

$$(\nabla P)_r = (\nabla P)_x \, cos\theta \tag{4.2a}$$

$$(\nabla P)_\theta = -(\nabla P)_x \, sin\theta \tag{4.2b}$$

$$(\nabla P)_z = (\nabla P)_z \tag{4.2c}$$

Continuity Equation (within the volume of the fluid)

$$\left(\frac{1}{r}\partial_r(r\, u_r) + \frac{1}{r}\partial_\theta u_\theta + \partial_z u_z\right) = 0 \tag{4.3}$$

Boundary Conditions (over the interface)

On the cylinder, $r = R_1$

$$u_r(r, \theta, z) = 0 \tag{4.4a}$$

$$u_\theta(r, \theta, z) = 0 \tag{4.4b}$$

$$u_z(r, \theta, z) = 0 \tag{4.4c}$$

Where p and $\overrightarrow{u(r,\theta,z)}$ are the pressure and velocity, respectively of the fluid surrounding the fibre while $\nabla P(r,\theta,z)$ is externally applied oblique oscillatory pressure gradient on single fibre system.

Based on HPM, incompressibility can be assumed for the fluid at the microscopic scale. Thus, $\overrightarrow{u(r,\theta,z)} = \overrightarrow{v(r,\theta,z)} + curl\vec{A}$. Here $\vec{A}$, acts as the velocity potential.

In cylindrical coordinates, the velocity corresponding to the oblique oscillatory pressure gradient $\overrightarrow{v(r,\theta,z)} = v(r,\theta,z)e^{-i\omega t}\overrightarrow{e(r,\theta,z)}\ and,\ v(r,\theta,z) = \frac{1}{i\omega\rho_0}\left(\nabla P_{r,\theta,z}\right)$.

In the following it is considered that the pressure gradient is applied in the direction perpendicular to the fibre, so v does not have $z-$component and does not vary along z.This implies that when considering in r and θ coordinates separately, $i\omega\rho_0\ v\ cos\theta = (\nabla P)_r$ and $i\omega\rho_0\ v\ sin\theta = (\nabla P)_\theta$ The vector potential has only A_z component with both $A_r = A_\theta = 0$. The velocity components are $u_r = v\ cos\theta + \left(\frac{1}{r}\right)(\partial_\theta A_z)$ and $u_\theta = -v\ sin\theta - (\partial_r A_z)$.

Here A_z is a function of (r,θ) so let $A_z = A(r,\theta) = A$.

The velocities can be rewritten as

$$u_r = v\ cos\theta + \left(\frac{1}{r}\right)\partial_\theta A \tag{4.5a}$$

$$u_\theta = -v\ sin\theta - \partial_r A \tag{4.5b}$$

Vorticity of velocity $\vec{u}$ can be calculated as the curl of the vector. This is needed, because a zero-velocity vorticity boundary condition is applied at the outer boundary of the elementary cell [49]. In cylindrical coordinate system

$$curl\ \vec{u} = \left(\frac{u_\theta}{r} + \partial_r u_\theta - \frac{1}{r}\partial_\theta u_r\right)\overrightarrow{e_z} \tag{4.6}$$

Substituting u_r and u_θ in equation (4.6),

$$curl\ \vec{u} = -\left[\frac{1}{r}\partial_r A + \partial_{rr}A + \frac{1}{r^2}\partial_{\theta\theta}A\right]\overrightarrow{e_z} \tag{4.7}$$

Introducing $f(r,\theta)$ as a function equating to terms in bracket for $curl\ \vec{u}$,

$$f(r,\theta) = \left[\frac{1}{r}\partial_r A + \partial_{rr}A + \frac{1}{r^2}\partial_{\theta\theta}A\right] = \frac{1}{r^2}[r\ \partial_r A + r^2\ \partial_{rr}A + \partial_{\theta\theta}A] \tag{4.8}$$

Then $curl\ \vec{u} = -f(r,\theta)\overrightarrow{e_z}$.

For incompressible fluid, the following identity is valid: $\Delta\vec{u} = -curl\ curl\ \vec{u}$

Which implies $\Delta\vec{u} = -curl\ (-f(r,\theta)\overrightarrow{e_z}) = curl\ (f(r,\theta)\overrightarrow{e_z})$

Thus, $\Delta\vec{u} = curl\ (f(r,\theta)\overrightarrow{e_z}) = \begin{vmatrix} \frac{e_r}{r} & e_\theta & \frac{e_z}{r} \\ \partial_r & \partial_\theta & \partial_z \\ 0 & 0 & f(r,\theta) \end{vmatrix}$ and

$$\Delta\vec{u} = \left(\frac{1}{r}\partial_\theta f(r,\theta)\right)e_r - \big(\partial_r f(r,\theta)\big)e_\theta \tag{4.9}$$

The Dynamic Navier-Stokes Equations (4.1 a,b), can be rewritten in terms of two velocity components by substituting the equations for u_r, u_θ, $\Delta\overrightarrow{u_r}$ and $\Delta\overrightarrow{u_\theta}$, as follows:

$$-i\omega\rho_0\big(r^2\ v\ cos\theta + r\ (\partial_\theta A)\big) = -r^2\partial_r p + \eta\ r(\partial_\theta f) - r^2(\nabla P)_r$$

$$-i\omega\rho_0 r^2(-v\ sin\theta - \partial_r A) = -r\ \partial_\theta p - \eta\ r^2(\partial_r f) - r^2(\nabla P)_\theta$$

This could be simplified further,

$$-i\omega\rho_0\ r\ \partial_\theta A = -r^2\partial_r p + \eta\ r\ (\partial_\theta f) \tag{4.10a}$$

$$+i\omega\rho_0 r^2\partial_r A = -r\ \partial_\theta p - \eta\ r^2(\partial_r f) \tag{4.10b}$$

Processing equation (4.10 a,b) and differentiating them finally gives,

$$-i\omega\rho_0 \frac{1}{r}\partial_{\theta\theta}A = -\partial_{r\theta}p + \eta\frac{1}{r}(\partial_{\theta\theta}f) \tag{4.11a}$$

$$+i\omega\rho_0\partial_r(r\partial_r A) = -\partial_{\theta r}p - \eta\partial_r(r\partial_r f) \tag{4.11b}$$

Subtracting the equations (4.11a) and (4.11b),

$$-i\omega\rho_0\left(\frac{1}{r}\partial_{\theta\theta}A + \partial_r(r\partial_r A)\right) = \eta\left(\frac{1}{r}(\partial_{\theta\theta}f) + \partial_r(r\partial_r f)\right) \tag{4.12}$$

On expanding the equation (4.12),

$$-\frac{i\omega\rho_0}{r}(\partial_{\theta\theta}A + r\partial_r A + r^2\partial_{rr}A) = \eta\left(\frac{1}{r}\partial_{\theta\theta}f + r\partial_{rr}f + \partial_r f\right) \tag{4.13}$$

From equations (4.8) and (4.13), $\partial_{\theta\theta}A + r\partial_r A + r^2\partial_{rr}A = r^2 f$

This, finally, leads to a single equation for f

$$\therefore\ -i\omega\rho_0 rf = \eta\left(\frac{1}{r}\partial_{\theta\theta}f + r\partial_{rr}f + \partial_r f\right) \tag{4.14}$$

On rearranging,

$$\therefore\ -\frac{i\omega\rho_0}{\eta}rf = \frac{1}{r}\partial_{\theta\theta}f + r\partial_{rr}f + \partial_r f \tag{4.15}$$

Applying $\frac{i\omega\rho_0 R_1^2}{\eta} = k^2$ gives $k^2 rf + \frac{1}{r}\partial_{\theta\theta}f + r\partial_{rr}f + \partial_r f = 0$

On further rearranging the terms,

$$k^2 f + \frac{1}{r^2}\partial_{\theta\theta}f + \partial_{rr}f + \frac{1}{r}\partial_r f = 0 \tag{4.16}$$

If $y = kr$ then

$$\partial_r f = k\, \partial_y f \tag{4.17a}$$

$$\partial_{rr} f = k^2\, \partial_{yy} f \tag{4.17b}$$

This implies,

$$f + \frac{1}{y^2}\partial_{\theta\theta} f + \partial_{yy} f + \frac{1}{y}\partial_y f = 0 \tag{4.18}$$

If $f = \Sigma f_n e^{in\theta}$,

$$y^2 \partial_{yy} f_n + y\partial_y f_n + (y^2 - n^2) f_n = 0 \tag{4.19}$$

Equation (4.19) is a standard Bessel differential equation of order n [106]. The general solution of this equation is expressed as a linear combination of two independent Bessel functions of order n:

$$f_n = C_{1n} J_n(y) + C_{2n} H_n(y) \tag{4.20}$$

Where $C_{1,2n} = const$. Here a linear combination of Bessel function of the first kind J_n and Hankel function H_n has been chosen, although other combinations such as J_n and Y_n are also possible. Thus, f is now expressed as a Fourier series

$$f = \sum_{n=-\infty}^{n=+\infty} [C_{1n} J_n(kr) + C_{2n} H_n(kr)] e^{in\theta} \tag{4.21}$$

According to equations (4.5), velocity components are expressed in terms of potential function A. So, the next step is to derive solution for A using (4.21).

Writing in terms of A, from equation (4.8),

$$\frac{1}{r}\partial_r A + \partial_{rr} A + \frac{1}{r^2}\partial_{\theta\theta} A = \sum_{n=-\infty}^{n=+\infty} [C_{1n} J_n(kr) + C_{2n} H_n(kr)] e^{in\theta} \tag{4.22}$$

Expanding A in Fourier series, $A = \Sigma A_n e^{in\theta}$ and using orthogonality conditions,

$$r^2 \partial_{rr} A_n + r\, \partial_r A_n - n^2 A_n = r^2 \left(C_{1n} J_n(kr) + C_{2n} H_n(kr) \right) \tag{4.23}$$

Rewriting this equation in terms of previously introduced $y = kr$, this can be rewritten as

$$\left(\frac{y}{k}\right)^2 k^2\, \partial_{yy} A_n + \left(\frac{y}{k}\right) k\, \partial_y A_n - n^2 A_n = \left(\frac{y}{k}\right)^2 \left(C_{1n} J_n(y) + C_{2n} H_n(y) \right) \tag{4.24}$$

From equations (4.20) and (4.24),

$$y^2\, \partial_{yy} A_n + y\, \partial_y A_n - n^2 A_n = \left(\frac{y}{k}\right)^2 f_n \tag{4.25}$$

Dividing equation (4.19) by k^2 and replacing the RHS of equation (4.25),

$$\left(\frac{y}{k}\right)^2 \partial_{yy} f_n + \frac{y}{k^2} \partial_y f_n + \left(\frac{y}{k}\right)^2 f_n - \left(\frac{n}{k}\right)^2 f_n = 0$$

$$\therefore \left(\frac{y}{k}\right)^2 f_n = \left(\frac{n}{k}\right)^2 f_n - \frac{y}{k^2} \partial_y f_n - \left(\frac{y}{k}\right)^2 \partial_{yy} f_n$$

$$\therefore y^2\, \partial_{yy} A_n + y\, \partial_y A_n - n^2 A_n = \left(\frac{n}{k}\right)^2 f_n - \frac{y}{k^2} \partial_y f_n - \left(\frac{y}{k}\right)^2 \partial_{yy} f_n$$

Multiplying throughout by k^2 and gathering like terms,

$$y^2 (k^2+1) \partial_{yy} (k^2 A_n + f_n) + y(k^2+1) \partial_y (k^2 A_n + f_n) - \left(n^2 (k^2+1)(k^2 A_n + f_n) \right) = 0 \tag{4.26}$$

Letting $k^2 A_n + f_n = Z_n$, then equation (4.26) becomes

$$y^2 \partial_{yy} Z_n + y \partial_y Z_n - n^2 Z_n = 0 \tag{4.27}$$

Or it can be rearranged as

$$\partial_{yy}Z_n + \frac{1}{y}\partial_y Z_n - \left(\frac{n}{y}\right)^2 Z_n = 0 \tag{4.28}$$

This second order Ordinary Differential Equation [107] is known as Euler equation. The generic form of such equations can be expressed as:

$$y''_{xx} + \frac{a}{x}y'_x + \frac{b}{x^2}y = 0 \tag{4.29}$$

Comparing between equations (4.28) and (4.29),

$$y = x, Z_n = y, a = 1, b = -n^2 \tag{4.30}$$

Its exact solution (Kamke 1977, Polyanin and Zaitsev, 2003) [108]:

$$y = \begin{cases} |x|^{\frac{1-a}{2}}(C_1|x|^{\mu} + C_2|x|^{-\mu}) & if\ (1-a)^2 > 4b, \\ |x|^{\frac{1-a}{2}}(C_1 + C_2\ln|x|) & if\ (1-a)^2 = 4b, \\ |x|^{\frac{1-a}{2}}(C_1\sin(\mu\ln|x|) + C_2\cos(\mu\, ln|x|)) & if\ (1-a)^2 < 4b, \end{cases} \tag{4.31}$$

where $\mu = \frac{1}{2}|(1-a)^2 - 4b|^{\frac{1}{2}}$; C_1 and C_2 are arbitrary constants.

Calculating μ using relations from equation (4.30),

$$\mu = \frac{1}{2}|(1-1)^2 - 4(-n^2)|^{\frac{1}{2}} = \frac{1}{2}|(2n)^2|^{\frac{1}{2}} = +n \tag{4.32}$$

Also, for the condition for the solution,

$$(1-a)^2 = 0 \text{ and } 4b = -(2n)^2 \tag{4.33}$$

implies that $0 > -(2n)^2$ and first solution form from (4.31) is valid.

Also let $C_1 = D_1$and $C_2 = D_2$ to avoid confusion from previous coefficients.

Thus, from equation (4.31) the selected solution for the Euler equations (4.27) or (4.28) is,

$$y = |x|^{\frac{1-a}{2}}(D_1|x|^{\mu} + D_2|x|^{-\mu}) \tag{4.34}$$

Writing in the original variables from equation (4.30) and (4.32),

$$Z_n = (D_{1n}|y|^n + D_{2n}|y|^{-n}) \tag{4.35}$$

Equation (4.35) can also be expressed using conditions before equations (4.24) and (4.27),

$$k^2 A_n + f_n = Z_n = (D_{1n}(kr)^n + D_{2n}(kr)^{-n}) \tag{4.36}$$

Here the modulus for kr can be eliminated even if k is a complex term as the negative sign can be incorporated within the coefficients D before them.

On rearranging equation (4.36) and using equation (4.20) and (4.24),

$$A_n = \frac{1}{k^2}\{[D_{1n}(kr)^n + D_{2n}(kr)^{-n}] - [C_{1n}J_n(kr) + C_{2n}H_n(kr)]\} \tag{4.37}$$

Or equation (4.37) can also be written as,

$$A = \sum_{n=-\infty}^{n=+\infty} \frac{1}{k^2}\{[D_{1n}(kr)^n + D_{2n}(kr)^{-n}] - [C_{1n}J_n(kr) + C_{2n}H_n(kr)]\}\, e^{in\theta} \tag{4.38}$$

Solutions for the velocity components u_r and u_θ, can be obtained from equations (4.5a) and (4.5b),

$$u_r = v\,cos\theta + \left(\frac{1}{r}\right)\partial_\theta \sum_{n=-\infty}^{n=+\infty} \frac{1}{k^2}\{[(D_{1n}(kr)^n + D_{2n}(kr)^{-n})] - [C_{1n}J_n(kr) + C_{2n}H_n(kr)]\}\, e^{in\theta} \tag{4.39a}$$

$$u_\theta = -v\sin\theta - \partial_r \sum_{n=-\infty}^{n=+\infty} \frac{1}{k^2}\{[D_{1n}(kr)^n + D_{2n}(kr)^{-n}] - [C_{1n}J_n(kr) + C_{2n}H_n(kr)]\}\, e^{in\theta} \tag{4.39b}$$

On solving and consuming the negative sign into the coefficients $C_{1,2n}$,

$$u_r = v\cos\theta + \left(\frac{i}{r}\right)\sum_{n=-\infty}^{n=+\infty}\frac{n}{k^2}\{[(D_{1n}(kr)^n + D_{2n}(kr)^{-n})] + [C_{1n}J_n(kr) + C_{2n}H_n(kr)]\}\,e^{in\theta} \tag{4.40a}$$

$$u_\theta = -v\sin\theta - \sum_{n=-\infty}^{n=+\infty}\frac{1}{k}\left[n(D_{1n}(kr)^n - D_{2n}(kr)^{-n}) + \left(C_{1n}J_n'(kr) + C_{2n}H_n'(kr)\right)\right]e^{in\theta} \tag{4.40b}$$

Additional simplification for u_θ following the equation (4.40b),

$$u_\theta = -v\sin\theta - \sum_{n=-\infty}^{n=+\infty}\frac{1}{k}\left[\frac{n}{kr}(D_{1n}(kr)^n - D_{2n}(kr)^{-n}) + \left(C_{1n}J_n'(kr) + C_{2n}H_n'(kr)\right)\right]e^{in\theta} \tag{4.41}$$

The next step is obtaining general solution for pressure p from equations (4.10).

Let $p = \Sigma p_n e^{in\theta}$ and by using rearranged equation (4.10b),

$$p_n = \frac{i\ r\ \eta}{n\ R_1}[k^2(\partial_r A_n) + (\partial_r f_n)] \tag{4.42}$$

Now using solutions for f and A given by equations (4.20) and (4.38),

$$p_n = \frac{i\ r\ \eta}{n\ R_1}\left[k^2\left(\partial_r\frac{1}{k^2}\{[D_{1n}(kr)^n + D_{2n}(kr)^{-n}] - [C_{1n}J_n(kr) + C_{2n}H_n(kr)]\}\right) + (\partial_r[C_{1n}J_n(kr) + C_{2n}H_n(kr)])\right] \tag{4.43}$$

On expanding and simplifying

$$p_n = \frac{i\,\eta}{R_1}[D_{1n}(kr)^n - D_{2n}(kr)^{-n}] \tag{4.44}$$

While the general solution for pressure p is defined by the following equation.

$$p = \sum_{n=-\infty}^{n=+\infty} \frac{i\,\eta}{R_1}[D_{1n}(kr)^n - D_{2n}(kr)^{-n}]e^{in\theta} \tag{4.45}$$

To summarise, general solutions of the equations of motion for two velocity components and pressure as given by equations (4.40a), (4.41) and (4.45).

The constant k can be accommodated within the coefficients (e.g. $D_{1n}\ for\ \frac{D_{1n}}{k}$) and the final expressions for the velocity components and pressure term are as per equations (4.46 a, b and c):

$$u_r = v\cos\theta + i\sum_{n=-\infty}^{n=+\infty}\Big\{n\big[D_{1n}(kr)^{n-1} + D_{2n}(kr)^{-(n+1)}\big] + \frac{n}{kr}[C_{1n}J_n(kr) + C_{2n}H_n(kr)]\Big\}e^{in\theta} \tag{4.46a}$$

$$u_\theta = -v\sin\theta - \sum_{n=-\infty}^{n=+\infty}\big[n\big(D_{1n}(kr)^{n-1} - D_{2n}(kr)^{-(n+1)}\big) + \big(C_{1n}J_n'(kr) + C_{2n}H_n'(kr)\big)\big]e^{in\theta} \tag{4.46b}$$

$$p = \frac{i\,\eta k}{R_1}\sum_{n=-\infty}^{n=+\infty}[D_{1n}(kr)^n - D_{2n}(kr)^{-n}]e^{in\theta} \tag{4.46c}$$

As velocity vorticity is required for further application of the boundary conditions, the solution for it is also derived using equation (4.47):

$$curl(\vec{u}) = k\sum_{n=-\infty}^{n=+\infty}\big(C_{1n}J_n(kr) + C_{2n}H_n(kr)\big)e^{in\theta} \tag{4.47}$$

Solutions derived in this part are more general than those given in [49], where only the first terms in the full Fourier series were considered. This was due to the axial symmetry of a unit cell with a centrally positioned cylindrical fibre, as considered in [49]. Solving beyond this stage in the dynamic form shall need computational intervention. To approach this problem in a simplified format, calls for deriving in the static (or stationary) state, $\omega = 0$. Similar work has been carried out by works of Boutin [75] as established in the literature review section.

4.2. STATIC CASE (SINGLE FIBRE IN THE UNIT CELL)

In line with the derivation steps followed for the dynamic case above, a static version of the derivation for a single cylinder case in the cylindrical coordinate system is elaborated (with some modifications) as under.

1. **Steady state solution for incompressible fluid motion under constant pressure gradient ∇P_i**

Assuming from the start that r is normalised to fibre radius R_0, the governing equations are (compare with equations (4.1) and (4.3))

$$-\frac{1}{R_0}\partial_r p + \frac{\eta}{R_0^2}(\Delta u)_r - \nabla P\cos\theta = 0, \tag{4.48}$$

$$-\frac{1}{rR_0}\partial_\theta p + \frac{\eta}{R_0^2}(\Delta u)_\theta + \nabla P\sin\theta = 0, \tag{4.49}$$

$$\frac{1}{r}\partial_r(r\,u_r) + \frac{1}{r}\partial_\theta u_\theta = 0, \tag{4.50}$$

Due to equation (4.50), $\vec{u} = \nabla \times \vec{A}$ then

$$\nabla \times \vec{u} = \nabla \times \nabla \times \vec{A} = \left(-\frac{1}{r}\partial_r A - \partial_{rr}A - \frac{1}{r^2}\partial_{\theta\theta}A\right)k = f(r,\theta) \tag{4.51}$$

And $(\Delta u)_r = -\frac{1}{r}\partial_\theta f$, $(\Delta u)_\theta = \partial_r f$.

This allows reformulations of equations (4.48) and (4.49) as

$$-\frac{1}{R_0}\partial_r p - \frac{\eta}{R_0^2 r}\partial_\theta f - \nabla P\cos\theta = 0, \tag{4.52}$$

$$-\frac{1}{R_0}\partial_\theta p + \frac{\eta r}{R_0^2}\partial_r f + r\nabla P\sin\theta = 0, \tag{4.53}$$

Eliminating p, a single equation for f can be written down.

$$\partial_{rr} f + \frac{1}{r}\partial_r f + \frac{1}{r^2}\partial_{\theta\theta} f = 0, \tag{4.54}$$

This equation is the same as (4.16), but with $k = 0$ which corresponds to $\omega = 0$. The solution is sought in the form of Fourier series $f = \Sigma_n a_n(r) e^{in\theta}$, where $a_n(r)$ satisfies.

$$a_n'' + \frac{1}{r} a_n' - \frac{n^2}{r^2} a_n = 0 \tag{4.55}$$

With solutions

$$\begin{aligned} a_n &= \alpha_n r^n + \beta_n r^{-n}, if\ n \neq 0 \\ a_n &= \alpha_0 \ln r + \beta_0, if\ n = 0 \end{aligned} \tag{4.56}$$

And the corresponding solution for f is,

$$f = \alpha_0 \ln r + \beta_0 + \Sigma_{n\neq 0}(\alpha_n r^n + \beta_n r^{-n}) e^{in\theta} \tag{4.57}$$

According to (4.51), this results in the following equation for A

$$-\frac{1}{r}\partial_r A - \partial_{rr} A - \frac{1}{r^2}\partial_{\theta\theta} A = \alpha_0 \ln r + \beta_0 + \Sigma_{n\neq 0}(\alpha_n r^n + \beta_n r^{-n}) e^{in\theta} \tag{4.58}$$

Again, the solution is sought in the form of a Fourier series $A = \Sigma b_n e^{in\theta}$, where due to orthogonality equations for coefficients are,

$$-b_0'' - \frac{1}{r} b_0' = \alpha_0 \ln r + \beta_0 \tag{4.59}$$

$$-b_n'' - \frac{1}{r} b_n' + \frac{n^2}{r^2} b_n = \alpha_n r^n + \beta_n r^{-n} \tag{4.60}$$

Solution of (4.60) is,

$$b_0 = -\frac{\alpha_0}{4} r^2 \ln r + \frac{\alpha_0 - \beta_0}{4} r^2 + C \ln r + D \tag{4.61}$$

Equation (4.61) is inhomogeneous Cauchy – Euler equation [107], its general solution is the sum of the particular solution b_n^p and complimentary function b_n^c, $b_n = b_n^p + b_n^c$. The complimentary function is the general solution of homogeneous equation.

$$b_n^c = s_n r^n + q_n r^{-n} \tag{4.62}$$

Formula for the particular solution b_n^p [108] is,

$$b_n^p = -y_1 \int \frac{y_2(\alpha_n r^n + \beta_n r^{-n})}{W(y_1, y_2)} dr + y_2 \int \frac{y_1(\alpha_n r^n + \beta_n r^{-n})}{W(y_1, y_2)} dr \tag{4.63}$$

Where $y_1 = r^n$, $y_2 = r^{-n}$ and $W(y_1, y_2) = y_1 y_2' - y_2 y_1' = -\frac{2n}{r}$.

The end result is,

$$b_n^p = \frac{1}{2n}\left(-\alpha_n\left(\frac{r^{n+2}}{2} - r^{-n}\int r^{2n+1} dr\right) + \beta_n\left(\frac{r^{-n+2}}{2} - r^{n}\int r^{-2n+1} dr\right)\right) \tag{4.64}$$

Combining (4.61) and the sum of (4.62), (4.64), for A gives,

$$\begin{aligned} A = \Sigma b_n e^{in\theta} &= -\frac{\alpha_0}{4} r^2 \ln r + \frac{\alpha_0 - \beta_0}{4} r^2 + C \ln r + D \\ &+ \sum_{n\neq 0} (s_n r^n + q_n r^{-n}) e^{in\theta} \\ &+ \sum_{n\neq 0} \frac{1}{2n}\left(-\alpha_n\left(\frac{r^{n+2}}{2} - r^{-n}\int r^{2n+1} dr\right)\right. \\ &\left. + \beta_n\left(\frac{r^{-n+2}}{2} - r^{n}\int r^{-2n+1} dr\right)\right) e^{in\theta} \end{aligned} \tag{4.65}$$

As $\vec{u} = \nabla \times \vec{A}$, the components of velocity can be found.

Differentiation of (4.65) gives,

$$u_r = \frac{i}{r}\sum_{n\neq 0} n(s_n r^n + q_n r^{-n})e^{in\theta} + \sum_{n\neq 0}\frac{i}{2}\left(-\alpha_n\left(\frac{r^{n+1}}{2} - r^{-n-1}\int r^{2n+1}dr\right) + \beta_n\left(\frac{r^{-n+1}}{2} - r^{n-1}\int r^{-2n+1}dr\right)\right)e^{in\theta} \tag{4.66}$$

$$u_\theta = \frac{\alpha_0}{2} r\ln r + \frac{\alpha_0}{4} r - \frac{\alpha_0 - \beta_0}{2} r - \frac{C}{r} - \sum_{n\neq 0} n(s_n r^{n-1} - q_n r^{-n-1})e^{in\theta} + \sum_{n\neq 0}\frac{1}{2}\left(\alpha_n\left(\frac{r^{n+1}}{2} + r^{-n-1}\int r^{2n+1}dr\right) + \beta_n\left(\frac{r^{-n+1}}{2} + r^{n-1}\int r^{-2n+1}dr\right)\right)e^{in\theta} \tag{4.67}$$

Next is, to find pressure p, appearing in equations (4.52), (4.53) from the knowledge of f as given by equation (4.58). This gives equation for p as,

$$\partial_r(p + \nabla PrR_0\cos\theta) = -\frac{\eta}{R_0 r}\partial_\theta f = -\frac{i\eta}{R_0}\sum_{n\neq 0} n(\alpha_n r^{n-1} + \beta_n r^{-n-1})e^{in\theta} \tag{4.68}$$

And on solving equation (4.66) further gives,

$$p + \nabla PrR_0\cos\theta = -\frac{i\eta}{R_0}\sum_{n\neq 0}(\alpha_n r^n - \beta_n r^{-n})e^{in\theta} + S(\theta) \tag{4.69}$$

On the other hand

$$\partial_\theta(p + \nabla PrR_0\cos\theta) = \frac{\eta r}{R_0}\partial_r f = \frac{\eta}{R_0}(\alpha_0 + \sum_{n\neq 0} n(\alpha_n r^n - \beta_n r^{-n})e^{in\theta} \tag{4.70}$$

And thus, equation (4.70) becomes,

$$p + \nabla PrR_0\cos\theta = -\frac{i\eta}{R_0}\sum_{n\neq 0}(\alpha_n r^n - \beta_n r^{-n})e^{in\theta} + \frac{\eta\alpha_0}{R_0}\theta + B(r) \tag{4.71}$$

In cylindrical geometry, p should be periodic in θ,

consequently $\alpha_0 = 0$, $B(r) = 0$ and $S(\theta) = 0$.

So, finally

$$p = -\nabla P r R_0 \cos\theta - \frac{i\eta}{R_0}\sum_{n\neq 0}(\alpha_n\, r^n - \beta_n r^{-n})e^{in\theta} \tag{4.72}$$

Also $f = |\nabla \times u|$ is,

$$f = \beta_0 + \Sigma_{n\neq 0}(\alpha_n r^n + \beta_n r^{-n})e^{in\theta} \tag{4.73}$$

This completes the derivation of the general solutions of the equations of motion of incompressible fluid in cylindrical coordinates under the action of the stationary pressure gradient applied perpendicular to z axis.

2. Boundary conditions at the outer cell

In an empirical way, as in [49], it is assumed that $p(r) = 0$ and $f(r) = 0$ at $r = 1$. This means, that the characteristic distance R_0 introduced earlier is equal to the outer radius of the cell. This results in the following set of conditions for Fourier coefficients as expressed in equation (4.74).

$$\begin{aligned} \beta_0 &= 0, \\ \alpha_n + \beta_n &= 0, \\ -\frac{\nabla P R_0}{2} &= \frac{i\eta}{R}(\alpha_1 - \beta_1), \\ -\frac{\nabla P R_0}{2} &= \frac{i\eta}{R_0}(\alpha_{-1} - \beta_{-1}), \\ \alpha_n - \beta_n &= 0, for\ n \neq \pm 1. \end{aligned} \tag{4.74}$$

This implies that $\alpha_n = \beta_n = 0$ if $n \neq \pm 1$

and $\alpha_1 = \alpha_{-1} = \frac{i\nabla P R_0^2}{4\eta}$, $\beta_1 = \beta_{-1} = -\frac{i\nabla P R_0^2}{4\eta}$

Such that pressure p can be processed and represented as equation (4.75) below.

$$\begin{aligned} p = &-\nabla P r R_0 \cos\theta - \frac{i\eta}{R}\left(\frac{i\nabla P R_0^2}{4\eta} r + \frac{i\nabla P R_0^2}{4\eta}\frac{1}{r}\right) e^{i\theta} \\ &- \frac{i\eta}{R}\left(\frac{i\nabla P R_0^2}{4\eta} r + \frac{i\nabla P R_0^2}{4\eta}\frac{1}{r}\right) e^{-i\theta} \\ &= -\frac{1}{2}\nabla P r R_0 \cos\theta + \frac{1}{2}\nabla P R_0 \cos\theta \frac{1}{r} \end{aligned} \tag{4.75}$$

The expressions for u_r and u_θ thus need to be updated as equations (4.76) and equation (4.77).

$$\begin{aligned} u_r = &\frac{i}{r}\sum_{n\neq 0} n(s_n r^n + q_n r^{-n}) e^{in\theta} \\ &+ \frac{i}{2}\left(-\alpha_1\left(\frac{r^2}{2} - r^{-2}\int r^3 dr\right) - \alpha_1\left(\frac{1}{2} - \int r^{-1} dr\right)\right) e^{i\theta} \\ &+ \frac{i}{2}\left(-\alpha_1\left(\frac{1}{2} - \int r^{-1} dr\right) - \alpha_1\left(\frac{r^2}{2} - r^{-2}\int r^3 dr\right)\right) e^{-i\theta} \\ &= \frac{i}{r}\sum_{n\neq 0} n(s_n r^n + q_n r^{-n}) e^{in\theta} \\ &+ \frac{i}{2}\,(-\alpha_1)\left[\left(\frac{r^2}{2} - r^{-2}\int r^3 dr\right)\left(e^{i\theta} + e^{-i\theta}\right)\right. \\ &\left. + \left(\frac{1}{2} - \int r^{-1} dr\right)\left(e^{i\theta} + e^{-i\theta}\right)\right] \\ &= \frac{i}{r}\sum_{n\neq 0} n(s_n r^n + q_n r^{-n}) e^{in\theta} + i(-\alpha_1)\left(\frac{r^2}{4} + \frac{1}{2} - \ln r\right) \\ &= \frac{i}{r}\sum_{n\neq 0} n(s_n r^n + q_n r^{-n}) e^{in\theta} - i\frac{i\nabla P R^2}{4\eta}\cos\theta\left(\frac{r^2}{4} + \frac{1}{2} - \ln r\right) \end{aligned} \tag{4.76}$$

$$
\begin{aligned}
u_\theta = &-\frac{C}{r} - \sum_{n\neq 0} n(s_n r^{n-1} - q_n r^{-n-1}) e^{in\theta} \\
&+ \frac{1}{2}\left(\alpha_1\left(\frac{r^2}{2} + r^{-2}\int r^3 dr\right) - \alpha_1\left(\frac{1}{2} + \int r^{-1} dr\right)\right) e^{i\theta} \\
&+ \frac{1}{2}\left(\alpha_1\left(\frac{1}{2} + \int r^{-1} dr\right) - \alpha_1\left(\frac{r^2}{2} + r^{-2}\int r^3 dr\right)\right) e^{-i\theta} \\
&= -\frac{C}{r} - \sum_{n\neq 0} n(s_n r^{n-1} - q_n r^{-n-1}) e^{in\theta} \\
&+ \frac{\alpha_1}{2}\left[\left(\frac{r^2}{2} + r^{-2}\int r^3 dr\right)\left(e^{i\theta} - e^{-i\theta}\right) - \left(\frac{1}{2} + \int r^{-1} dr\right)\left(e^{i\theta} - e^{-i\theta}\right)\right] \\
&= -\frac{C}{r} - \sum_{n\neq 0} n(s_n r^{n-1} - q_n r^{-n-1}) e^{in\theta} + i\alpha_1 \sin\theta\left[\frac{3}{4}r^2 - \frac{1}{2} - \ln r\right] \\
&= -\frac{C}{r} - \sum_{n\neq 0} n(s_n r^{n-1} - q_n r^{-n-1}) e^{in\theta} - \frac{\nabla P R^2}{4\eta}\sin\theta\left[\frac{3}{4}r^2 - \frac{1}{2} - \ln r\right]
\end{aligned}
\tag{4.77}
$$

Results for the velocity components are,

$$
u_r = i\sum_{n\neq 0} n(s_n r^{n-1} + q_n r^{-n-1}) e^{in\theta} + \frac{\nabla P R^2}{4\eta}\cos\theta\left(\frac{r^2}{4} + \frac{1}{2} - \ln r\right), \tag{4.78}
$$

$$
u_\theta = -\frac{C}{r} - \sum_{n\neq 0} n(s_n r^{n-1} - q_n r^{-n-1}) e^{in\theta} - \frac{\nabla P R^2}{4\eta}\sin\theta\left[\frac{3}{4}r^2 - \frac{1}{2} - \ln r\right]. \tag{4.79}
$$

3. Boundary conditions at a single concentric particle and permeability results

If the particle is concentric with the outer cell, as in [49], then the cell averaged velocity in the direction of pressure gradient is,

$$< u_x > = \frac{1}{S} \iint_{S_f} (u_r \cos\theta - u_\theta \sin\theta) dA \tag{4.80}$$

where $S = \pi$ is normalised surface area of the unit cell

and the integration is performed over the portion of the cell filled with the fluid, s_f i.e.

$\iint_{S_f} dA = \int_0^{2\pi} \int_a^1 r dr\, d\theta$, where $a = \frac{R_1}{R_0} = \sqrt{1-\phi}$ and ϕ is porosity.

Integration over the angle will give,

$$\begin{aligned}
&\int_0^{2\pi} \Bigg[\Bigg(i \textstyle\sum_{n\neq 0} n(s_n r^{n-1} + q_n r^{-n-1}) e^{in\theta} \cos\theta + \frac{\nabla P R^2}{4\eta} \cos^2\theta \left(\frac{r^2}{4} + \frac{1}{2} - \ln r \right) + \\
&\textstyle\sum_{n\neq 0} n(s_n r^{n-1} - q_n r^{-n-1}) e^{in\theta} \sin\theta + \frac{\nabla P R^2}{4\eta} \sin^2\theta \left[\frac{3}{4} r^2 - \frac{1}{2} - \ln r \right] \Bigg] d\theta = \\
&i\pi \big((s_1 + q_1 r^{-2}) - (s_{-1} r^{-2} + q_{-1}) \big) + \pi \frac{\nabla P R^2}{4\eta} \left(\frac{r^2}{4} + \frac{1}{2} - \ln r \right) + i\pi (s_1 - q_1 r^{-2} + \\
&s_{-1}\, r^{-2} - q_{-1}) + \pi \frac{\nabla P R^2}{4\eta} \left(\frac{3}{4} r^2 - \frac{1}{2} - \ln r \right) \\
&= i\pi 2(s_1 - q_{-1}) + \pi \frac{\nabla P R^2}{4\eta} (r^2 - 2\ln r)
\end{aligned} \tag{4.81}$$

Then further integration gives,

$$\begin{aligned}
< u_x > &= 2i \int_a^1 (s_1 - q_{-1}) r dr + \frac{\nabla P R_0^2}{4\eta} \int_a^1 (r - r^3) dr \\
&= i(s_1 - q_{-1})(1 - a^2) + \frac{\nabla P R_0^2}{4\eta} \left(\frac{1 - a^4}{4} + a^2 \ln a + \frac{1 - a^2}{2} \right)
\end{aligned} \tag{4.82}$$

Boundary conditions $u_r(a) = u_\theta(a) = 0$ for velocity components on the surface of rigid fibre together with equations (4.78) and (4.79) result in

$$0 = i\sum_{n\neq 0} n(s_n a^{n-1} + q_n a^{-n-1})e^{in\theta} + \frac{\nabla P R_0^2}{4\eta}\cos\theta\left(\frac{a^2}{4} + \frac{1}{2} - \ln a\right), \tag{4.83}$$

$$0 = -\frac{C}{r} - \sum_{n\neq 0} n(s_n r^{n-1} - q_n r^{-n-1})e^{in\theta} - \frac{\nabla P R_0^2}{4\eta}\sin\theta\left[\frac{3}{4}r^2 - \frac{1}{2} - \ln r\right]. \tag{4.84}$$

From orthogonality conditions this gives,

$$(s_1 + q_1 a^{-2}) = -\frac{\nabla P R_0^2}{4\eta\, i2}\left(\frac{a^2}{4} + \frac{1}{2} - \ln a\right), \tag{4.85a}$$

$$(s_{-1}a^{-2} + q_{-1}) = \frac{\nabla P R_0^2}{4\eta i\, 2}\left(\frac{a^2}{4} + \frac{1}{2} - \ln a\right) \tag{4.85b}$$

$$(s_1 - q_1 a^{-2}) = -\frac{\nabla P R_0^2}{4\eta\, 2i}\left[\frac{3}{4}a^2 - \frac{1}{2} - \ln a\right]. \tag{4.85c}$$

$$(s_{-1}a^{-2} - q_{-1}) = -\frac{\nabla P R_0^2}{4\eta\, 2i}\left[\frac{3}{4}a^2 - \frac{1}{2} - \ln a\right] \tag{4.85d}$$

$$C = 0 \tag{4.85e}$$

And $s_n = q_n = 0$ if $n \neq 1$.

The equations (4.85) above give $q_{-1} = -s_1$, $s_{-1} = -q_1$,

as also, $(2s_1) = -\frac{\nabla P R^2}{4\eta\, i2}(a^2 - 2\ln a)$ and $(2q_1) = -\frac{\nabla P R^2}{4\eta\, i2}a^2\left(1 - \frac{a^2}{2}\right)$.

Then,

$$< u_x > = -\frac{\nabla P R_0^2}{16\eta}(-\phi^2 - 2\phi - 2\ln(1-\phi)) \tag{4.86}$$

This gives the following expression for static flow resistivity,

$$\sigma_x = -\frac{\nabla P}{< u_x >} = \frac{16\eta(1-\phi)}{a^2(-\phi^2 - 2\phi - 2\ln(1-\phi))} \tag{4.87}$$

This equation (4.87) coincides with the numerator of equation (46) in [49]. The term in the numerator corresponds to expression for the airflow resistivity for the perpendicular flow case derived assuming no slip boundary conditions at zero Knudsen number.

High frequency transport parameters, as shown in [49], are not affected by $Kn \neq 0$ so expressions, derived in that paper could be directly applied to the case of concentric cell considered here.

Namely, expression for high frequency tortuosity is,

$$\alpha_\infty = -\frac{\nabla P}{-i\omega\rho_0 < v_x >} = 1 + a^2 = 2 - \phi \tag{4.88}$$

And characteristic viscous length is given by the following equation.

$$\Lambda = \frac{\phi(2-\phi)}{2(1-\phi)} R_1 \tag{4.89}$$

Chapter 5

SINGLE FIBRE MODELS

Overview:

5.1. *Empirical models*

5.2. Theoretical approaches

5.3. Numerical studies

To understand the behaviour of nonwoven fibrous materials, various techniques have been suggested which have been explored in the literature review section. It has shown that overall properties of materials can be estimated by the knowledge of the non-acoustic properties of its component fibre(s). Equations were derived in the previous chapter while in this section, modelling techniques have been explored to understand sound propagation around a single fibre or its equivalent. The models elaborated in this section, shall focus on polyester-based nonwovens, and highlight the role of bico- material in a nonwoven mix by considering a single fibre case. Three approaches to modelling have been considered. The first part shall look at the empirical models that apply to fibrous materials in general and thermally bonded polyesters, in particular. Before considering the numerical modelling technique, the transitioning approach of analytical modelling has been covered as well.

Common to all modelling processes through this chapter, initially, it is considered that the fibre under examination is of the staple variety, which is also occasionally referred as the main fibre. Then a comparison is made by computing the parametric variations for an averaged case where the bico- has been considered proportionally. It is understood that the averaging will lead to a smaller radius of the fibre thereby changing the overall scope. The variations will be compared for their overall performance through various acoustic and non-acoustic properties of nonwovens.

The polyester sample materials used throughout this study compose of the following staple and bico- fibre types as detailed in Table 5.1 below.

Table 5.1.: Polyester sample properties

Fibre properties	**Units**	**Combinations**
Staple fibre radii	µm	12.50, 20.00
Bico- fibre radius	µm	10.20
Blend ratios (main : bico)	-	66:34, 75:25, 80:20
Sample thickness	Mm	10, 20, 30
Approximate bulk densities	kg/m^3	20, 40, 60

To calculate the effective single fibre radius, averaging technique is based on the weighted average of fibre blend. This has been calculated by using the SRSS (Square root of the Sum of Squares) statistical approach. Hence, for a case of bi-disperse fibrous material, the averaged fibre radius is,

$$r = \sqrt{X_1 r_1^2 + X_2 r_2^2} \tag{5.1}$$

where $r_{1,2}$ are radii of the two fibres and $X_{1,2}$ are the weighted average fractions of the blend.

Based on the general formula (5.1), the variation in radius values with blend ratios have been obtained as per Table 5.2.

Table 5.2.: Average radii calculations based on blend ratio

Blend ratio (Main : Bico)	**Average radius calculated**
50-50	$r = \sqrt{\frac{1}{2}r_1^2 + \frac{1}{2}r_2^2} = \frac{1}{\sqrt{2}}\sqrt{r_1^2 + r_2^2}$
75-25	$r = \sqrt{\frac{3}{4}r_1^2 + \frac{1}{4}r_2^2} = \frac{1}{2}\sqrt{3(r_1^2) + r_2^2}$
80-20	$r = \sqrt{\frac{4}{5}r_1^2 + \frac{1}{5}r_2^2} = \frac{1}{\sqrt{5}}\sqrt{4(r_1^2) + r_2^2}$

5.1. EMPIRICAL MODELS

As discussed previously in the literature review section, empirical models are developed because of the observations that are made during the group study of like materials. Due to which, these models are unique for characteristically similar materials. For instance, among porous materials, there shall be a particular equation obtained from fitting a group of polyurethane foams, which shall be slightly different for fibrous materials. Within fibrous materials, equation governing polyester may vary from a recycled nonwoven blend and quite interestingly, there would be variation in equating polyesters that were bonded thermally versus by mechanical needle-punching process. These models are used to obtain the airflow resistivity, which is the other most popularly known or utilised property of a porous material after porosity. The knowledge of bulk input parameters of a material as well as the constituents of the material is equally important. Such information can normally be obtained from the fabric manufacturer or during the product development phase where the components are being selected for blending at laboratory scale fabric preparation. In other cases, various other experimental techniques can be applied to arrive at the material's physical properties.

Several ways of simplifying the empirical expressions for nonwoven materials have been explored. The simple representation provided by Bies and Hansen [40] for glass wool, yields airflow resistivity values from the knowledge of bulk density and fibre diameter. The equation works with the provision of two constants that are specific to glass wool material that they base their equation on. New Resistivity Model (NMR) model [42] developed by Garai and Pompoli was an improvement to the Bies and Hansen model who derived the constants specifically with polyester material in mind. Inputs required for both these models include:

1. Fabric properties: Bulk density
2. Fibre properties: mean diameter, constants K1 and K2 (material specific)

As mentioned, Bies and Hansen calculated K1 and K2 for fibre glass while Garai and Pompoli adapted the approach for polyester material by least squares best-fitting values of calculated airflow resistivity on measured data. Bies and Hansen assumed that contribution of the binder material was insignificant. For devising the best fit values, both their formulae have assumed a mean diameter based on the choice of samples. Since Garai and Pompoli focused on polyester

materials specifically, they recalculated the mean diameter for the Bies and Hansen model (that was developed originally for fibre glass). The mean diameter that the model considers is an arithmetic average of the range of fibres being studied. Garai and Pompoli, for instance, were examining polyester fibres, that generally are coarser that fibre glass (typical range of 1 – 10 μm), having a range of 18 – 48 μm thus generating a mean of 33 μm. Although the polyester samples selected in their study specify the blending of bico- fibres, the lower end of the diameter range is probably inclusive of the binder material. On similar lines, Manning and Panneton [43] have proposed empirical regression equations for nonwovens based on their manufacturing approach. To suit the scope of study in this chapter, thermally bonded type of nonwoven polyester materials shall be correlated, hence the equation (5.2) for airflow resistivity, σ, is considered.

$$\sigma = \left(\frac{K_2}{d^2}\right)\rho_m^{K_1} \tag{5.2}$$

Table 5.3.: Summary of Empirical models

Method	**Material**	**K1**	**K2**
Bies and Hansen (BH) model	Glass wool	1.53	3.18×10^{-9}
Garai and Pompoli (NMR) model	Polyester	1.404	2.83×10^{-8}
Manning and Panneton (MP-Th) model	Thermally bonded polyester	1.516	1.94×10^{-8}

Utilising the constant values suggested by these empirical regression studies, airflow resistivity has been inspected for a selection of 9 samples comprising of the main and bico- fibres of diameters 25 – 20.4 μm blended at a constant ratio but with varying bulk densities. The plot shows airflow resistivity against the bulk densities to compare the variation of the pre-existing models with respect to the flow resistivity values of these samples obtained experimentally. The trends presented in Figure 5.1 show the difference between the staple fibre only case compared to the consideration of an averaged value. The cases for averaged fibre radii tend to show a higher airflow resistivity value in comparison to the corresponding staple or main fibre cases. Never-the-less, none of the three models considered present a true representation of the samples. This also implies that for the set of samples considered, a unique regression relation would need to be developed.

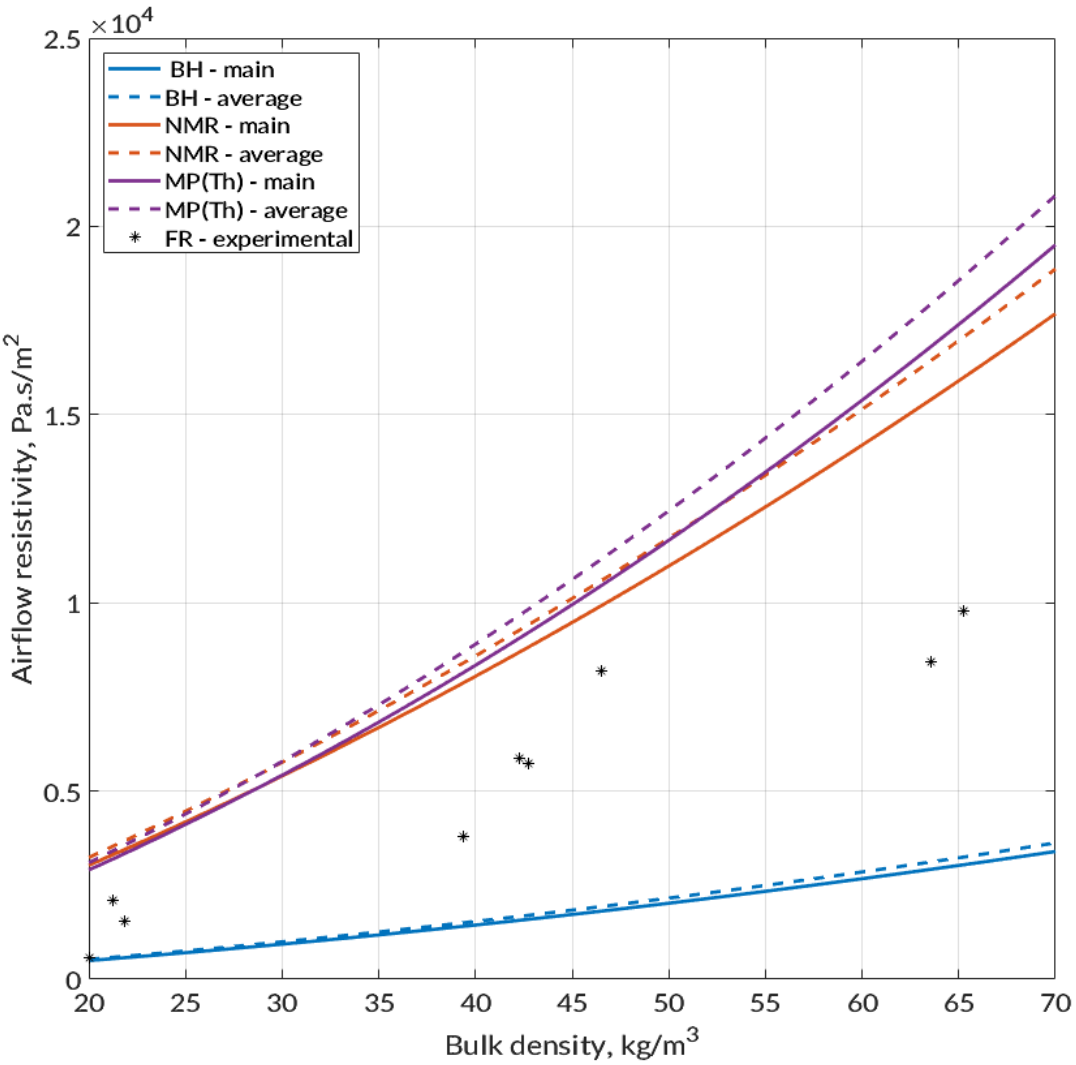

Figure 5.1.: Comparison of airflow resistivity at various bulk densities using basic empirical models

5.2. THEORETICAL APPROACHES

Progressing from experiential understanding, theoretical developments have systematically been examined to better represent the said polyester nonwovens. Deriving properties from the Poiseuille's equation for laminar flowing liquids, the Kozeny-Carman (KC) model [53] has been studied for air saturated porous media. Like the other referred capillary channel theory models, for evaluating the KC model, the following inputs are needed:

1. Fabric properties: volume and weight of the fabric pad/ batt
2. Fibre properties: density, mean fineness or diameter and fraction

From this material information and using dynamic density of air, bulk porosity is calculated using the density ratio of fibre to fabric content and the bulk density of the fabric. This porosity ultimately leads to the airflow resistivity value. This formula considers the presence of a mean fibre diameter in the case of two or more fibre components being present, like the above-mentioned models. An approximate model [57] as an alternative to the KC model has been included as a comparison. In the reference, the said approximation has been expressed for polyester materials and provides constants K1 and K2, linking back to the NMR [42] based empirical approach studied previously.

$$\sigma = \frac{180\mu(1-\phi)^2}{d^2\phi^3} \tag{5.3}$$

where, μ is the dynamic density of air, as obtained by the Poiseuille's equation is 1.81×10^{-5}, d is the main or equivalent fibre diameter and ϕ is the porosity of the material.

The KC equation (5.3) was initially developed for studying granular media but is also applicable to other porous materials such as fibrous materials.

The approximation of the KC equation to correlate with the empirical relations, can be expressed in terms of the constants as per equation (5.4).

$$\sigma \cong \frac{180\mu}{\rho_f^2}\left(\frac{\rho_m}{d_f}\right)^2 \cong A\rho_m^B \tag{5.4}$$

Such that, $A = \frac{K_2}{d_f^2}$, $K_2 = \frac{180\mu}{\rho_f^2}$ and $B = K_1 = 2$, giving the values in the Table 5.4 for the case of air saturated polyester nonwoven sample.

Table 5.4.: KC model summary

Method	**Material**	**K1**	**K2**
Approximated Kozeny-Carman (KC) model	Polyester	2	1.736×10^{-9}

The KC model and its approximate empirical model as explained above have been used to plot the airflow resistivity parameter for the 9 polyester samples shortlisted above. The trends for airflow resistivity versus bulk densities have been compared with experimental airflow resistivity values

that were obtained for the corresponding samples using the large 100 mm diameter tube-based airflow resistivity test rig, as described in section 3.3.2 of Chapter 3.

Figure 5.2. presents the two variations of the KC models, both for the main fibre only and the averaged fibre cases, comparing the airflow resistivity values over various bulk densities for the polyester samples. Unlike the empirical relations presented in Figure 5.1 previously, the KC and its approximate model shows good agreement with the samples around the low-density regions of 20 – 50 kg/m3. The trends show that the variation between the KC model, its empirical approximate and the experimentally obtained values is less at the lower bulk density values while it tends to deviate further with higher densities. In the higher region, the approximated KC values are closer to the experimental ones as compared to the trend deviation to experiments for the KC model. This could be reasoned as the approximation has been carried out specifically for the polyester materials, similar to the samples that were studied.

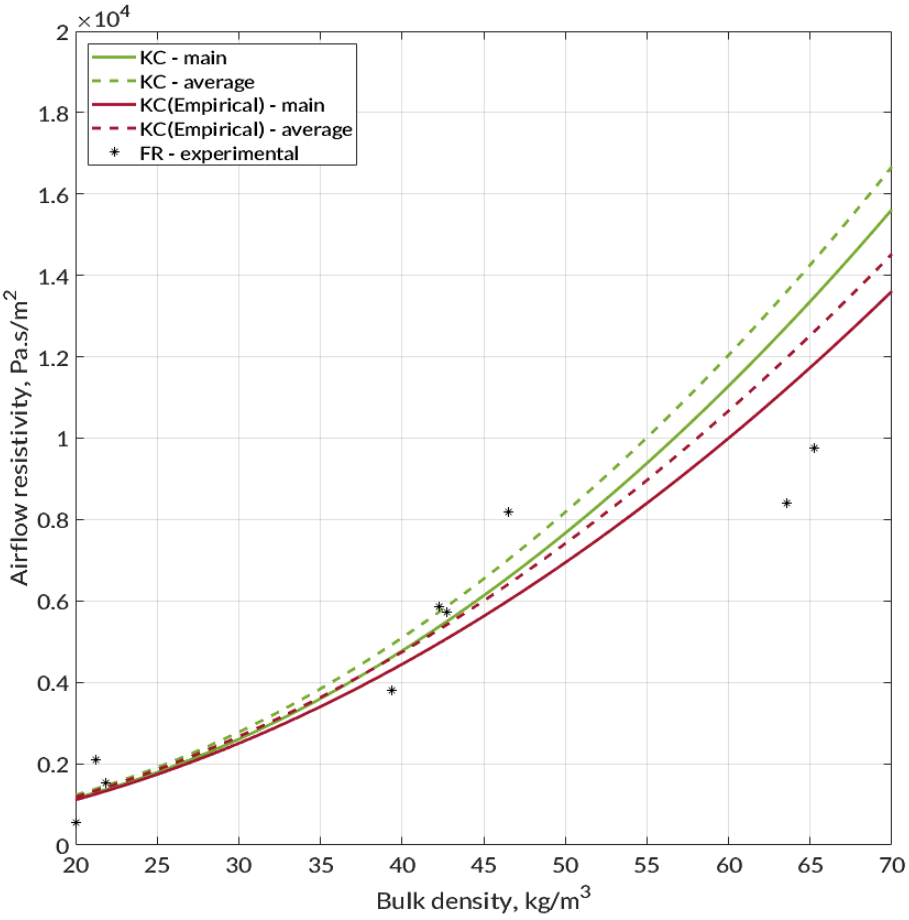

Figure 5.2.: Comparison of airflow resistivity using KC and its empirical approximate model

In the literature review section detailing theoretical models, two thought processes were introduced that formulate the empirical models. The KC model examined above correspond to the capillary channel theory while the other chain of thoughts emerges from the drag force theory. Both these varieties of models can be represented with the fibre and fabric input information as required by the KC model. The solid phase of the material is given emphasis here.

Studies that acknowledge the multi-fibre composition of nonwoven materials present airflow resistivity trends in different perspectives. In a prediction study [31], the focus has been on fibrous materials comprising of two fibres having varying radii. The airflow resistivity calculation presented in their work uses similar inputs but highlights on the fibre properties and the blend. Using the weighted ratio of fabric to fibre densities, they define the solidity, C for the two fibre components as per equation (5.5) below,

$$C = X_1 \frac{\rho_m}{\rho_{f1}} + X_2 \frac{\rho_m}{\rho_{f2}} \tag{5.5}$$

where, X_1 and X_2 are the weighted fractions of fibres constituting the blend such that $X_2 = 1 - X_1$.

As this parameter is a ratio of the bulk and fibre densities, it is also sometimes called as relative density in some reference studies (refer Table 2.4) which is probably obvious when the blending weighted fractions are not considered in the formula.

At this stage, defining this solidity parameter as per equation (5.6). which gives attention to the solid phase of the material, can be corelated directly to porosity. It is also used to define the mean spacing between fibres for circular cross-sectional fibres as per equation (5.7).

$$C = (1 - \phi) \tag{5.6}$$

$$C = \frac{n_{fib_1} \pi r_1^2 + n_{fib_2} \pi r_2^2}{b^2 \left(n_{fib_1} + n_{fib_2} \right)} \tag{5.7}$$

where, n_{fib} is the fibre count and b^2 is the mean spacing between fibres.

Note that solidity C can be correlated with the textile-based parameter ϵ, from in equation (2.2).

Airflow resistivity can also be calculated using dynamic viscosity of air constant in combination with the solidity and the mean spacing between fibres as defined above. Both single staple fibre based as well as dual fibre composition can be studied using such models [31]. In this research work consists of various model comparisons for parallel and perpendicular orientations as well. Most of the constituent fibre information can be directly obtained from the textile manufacturer. However, the fibre specifications are in textile parlance that need to be translated in the SI units for further calculation. A MATLAB code (see Appendix A) in this effect has been prepared that has been used for calculating the airflow resistivity values of nonwoven materials using the fibre textile data and can be used for fibres made up of other nonwovens besides polyesters as well. The code can be easily adapted to run with or without the consideration of the bico- fibre. This method is equally useful in understanding the significance of the bico- in a typical nonwoven mix.

Models proposed initially by Tarnow [58] have been considered to be the closest to represent the selected samples. Tarnow's models for the parallel and perpendicular flow conditions respectively, considering a random lattice of fibre cylinders is as expressed in equations (5.8 and 5.9),

$$\sigma_{\parallel} = \frac{4\eta C}{r^2[-0.640 \ln C + C - 0.737]} \tag{5.8}$$

$$\sigma_{\perp} = \frac{4\eta C}{r^2[-1.280 \ln C + 2C - 1.474]} \tag{5.9}$$

These formulae have been provided for a generic single uniform fibre composition. The solidity factor, C can be used to further introduce the multi-component nature of the nonwoven. Figure 5.3 shows a comparison between the Pelegrini *et.al*. [57], Tarnow Random Parallel and Tarnow Random Perpendicular models [58] with the experimentally obtained airflow resistivity rig data. As observed the test data best fits around the Tarnow Random Parallel model suggesting the likelihood of the parallel orientation of the fibres within these specific samples. An interesting aspect added onto this study is the consideration of the single staple fibre and the averaged combination of main and bico- fibres. On the graph, the Tarnow Random Parallel curves with circles represent the regression data for two fibre consideration while the rhombus shapes represent the main fibres only. It is evident that when the main fibre is considered as a lone representative of the material, the flow resistivity values are higher than those for the dual nature. An upward

offset is depicted in the shift in trends similar to the resistivity values as seen from the empirical studies plotted earlier. The experimental test data matches well with the two-fibre consideration, validating that contribution of the presence of the other fibre. This plot has been presented with a specific interest to substantiate the fact that with a theoretical basis, if the dual nature of nonwovens is not considered then it could lead to misinterpreted performance of the bulk material. This approach of highlighting the solid phase of the porous fibrous media provides further insight into the material's acoustic performance at the fibre scale.

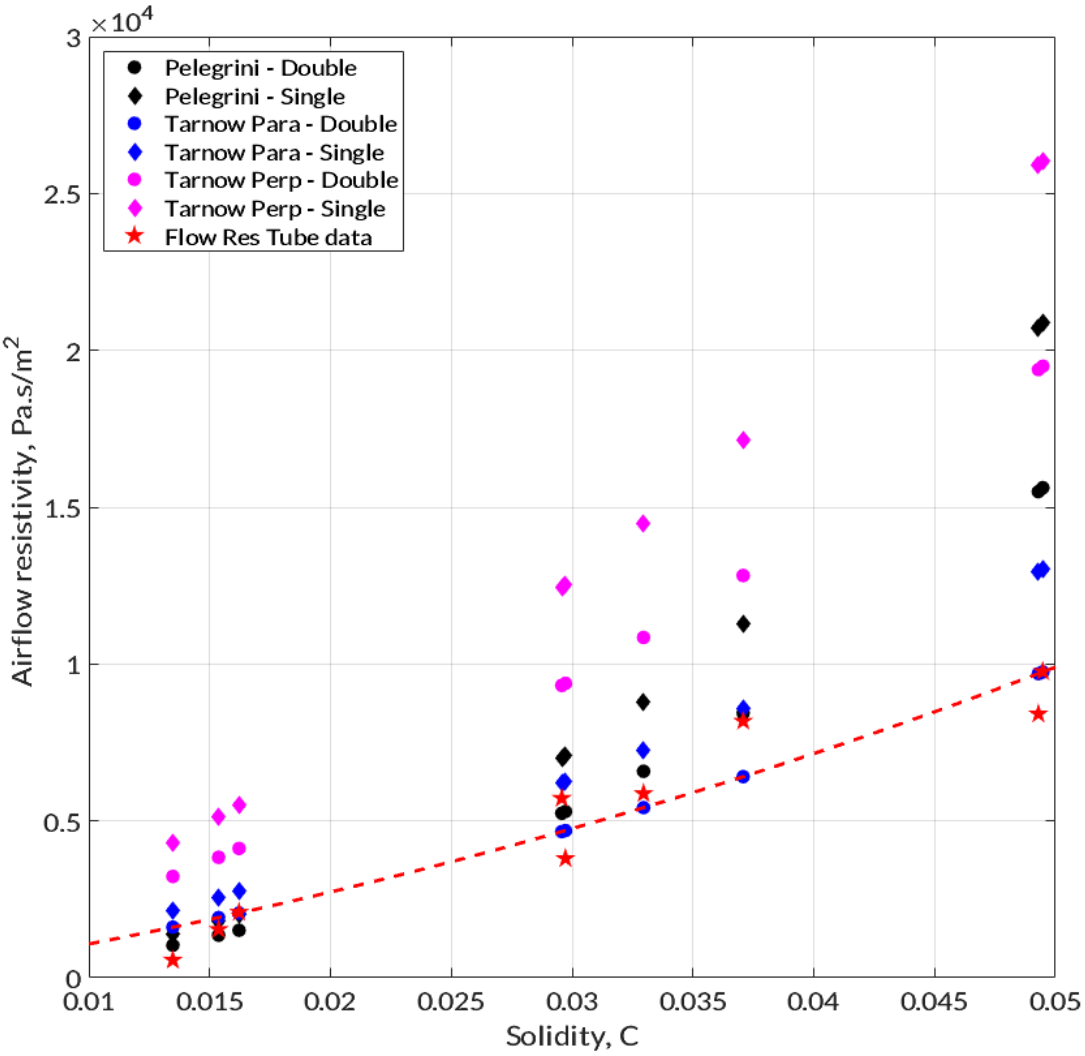

Figure 5.3.: Comparison of theoretical models for airflow resistivity against solidity

Using the best fit theoretical model, the flow resistivity values for the measured samples were then used to obtain the sound absorption characteristics (refer equation (2.14c)) using the empirical Delany-Bazley-Miki [46] model. These values over a frequency range of 200 – 6.4k Hz were then compared with the two-microphone impedance tube data of the corresponding samples. For a particular case of each blend type considered, the results show decent agreement with the experimental data as shown in Figure 5.4. It is important to note that the non-acoustic factors do play a significant role in entirely tracing the actual performance of the material.

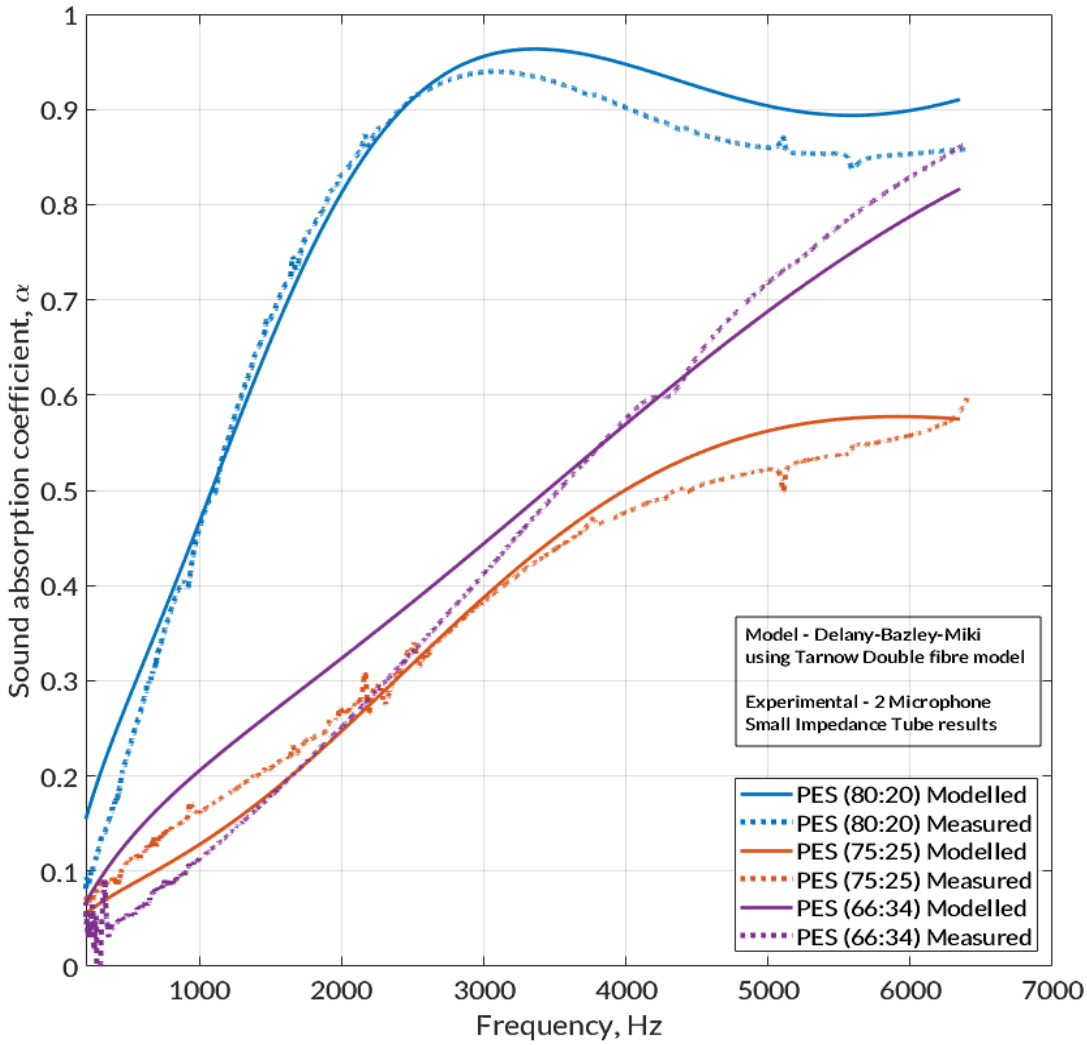

Figure 5.4.: Comparison of absorption coefficients between model and test data

Analytical single fibre model development

The fundamental theories have established that to better represent acoustic performance of the porous fibrous materials, particularly in terms of the sound absorption characteristics, if there is more insight into how the material interacts with sounds at various frequency ranges, then one can replicate such materials with improvements. This leads to the introduction of semi-phenomenological and the micro-macro modelling approaches. Utilising the understanding developed from the Tarnow's models examined earlier, Umnova, *et. al*. [49] have developed the models further to formulate analytical equations of wave motion for a single fibre under the influence of small amplitudes of parallel and perpendicular constant pressure gradients.

Sound propagation and attenuation through a rigid frame of fabric is a combined effect of the viscous and thermal dissipation of the incident sound energy. The viscous dissipation is due to the generation of viscous stresses and the thermal dissipation is due to the conductive heat dissipation because of the heat interaction between the solid and the fluid. In the case of a nonwoven material as well, the saturated air between the fibrous media does not move in phase with the fibres (which are generally treated as limp or rigid), visco-inertial and thermal effects are observed. These effects are frequency dependent, which is why the equation sets [49] have been treated based on the low and high frequency asymptotes. In the low frequency range, the viscous forces tend to dominate the inertial ones. The airflow around the fibres is governed by the Darcy Law [82]. In the high frequency range, however, vice-versa occurs, where the inertial forces dominate viscous forces. Thermal effects undergo similar two-asymptotic behaviour where the low frequency range witness an isothermal regime while at the high frequencies the heat transfer between the air and the fibres is negligible and so the adiabatic regime is followed.

Two main quantities that determine the propagation of sound through porous media, viz., frequency dependent complex characteristic wave number and impedance. These macroscopic properties sufficiently define the mechanism of dissipation and can be obtained from the microstructure of the material. The derivation of the wave equation for the porous fabric generally uses the Theory of Homogenisation of Porous Media [82].

This derivation for a single fibre system has been detailed in the following references [49, 58, 96] for parallel and perpendicular fibres. Also, exact analytical expressions for ideal shapes have been determined by various researchers and has been covered in section 2.2 of the literature review.

To understand the formulation better, a rigorous derivation for the general wave equation for an obliquely inclined fibre has been attempted in the section 4.1, Chapter 4. This has led to the first simplification by considering the static version single fibre case. Referring to Umnova *et. al.* [49], steady state solutions obtained for a single fibre case elaborated further in section 4.2, Chapter 4. On application of the appropriate boundary conditions, the permeability and high frequency limit parameters have been validated with those obtained in the reference [49]. The equations thus obtained for the basis for the analytical correlations in this part of the study.

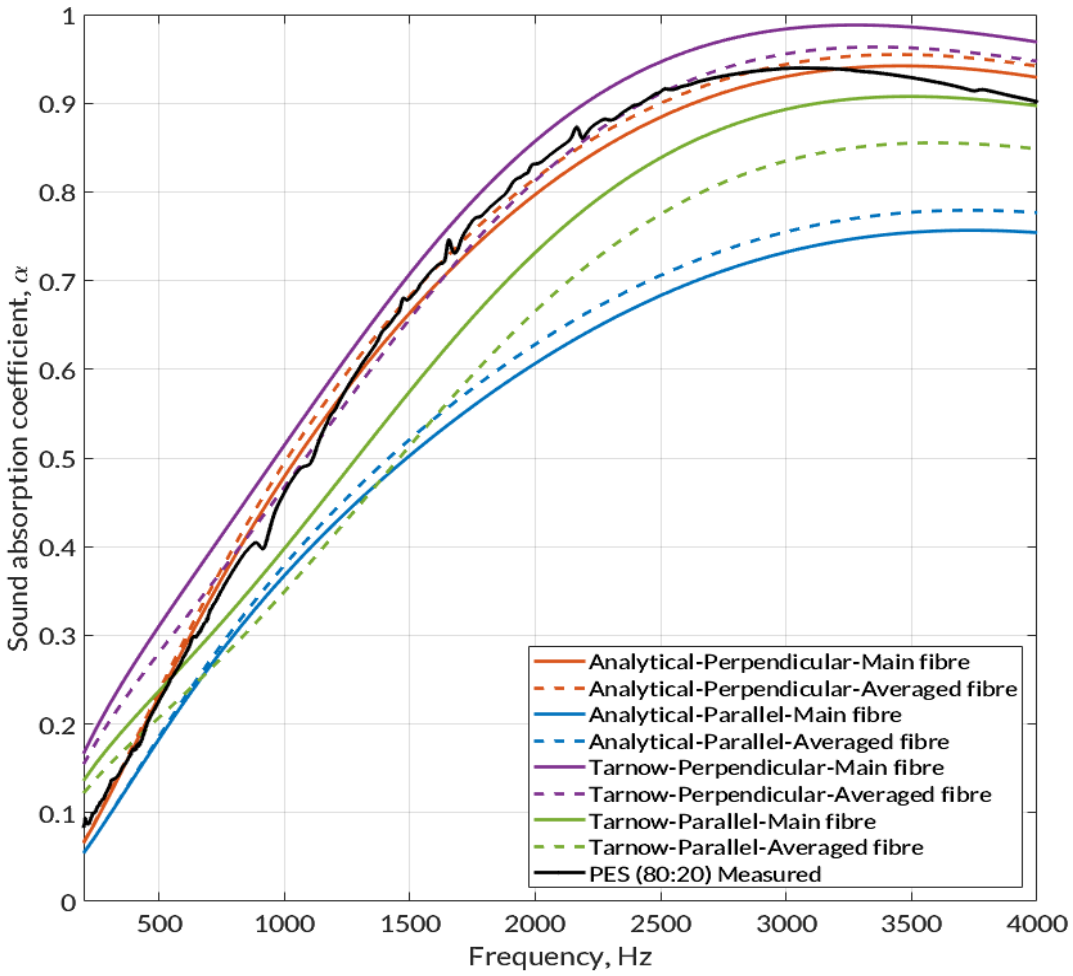

Figure 5.5.: Sound absorption coefficient comparison between the Tarnow and analytical models for perpendicular and parallel fibre orientations and validation with experimental data

Tarnow and Analytical models for perpendicular and parallel fibre orientations have been compared with experimentally measured data as shown in Figure 5.5 for sound absorption characteristics (as in equation (2.7c)).

The measurements were conducted using the 2-mic impedance tube detailed in Chapter 3. Experimental data aligns well with the analytical perpendicular case results. It is also observed that perpendicular set of models have higher absorption coefficients in comparison to the parallel configuration as this orientation imparts a higher characteristic impedance and wave number to the propagating sound waves as seen from Figures 5.6 and 5.7.

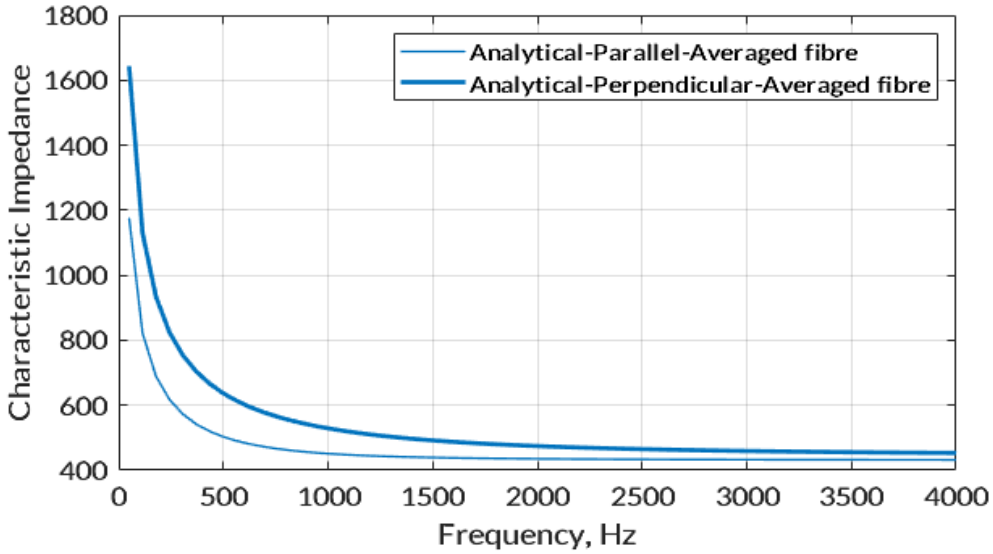

Figure 5.6.: Comparing real part of characteristic impedances for parallel and perpendicular fibres

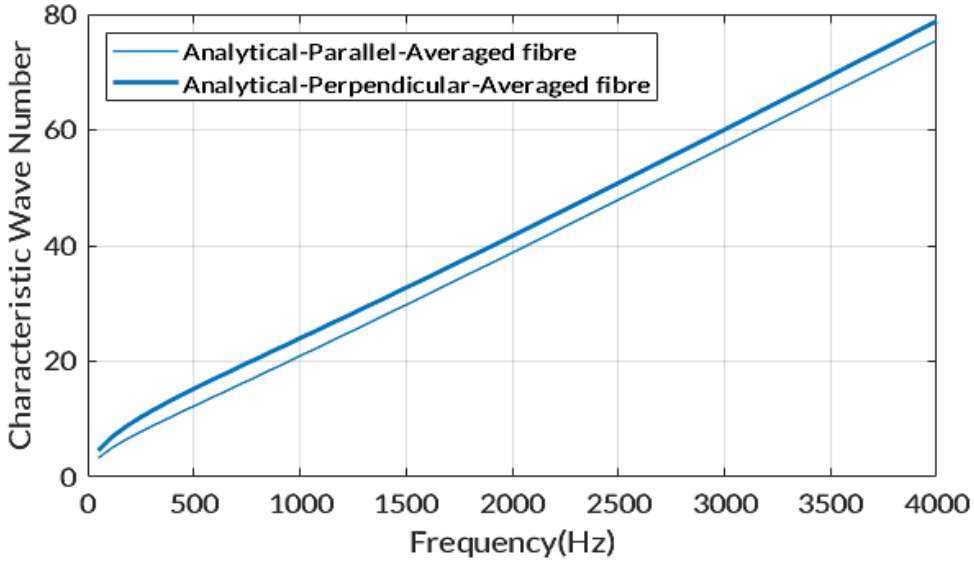

Figure 5.7.: Comparing characteristic wave numbers for parallel and perpendicular fibres

The equations providing parallel and perpendicular static flow transport properties which were used to analytically acquire further information about nonwovens with the knowledge of fibre radius and porosity were coded in MATLAB (see Appendix B). These have been transformed to obtain complex dynamic density and bulk modulus leading to characteristic surface impedance and wave number which are then used to obtain the reflection factor and ultimately expressing the sound absorption characteristics of the material. Since the model is a single cell approach, the comparison includes a study of staple fibre versus the weighted average fibre as used throughout this chapter.

The models have been validated against experimental data for the sample under observation and three key points have been noted. First, the coincides well in the low-mid frequency range with the analytical model. Second, the measured values of the sample align more towards the modelled curves based on the averaged fibre radii rather than the main fibre only. Lastly, the material sample has been suitably prepared and tested with majority of the fibres oriented in the perpendicular direction to the propagating sound waves. This can be verified by visual observation as well.

Understanding estimate conditions (Boutin's work – HPM-SCM [77])

Although HPM is a well-established approach, it has been meticulously used for idealised geometry such as circular cylinders to replace the realistic fibres in the case of nonwoven materials. To account for the realistic features of a porous fibrous material, an alternative has been provided by the Self-Consistent method (SCM), which has been reviewed in comparison to HPM method. The SCM based models work on analytical expressions that use the key physical features of a material and are easy to process. Boutin's work on combining the HPM and SCM techniques has provided another perspective to obtain the transport parameters.

To reiterate from the review section, the combining process of HPM and SCM involve the derivation of dynamic permeability, covered at length by Auriault *et. al* [82]. Following the HPM approach, Darcy law is derived to obtain the macroscopic description in terms of the mass balance. Then by using the SCM approach, the overall equilibrium with regards to the momentum balance is established, which cannot be typically obtained from the Darcy law. This is followed by the deriving the energy consistency between the micro- and macroscopic details. The energy consistency condition leads to certain alternatives for arriving at the dynamic permeability that are expressed as the three estimates of dynamic permeability. Boutin classifies them as the P-estimate,

V-estimate and C-estimate based on their respective assumptions. These estimates have been simplified and provided in the Table 5.5 to obtain normalised airflow resistivity values for the selected samples to be compared with the previous approaches.

Table 5.5.: Summary of Estimates

Estimates	Normalised flow resistivity equations
P- estimate	$pest = \frac{8(1-\phi)}{\left[-\frac{1-(1-\phi)^2}{1+(1-\phi)^2} - \ln(1-\phi)\right]}$
V- estimate	$vest = \frac{2(1-\phi)(4-\phi)}{-\phi - \frac{(2-\phi)\ln(1-\phi)}{2}}$
C- estimate	$zervor = \frac{16(1-\phi)}{-\phi^2 - 2\phi - 2\ln(1-\phi)}$

Figure 5.8. provides a visual comparison between airflow resistivity values obtained for polyester samples of different blend types using the averaged cases of analytical and estimate models. The results have been compared with the measured airflow resistivity. The Pelegrini model [57] best represents the measured values followed by the Tarnow parallel model. P-estimate and C-estimate values are quite comparable with the Tarnow perpendicular model, while the V-estimate for both the samples falls beyond the typical range of expected airflow resistivity value.

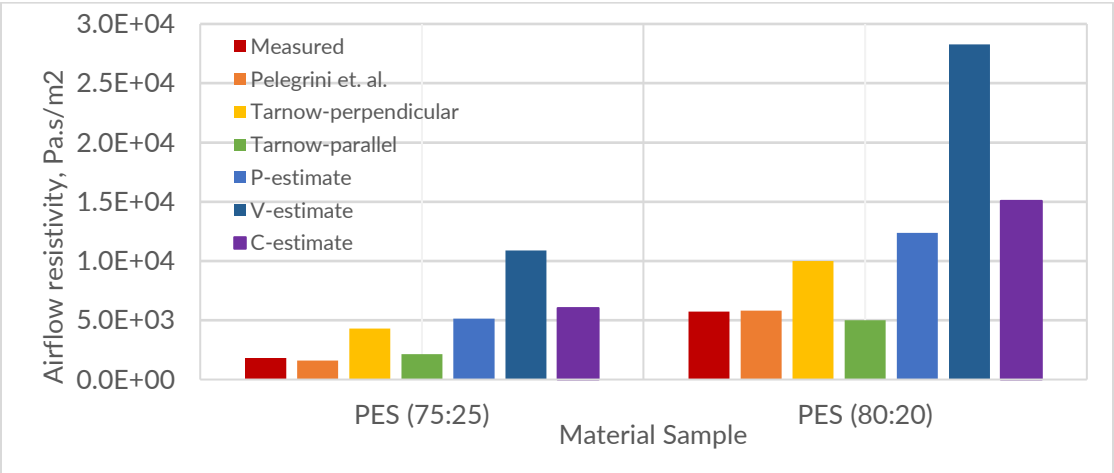

Figure 5.8.: Comparison of averaged model results for airflow resistivity

5.3. NUMERICAL MODELLING

Fibrous materials can be represented as a matrix of cylinders to denote periodic arrangement.

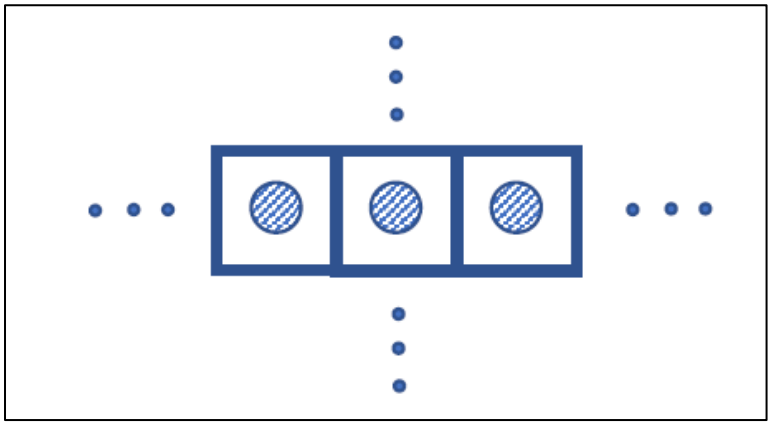

Figure 5.9.: 2D cellular view of periodically arranged cylinders as fibrous materials.

In Figure 5.9, the circle represents the fibrous material, or a single strand of fibre to be specific. This fibre is enclosed in the void that represents the pore of the material, which is also the air (fluid) cavity in between the adjacent fibres. The square represents the domain defining the cell comprising of a single fibre along with the fluid domain around it. Equally spaced cells depicting periodicity of their arrangement can be present in plurality in all directions as represented by the dots. A key point to note here is that the frame of the fibrous material in consideration is assumed rigid. This cell or a similar modification (where a few cylinders/ fibres are considered together) can also be termed as the Representative Elementary Volume (REV) as referred in several instances through the literature. The REV is defined in the microscopic scale such that $\varepsilon \ll 1$.

Porosity of the material can be obtained as the ratio of the volume (area in 2D case) occupied by the fluid domain to the total volume of the porous material (solid and fluid domain included).

Similar to the single fibre model as discussed analytically, this model can also be visualised numerically using COMSOL Multiphysics 5.5 software. To begin with 2D planar models for solving stokes equation with the variables being fibre dimension and porosity. Figure 5.10. shows the geometric representation of a single fibre model.

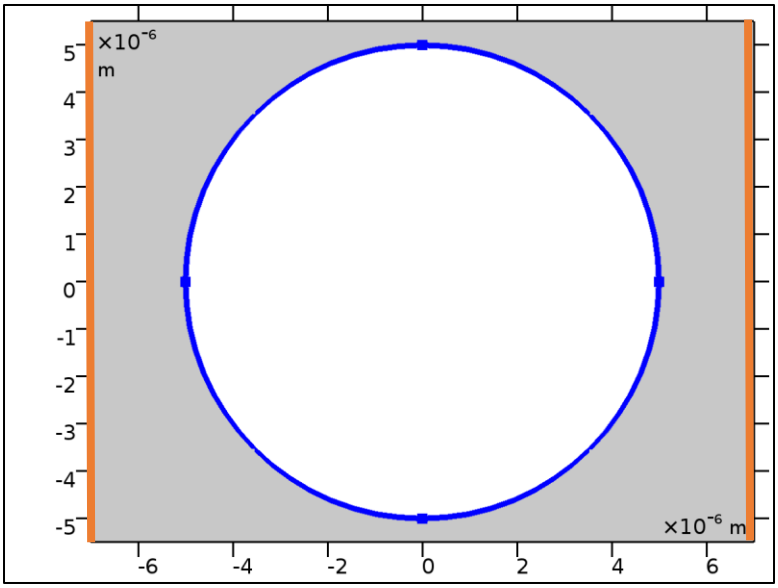

Figure 5.10.: 2D planar model showing geometry of fibre within fluid on COMSOL.

The circle represents the cylindrical fibre and the shaded zone around it represents the fluid domain with laminar flow. For this initial analysis, the solid frame of the fibre was considered as rigid and hence the circle boundary highlighted is assumed stationary.

Periodic flow conditions are added selecting the source and destination. The opposite sides of fluid domain are selected such that one edge is the source and the other is the destination; and similarly selected for the other two sides accordingly. The external pressure gradient is chosen as the volume force on the domain from the orientation as desired. Besides these, yet another condition is applied to assume the constant pressure term, by selected a corner of the domain as a pressure point constraint, which is set to zero for this analysis.

Computing the problem defined based on these settings; the solution is obtained, quite similar to the analytical approach, in terms of the velocity. This velocity is averaged and integrated over the entire area, on the basis of which, the static viscous permeability is calculated. A parametric variation between fibre radius and porosity is solved for and values for permeability are obtained.

The linearised equations of motion of a fluid around a cylindrical fibre in a REV under constant small amplitude harmonic oscillatory pressure gradient $(\nabla_x p)e^{-i\omega t}\overrightarrow{e_x}$ are governed by the following set of rescaled equations deduced using HPM, as in equations (2.4 – 2.10).

At the Low Frequency Limits (LFL), the rescaled equations (with $\nabla = \nabla_x + \varepsilon^{-1}\nabla_y$) are,

Stokes Problem (Low Reynold's Number Flow implying negligible inertial term $(\rho.\vec{u}.\nabla\vec{u})$:

$$\eta\Delta_y\vec{u}^0 - \nabla_y p^1 = -\nabla_x p^0 \qquad \text{in } \Omega_f \qquad (5.10)$$

Continuity equation suggesting incompressibility:

$$\nabla_y.\vec{u}^0 = 0 \qquad \text{in } \Omega_f \qquad (5.11)$$

No-Slip Boundary Condition:

$$\vec{u}^0 = 0 \qquad \text{on } \Gamma_s \qquad (5.12)$$

where,

$p^{(i)}$ and $\vec{u}^{(i)}$ are the pressure and the velocity of the fluid where $\vec{u}^{(i)}$ is y-periodic.

Ω_f and Γ_s symbolize the volume of the fluid and the fluid-solid interphase respectively.

The term on the right-hand side of equation (5.10) is the applied pressure gradient. Therefore, F, which is the external volume force or $\nabla_x p^0 = (\nabla_x p)e^{-i\omega t}\overrightarrow{e_x}$ say for instance, being applied along the x direction. In this case, the coordinates for pressure force are $P.\overrightarrow{e_x} = (P,0).(1,0)$ with $\overrightarrow{e_x}$ as the unit vector in the x direction. Now this $p = \tilde{p} + c$ implies that the p is unique and would need defining of a pressure point constraint for indicating the location of constant pressure application. Once the geometry and these equations have been defined in the COMSOL interface choosing the Laminar Flow Stationary module, the model is meshed and computed for the solutions.

The solution to the Stokes problem, equation (5.10), is in terms of x- component of the velocity vector, u_x, in the direction of the pressure gradient. To obtain the remaining parameters from the following problem, Darcy's Law is used:

$$\langle u^0 \rangle = -\frac{\langle \hat{k} \rangle}{\eta}\nabla_x p^0 \qquad (5.13)$$

Here $\langle \hat{k} \rangle$ is the viscous permeability and $\langle u^0 \rangle$ represents the x- component of the velocity averaged over the volume of the fluid domain. In COMSOL, this is done using the integral operator $intop1 = \int_{\Omega_f} d\Omega$

$$u_{avg} = \langle u^0 \rangle = \frac{1}{A}\int_{\Omega_f} u \, d\Omega = \frac{1}{\int_{\Omega_f} 1 \, d\Omega}\int_{\Omega_f} u \, d\Omega = \frac{1}{intop1(1)} intop1(u) \qquad (5.14)$$

is to be thus defined in the global variables. The static viscous permeability is used to obtain the dynamic viscous permeability after obtaining the HFL parameters such as the characteristic lengths and tortuosity from the HFL-based COMSOL model [96].

In this other COMSOL model, the HFL has been considered for obtaining some of the other relevant properties that effectively define the porous material. Here the COMSOL interface is developed by opting for the Laplace Equation based mathematical module.

$$\nabla^2 or \, \Delta\vartheta = 0 \qquad \text{in } \Omega_f \qquad (5.16)$$

Now the general theory of solutions to the Laplace Equation is the Potential Theory. The solutions of Laplace Equation are harmonic functions, and they can be used to accurately describe the behaviour of electric, gravitational and fluid potentials. For instance, in the study of heat conduction, the Laplace Equation is the steady state heat equation. This derivation has been correlated using the electric analogy as elaborated in [96].

$$\vec{n}.\nabla\vartheta = \vec{n}.\vec{e} \qquad \text{on } \Gamma_s \qquad (5.17)$$

where $\vec{n}$ is the unit normal vector directing away from the pore or inclusion such that $(n_x, n_y).(\partial_x\vartheta, \partial_y\vartheta) = (n_x, n_y).(e_x, e_y)$, ϑ is the deviatoric part of an electric potential which is y-periodic and e is the unit electric field.

Let unit electric field $(e_x, e_y) = (0,1)$ along the y axis. The scaled electric field $\vec{E}$ which is the local electric field divided by applied macroscopic potential gradient implies,

$$\vec{E} = \vec{e} - \nabla\vartheta \qquad (5.18)$$

Such that,

$$\vec{E} = (0,1) - \left(\partial_x \vartheta, \partial_y \vartheta\right) = (-\partial_x \vartheta, 1 - \partial_y \vartheta)$$

For an isotropic material or a preferential flow direction, the following properties can be obtained: Tortuosity α_∞ from the equation:

$$\alpha_\infty^{-1} = \frac{1}{\Omega_f} \int_{\Omega_f} \vec{E}.\vec{e}\, d\Omega \tag{5.19}$$

Where $\vec{E}.\vec{e} = (\vec{e} - \nabla\vartheta).\vec{e}$ and for the specific case being discussed as above,

$$\vec{E}.\vec{e} = \left(-\partial_x \vartheta, 1 - \partial_y \vartheta\right).(0,1) = (1 - \partial_y \vartheta)$$

Viscous Characteristic Length Λ is obtained as:

$$\frac{2}{\Lambda} = \frac{\int_{\Gamma_s} \vec{E}.\vec{E}\, d\Gamma_s}{\int_{\Omega_f} \vec{E}.\vec{E}\, d\Omega_\mathrm{f}} \tag{5.20}$$

Where $\vec{E}.\vec{E} = (\vec{e} - \nabla\vartheta).(\vec{e} - \nabla\vartheta)$ and for the specific case being discussed as above,

$$\vec{E}.\vec{E} = \left(-\partial_x \vartheta, 1 - \partial_y \vartheta\right).\left(-\partial_x \vartheta, 1 - \partial_y \vartheta\right) = \partial_\mathrm{x}^2 \vartheta + \left(1 - \partial_y \vartheta\right)^2$$

Thermal Characteristic Length Λ' is calculated as:

$$\Lambda' = 2\frac{\Omega_f}{\Gamma_s} \tag{5.21}$$

The REV cells for a single fibre model have been developed initially as generic cases and have been defined in two ways:

1. Fixed cell volume approach where the variation of transport parameters is studied against varying fibre radii values (ranging as 1, 5, 10, 15, 20 and 25 μm)
2. Controlled porosity approach where the parameters vary over porosity for a fixed radius ($15\mu m$), but the cell volume changes to accommodate porosities (from 0.4 – 0.99).

Transport parameters for a fixed fibre radius of 15 μm have been presented for LFL. Figure 5.11 shows velocity magnitude along with volume force (left) and pressure contours (right) to visualise pressure gradient that is applied along the y-direction.

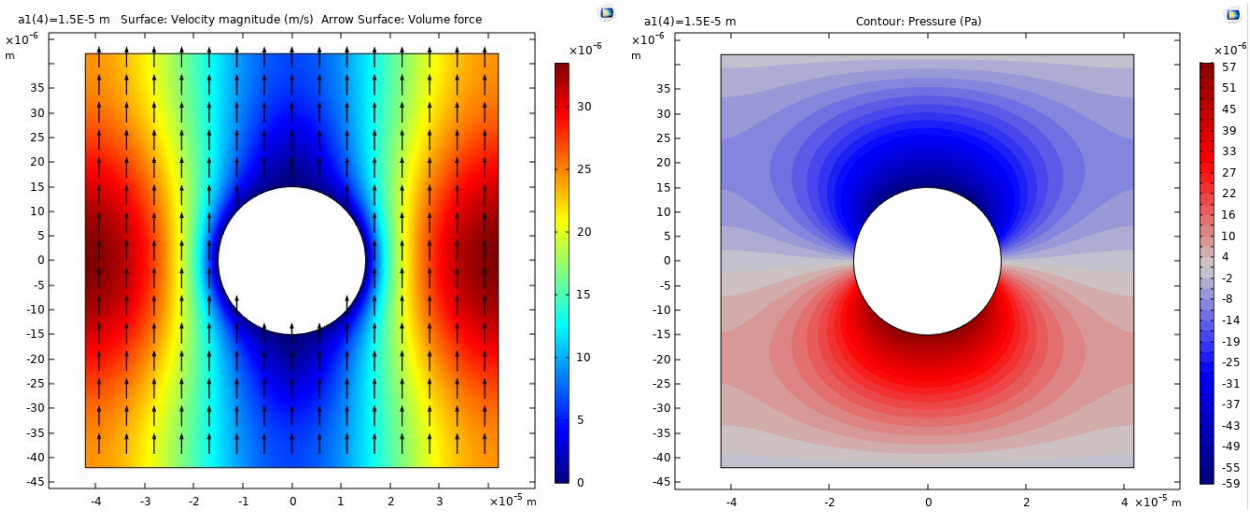

Figure 5.11.: Single fibre-based a) velocity magnitude (volume force - arrows) b) pressure contour

The symmetricity of the velocity components can be realised from Figure 5.12. The y component of velocity coincides with the velocity magnitude plot suggesting the preferential flow direction.

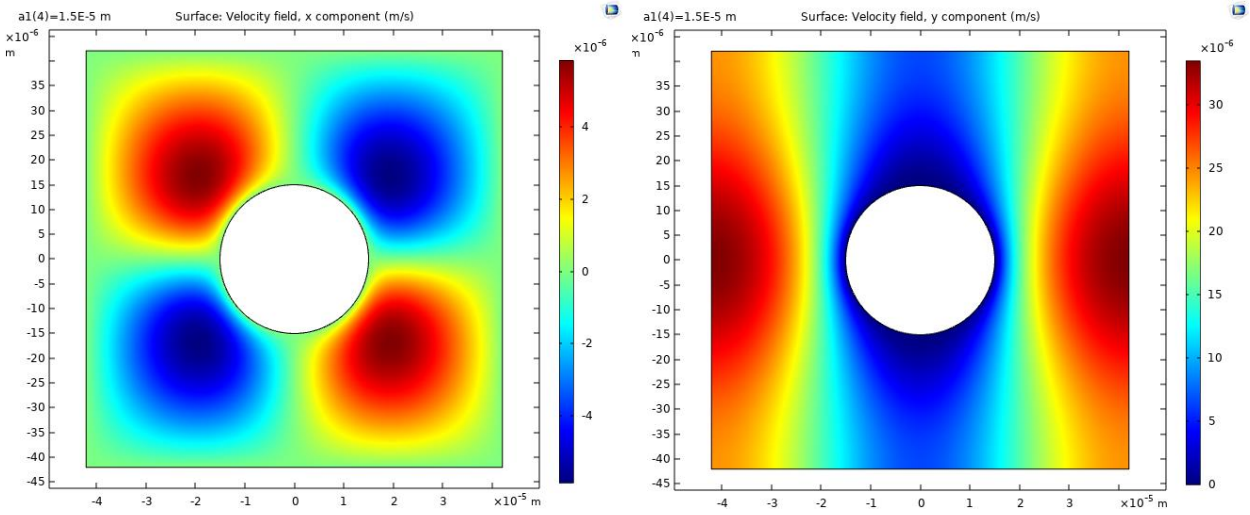

Figure 5.12.: x and y components of velocity field at LFL for single fibre

While the pressure and velocity graphics demonstrate periodic boundary condition, zero vorticity at the cell boundary condition can be represented by the vorticity magnitude plot as in Figure 5.13.

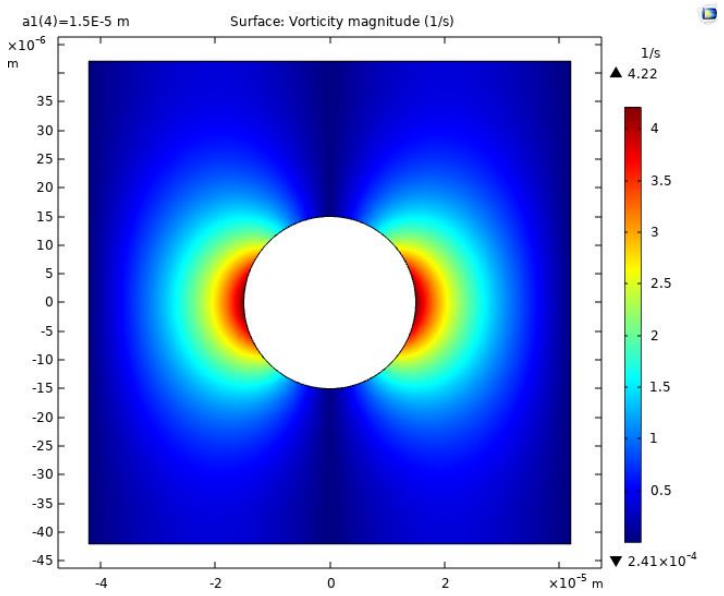

Figure 5.13.: Vorticity magnitude for single fibre

Viscous permeability has been calculated for a single fibre cell approach and has been plotted in Figure 5.14 to show the inversely proportional variation with the fibre radius.

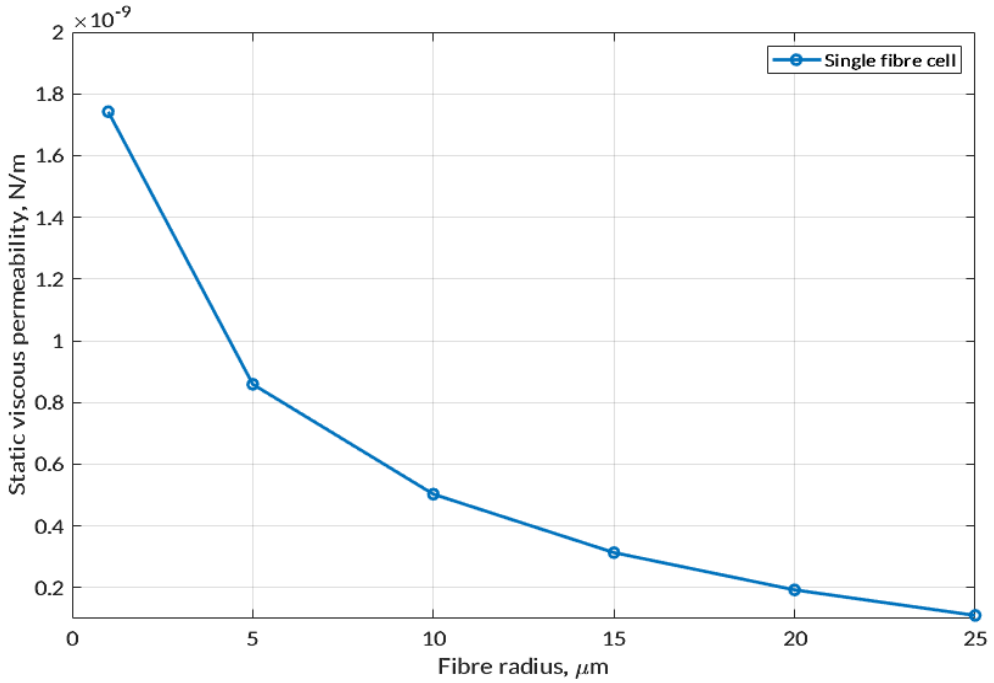

Figure 5.14.: Permeability of a single fibre case variation with fibre radius

At HFL, x and y velocity components have been presented to show similar impact of pressure flow along the y-direction. Symmetricity of velocity field is observed at this condition as in Figure 5.15.

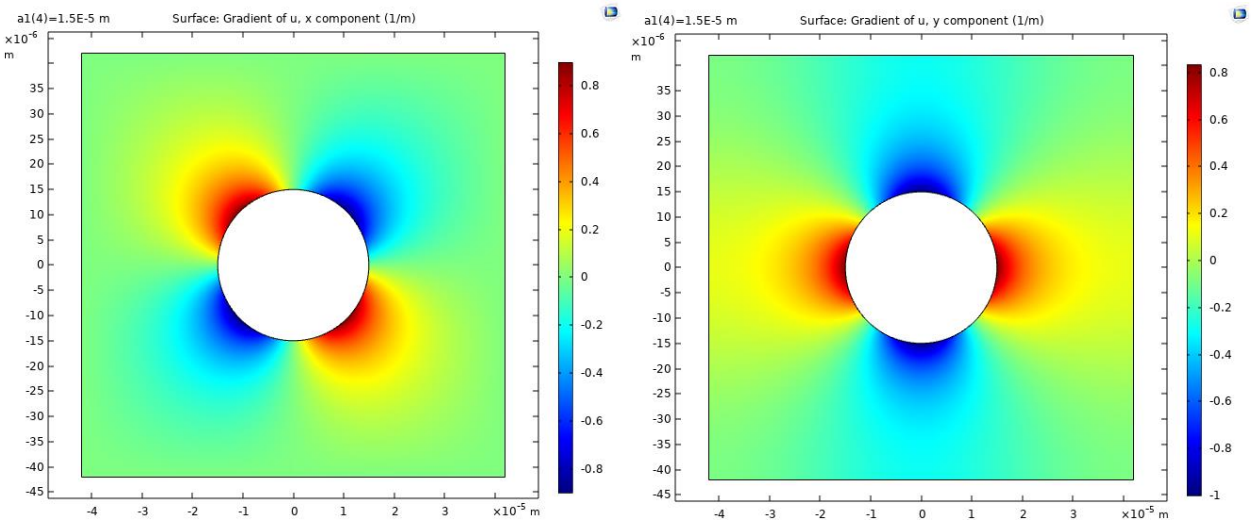

Figure 5.15.: x and y components of velocity field at HFL for single fibre

The HFL transport parameters, tortuosity and viscous and thermal characteristic lengths have been calculated using the Laplace equation-based model derived from equation (5.17) onwards, comprising of the single fibre cell. These have been plotted as per the Figures 5.16 and 5.17.

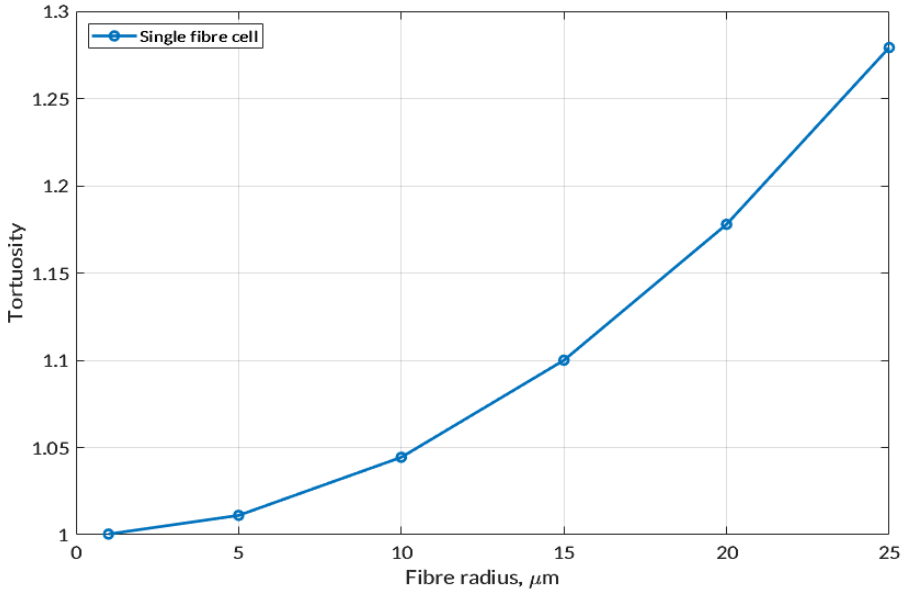

Figure 5.16.: Tortuosity variation with varying fibre radius

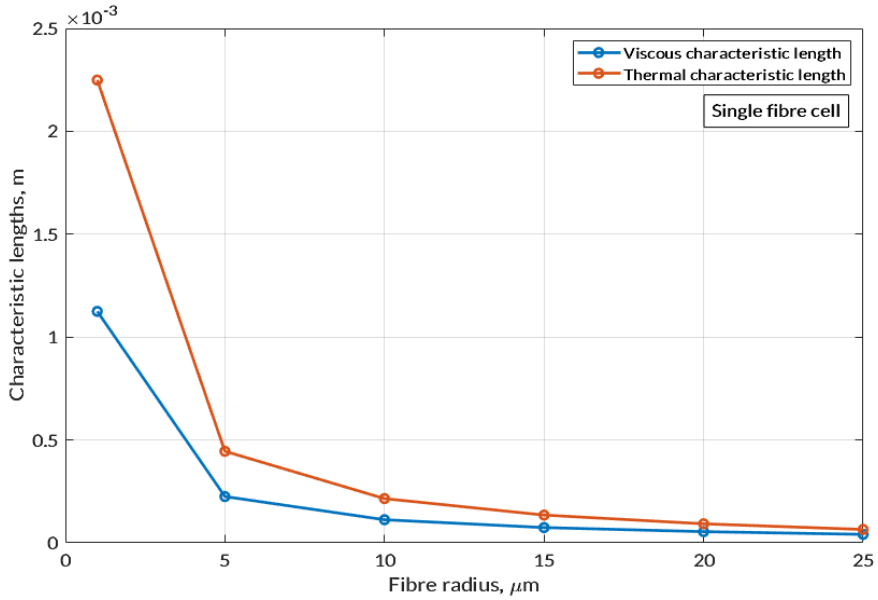

Figure 5.17.: Single fibre cell based characteristic lengths against increasing fibre radii

The other approach of defining the REV cell where the variations are plotted with respect to porosity. For the comparison with the estimates [77] defined in the analytical model (here refer Table 5.5), the single fibre cell has been simulated for porosities ranging from 0.4 – 0.99. However, it should be noted that porosities lower than 0.6 are uncommon for the material to be classified as a fibrous absorber. Figure 5.18 provides a comparison of estimates in the form of ratios and indicates that P- and C- estimates have better alignment with the numerically calculated permeability.

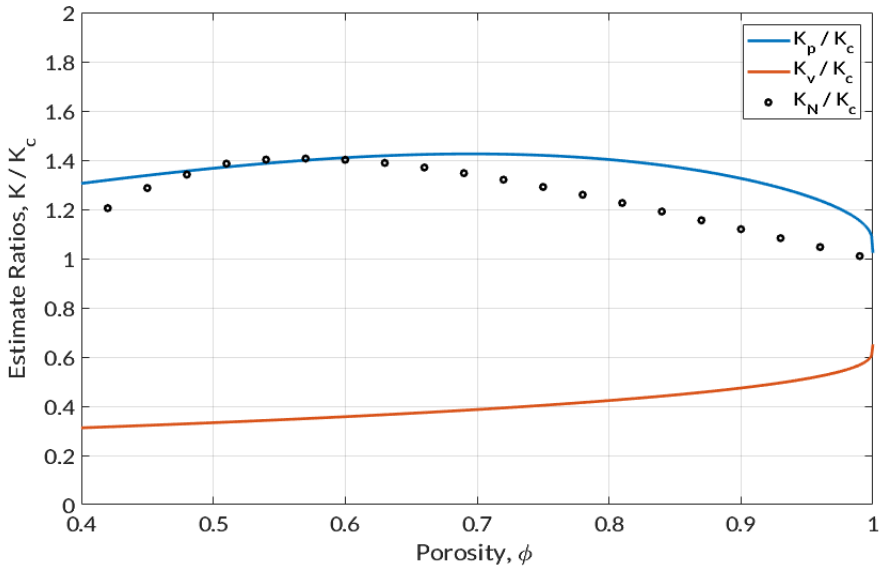

Figure 5.18.: Ratios of the estimates with C-estimates and the numerically calculated permeability K_N

Figure 5.19 is a plot of the dimensionless permeability K/r_f^2 normalised using fibre radius varying with porosity. The three self-consistent estimates have been correlated with numerically calculated values. For the case of single cylindrical fibres, this figure also reassures that permeability is closer to P- and C- estimates as compared to V-estimate. This also validates bar chart data (here refer Figure 5.8) where V-estimate is off the range of airflow resistivities suggested by other analytical models.

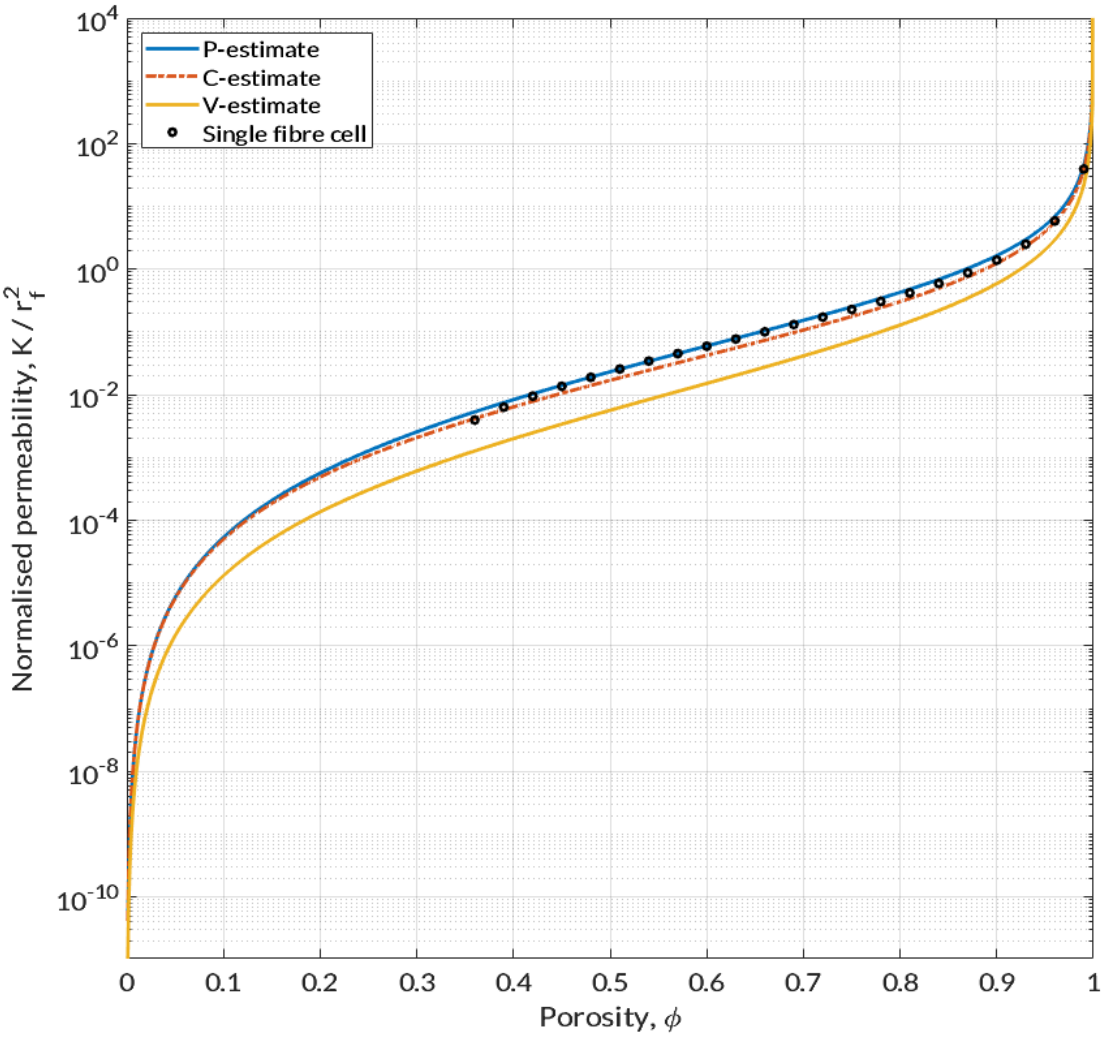

Figure 5.19.: Dimensionless permeability K/r_f^2 plotted against porosity for comparing estimates with numerical results for single fibre model

Figures 5.18 and 5.19 have been presented for cylindrical fibres and have been inspired by Boutin's work (Figure 5 of [77]) where the spheres have been studied similarly by SCM detailed earlier.

The single fibre cell model has been trained to run for a porosity range of 0.7 – 0.99 as this is the typical range of porosities for a nonwoven material, particular of the polyester make. The calculations have been made for the same set of generic fibre diameters of 2 – 50 μm. The generic single fibre variation for viscous permeability over the porosity parameter is shown in Figure 5.20.

It has been noted that the high frequency limit tortuosity remains unchanged for the various single radius fibres calculated over the porosity range.

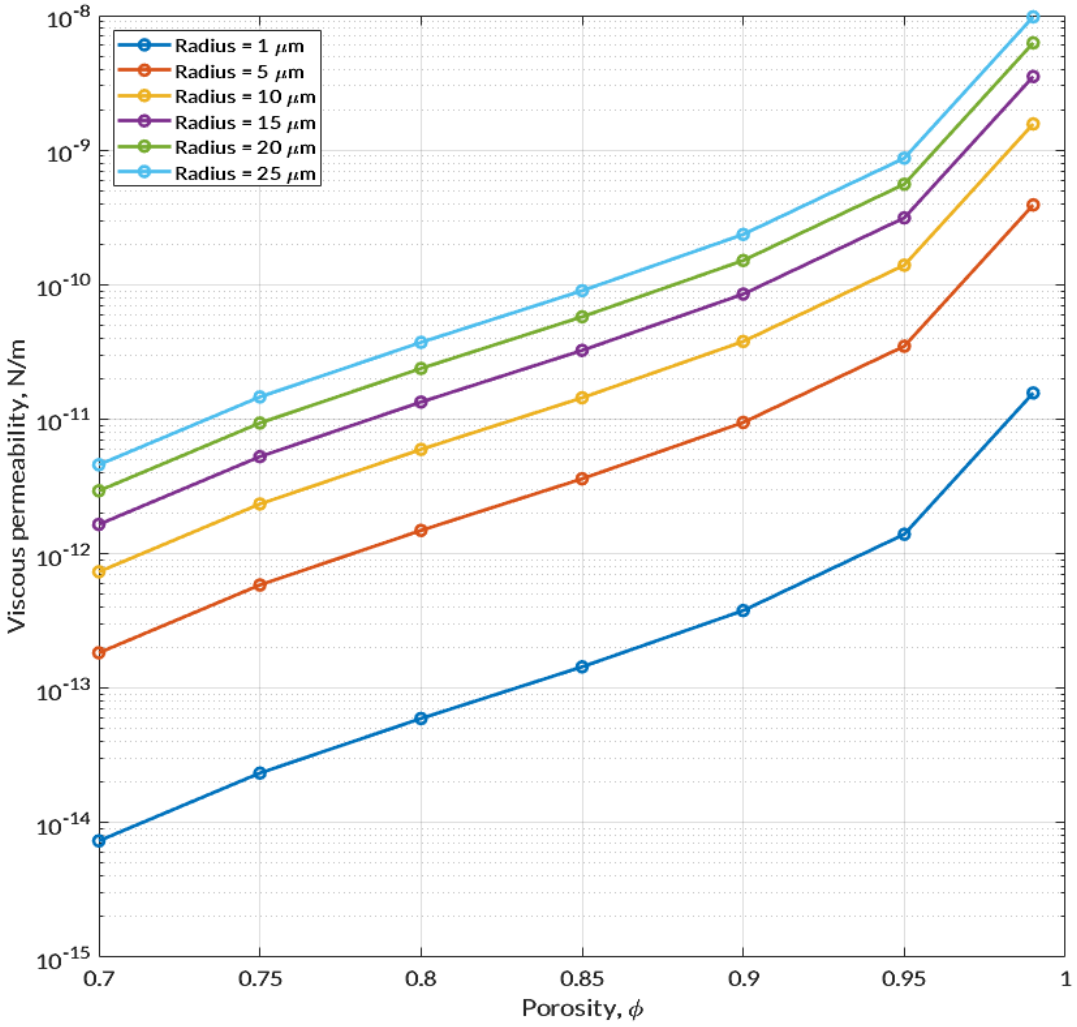

Figure 5.20.: Permeability variation over porosity for various fibre radii

Finally, to represent the test samples using numerical methods, PES variety have been compared for single staple or main fibre with the weighted average fibre diameters. The same single cell model approach has been adapted to compute the material's transport parameters. At the low frequency limits, the properties referred are the permeability and flow resistivity. These have been presented in the Figures 5.21 and 5.22.

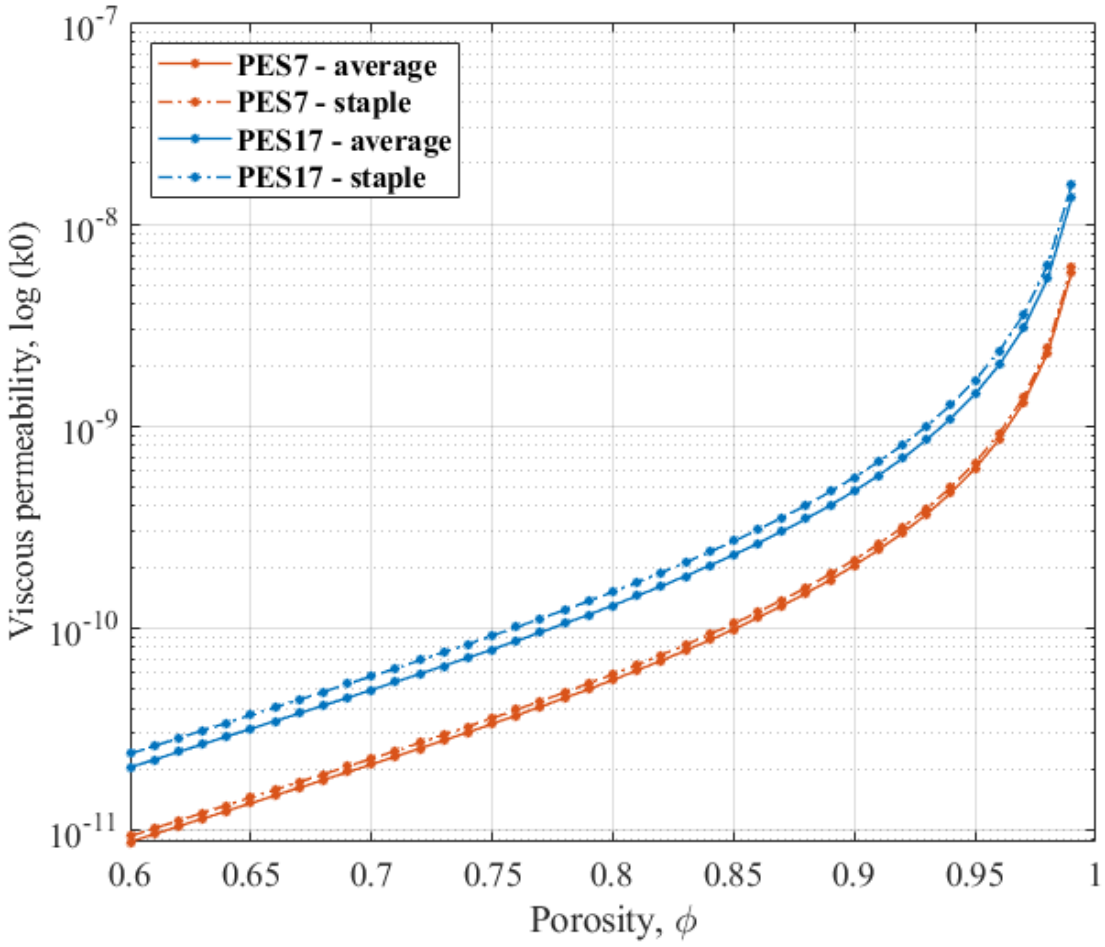

Figure 5.21.: Permeability variation for PES 7 and PES 17 – main vs average

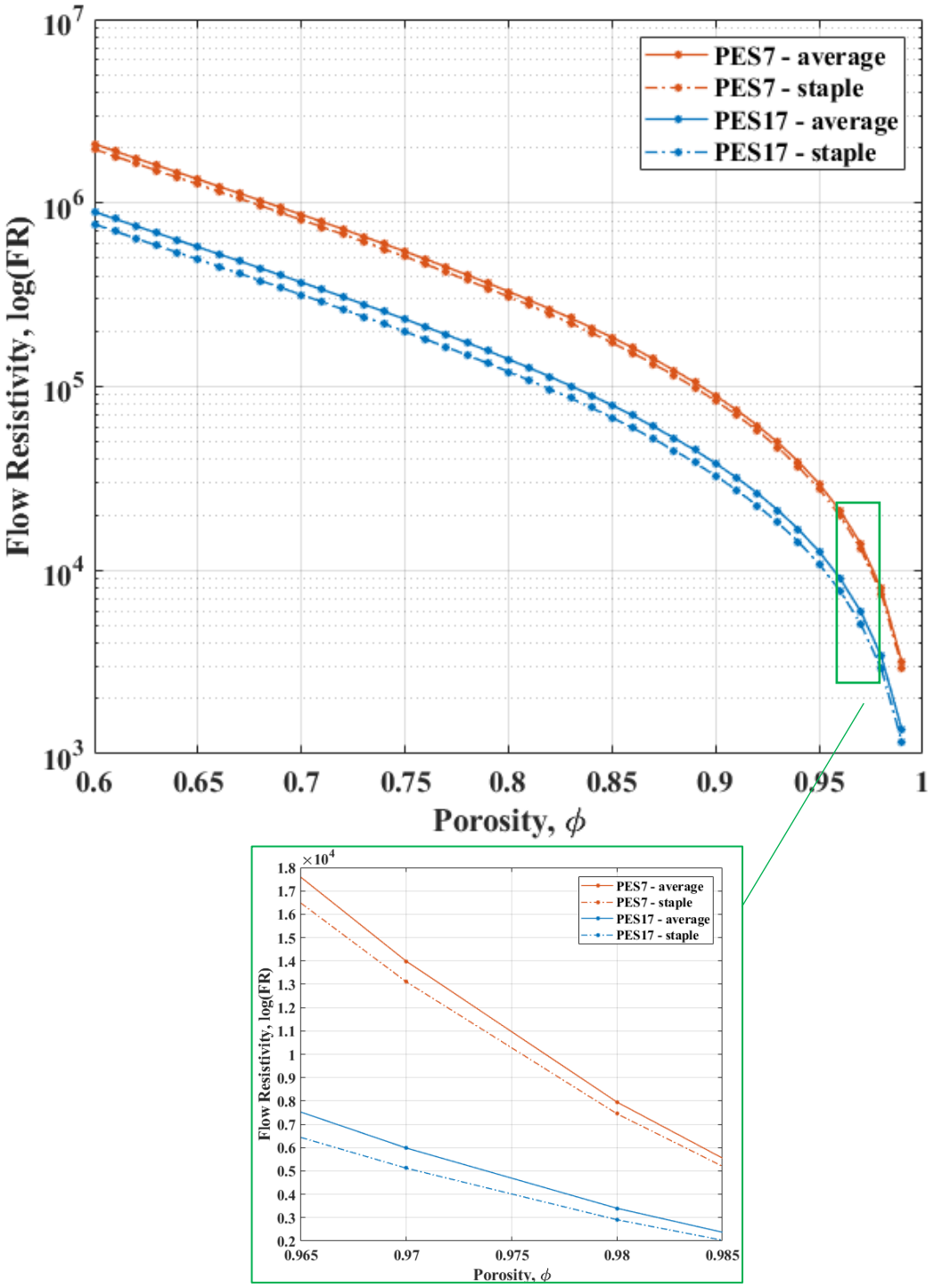

Figure 5.22.: Airflow resistivity variation for PES 7 and PES 17 – main vs average

At the high frequency limits, the transport properties considered are tortuosity and the characteristic lengths. Note that for the case of a single cell consideration, any of the variables have no impact on the tortuosity as this parameter is solely influenced by the structural variations

if they were to be included as a part of the study. The Figure 5.23 shows that viscous characteristic lengths are typically smaller than the thermal characteristic lengths as expected. Also, although very minor, the single fibre cell suggests that there is a difference even in the characteristic lengths when the average fibre is considered instead of only the staple component of the nonwoven blend.

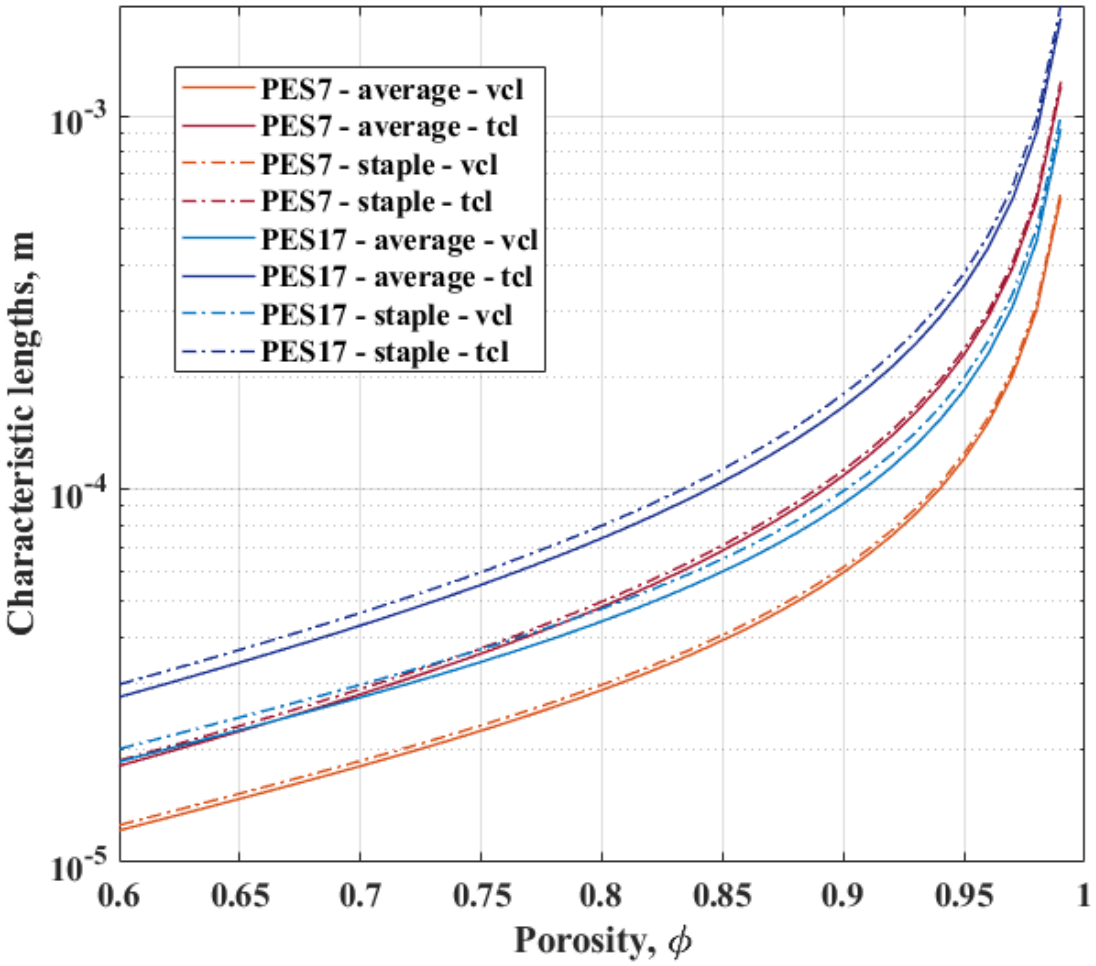

Figure 5.23.: Characteristic Length variations for PES 7 and PES 17 – main vs average (sub plots)

Repeatability Validation of Single Fibre Cell as a Unit and Repetition of such Units

In this part of the COMSOL study, the single fibre cell has been defined based on the fibre radius and square cell dimension as an influence of the porosity. The cell is arranged in a matrix of four-unit cells to resemble a multi-fibre homogeneous material as in Figure 5.24 b. The unit cell is also arranged in an array of twos, suggesting two fibre cells. These models have been prepared in two different alignments (Types 1 and 2) as in Figures 5.25 a and 5.25 b.

The aim of this study is to validate the repeatability of the static viscous permeability values for the single fibre radius considered. This process has been carried out for numerous porosities ranging from 0.8 – 0.99 with focus on the higher end of the range.

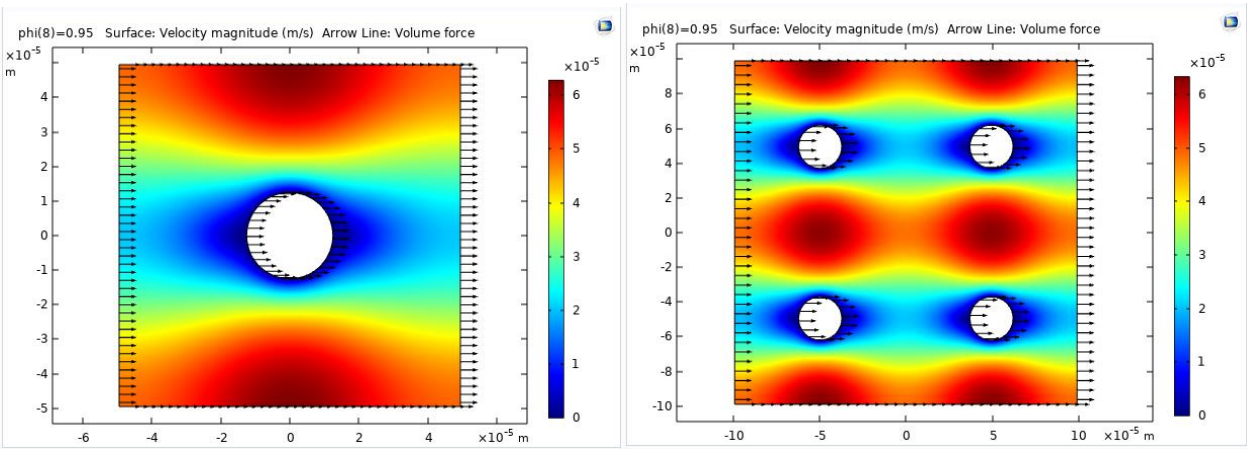

Figure 5.24.: a) Single fibre unit cell b) 4 Single fibre unit cells

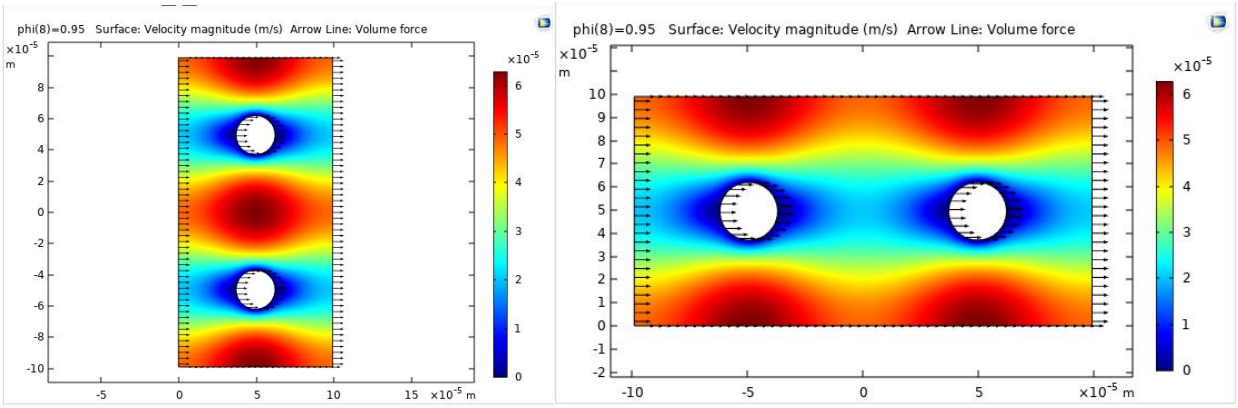

Figure 5.25.: a) 2 vertical single fibre unit cells b) 2 horizontal single fibre unit cells

To express viscous permeability, both normalised (Nor VP) and unnormalised (VP) have been cross checked for validation. The normalisation has been carried out using square of the fibre radius value used. As per the comparison for the four-unit cell types shown in Figures 5.24 and 5.25, the viscous permeability values shown in Table 5.6 indicate that the models prepared works in good agreement with each other. However, this variation increases with increase in the number of cells with a maximum of <0.5% error rate at the lower porosity values for four-unit cell as compared to the single unit.

Table 5.6.: Comparison of normalised and unnormalised permeabilities for various single cells

phi	Single Fibre Unit		2 Single Fibre Unit_1		2 Single Fibre Unit_2		4 Single Fibre Unit	
	Nor VP	VP	Nor VP	VP	Nor VP	VP	Nor VP	VP
0.8	0.38005	5.94E-11	0.3799	5.94E-11	0.38013	5.94E-11	0.3785	5.91E-11
0.85	0.67687	1.06E-10	0.67676	1.06E-10	0.67698	1.06E-10	0.6761	1.06E-10
0.9	1.4022	2.19E-10	1.4019	2.19E-10	1.4024	2.19E-10	1.3975	2.18E-10
0.91	1.6745	2.62E-10	1.6742	2.62E-10	1.6748	2.62E-10	1.6725	2.61E-10
0.92	2.0328	3.18E-10	2.0325	3.18E-10	2.0332	3.18E-10	2.0338	3.18E-10
0.93	2.5197	3.94E-10	2.5193	3.94E-10	2.5202	3.94E-10	2.5121	3.93E-10
0.94	3.209	5.01E-10	3.2085	5.01E-10	3.2096	5.01E-10	3.2069	5.01E-10
0.95	4.2404	6.63E-10	4.2399	6.62E-10	4.2414	6.63E-10	4.2379	6.62E-10
0.96	5.9091	9.23E-10	5.9084	9.23E-10	5.9099	9.23E-10	5.9042	9.23E-10
0.97	8.9475	1.40E-09	8.9468	1.40E-09	8.9487	1.40E-09	8.9319	1.40E-09
0.98	15.744	2.46E-09	15.742	2.46E-09	15.747	2.46E-09	15.718	2.46E-09
0.99	39.67	6.20E-09	39.664	6.20E-09	39.677	6.20E-09	39.59	6.19E-09

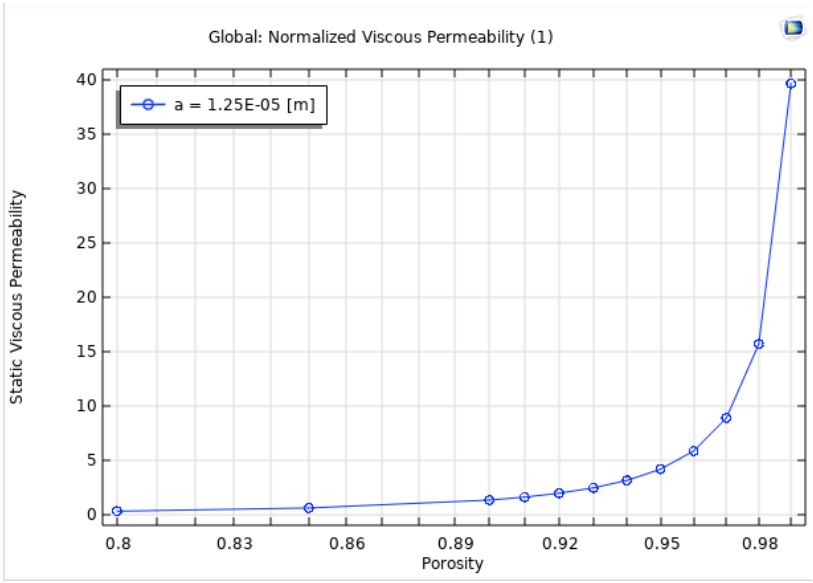

Figure 5.26.: COMSOL graphic showing normalised permeability plot

The Figure 5.26 extracted from COMSOL for the case of a single fibre PES sample, has been the basis for the correlations between the unit cell replications. In this chapter, single fibre cell-based models have been studied. This comparison frames the motivation to explore the concepts with cells that comprise of more than one fibre types that shall be covered in the following chapters.

Chapter 6

SOUND PROPAGATION AROUND DUAL FIBRES

Overview:

6.1.Adjacent bi-disperse fibre models

6.2.Staggered bi-disperse fibre models

6.3.Acoustic influence of key parameters

The previous chapter looked at single fibre-based modelling and a comparison of several modelling approaches. The single fibre models had the capability to study mono-disperse fibres. For the case of poly-disperse media, approximations must be carried out in the form of effective fibre diameter calculations based on which the various averaging techniques had been reviewed.

In this chapter, bi-disperse or dual fibre nature of models have been examined. The transition from single fibre models to dual fibre cases has been carried out to attain better clarity of the properties of nonwovens. While single-fibre models have provided valuable insights into the behaviour of individual or averaged fibres within these complex structures, they often fall short in capturing the intricate interactions that occur between realistic nonwoven fibres. Dual-fibre models aim to consider the interplay between two neighbouring fibres.

This part of the research has been inspired by the Scanning Electron Microscope (SEM) based observation of a nonwoven sample. As discussed previously, the nonwoven materials are a complex mix of a main fibre web that is bound together by the bi-component fibres. Although randomly distributed throughout, the proportions are typically set during the pre-manufacturing stage. Randomisation is important to a nonwoven for the individual fibres to stay bonded together.

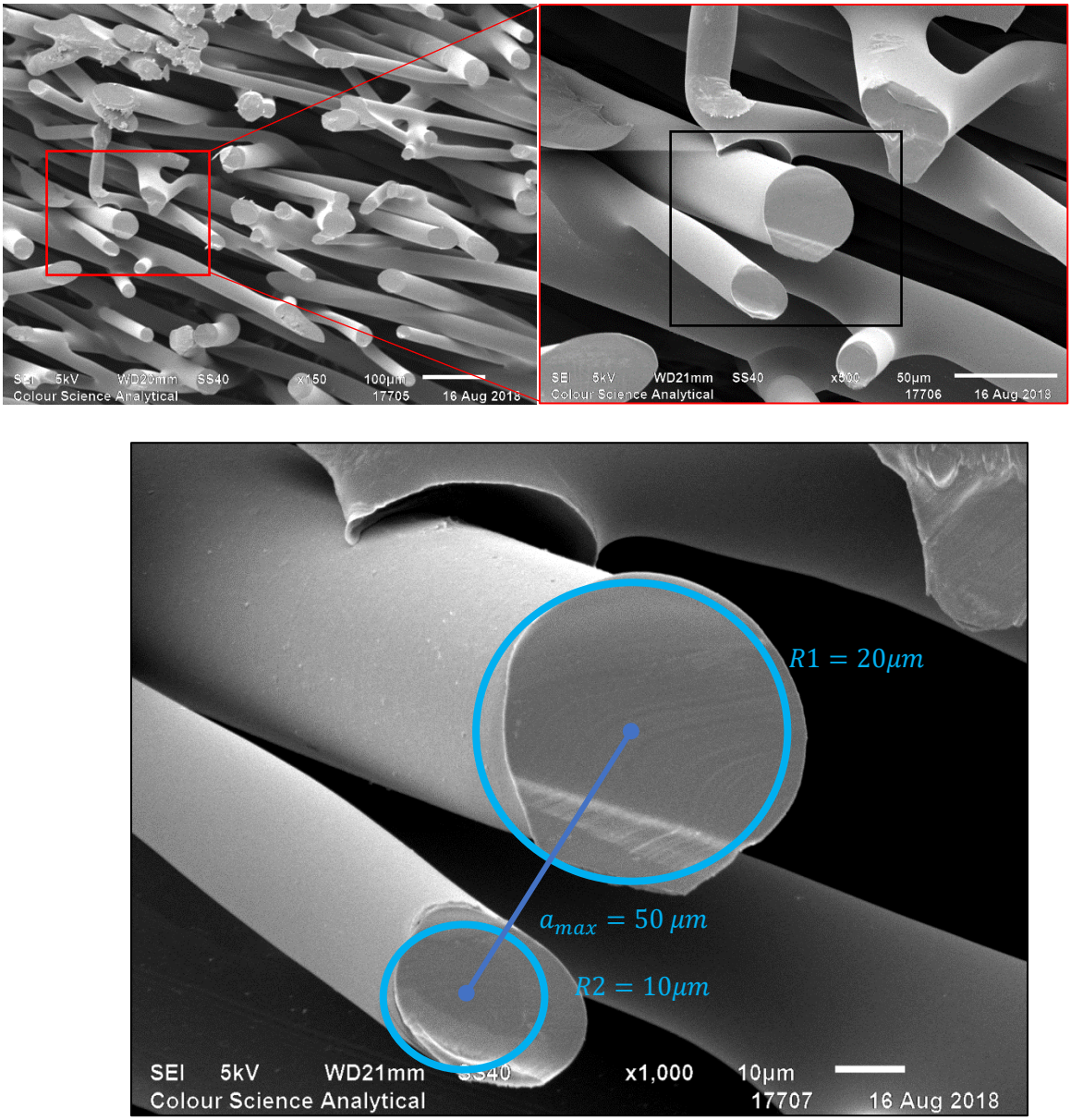

Figure 6.1.: SEM image of nonwoven sample at three scales of magnification (bottom) typical dimensions of fibres and inter fibre spacing

Figure 6.1. shows the cut-section of a nonwoven at magnifications from 150 to 1000 times zoom corresponding to a resolution size varying from 100 to 10 μm. The SEM images help to visualise the actual morphology of the sample, the dimensions, alignment, and proximity traits at the microscopic scale. This cannot always be appreciated at the macroscopic version or the bulk scale of a typical fibrous nonwoven material.

This study has been carried out using two powerful modelling techniques developed for the adjacent and expanded for staggered [73] alignments, forming the first two sections of this chapter. For both the study sets, initially the theoretical basis for the development of these models is discussed. As the chapter progresses, material properties shall be correlated, they shall be compared with the single (average) case that has been established in the previous chapter and ultimately, in the final section the acoustic influence on key parameters shall be assessed. As per the numerical model for Single fibre cell developed in the previous chapter, the models studied in this chapter have been examined on the basis of a fixed cell volume approach for understanding the parametric variations with respect to the fibre radius and the controlled porosity approach for the variations over a suitable range of porosities.

6.1. ADJACENT BI-DISPERSE FIBRE MODELS

For a typical adjacent alignment, there can be two possibilities based on the direction of the application of the external pressure gradient and fluid velocity. For this study, the pressure gradient has been applied along the y- direction. Hence, these alignments have been termed as

- Tandem Arrangement for vertically positioned cells, where the lower cell encounters the volume force first followed by the upper cell.
- Side-by-side Arrangement for horizontal cell orientation where both the sub-cells encounter the volume force simultaneously.

Theoretical basis for the development of this model has evolved from the single fibre cell derivation covered in the previous chapter. Further development of the HPM based model involves the consideration of two sub-cells comprising of cylindrical fibres, such that the common interface between the sub-cells shall be assigned continuity of velocity, pressure, and stress, while rest of the boundaries shall have the periodic boundary condition. For the case of this bi-disperse fibre arrangement, the equation sets are solved for each sub-cell individually and are then combined for the overall ‘super cell’ performance.

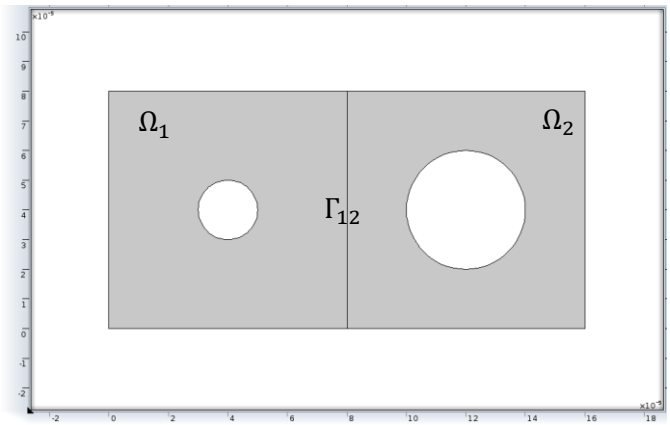

Figure 6.2.: REV with 2 sub-cells with unequal fibre cylinders of the bi-disperse fibre model

The Figure 6.2 shows the REV comprising of the bi-disperse fibre as visualised by COMSOL geometry. All treatments of the unit cell for this dual fibrous media will be applied to the sub-cells instead of the super cell. Accordingly, the sub-cell domains shall be referred by $\Omega_{1,2}$ and their common interface as Γ_{12}. Periodic boundary conditions are set for rest of the boundaries of the super cell.

The governing problem sets for these sub-domains are as follows

Stokes problems:

$$\eta \Delta \overrightarrow{v_1} - \nabla p_1 = 0 \qquad \text{in } \Omega_1 \qquad (6.1a)$$

$$\eta \Delta \overrightarrow{v_2} - \nabla p_2 = 0 \qquad \text{in } \Omega_2 \qquad (6.1b)$$

Continuity equations suggesting incompressibility:

$$\nabla . \overrightarrow{v_1} = 0 \qquad \text{in } \Omega_1 \qquad (6.2a)$$

$$\nabla . \overrightarrow{v_2} = 0 \qquad \text{in } \Omega_2 \qquad (6.2b)$$

No-Slip boundary conditions:

$$\overrightarrow{v_1} = 0 \qquad \text{on } \Gamma_1 \qquad (6.3a)$$

$$\overrightarrow{v_2} = 0 \qquad \text{on } \Gamma_2 \qquad (6.3b)$$

Considering the preferential direction along the y-axes, continuity condition shall be assigned to the vertical boundaries ($\Gamma_{v\pm}$) in terms of the pressure, normal velocity and stress, where $\pm$ indicates the sub-cells situated to the left and right in this case.

Common interface continuity condition:

$$(\overrightarrow{v_1} - \overrightarrow{v_2}).n = 0 \qquad \text{on } \Gamma_{v\pm} \qquad (6.4)$$

The horizontal boundaries shall have the periodic boundary conditions, while the interface Γ_{12} follows continuity of velocity, pressure, and stress. Applying the rescaled equations as used for single fibre case in the previous chapter (with $\nabla = \nabla_x + \varepsilon^{-1}\nabla_y$) and solving for the two indices indicates that $\nabla_y p_1^0 = 0$ and $\nabla_y p_2^0 = 0$. Hence it is assumed that $p^0(x) = p_1^0(x) = p_2^0(x)$. Thus, the problem equations (6.1 – 6.3) thus transform to

$$\eta\nabla_y^2\overrightarrow{v_1^0} - \nabla p_1^1 = \nabla_x p^0 \qquad \text{in } \Omega_1 \qquad (6.5a)$$

$$\eta\nabla_y^2\overrightarrow{v_2^0} - \nabla p_2^1 = \nabla_x p^0 \qquad \text{in } \Omega_2 \qquad (6.5b)$$

$$\nabla_y.\overrightarrow{v_1^0} = 0 \qquad \text{in } \Omega_1 \qquad (6.6a)$$

$$\nabla_y.\overrightarrow{v_2^0} = 0 \qquad \text{in } \Omega_2 \qquad (6.6b)$$

$$\overrightarrow{v_1} = 0 \qquad \text{on } \Gamma_1 \qquad (6.7a)$$

$$\overrightarrow{v_2} = 0 \qquad \text{on } \Gamma_2 \qquad (6.7b)$$

These set of equations are then solved to derive their variational formulation [75, 96]. This approach is also called as a weak formulation and is typically used as a discretisation strategy for boundary value problems.

This leads to a linear problem that is subjected to a volume force of macroscopic pressure gradient. The solution of which is then expressed as

$$\overrightarrow{v^0} = -\frac{k(y)}{\eta}.\nabla_x p^0 \tag{6.8}$$

$$p^1 = -\pi.\nabla_x p^0 + \tilde{p}^1(x) \tag{6.9}$$

where the velocity is defined as $\overrightarrow{v^0} = \overrightarrow{v_1^0} \in \Omega_{f1}$ and $\overrightarrow{v^0} = \overrightarrow{v_2^0} \in \Omega_{f2}$ and $\tilde{p}$ provides the pressure point constraint to the pressure equation.

The solution is used as a test field by applying to the weak formulation, then diving all through by $\Omega = \Omega_1 + \Omega_2$ for the volumetric fractions contributed by each sub-cell, $\varphi_1 = \frac{\Omega_1}{\Omega}$ and $\varphi_2 = \frac{\Omega_2}{\Omega}$ gives

$$\eta\left(\frac{\Omega_1}{\Omega}\frac{1}{\Omega_1}\int_{\Omega_{f1}}\left|\nabla_y\overrightarrow{v_1^0}\right|^2 d\Omega + \frac{\Omega_2}{\Omega}\frac{1}{\Omega_2}\int_{\Omega_{f2}}\left|\nabla_y\overrightarrow{v_2^0}\right|^2 d\Omega\right) = \nabla_x p^0.\frac{k}{\eta}.\nabla_x p^0 \tag{6.10}$$

$$\eta\left(\varphi_1\frac{1}{\Omega_1}\int_{\Omega_{f1}}\left|\nabla_y\overrightarrow{v_1^0}\right|^2 d\Omega + \varphi_2\frac{1}{\Omega_2}\int_{\Omega_{f2}}\left|\nabla_y\overrightarrow{v_2^0}\right|^2 d\Omega\right) = \nabla_x p^0.\frac{k}{\eta}.\nabla_x p^0 \tag{6.11}$$

The transport parameters can thus be formulated for the super cell by combining their individual weighted contributions as follows:

At the low frequency limit (LFL), the total viscous permeability can be computed based on the sub-cell permeabilities as

$$\kappa = \varphi_1\kappa_1 + \varphi_2\kappa_2 \qquad \text{LFL} \tag{6.12}$$

Similarly, at the high frequency limits (HFL), the high frequency tortuosity α_∞ and the viscous and thermal characteristic lengths (Λ, Λ') can be computed for the super cell as

$$\frac{\phi}{\alpha_\infty} = \frac{\varphi_1\phi_1}{\alpha_{\infty 1}} + \frac{\varphi_2\phi_2}{\alpha_{\infty 2}} \qquad \text{HFL} \tag{6.13}$$

$$\Lambda = \frac{S_1}{S}\Lambda_1 + \frac{S_2}{S}\Lambda_2 \qquad \text{HFL} \qquad (6.14)$$

$$\Lambda' = 2\frac{V}{S} = \frac{S_1}{S}\Lambda'_1 + \frac{S_2}{S}\Lambda'_2 \qquad \text{HFL} \qquad (6.15)$$

At this theoretical stage, it is important to note that the result obtained for the super cell is a combined effect of not only the pressure, velocity and stress variation within the individual sub-cells but also involve the influence of one sub-cell over the other. It is difficult to calculate this aspect by theory. For instance, the problem shall have an exact solution when the velocities in the sub-cell are considered to not interfere with one another for situations where the common interface was treated as an impermeable wall. However, in fibrous model under consideration, this is not the case and the $\overrightarrow{v_1^0}$ shall affect $\overrightarrow{v_2^0}$. To best assess this situation, the numerical studies that follow shall be useful.

The above enlisted formulations shall be used to obtain the effective properties of the bi-disperse medium with an aim of providing further understanding of how such materials behave than what has been established in the single fibre cell models. The numerical study has been carried out using COMSOL 5.5 software and has looked at generic fibre radii within sub-cells. To lead the way from a single fibre cell approach, the models have looked as fibres of equal diameter that was initiated as a cell repetition study in the previous chapter. This is followed by unequal diameter models that drive the attention to replicating real samples.

1. 2 cylindrical fibres of equal diameter

Visualising a bi-disperse fibre model from an adjacent cell approach, can be seen from the tandem (vertical arrangement) versus side-by-side (horizontal arrangement) as detailed above. This part of the adjacency study looks at both fibres having equal diameters. Generic fibre radii selected for this study are same as the single fibre cell study, ($r_{1,2} = 1, 5, 10, 15, 20, 25\ \mu m$). It is important to validate the duplication of single cell approach from various aspects, particularly in terms of how the pressure and velocity interacts with the fibre and between the two sub-cells. Developing this understanding of the cell provides a control point to compare with the unequal diameters or cases handling realistic fibre dimensions.

Figures 6.3, 6.4 show symmetric replication of the velocity and pressure magnitudes for each sub-cell comprising of the fibre radius of 15 μm. The REV super cell is equally split into two sub-cells based on a fixed cell volume. This fixes the overall porosity which is contributed by both the sub-cells. The arrows in the velocity magnitude plots indicate the y- directional application of the volume force. It is evident that for tandem and side-by-side configurations, their orientations impact the sub-cells in the way they encounter the externally applied pressure gradient. It also observed that there is uniformity in the magnitudes validating the continuity at the common interface and periodicity at the super cell boundaries.

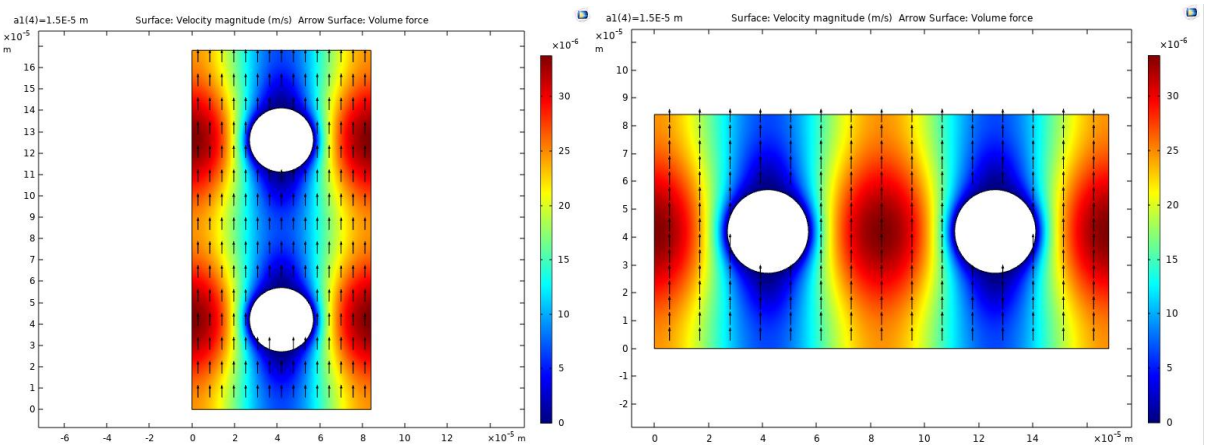

Figure 6.3.: Velocity magnitude (arrow – volume force) for a) tandem b) side-by-side

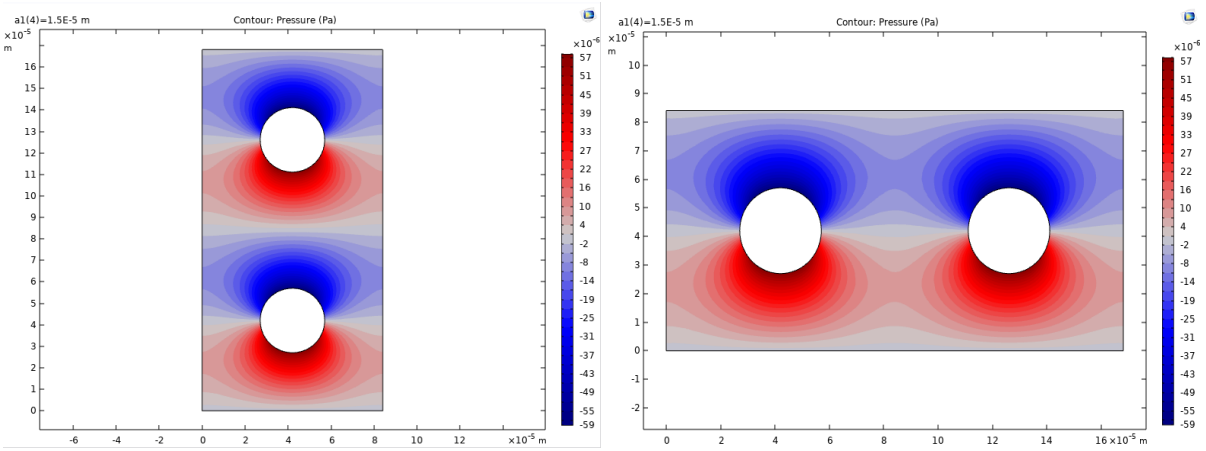

Figure 6.4.: Pressure contours for a) tandem b) side-by-side

In the next pair of Figures 6.5, the x- and y- components of velocity field have been presented for the tandem case on the top and side-by-side orientation at the bottom of the figure sub-divisions. The effects of orientating the sub-cells can be observed for both the components.

The preferential direction being along the y- axis indicates the overall magnitude to replicate the y- component case. Again, the symmetry can be observed between each sub-cell. This is also true for the velocity components obtained from the models computed at HFL as seen in Figure 6.7.

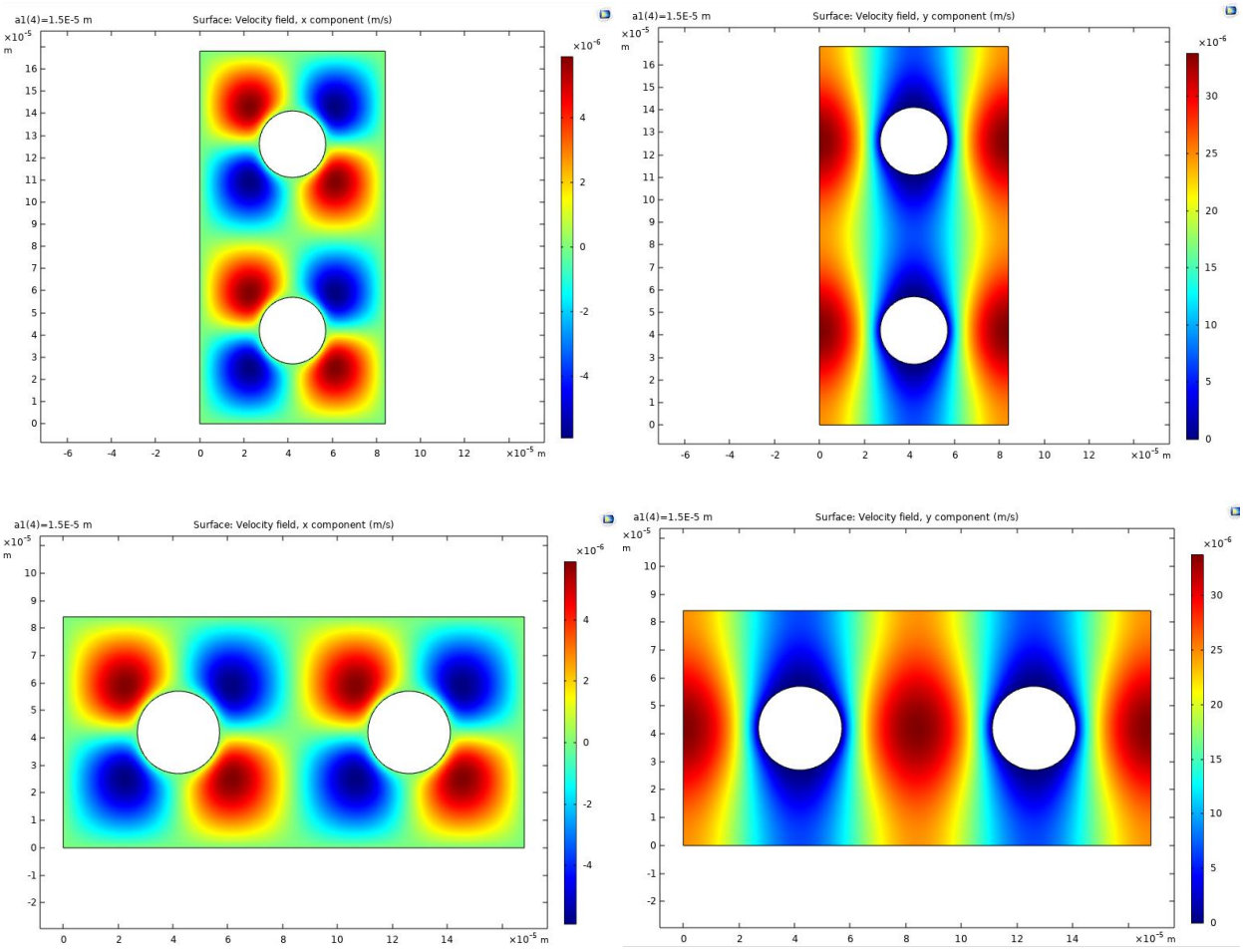

Figure 6.5.: x and y components of velocity field for tandem (top) side-by-side (bottom)– LFL

An observation from comparing the vorticity magnitude plots in Figure 6.6 can be made. For the side-by-side (horizontal arrangement) case, the vorticity tends to zero at the common interface which is not the case of the tandem case due to its orientation. The estimating condition of zero vorticity discussed in the previous chapter would apply to the super cell but not to all cases of the adjacent alignment situations. The choice of orientation would be critical to identify the impact.

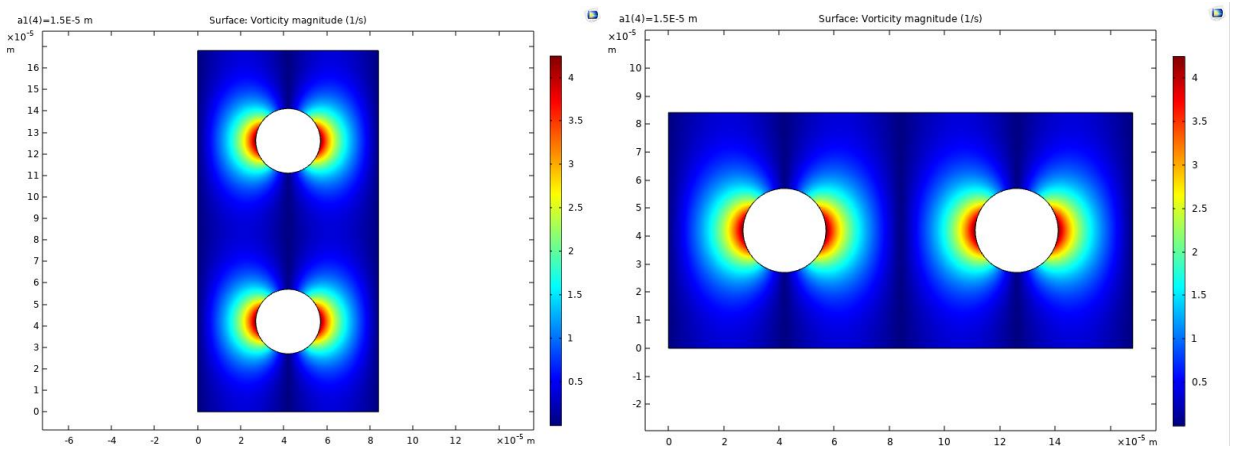

Figure 6.6.: Vorticity magnitude a) tandem b) side-by-side

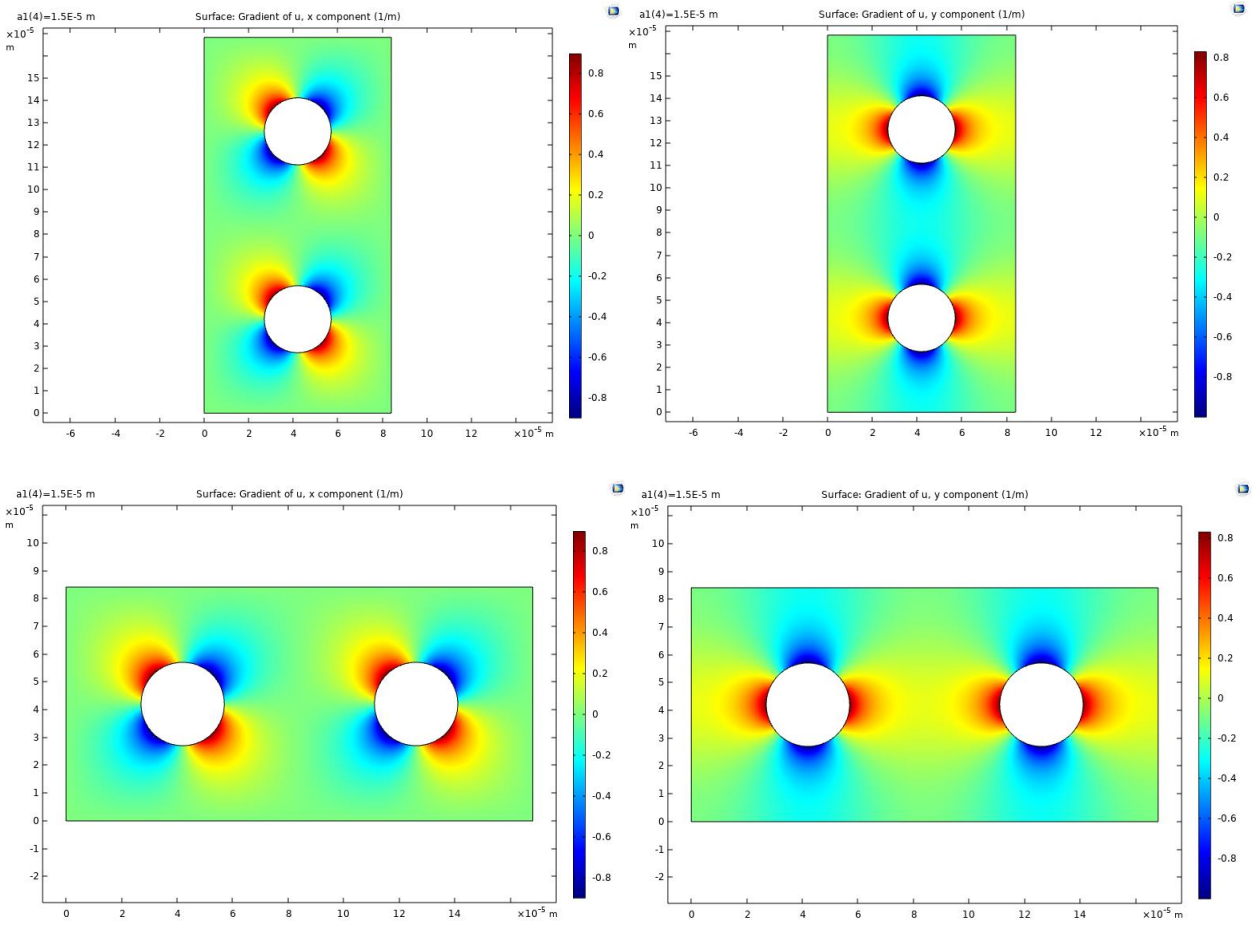

Figure 6.7.: x and y components of velocity field for tandem (top) side-by-side (bottom)– HFL

2. 2 cylindrical fibres of unequal diameter

Progressing from the equal diameter case, the range of fibre radii have been kept the same in this study. The impact of considering different fibre types based on their size have been studied for two sets from the generic radii range ($r_{1,2} = 1, 5, 10, 15, 20, 25\ \mu m$) as adopted for the equal diameter selection. The fixed radius is however taken as 12.5 μm which falls in between the 10 and 15 μm of the range. Keeping this fibre value fixed, the lower (in case of the tandem arrangement) and the left (in case of the side-by-side arrangement) is varied for comparison.

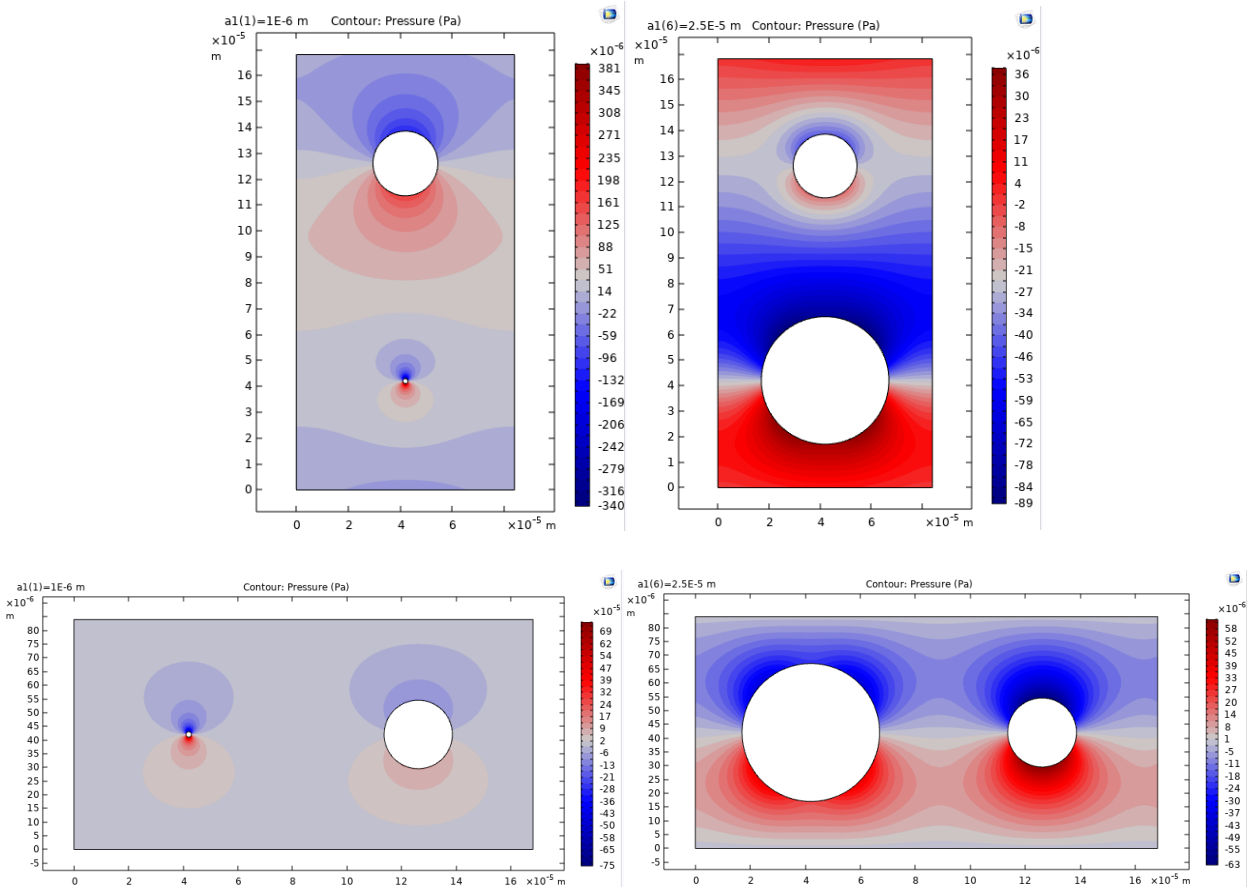

Figure 6.8.: Pressure contours for tandem (top) side-by-side (bottom) unequal diameter sub-cells

The pressure component trends shown in Figure 6.8 depict a striking difference between the equal diameter cases and the dissimilar diameter fibres. The prominent distinctions are seen between the tandem and side-by-side cell orientations. With application of the y- direction pressure gradient, the upper sub-cell is now influenced by the lower sub-cell content for the tandem case. On the

other hand, the symmetricity is intact for the side-by-side located sub-cells as both the cells intercept the volume force simultaneously.

Comparing the tandem and side-by-side cases again for the x- and y- velocity coefficients as seen in Figures 6.9 and 6.10 respectively, it can be noticed that none of the sub-cells have the same velocity profiles. For the tandem arranged sub-cells, the diameter of the lower fibre has a strong influence on the velocity field of the upper cell.

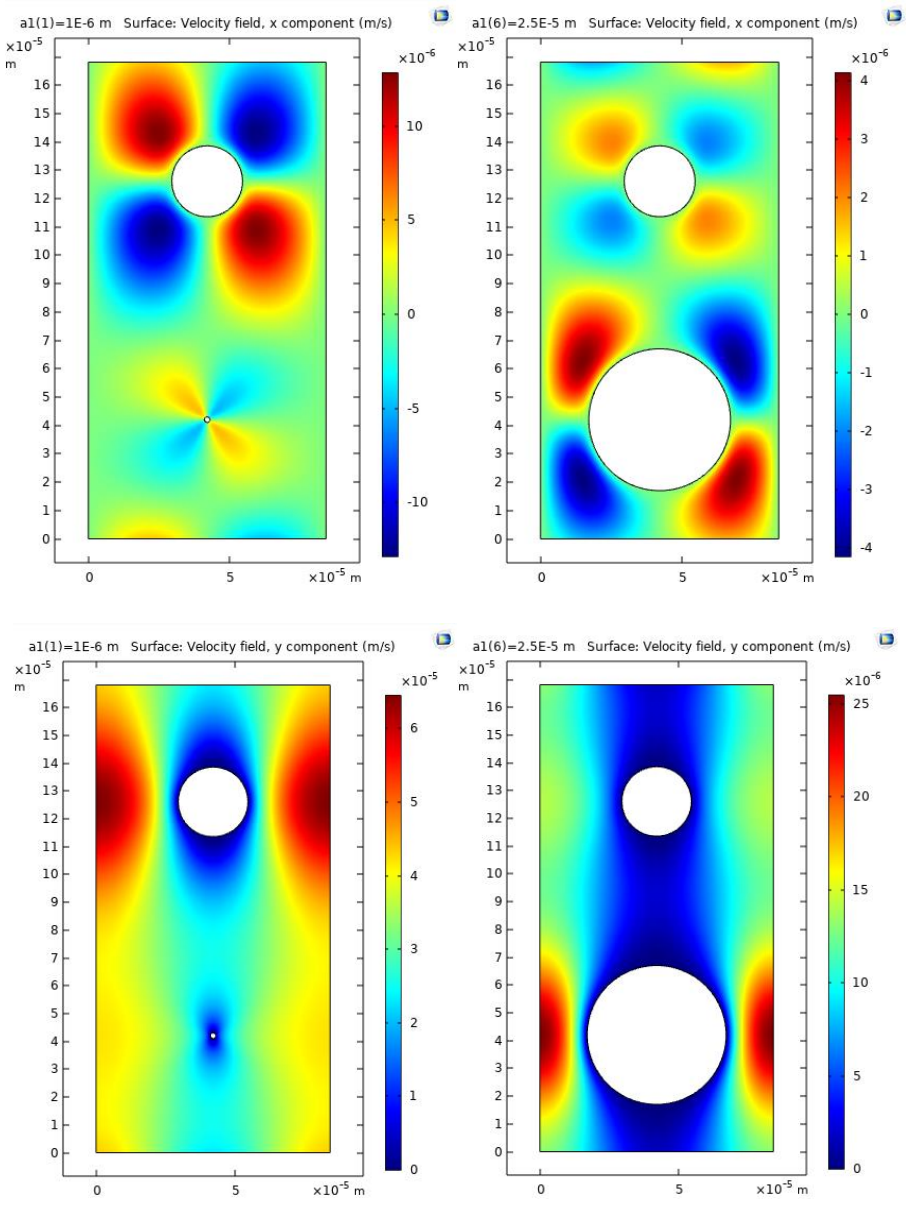

Figure 6.9.: x- and y- components of velocity field – LFL for tandem unequal diameter sub-cells

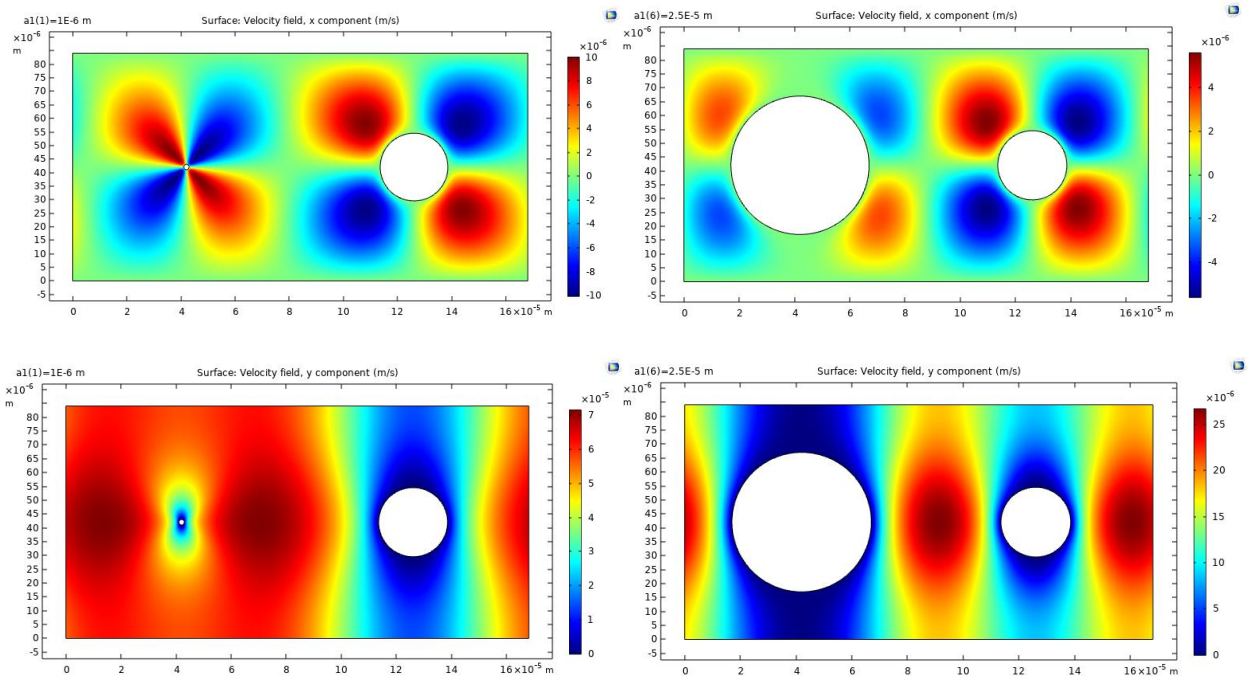

Figure 6.10.: x- and y- components of velocity field – LFL for side-by-side unequal diameter sub-cells

In case of the side-by-side arrangement, although the flow is perceived along the y-axis, the field is dominated by the dissimilar fibre dimension. Comparing the two y- component velocity graphics for this horizontal orientation, the velocity field around the same diameter (right sub-cell) is affected by the field resulting from the left sub-cell.

Similar observations can be made from the vorticity magnitude as in Figure 6.11 sub-plots. It is noted that if the fibre is too small, implying that the porosity is very high, indicates that the local sub-cell vorticity effects are very low. This in comparison to the large fibre, the effects are very dramatic affecting the adjacent cell as noticed from the super cells comprising of the large 25 μm radius fibres that nearly fill up the sub-cell space.

This trend is replicated at the HFL cases that show the influence on the velocity components, quite noticeably from that of the tandem type. This is noted from Figure 6.12 for tandem orientation and from Figure 6.13 for side-by-side orientations.

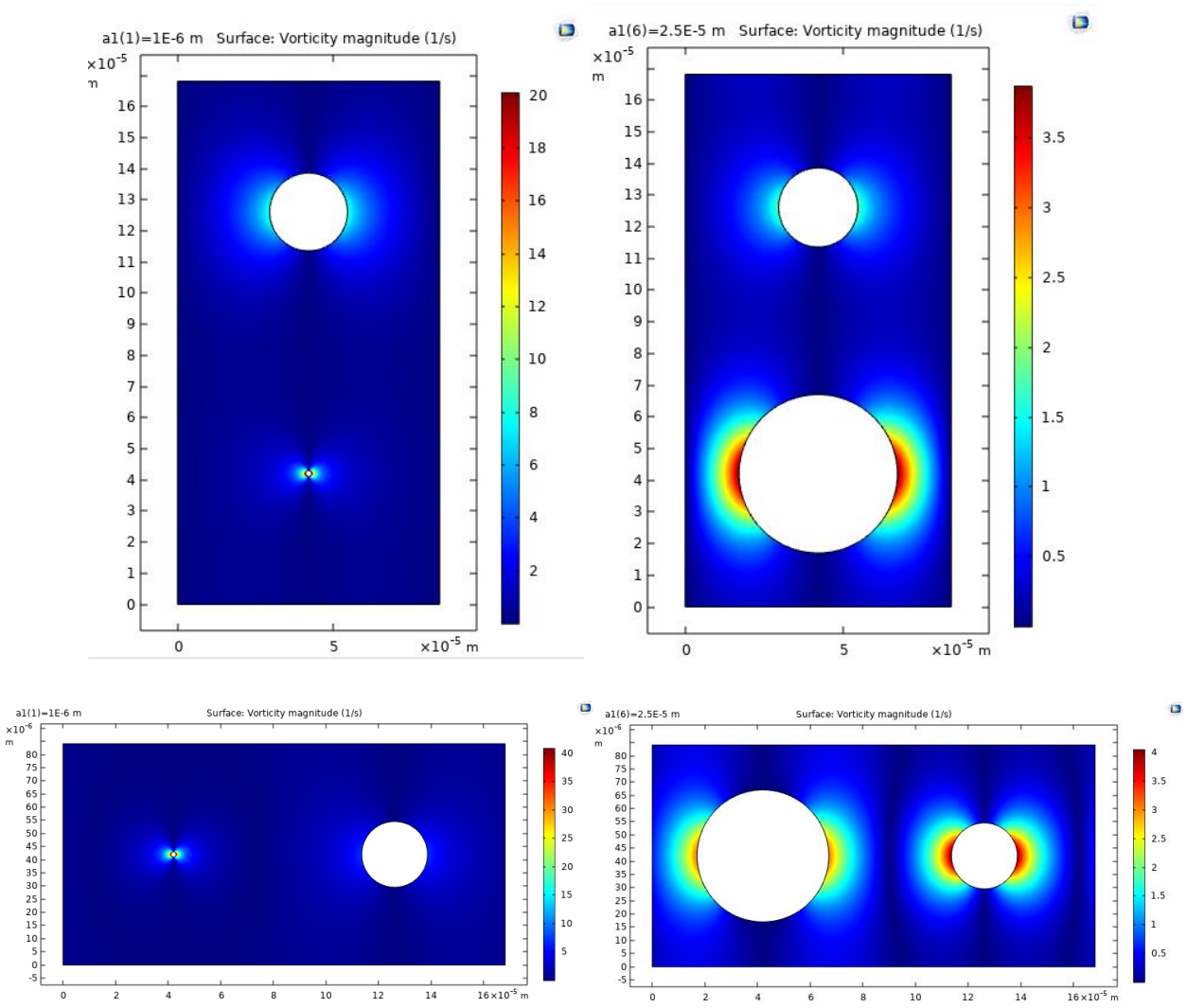

Figure 6.11.: Vorticity magnitude for tandem (top) side-by-side (bottom) unequal diameter sub-cells

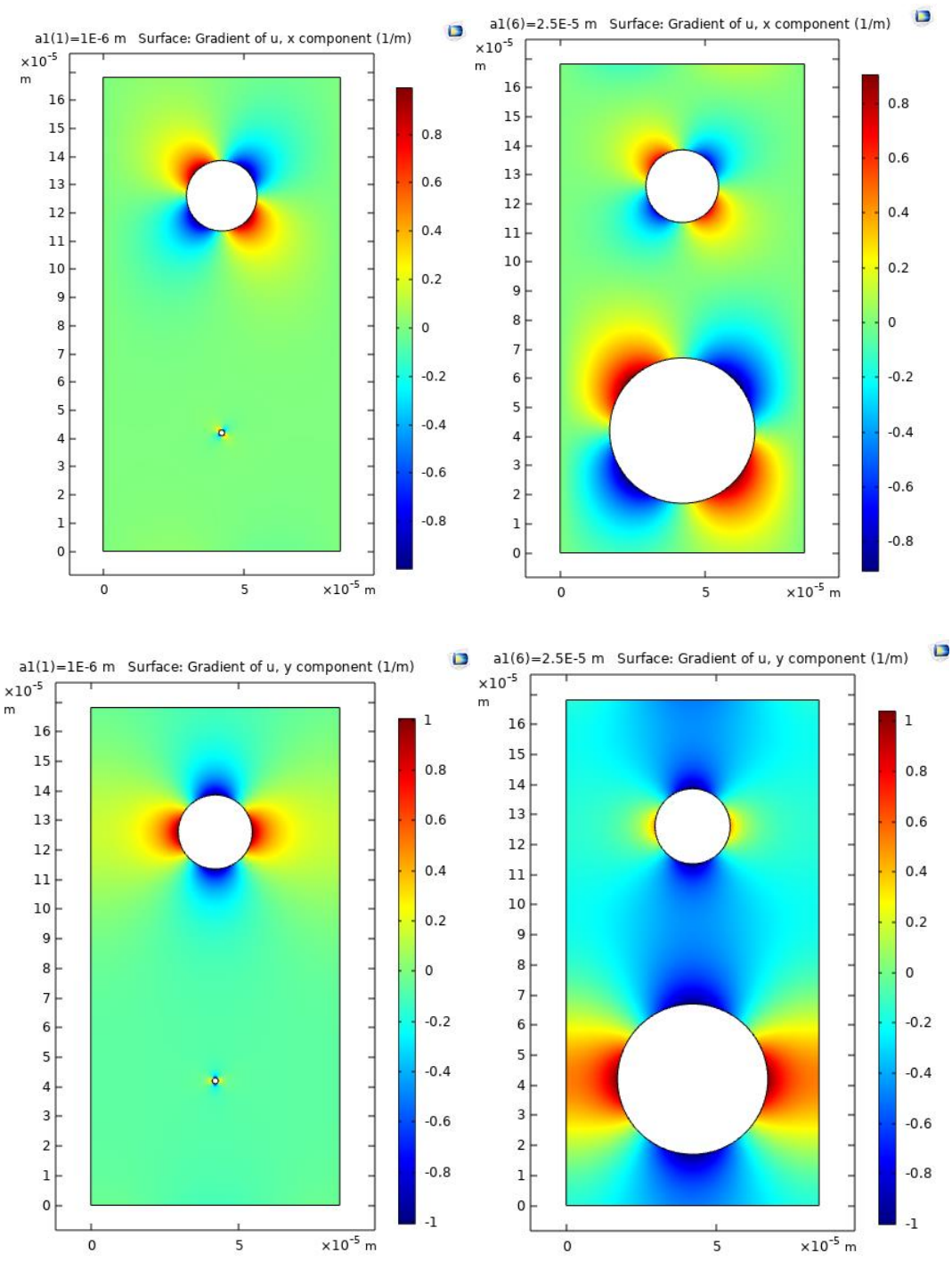

Figure 6.12.: x- and y- components of velocity field – HFL for tandem unequal diameter sub-cells

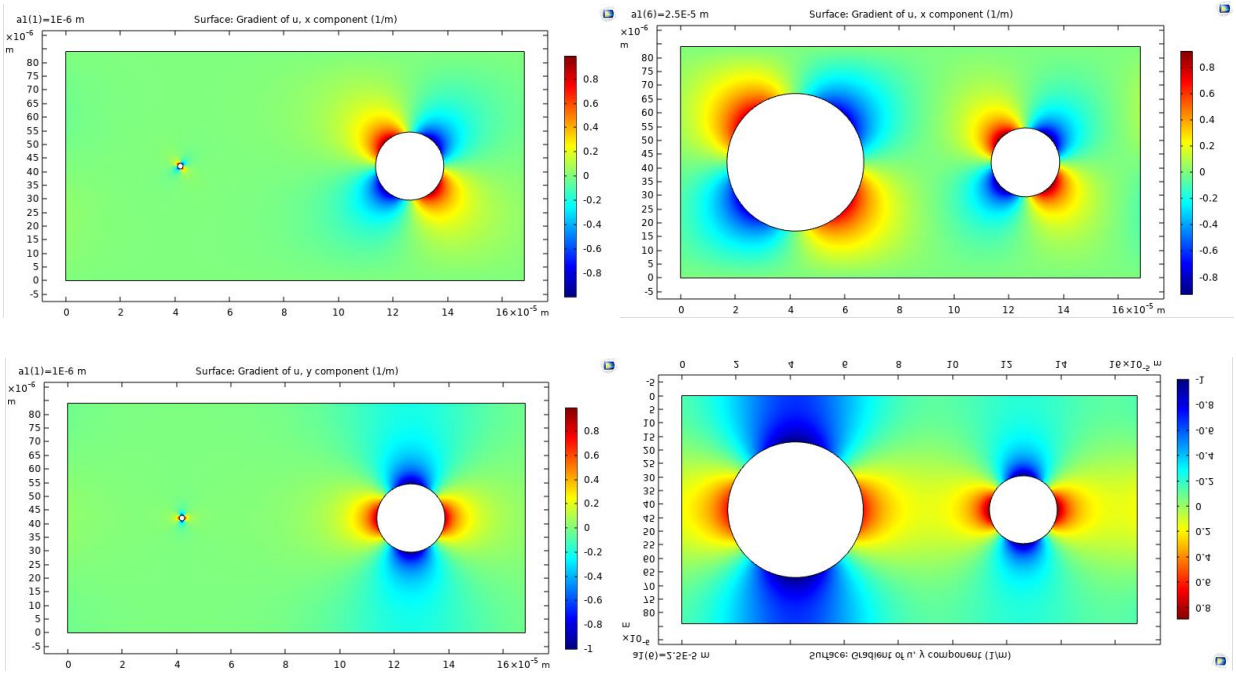

Figure 6.13.: x- and y- components of velocity field – HFL for side-by-side unequal diameter sub-cells

6.2. STAGGERED BI-DISPERSE FIBRE MODELS

The staggered bi-disperse or dual fibre case has been mentioned as the hybrid method from the Benchmarks paper as elaborated in the reference paper [73]. The cell development and description has been well elaborated in the paper. In this section, a parametric approach has been applied to a similar orientation of a bi-disperse case-based numerical model. The dimensions of the overall cell are fixed as per the supercell volume coverage in the models studied earlier. This is done to maintain consistency in the comparisons. First set of variations have been carried out to assess the variations in transport parameters over fibre radius values. Then the trends have been presented for particular radius for typical porosity values. Like the adjacent cases, this section shall deal with staggered case where two sets of outcomes are observed:

1. Dual fibre model with equal fibres
2. Dual fibre models with unequal fibres

For the equal fibre dimension cases, the fixed fibre radius of 15μm has been used. These have been located in the cell bearing diagonal symmetry. As per the models covered in the sections above, the radii for the unequal diameter cases are taken as 12.5 μm for the fixed fibre and 1μm as the lower end of the range to 25 μm as the upper range of the other unequal fibre pair radius.

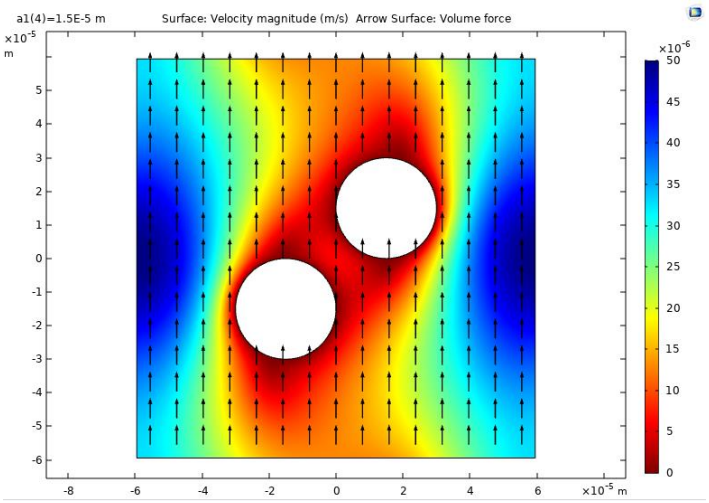

Figure 6.14.: Velocity magnitude (arrow – volume force) for staggered equal diameter cell

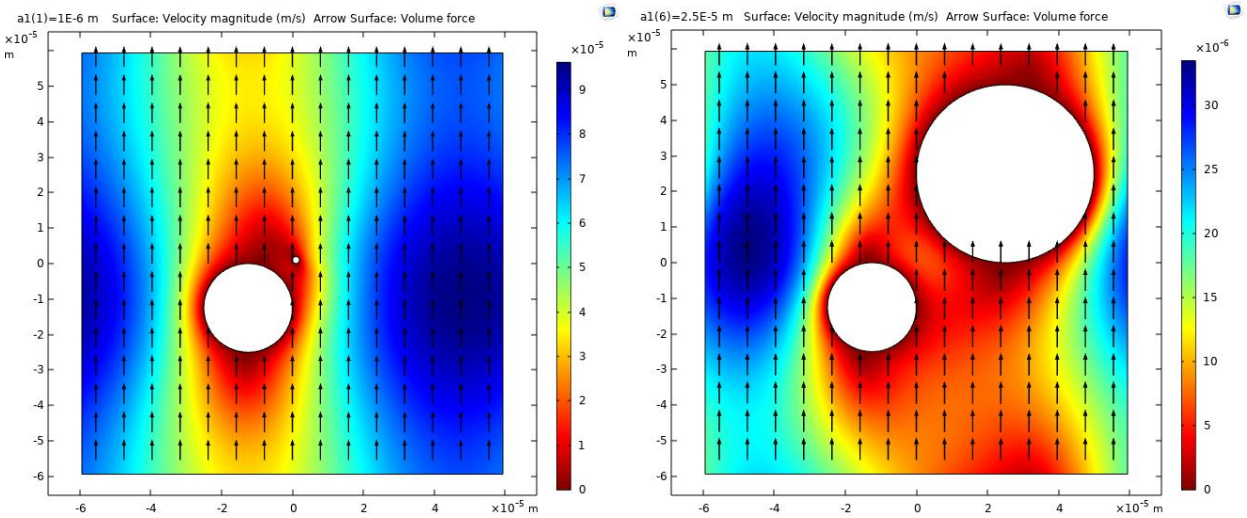

Figure 6.15.: Velocity magnitude (arrow – volume force) for staggered unequal diameter cells

Figure 6.14 shows uniform velocity magnitude for the equal case. This can be compared visually with the velocity magnitudes obtained for the unequal staggered case of fibres as shown in the Figure 6.15 plots. It can be noted that there is a strong impact on not only the placement of the secondary varying fibre but equally on the change in the velocity field.

A similar trend is observed for the pressure contours as seen from the Figures 6.16 and 6.17. Although not as much variation from the equal case, but when one of the fibres is extremely minute alongside the fixed fibre, the influence appears to be dominated by the larger of the two fibres.

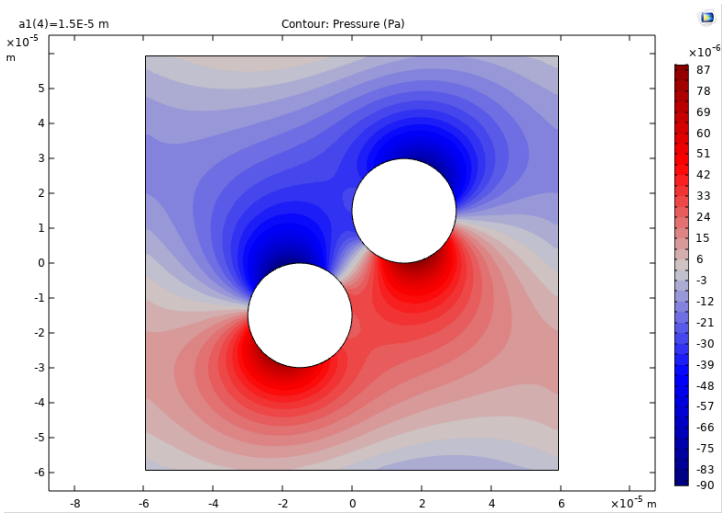

Figure 6.16.: Pressure contour for staggered equal diameter cell

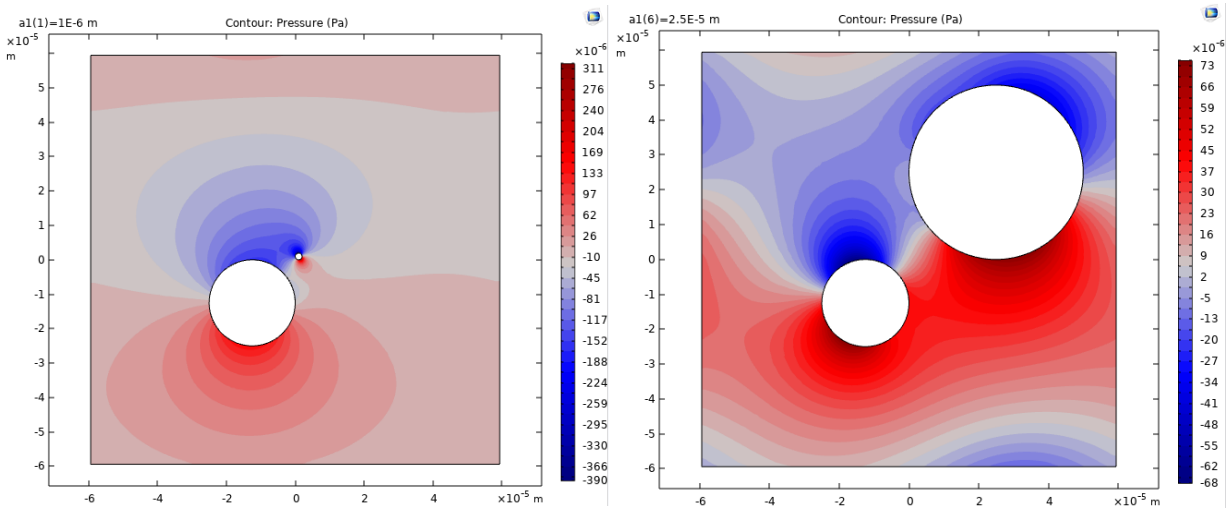

Figure 6.17.: Pressure contour for staggered unequal diameter cells

Vorticity magnitude plots in Figures 6.18 and 6.19 can be compared to demonstrate that the even distribution within the REV cell can be achieved by the symmetric model is disturbed for the unequal fibre radii. Particularly the larger end of fibre radii has a stronger impact on the magnitude adjacent to the cell boundaries.

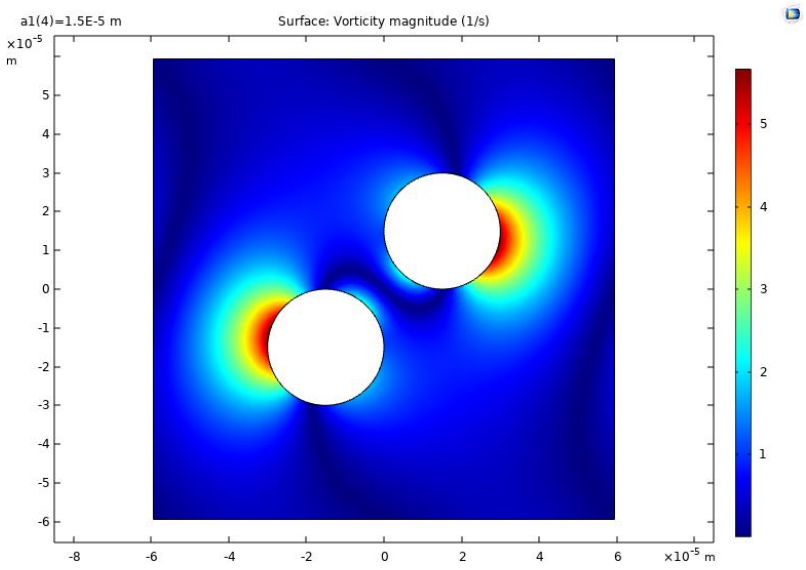

Figure 6.18.: Vorticity magnitude for staggered equal diameter cell

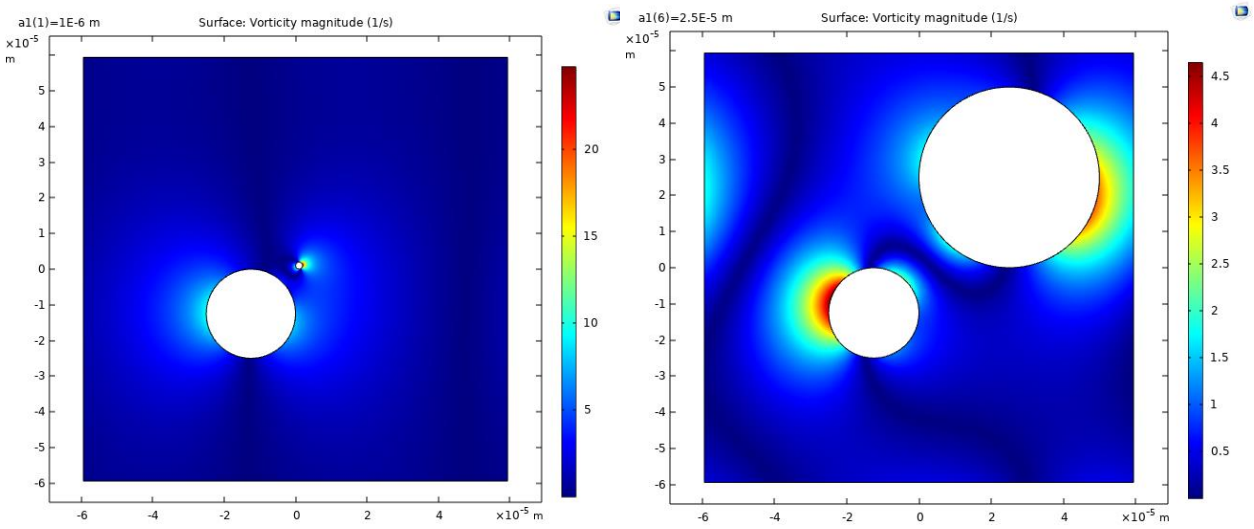

Figure 6.19.: Vorticity magnitude for staggered unequal diameter cells

Finally, a comparison between the key features of the transport parameters has been made between the two configurations of adjacent and staggered alignments to understand the variations between equal and unequal diametric variations for the dual fibres. The viscous permeability has been plotted for the six cases in Figures 6.20 and 6.21. The equal diameter cases for the adjacent type models coincide for all combinations of radii. The staggered arrangement has higher permeability values for smaller radii than adjacent models. At HFL, all the equal radii models perform like each other. The unequal case shows slight deviations for the larger fibre radii in the case of tortuosity.

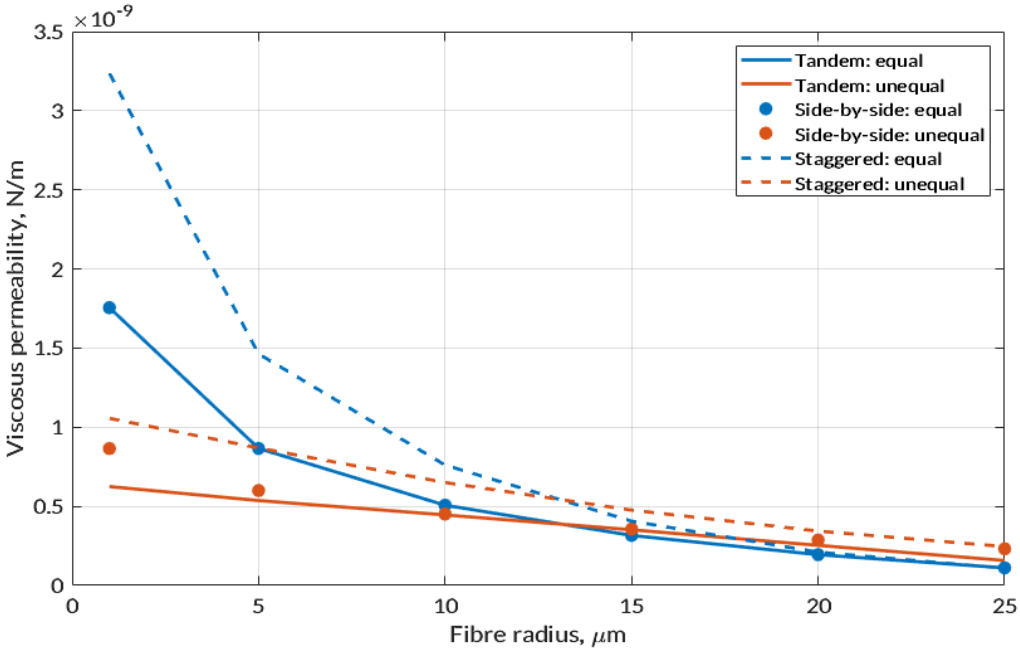

Figure 6.20.: Permeability comparison for bi-disperse models against fibre radius

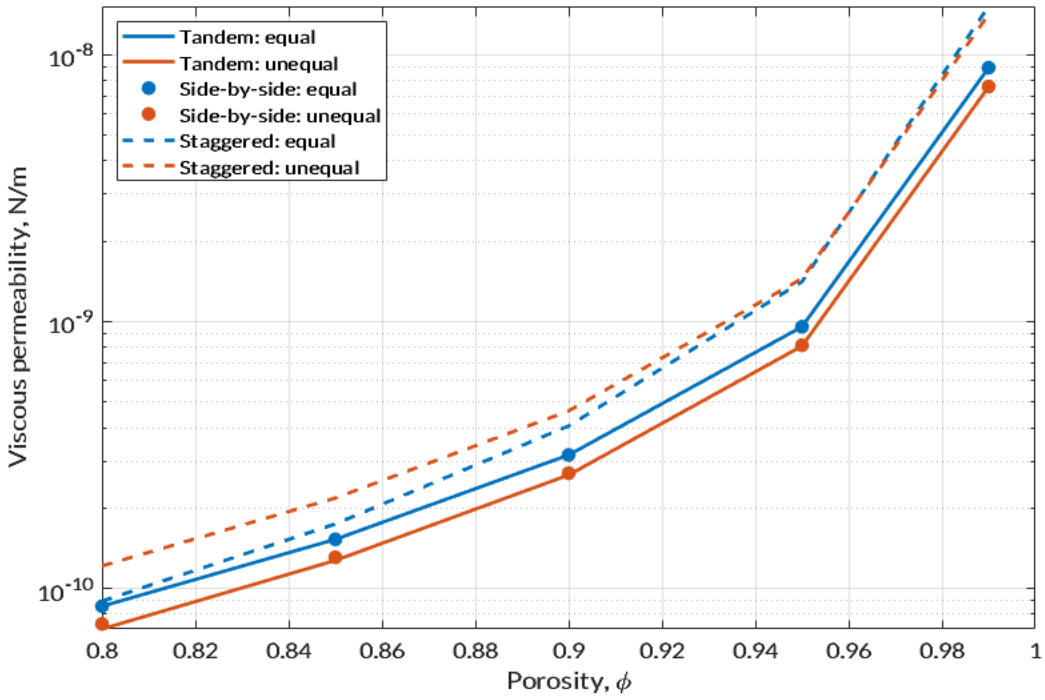

Figure 6.21.: Permeability comparison for bi-disperse models against porosity

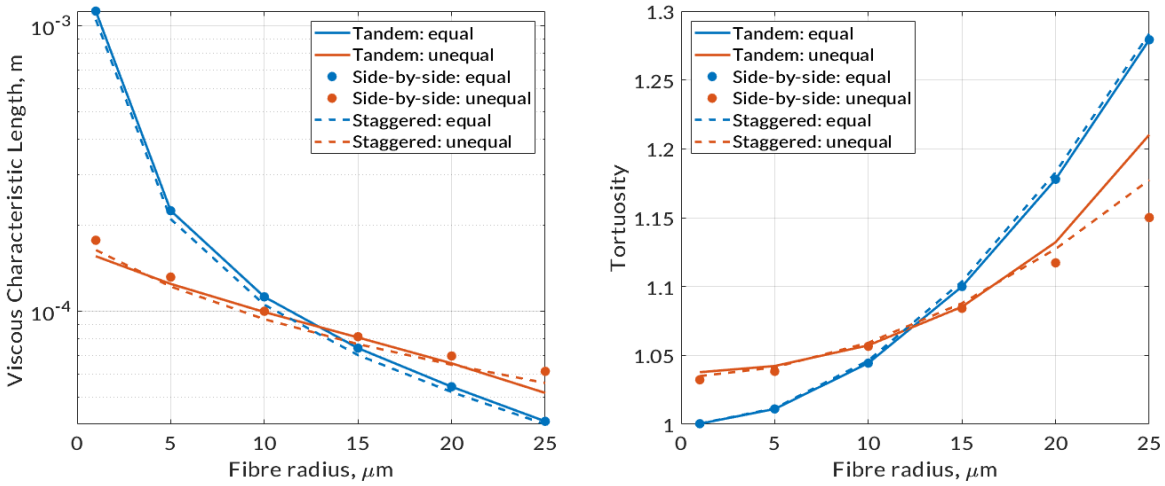

Figure 6.22.: a) Viscous characteristic length b) tortuosity for bi-disperse models against porosity

The characteristic lengths seen in Figure 6.22 follow similar trend with a is significant variation between equal and unequal cases indicating that by introducing a secondary fibre type, of different radius than the staple variety in a cell influences every transport parameter to a certain extent.

6.3. ACOUSTIC INFLUENCE OF KEY PARAMETERS

It is true that the effective properties of a porous fibrous material constitute the most essential aspects that define the understanding of its acoustic behaviour. Gathering some learning from the textile-based approach to replicate nonwovens, there are yet some non-acoustic parameters that can have an important role in their performance. Few of these properties have been identified in empirically or theoretically as intermediates to the formulation of governing equations. The focus of this part of the study is to highlight these key parameters.

Anisotropy

Earlier in this chapter a broad classification as made to segregate and understand the impact of two types of arrangements applicable for bi-disperse models, viz., the adjacent and the staggered arrangements. A comparison between these types has been considered imperative as they fundamentally contribute to the planar anisotropy concept. The study of variation in the orientation of fibres within an REV cell corresponds to the influence of geometrically induced anisotropy.

It can be noted that for each type of the arrangement itself, the fibres are aligned along either the central axis (as in the case of the adjacent orientation) and along the diagonal (for the staggered orientation). Hence, further intentional anisotropy can be introduced by offsetting the perfectly aligned fibres with reference to the centre or from the external boundaries of the REV cell. This aspect has been covered in the Benchmarks paper [73] where the fibres are placed at a predefined vertical and horizontal distance from the centre of the square cell, such that the vertical and horizontal spacings are not equal.

An instance of the variation in velocity magnitude with and without the diagonal symmetry is as plotted in Figure 6.23 below.

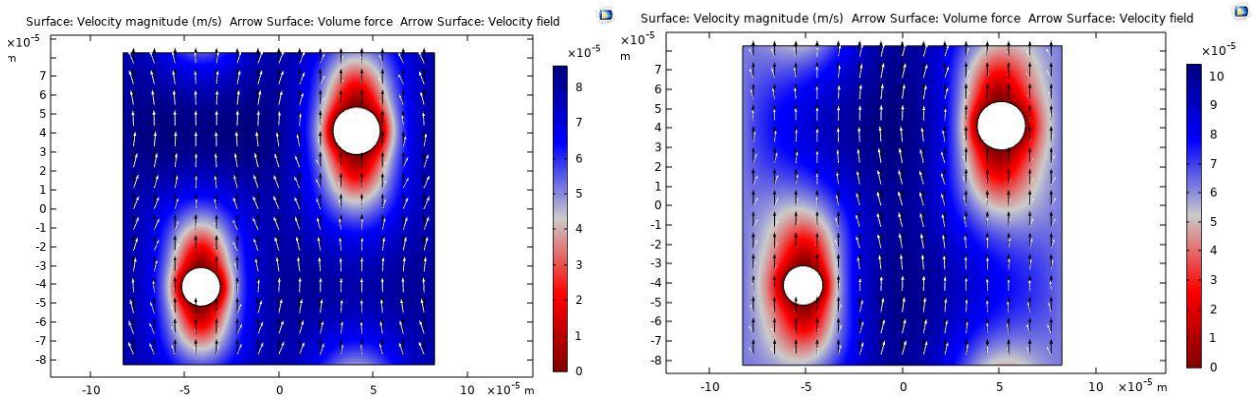

Figure 6.23.: PES7 staggered model arrangement a) symmetric b) asymmetric

Inter-fibre spacing

For all the numerical models a constant inter-fibre spacing value is assumed. However, there is a range of gaps that are generated as result of the randomness of the nonwoven binding process. This can be visualised and obtained by analysing cross-sectional SEM images of a sample. It is essential to note that this spacing is taken in the depth-wise orientation and is a result of the nonwoven web layers held together by the few binding fibres at orientations other than within the web itself. More importantly, inter-fibre spacing is a different parameter to the pore size distribution within nonwoven fibres that is generally considered on lateral plane of fabric's web. This parameter has been introduced in the analytical section previously and links to the solidity C factor of the fibres.

Referring to the PES sample-based REV cell, the main fibre arrangement has been varied to maintain the same positioning but at different spacing, *D* from the bico-fibre. Plots of velocity magnitude in Figure 6.24 and pressure in Figure 6.25 both show the striking impact of this variation. The vorticity magnitude as in Figure 6.26 shows how the compact placement of fibres leads to lower tending to zero vorticity around the cell boundary. The proximity, however, raises the vorticity in the region of the fibres themselves showing a variation in the fields.

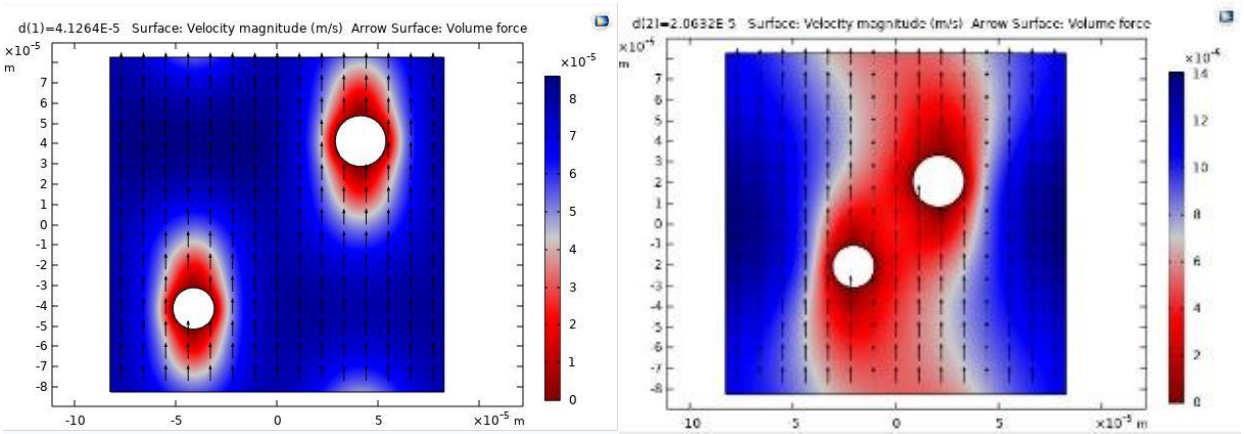

Figure 6.24.: Velocity magnitude variation with change in inter-fibre spacing for PES7 dual fibre case

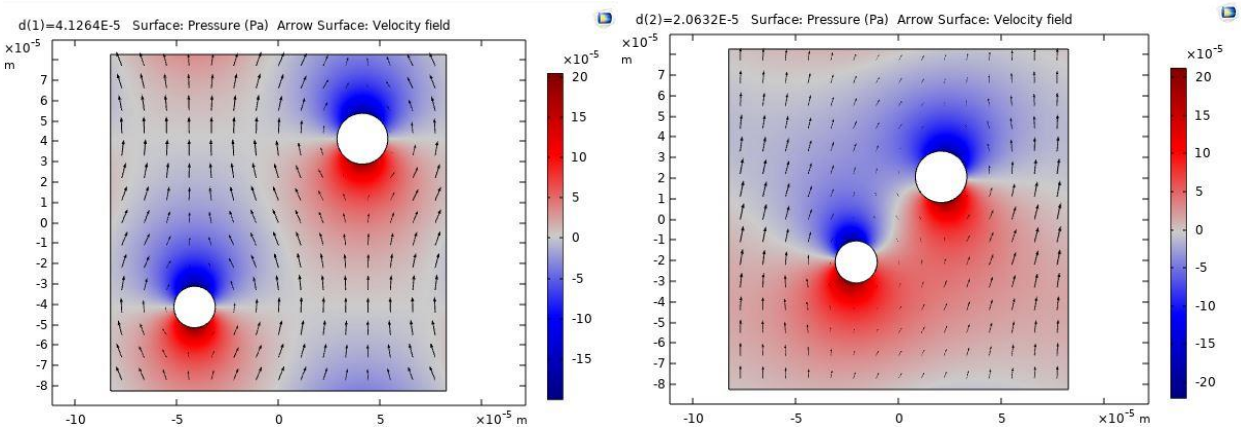

Figure 6.25.: Pressure variation with change in inter-fibre spacing for PES7 dual fibre case

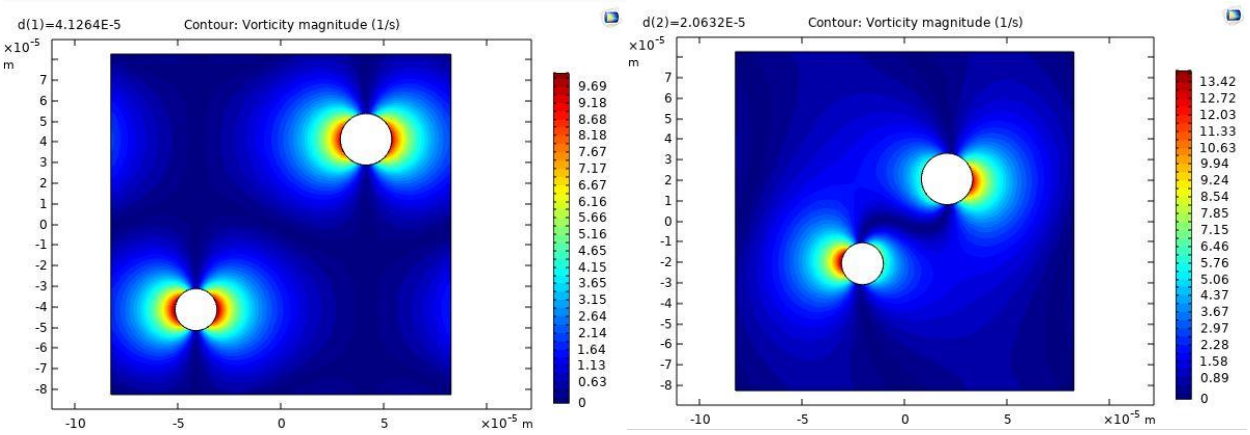

Figure 6.26.: Vorticity magnitude variation with change in inter-fibre spacing for PES7 dual fibre case

From the SEM images in Figure 6.1, not all fibres are spaced apart from one another. There are several instances where spacing is negligible and occasions where the binding process fuses the fibres causing them to intersect at junctions creating overlapping cross-sections. Touching fibres have been studied to understand the impact of the nonwoven fabrication process of binding planes of fibres. Magnitudes of velocity and pressure in Figure 6.27 and vorticity in Figure 6.28 have been plotted for PES7 based staggered model which can be compared with the plots that show inter-fibre spacing.

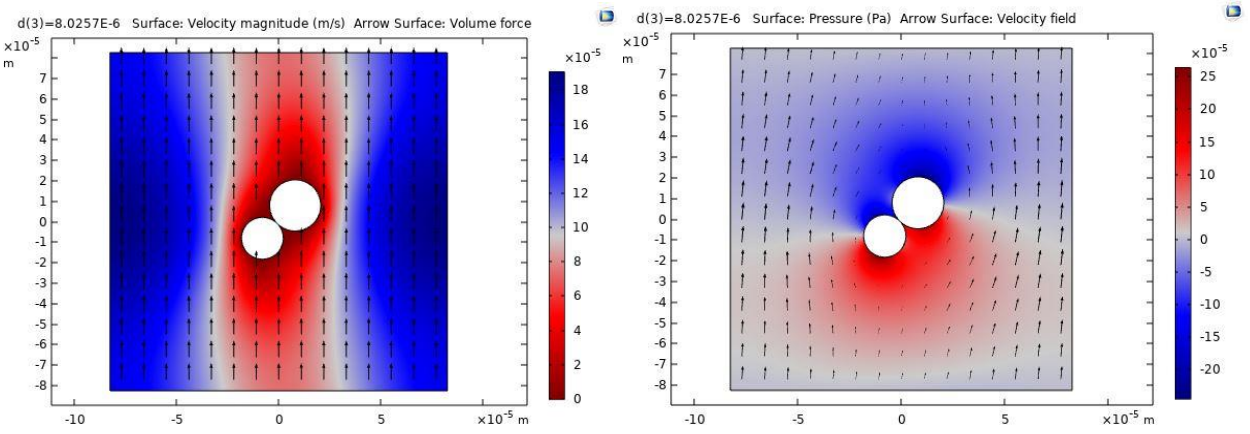

Figure 6.27.: Velocity and pressure plots for touching fibres of PES7 dual fibre case

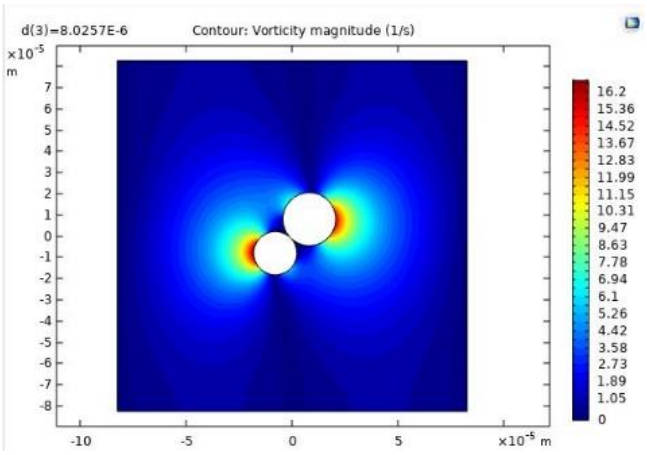

Figure 6.28.: Vorticity magnitude plot for touching fibres of PES7 dual fibre case

The results obtained for the three spacing trials has been tabulated in Table 6.1. It is noted that the closer the fibres, the resistance to the airflow reduces. Using the Daleny-Bazley-Miki model a correlation has been made to perceive the impact of this parameter.

Table 6.1.: Results of transport parameters for three spacing conditions of staggered configuration

Spacing	Permeability	AFR	Tortuosity	VCL	TCL
D/4	1.17E-09	15546	1.03	1.91E-04	3.71E-04
D/8	1.41E-09	12926	1.0301	1.90E-04	3.71E-04
touching	2.10E-09	8677.6	1.0434	1.25E-05	3.71E-04

From the absorption characteristics shown in Figure 6.29, not much variation is observed when the two fibres tend to come closer. However, the touching fibres lowers the overall trend by 5% across the mid-high frequency ranges. This is considered as the maximum possible fall in the absorption capability as far as inter-fibre spacing is concerned.

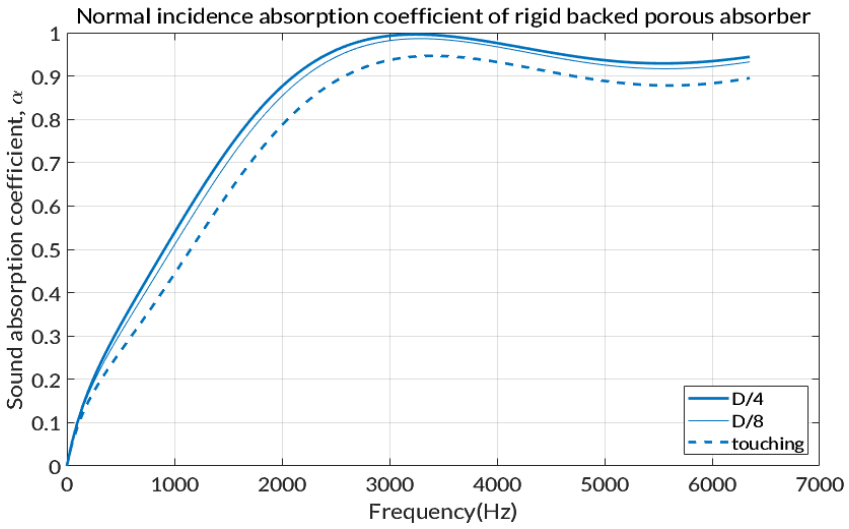

Figure 6.29.: Sound absorption variation with change in inter-fibre spacing for PES7 dual fibre case

Blend ratio

While deriving solutions to the bi-disperse adjacent arrangement case, the weighted averaged values of the individual sub-cells had been calculated to combine the individual contributions of the sub-cells to obtain the properties for the so-called supercell. The weighting corresponds to the volume fraction occupied by each sub-cell. Unless it is the fluid occupied regions, each sub-cell would normally occupy exactly half of the supercell. The fluid portions would be governed by the dimension of the fibre within the sub-cell. On a similar note, there has been a mention of the weighted fractions for the fibre content of a nonwoven mix. Here there is a direct reference to the solid phase component of the material. This is known to account for the blend ratio, which needs to be translated in the form of fibre diameter changes for a bi-disperse case. However, this may not imply an exact representation of the fibrous material. Hence, these is a need to seek a better approach to replicate the properties of the complex nonwoven material.

Chapter 7

ACOUSTICS OF FIBRE CLUSTER MODELS

Overview:

7.1.Symmetric multi-fibre models

7.2.Asymmetric multi-fibre models

7.3.Acoustic influence of key parameters

In the previous chapter the limitations of representing the dual fibre blended nonwoven materials have been identified. In this chapter, fibres have been studied as clusters. These clusters have been formed considering a least common multiple (LCM) based approach. As the clusters are developed for multi-disperse fibrous media, numerical models have been developed. This has been considered as a better approach since it provides a visual representation and analysis of sound wave propagation around multiple fibres of the material.

A typical nonwoven is a mix of fibres in a particular blend ratio. Consider a microscopic view of a certain fibre mix such that it comprises of the LCM based on the blend. Thus, for a blend mix of 50-50 there shall be one main fibre mixed with one bico- fibre, for 75-25, three main fibres shall be blended with one bico- fibre. The representative elementary volume (REV) of such a microscopic view shall then comprise of 2 fibres as described for 50-50 blend, 4 fibres for 75-25, 5 for 80-20 and so on. However, the 2 fibre models have been dealt in detail in the previous chapter. Based on the thought process that they could represent a 50:50 blend ratio, the need for undergoing

a multi-fibrous study has been realised. In this chapter, the models that involve an LCM of three fibres and beyond are considered.

While deciding the positioning of the fibres in a cluster, the primary geometric aspect that aids in determining the structure is the number of fibre cylinders to be accommodated within the REV cell. This is assumed to be a whole number which is either an odd number or an even multiple. As the REV is a square, the LCM number is crucial in deciding the layout of fibres. Typically, since the LCM number of fibres comprise of staple and bico- fibres, such that the upper limit of the bico- percentage is usually only around 30-40% of the blend for reasons covered in the literature review. This suggests that majority of the times, an odd number will lead to some form of symmetry in their placement while the even shall always lead to an asymmetric arrangement, no matter how wide the ratios develop. The contents of this chapter have been detailed based on the framework of this interesting concept of pattern.

7.1. SYMMETRIC MULTI-FIBRE MODELS

Following the basis established and the samples suitable for this part of the study, symmetric models have been developed for three and five fibre clusters. Based on their blends, both these models have one unit of bico- fibre, and the rest is the staple fibre. These models have been linked to their respective nonwoven samples for corroborating their acoustic behaviour.

Three-fibre model

A three-fibre model has been developed around the blend ratio of 66:34, such that there are two main fibres combined with a bico- fibre, which has a smaller radius. Figure 7.1a depicts a typical REV cell for the three fibres. Here the binder fibre is situated at the centre and equidistant to the two main fibres. The model is based on a selected sample that is known to have a porosity value of 0.97. The overall cell size has thus been fixed on this basis. The chosen sample is shown in the Figure 7.1b. The fibres are aligned diagonally in the REV cell like the staggered model developed in the previous chapter with the only difference being the placement of the bico- fibre in the centre.

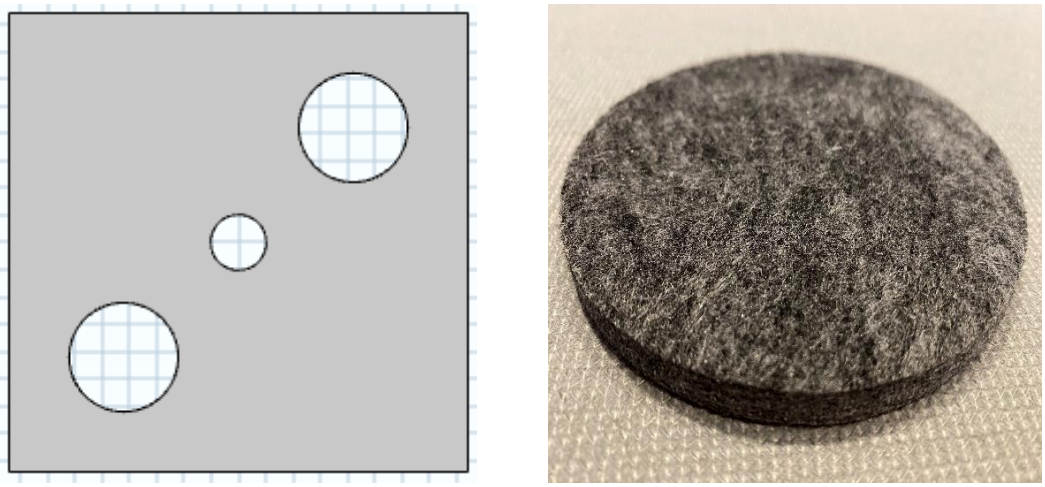

Figure 7.1.: a) REV cell of three-fibre model, b) PES (66:34) nonwoven sample

The model is computed at the low frequency limits (LFL) for the static viscous permeability. At LFL, the pressure, velocity, and vorticity magnitude have been observed to understand the propagation of sound around the three fibres. The preferential direction of sound propagation is parallel to the y- axis, same as the previous studies. Plots have been produced in accordance with the observed and calculated porosity of the actual material, which is $\phi = 0.89$ for this sample.

Symmetricity, similar to the equal fibre case from the staggered dual fibre model is seen in the velocity related plots as seen from the magnitude and the x- and y- components as in Figure 7.2 a. The pressure contour throughout the REV cell shown in Figure 7.2 b is influenced by the external pressure gradient and the presence to the odd bico- fibre in the centre. The vorticity magnitude plot (Figure 7.3) shows a diagonal pattern as well. At the cell boundary however, the vorticity does not tend to zero everywhere due to the proximity of larger fibre cylinders situated within the REV.

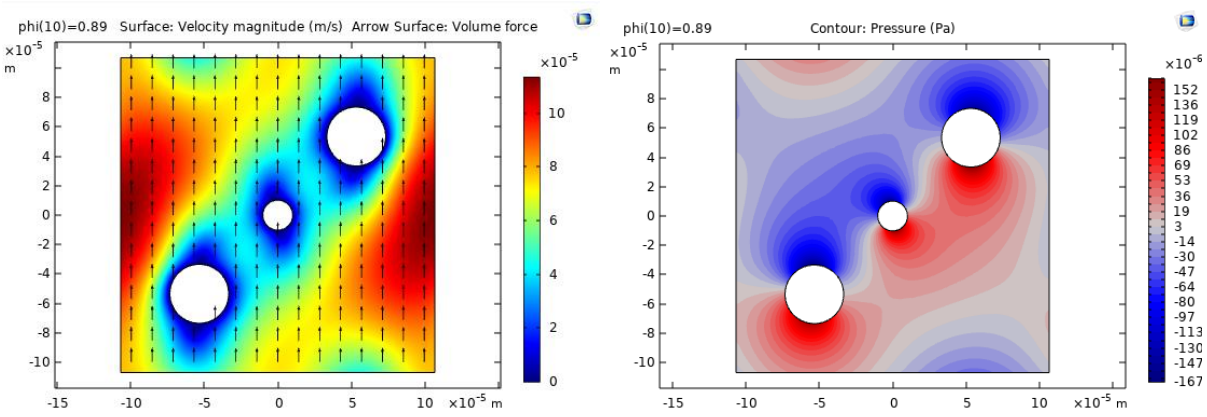

Figure 7.2.: Three fibre-model a) Velocity Magnitude (arrow – volume force) b) Pressure contour

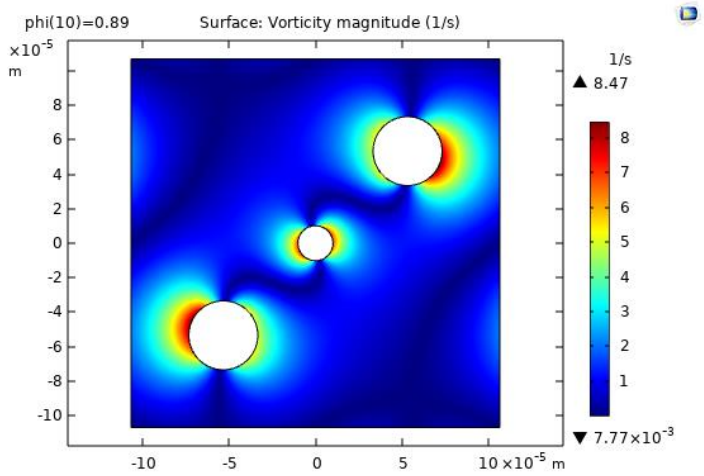

Figure 7.3.: Vorticity magnitude for three fibre-model

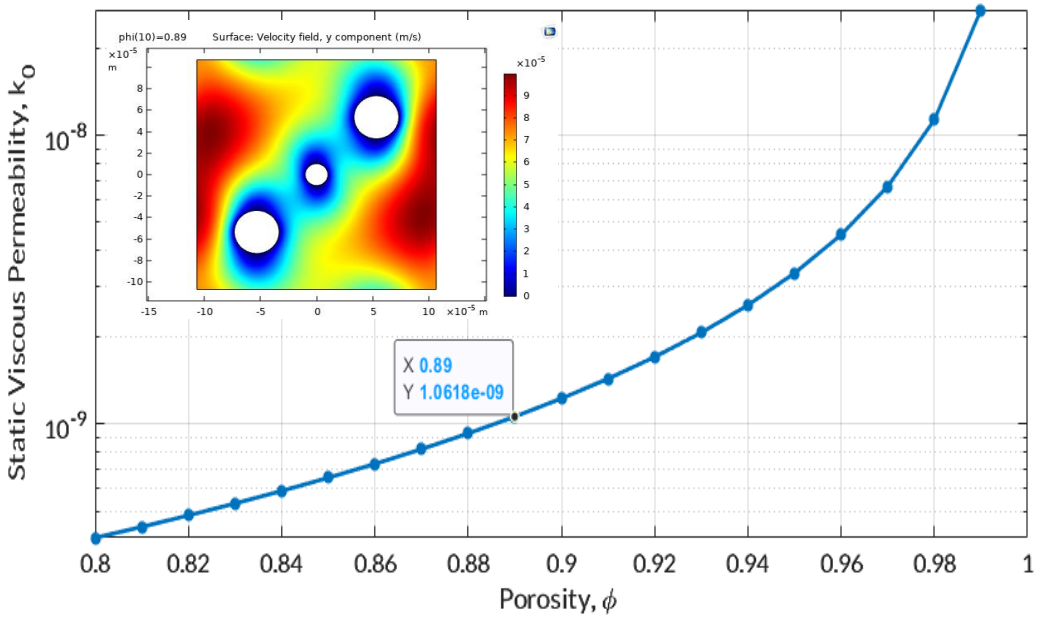

Figure 7.4.: Permeability for PES (66:34) at various porosities (Insert: y- component of velocity)

Figure 7.4 presents the static viscous permeability plotted against varying porosities and in the insert shows the velocity field behaviour at $\phi = 0.89$ point, which correlates to the observed porosity of the sample. It is important to visually understand the influence of the sound fields within the REV cell and correlate it with the trends. This is due to the sample having random alignment of fibres that influences the porosities observed in different local parts of the sample. This helps to introduce a margin of approximation when selecting the performances.

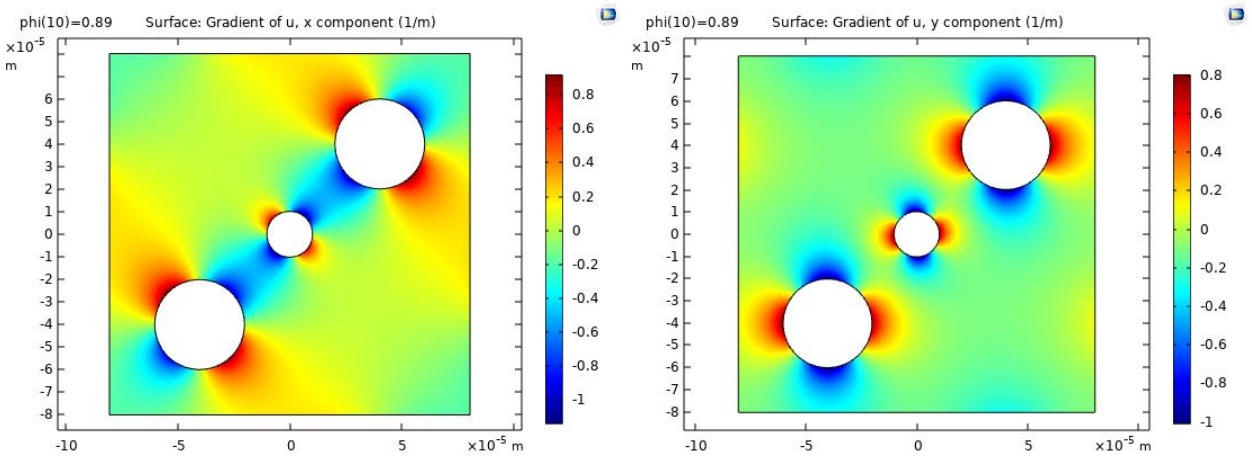

Figure 7.5.: x and y components of velocity field – HFL for three fibre model

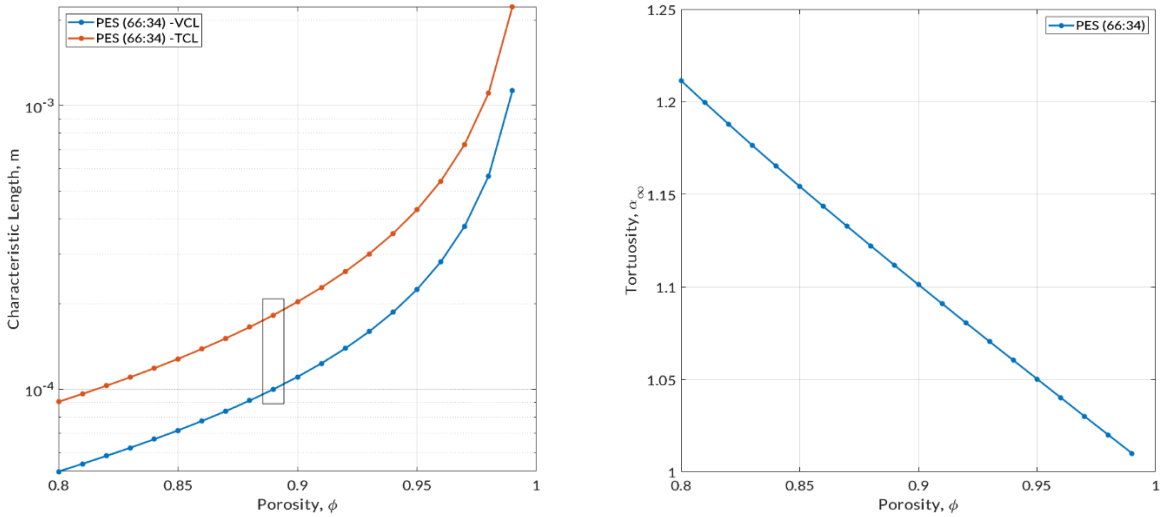

Figure 7.6.: a) Characteristic lengths b) high frequency limit of tortuosity for PES (66:34) sample

By treating it with the Laplace equation, this three-fibre cell is then evaluated for the high frequency limit (HFL) parameters of tortuosity and the thermal and viscous characteristic lengths. The diagonal symmetry is retained from the x- and y- velocity components as seen in Figure 7.5. In the Figure 7.6 a, the viscous and thermal characteristic lengths for the sample are shown indicating the values at 0.89 porosity while Figure 7.6 b presents the HFL tortuosity α_∞ varying with porosities. The effective properties at LFL and HFL corresponding to the porosity of interest can then be used to obtain other sound characteristics for the sample.

Five-fibre models

The next odd set to form the fibre clusters is the five-fibre model. These models comprise of four staple variety of fibres per unit of bico- binding them together in the ratio of 80:20. Since there are four large fibres with a single bico-fibre situated equidistantly in the centre of the REV cell, the adjacency arrangement type of symmetry has been established as in Figure 7.7 a. Based on ample availability of the test sample materials, two variants have been selected for the model correlations, one of which is as shown in Figure 7.7 b. The variations are based on the staple fibre diameter. Visual comparisons for both these types are presented for the key parameters. The sample plots have been shown for $\phi = 0.97$ based on the calculated porosity values.

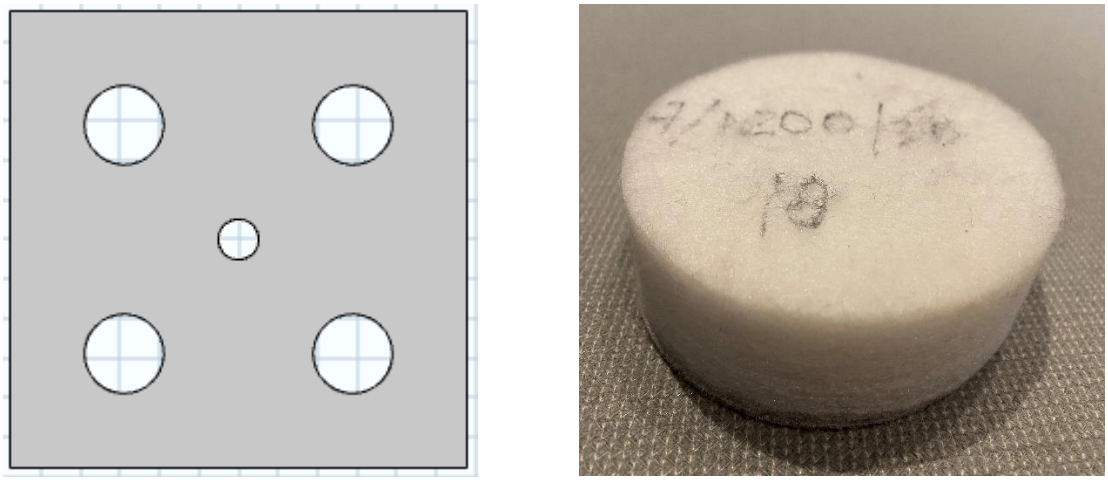

Figure 7.7.: a) Five-fibre model representation b) PES (80:20) nonwoven sample

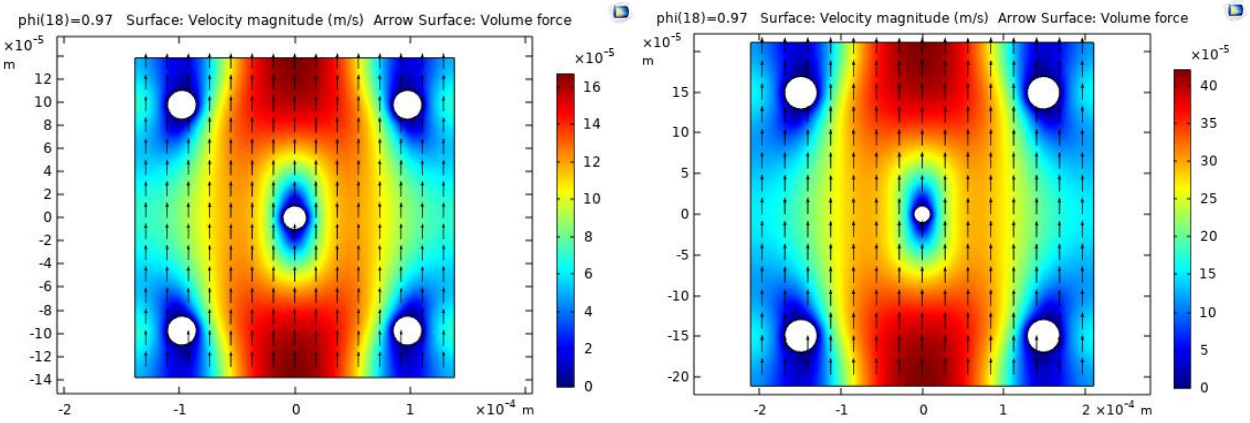

Figure 7.8.: Velocity Magnitude (arrow – volume force) a) PES7 b) PES17

The velocity magnitude plots are shown in Figure 7.8, where the REV cell dimensions are larger for the higher fibre radius sample. This is because the controlled porosity model approach has been used to express these models. To account for a fixed porosity value of 0.97 in this case, the sample with bigger fibres will occupy more space. This also implies that the bulk material will be sparser and limper, affecting the overall acoustic properties. This comparison will be seen from the trends for each material. The pressure contours have been shown alongside one another in Figure 7.9 while Figure 7.10 shows the y- components of the velocity fields for the two samples.

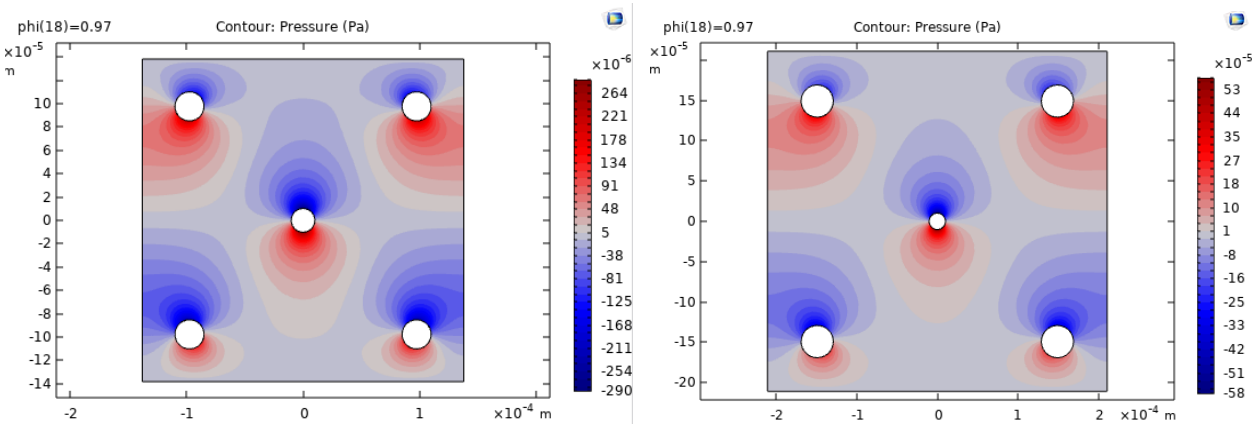

Figure 7.9.: Pressure contour a) PES7 b) PES17

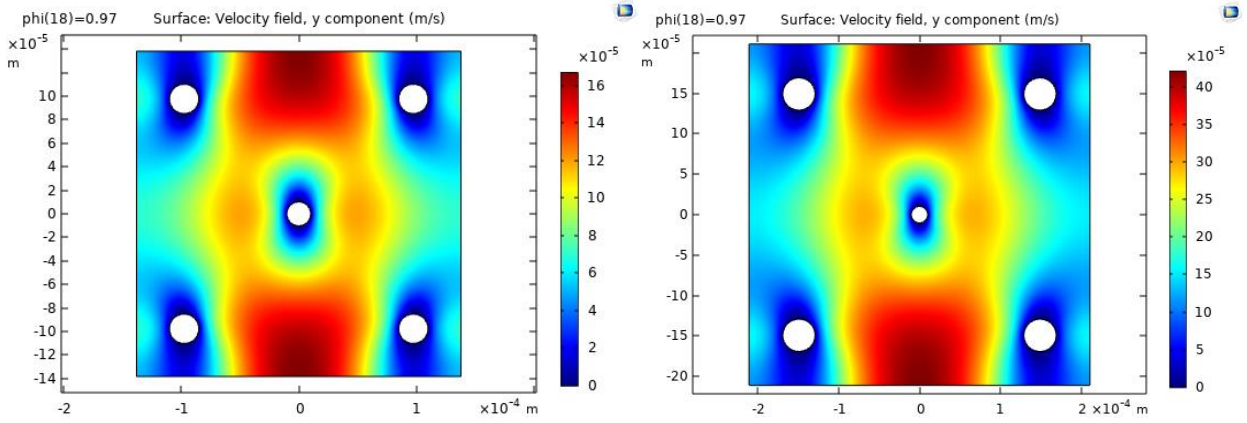

Figure 7.10.: LFL y- components of velocity field a) PES7 b) PES17

Static viscous permeability for the two samples is plotted in Figure 7.11. Porosity of 0.97 has been highlighted to depict that the finer fibre sample has higher permeability than the lower. There is a visible difference between the permeability values where they nearly double for the PES17 sample. A similar observation is made for the vorticity magnitude obtained at LFL as in Figure 7.12.

The values nearly double for the PES17 case in comparison to the PES7 at the said porosity. Symmetry is still maintained for both the REV cells. The concept of vorticity tending to zero at the cell boundary is obeyed for this type of model due to scale of cell volume and occupied portion.

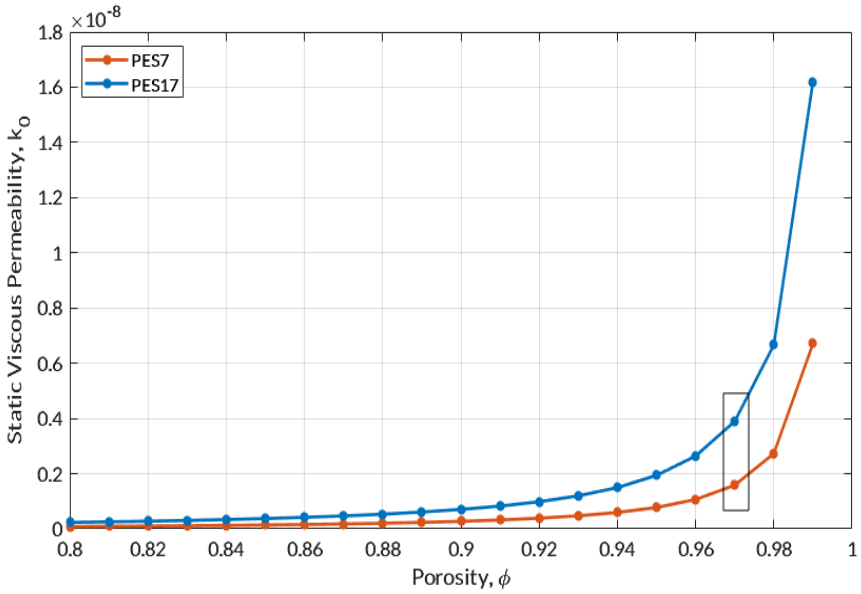

Figure 7.11.: Permeability comparison for the PES7 and PES17 variety

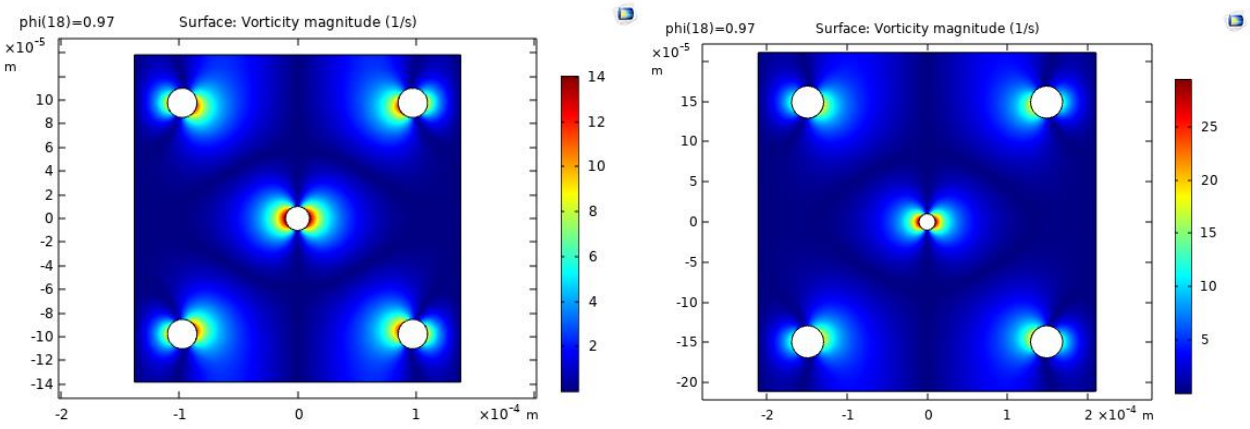

Figure 7.12.: Vorticity magnitude a) PES7 b) PES17

PES17 has bigger staple fibres than PES7 from the selection. Accounting for the proportion of the REV cell and its fibres, both the velocity components at LFL are scaled bigger as well. This however does not affect much at the HFL parameters and hence there is negligible variation between those components.

The characteristic lengths in Figure 7.13 a, show a variation with the fibre type and both viscous and thermal lengths are higher for the sample with larger fibre radius.

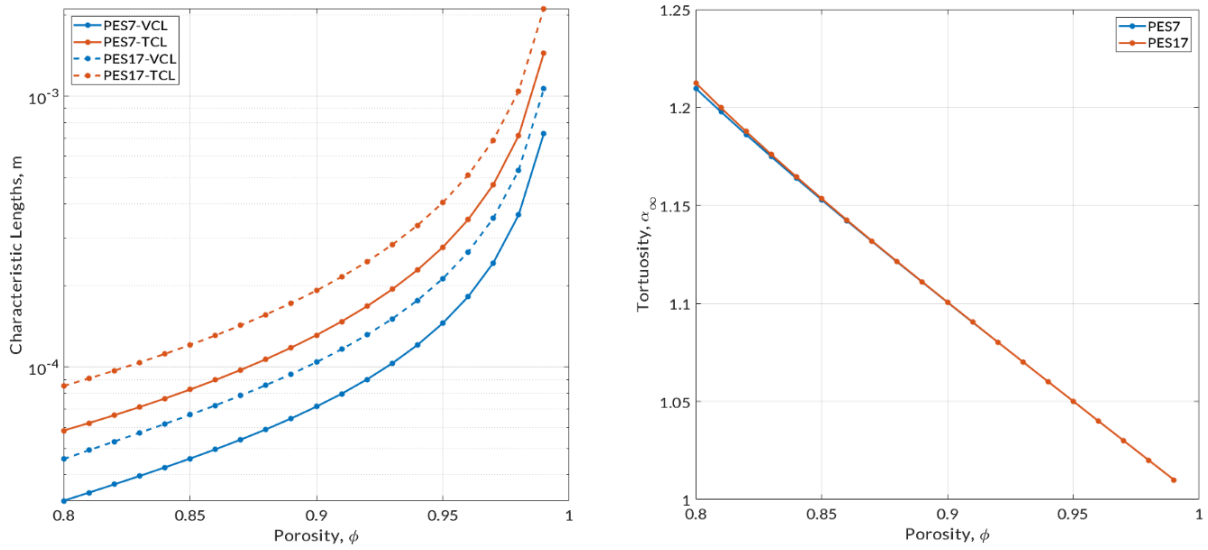

Figure 7.13.: a) Characteristic lengths b) high frequency limit of tortuosity for PES (80:20) samples

The HFL of tortuosity as shown in Figure 7.13 b, show that there is insignificant variation between the two sample types, particularly around the said porosity range.

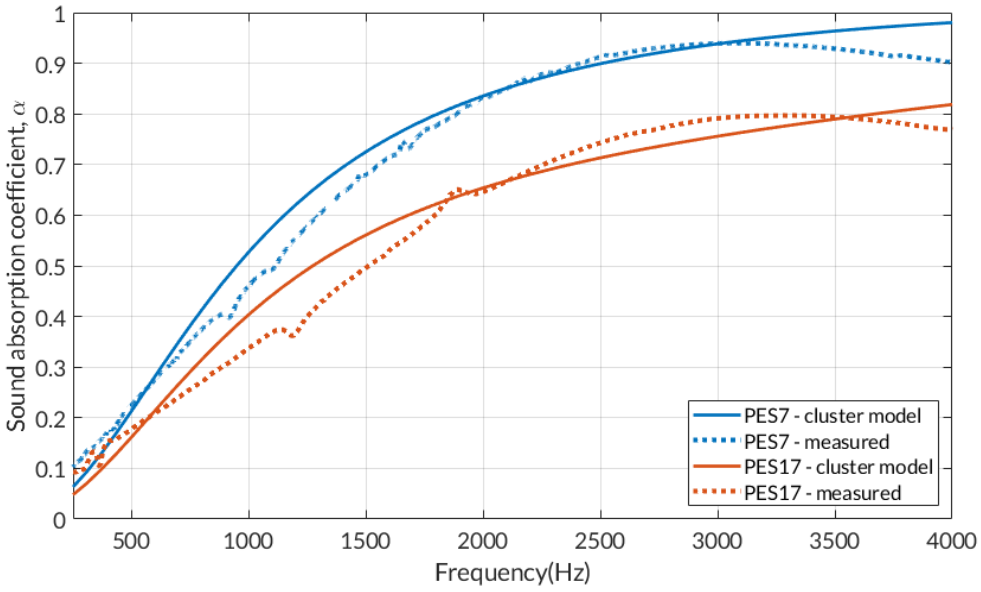

Figure 7.14.: Fibre cluster model-based prediction of sound absorption for PES (80:20)

Using the numerical transport parameters obtained from the cluster model, sound absorption has been obtained using Daleny-Bazley-Miki model and compared for the PES (80:20) varieties. Figure 7.14 expresses that there is a good agreement between the numerically modelled and experimentally measured characteristics in the frequency range of interest for absorbers.

7.2. ASYMMETRIC MULTI-FIBRE MODELS

Even number of fibres when spread over a square REV cell leads to unintentional asymmetry in either the geometry or the potentials developed as a result. This is because the ratio comprises of staple and bico- fibres in the nonwoven mix. Similar to the studies conducted above for the symmetric REV cell spreads, the models covered in this part of the study are the based on the available test samples. Accordingly, the lowest combination of four-fibre model and a highly compact option of twenty-fibre REV unit has been examined for sound propagation around the constituent fibres. Both the materials have nearly the same porosities and if the blend ratios are considered from staple to bico- then both samples are blended in 75:25.

Four-fibre model

This polyester material is composed of two fibre types the main fibre similar to PES7 and the bico-fibre. Due to higher porosity and blend proportion, this nonwoven performs much different from the PES7 sample studied above. The positioning of the fibres within the REV cell is randomised and can be placed in any pattern such that fibres are spaced well apart from one another.

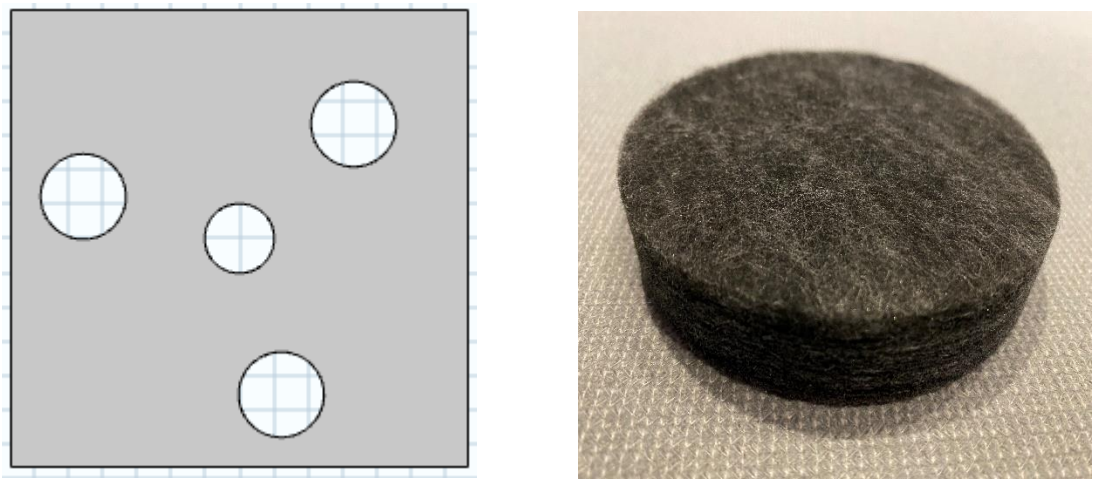

Figure 7.15.: a) REV cell for four-fibre model b) PES (75:25) nonwoven sample

Figure 7.15 shows an instance of the REV with the randomly placed staple fibres with binder or bico- fibre in its centre. The actual test sample is also shown alongside. Plots have been presented like before to visualise the asymmetry in sound propagation with this REV cell. Velocity magnitude and the pressure contours show the y- direction impacts under the influence of the external pressure gradient and due to the scattered fibres are shown in Figure 7.16.

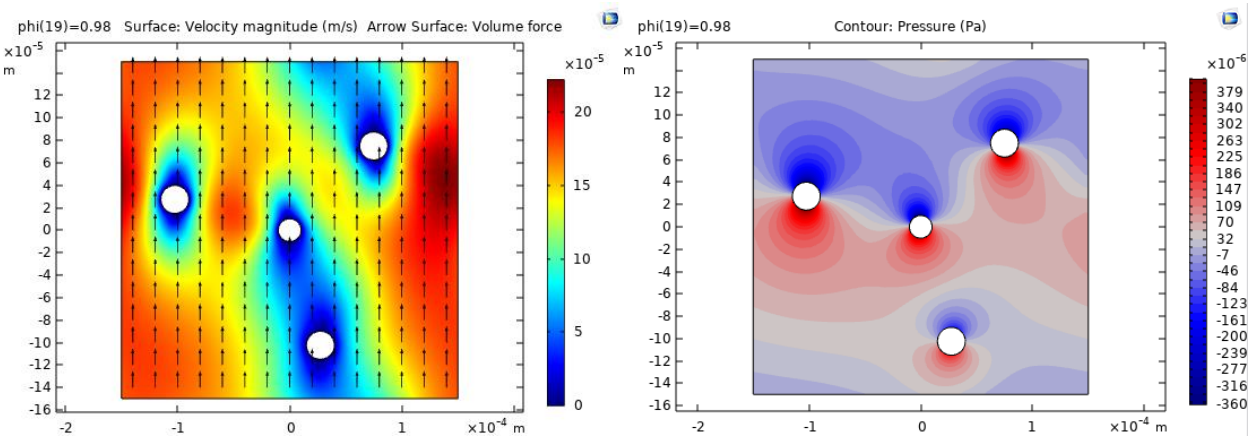

Figure 7.16.: Four fibre model a) Velocity Magnitude (arrow – volume force) b) Pressure contour

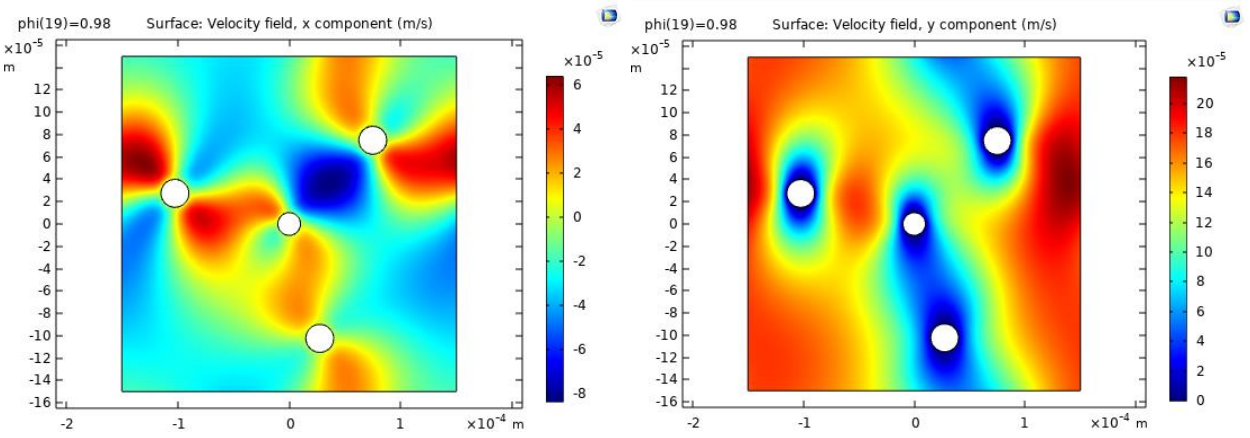

Figure 7.17.: x and y components of velocity field – LFL for four fibre model

Despite the nearly similar fibre diameters, the velocity field shown in Figure 7.17, indicates that every fibre impacts the sound in the locality of the other fibre.

Owing to high porosity value of this material, $\phi = 0.98$, a lot of space is available in the REV cell domain for the fluid medium to cause dramatic vorticity effects. This is seen from the Figure 7.18. Nearly zero values can be achieved with better rearranging of the fibres agreeing that vorticity tends to zero at the cell boundary.

In Figure 7.19, the sound absorption performance of the material has ben plotted using transport properties obtained form the model and compared with the experimentally obtained data. Results show that the random cluster fibre model is capable of representing the actual nonwoven sample arrangement and can be adapted for other variations of materials.

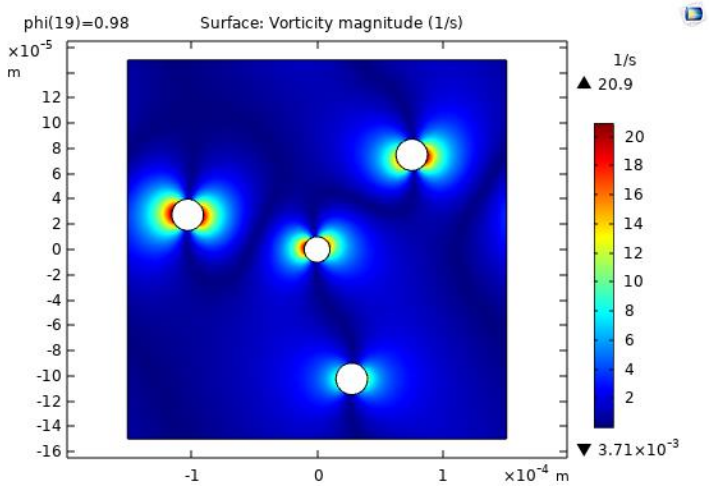

Figure 7.18.: Vorticity magnitude for four fibre model

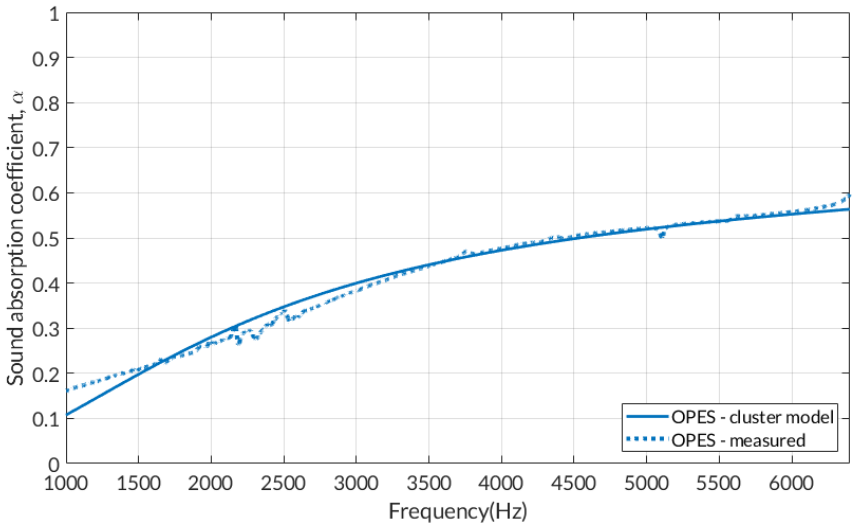

Figure 7.19.: Fibre cluster model-based prediction of sound absorption for OPES (75:25)

Twenty fibre model

When dealing with large multiples of fibres, an even integral can be uniformly distributed within a square REV cell to represent an ideal replica of the given nonwoven. From the REV cell shown in Figure 7. 20 a, the circular placement of nearly uniform fibres comprises of two types of staple fibres blended with single variety of bico- material. Staple fibres comprise of 15% of PES7 type but 60% of highly fine polyester variety. Bico- remains same as all other samples. Thus, the overall staple to bico- ratio is 75:25 as the previous sample. From Figure 7.20 b, it is seen that the actual material constitutes of a broad mixture of fine fibres, giving it the softer textural appearance.

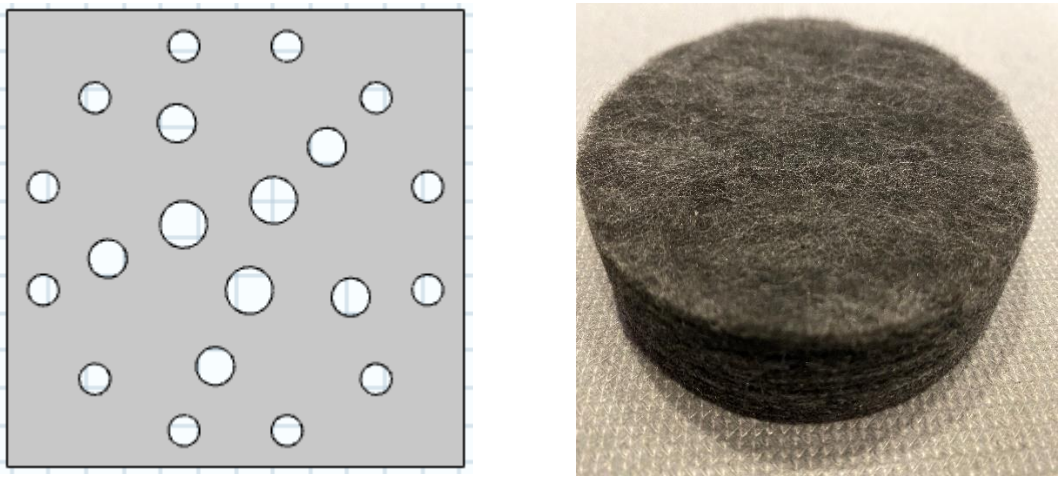

Figure 7.20.: a) REV cell for twenty-fibre model b) PES (60:15:25) nonwoven sample

The highly populated REV cell provides a wide scope for inter fibre scattering of waves. The asymmetricity is obvious from the velocity magnitude graphics as in Figure 7.21 a. The pressure contour from Figure 7.21 b, shows similar trends to the four-fibre model under the influence of the volume force. There are distinctive zones of high and low pressure locally created over the fluid domain with regional variations for each fibre type in the mix.

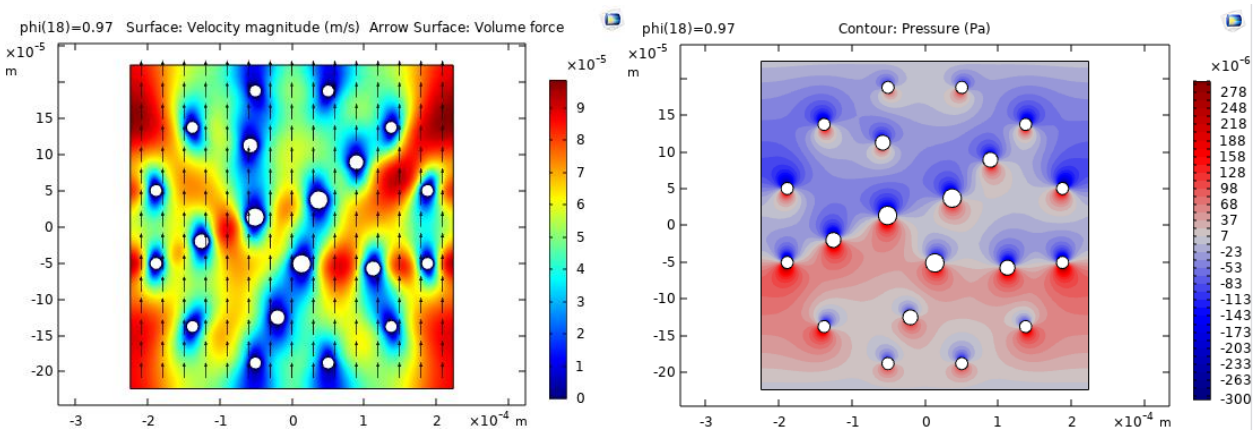

Figure 7.21.: Twenty fibre model a) Velocity Magnitude (arrow – volume force) b) Pressure contour

The x– and y- components of the velocity field in Figure 7.22 show high amounts of randomness for LFLs which is negligible when it comes to HFLs. Figure 7.23 suggests that the vorticity magnitude has similar trends like the previous model due to the high porosity of the material. For such a large mix of fibre types, plot in Figure 7.24 demonstrates that the sound absorption trends obtained from the cluster fibre models nearly trace the experimentally measured coefficient data at least at the mid to high frequency range.

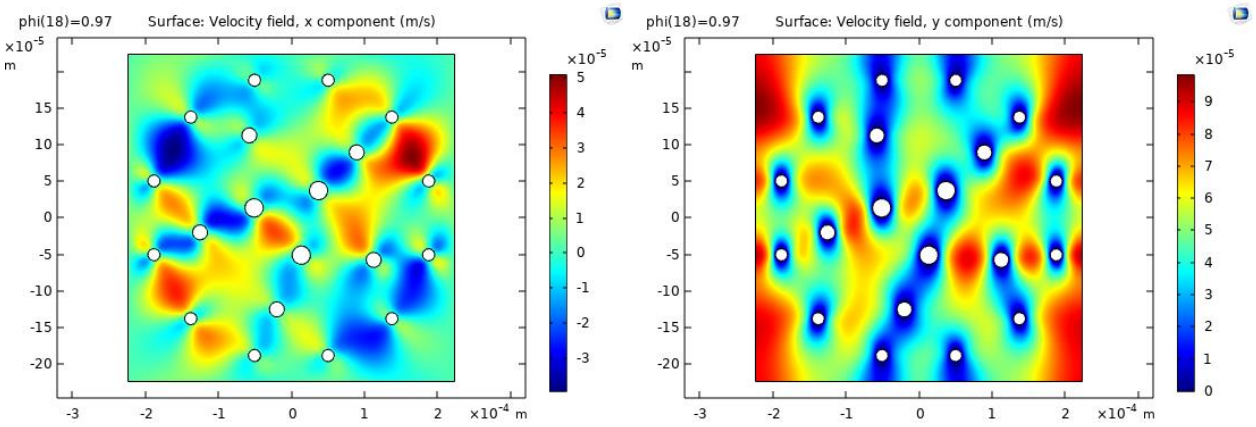

Figure 7.22.: x and y components of velocity field – LFL for twenty fibre model

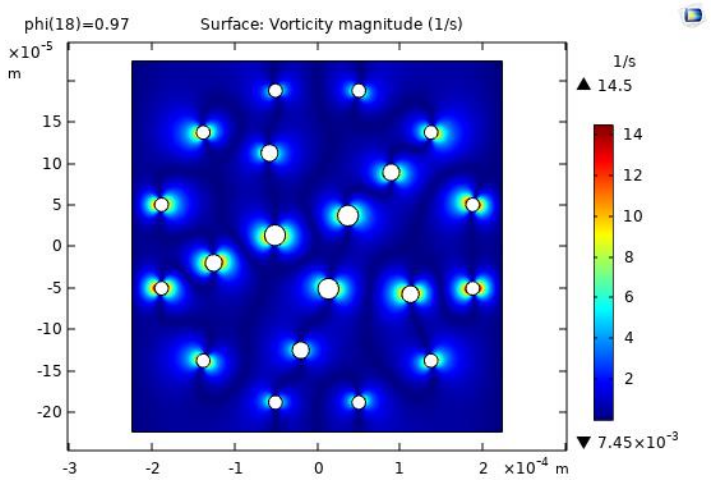

Figure 7.23.: Vorticity magnitude for twenty fibre model

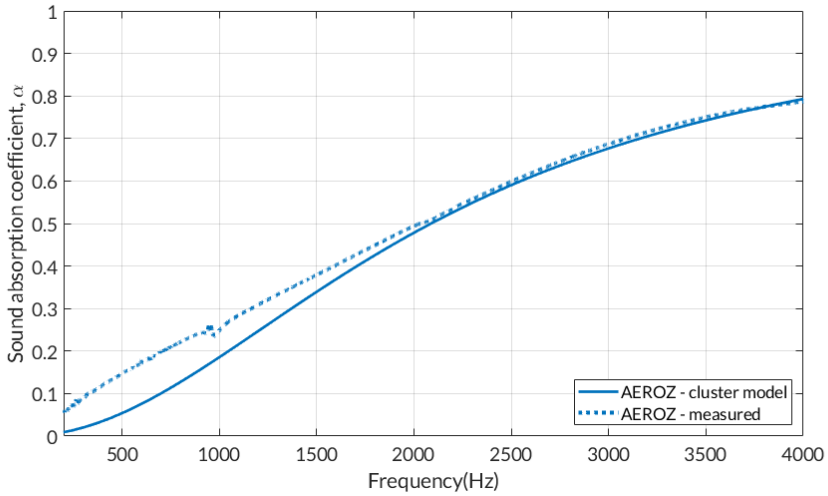

Figure 7.24.: Fibre cluster model-based prediction of sound absorption for AEROZ (60:15:25)

7.3. ACOUSTIC INFLUENCE OF KEY PARAMETERS

Besides the transport parameters that govern the overall micro-macro acoustic performance of the porous fibrous material, there are other non-acoustic parameters that have led to the development and study of multi-fibrous models based on cluster arrangements. These have been identified as a part of the progressive numerical model understanding from the single fibre cell to the poly-disperse fibres or the cluster fibre models covered in this chapter.

Blend ratio

On the basis of the fundamental feature of a nonwoven, the blend ratio is considered as a key parameter. This has been investigated on several occasions throughout the research work. It is also a primary reason to propose and explore the path of fibre cluster models as the approach, when adopted for structuring of the cluster provides the closest approximation to the realistic mix along with the treatment of other aspects. From literature it has been observed that the consideration of this parameter associated with nonwovens has generally been dealt with empirically. Although several semi-analytical and numerical acoustic models consider the influence of fibre size distribution, yet the ratio of blending of each size of fibre or the fibre count has not been accounted for acoustically. This is relevant for the equivalent fluid models that treat the solid phase as rigid and base their formulation on interaction of sound waves within the fluid alone.

To justify the blend ratio aspect within an REV, the bi-disperse version of the numerical models has been modified to the proposed cluster fibre models. As a recapitulation, this model is based on the least common blend ratio multiple of staple and bico- fibres present within a said nonwoven mix. This model is a representation of the post manufacturing experimental quantification laboratory test procedure, generally carried out to assess the accuracy of even distribution of both the fibre types. This test essentially cross-checks the controlled randomness ensuring that the blend ratio is nearly maintained throughout the bulk of the fabric batt. A nearly even blend confirms the structural integrity of the fabric all through and thus, blend ratio has been considered as a prime physical parameter of a nonwoven material.

It is essential here to understand the material properties that influence the blend ratio. As derived in the theoretical section, this ratio has been associated with the weighted fraction of the two fibre types that has a direct connection with the solidity or the bulk and fibre densities of the nonwoven. This is to say that a variation in the blend ratio must have an overall impact on the flow resistivity. The said effect has been examined with the various cluster fibre models covered in this chapter.

Inter-fibre spacing

The gap size distribution within a nonwoven in general and its REV cell in particular can be a critical factor to study the influence on the performance. Similar to the pore spacing, inter-fibre spacing can also be linked to the porosity of the material, but along the thickness of the bulk fabric. This is because when the porosity of a material increases, the pore size expands thus increasing the inter-fibre spacing. Within an REV, the inter-fibre spacing factor is connected with the cell size that in turn has the porosity element embedded within its calculation to account for the variation as described. This aspect can be studied using all the numerical models detailed previously. A comparison of this variation has been shown for the cluster fibre model.

The PES variety of test sample has been examined for the variation in the inter-fibre spacing. The symmetric sample was selected as it had sufficient number of fibres and can be proportionally arranged within the REV cell. Following the similar method of visualising the sound propagation fields as previously presented, the Figure 7.25 compares the influence on velocity magnitude for the varying fibre spacing within the REV cell. The pressure field variation for the two spacing configurations is seen in Figure 7.26. In this figure, the velocity field has been indicated by arrows indicating the influence of presence of fibres in the general pattern within the cell.

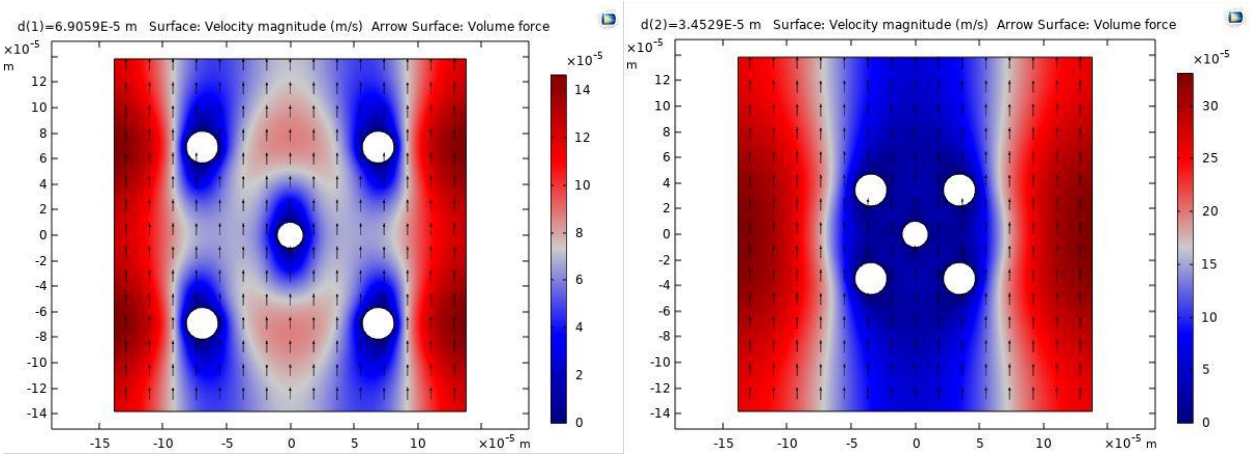

Figure 7.25.: Velocity magnitude variation with change in inter-fibre spacing for PES7

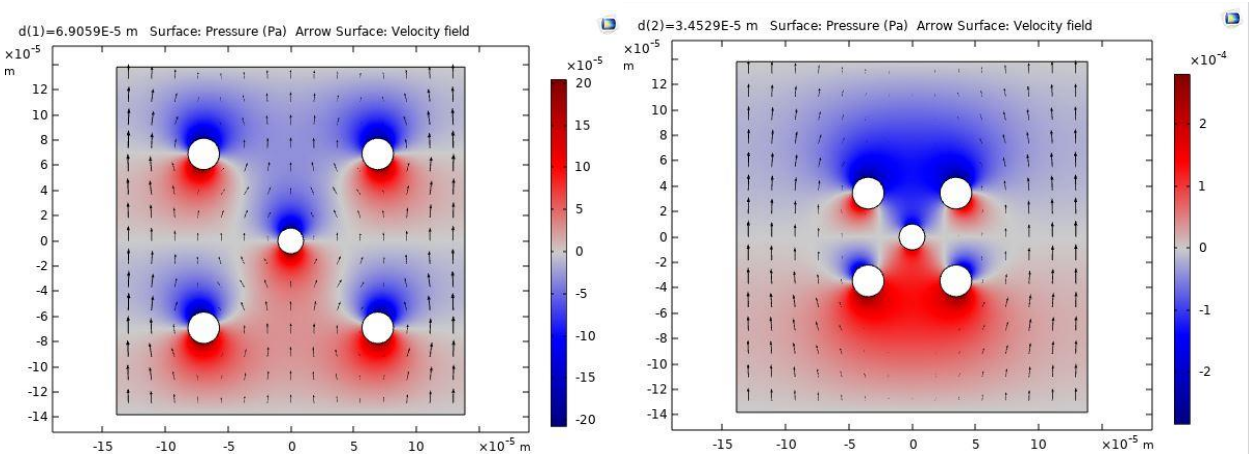

Figure 7.26.: Pressure variation with change in inter-fibre spacing for PES7

Figure 7.27 presents a comparison of the vorticity magnitude for the inter-fibre spacing cases. With the instance of closely packed fibres, there is more void present around the cell boundary with higher vorticity around the region where the fibres are located.

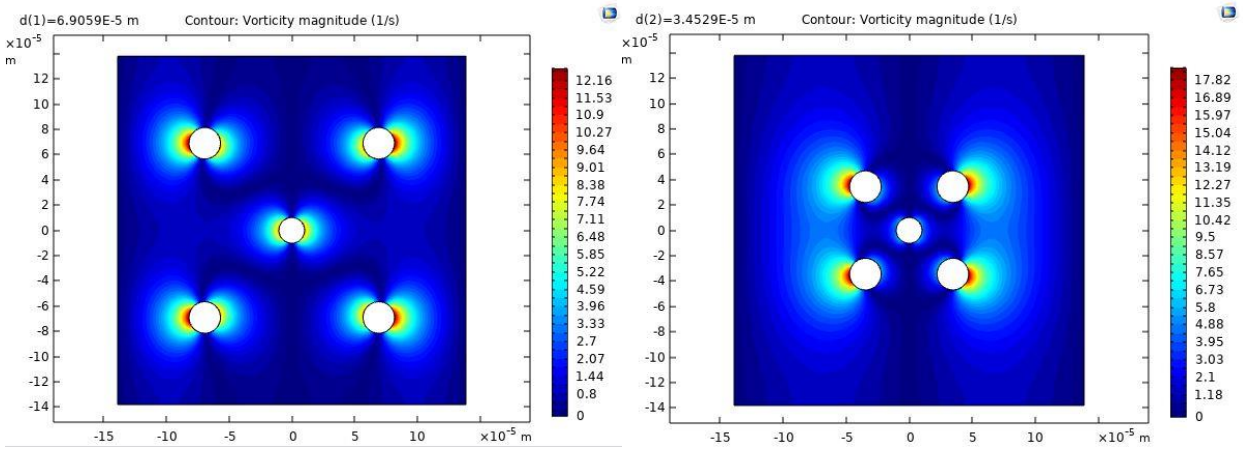

Figure 7.27.: Vorticity magnitude variation with change in inter-fibre spacing for PES7

Case of touching fibres

It is a general notion that a realistic nonwoven may be depicted such that, the binder material tends to hold on to the staple variety after the binding process has taken place. This is represented as a special case of touching fibres. This concept has been explored within the same PES7 based symmetric REV cell. Figure 7.28 shows the velocity and pressure plots with Figure 7.29 provides vorticity magnitude variation. This can be compared with other spacing options presented above.

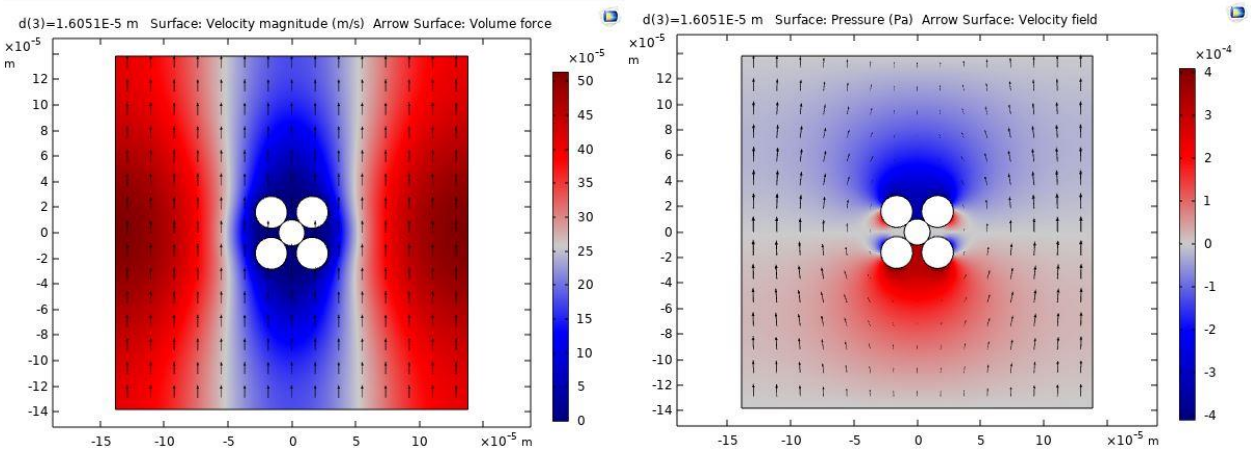

Figure 7.28.: Velocity and pressure plots for touching fibres of PES7 sample

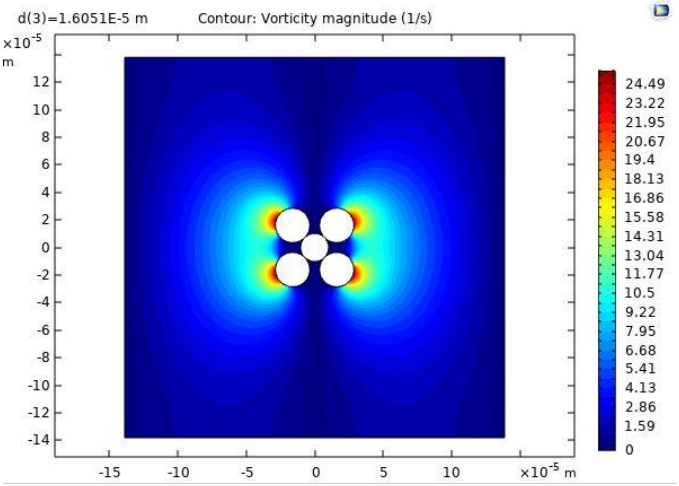

Figure 7.29.: Vorticity magnitude plot for touching fibres of PES7 sample

The results obtained for the three spacing trials has been tabulated below in Table 7.1. It is noted that the closer the fibres, the resistance to the airflow reduces. Again, using the Miki model, a correlation has been made to perceive the impact of this parameter presented in Figure 7.30.

Table 7.1.: Results of transport parameters for three spacing conditions of PES 7 configuration

Spacing	Permeability	AFR	Tortuosity	VCL	TCL
D/4	1.37E-09	13183	1.03	2.43E-04	4.71E-04
D/8	2.95E-09	6092.8	1.0302	2.41E-04	4.71E-04
touching	5.52E-09	3258.4	1.0498	1.94E-05	4.71E-04

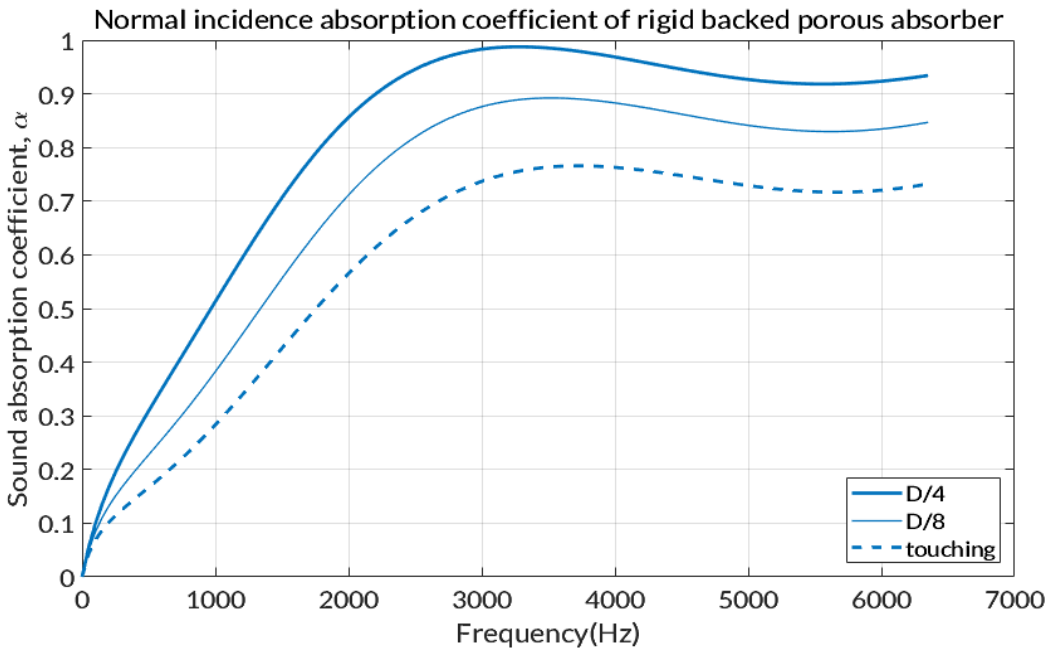

Figure 7.30.: Sound absorption variation with change in inter-fibre spacing for PES7 sample

From the absorption characteristics it can be seen that as the fibres come closer, the absorption property of the material drops by at least 10% until the touching fibres case has been reached. Unless the overlapping situation is being compared, the touching case is the lowest possible decline that can be expected from changing the inter-fibre spacing, D for the fibre cluster model.

Anisotropy

The fibre cluster representation of the PES7 model is that of a symmetric one. However, this need not always be the case. In fact, a realistic model shall never be as symmetric as represented by the model. Thus, an intentional asymmetricity has been introduced to inspect the effect on the various properties of the model.

In the fibre cluster model, based on the blend ratio, anisotropy is directly induced for even blends while this needs to be pseudo-created for the odd blends by offsetting the odd fibre. This can be seen in the following REV cells. A comparison between the velocity magnitudes has been depicted to compare between the case of symmetric REV cells (Figure 7.31) and the impact of two ways in which asymmetricity (Figure 7.32) can be deliberately introduced within the well aligned system. Similar trends may be obtained for the other transport properties to visualise the variation.

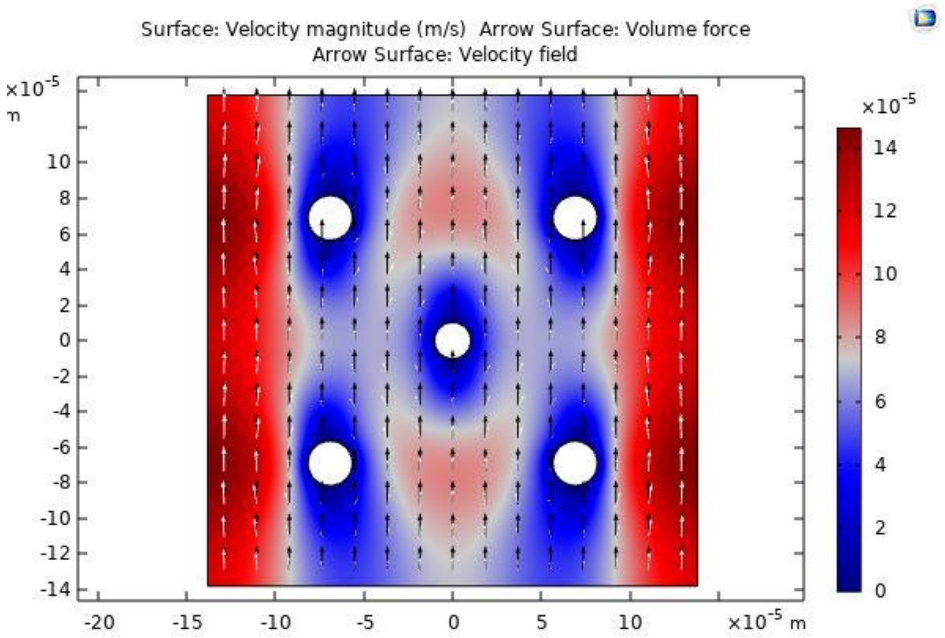

Figure 7.31.: Velocity magnitude influence due to anisotropy for perfectly symmetric PES7 cell

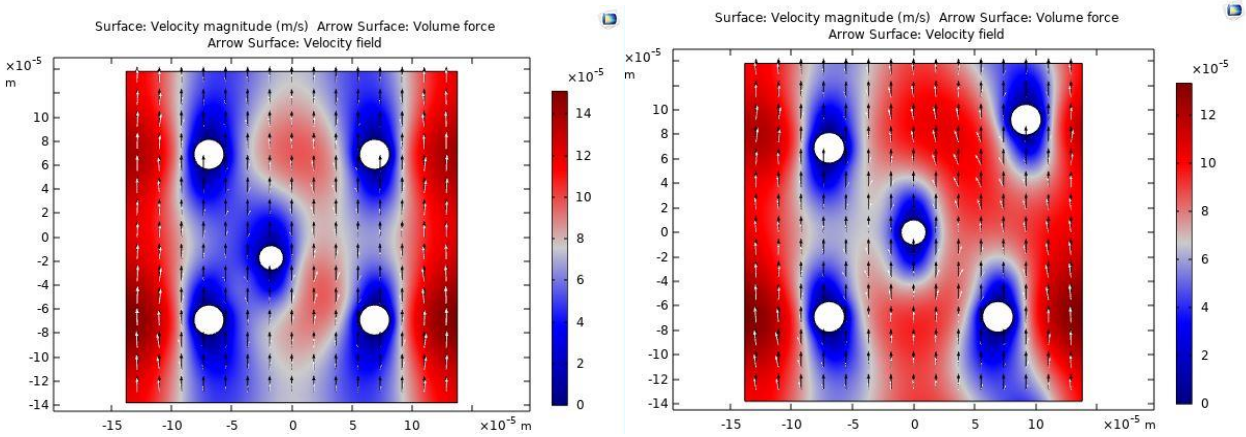

Figure 7.32.: Velocity magnitude influence due to anisotropy for asymmetric PES7 cells

This aspect has been introduced as the randomness in nonwovens naturally brings out anisotropy though the material. This may be assessed differently, say based on the direction in which anisotropy is considered. Oblique orientation of fibres may be represented by oval fibres rather than the regular circular cross-sections. Fibres have been positioned by offsetting the symmetry thereby losing the isotropy in the REV plane making the material nearly transversely isotropic due to the symmetry along the depth of the material.

Chapter 8

APPLICATIONS

Overview:

8.1. Impact of textile processes on nonwovens

8.2. Layered nonwovens and membranes

8.3. Study of sustainable materials

This chapter delves into the practical applications developed as a part of the research work conducted, highlighting three distinct areas where the research findings have significant relevance. These applications have been selected based on their close alignment with the overarching theme of this PhD thesis, representing impactful outcomes of the academic journey. Within this chapter, the numerical models and experimental investigations have been explored to culminate in real-world solutions, demonstrating the practical contributions of this research to various industries.

The first application investigates the impact of nonwoven textile processes on the bulk-scale acoustic properties of these materials, focusing on two key factors, crucial during manufacturing. One parameter is selection of cross-sectional shape that informs the presence of irregular shaped polyester and other nonwoven fibres than the simple cylindrical strands. The other is the impact of nonwoven fibre bonding process adopted during the manufacturing.

The second application looks at multi-layered porous materials exploring the role of gradation in layers and impact of membrane facings on enhancing the acoustic properties of nonwovens.

Technical textiles are currently being developed to meet the growing demand for sustainable alternatives. The third and final application deals with acoustic characterisation and optimisation of novel sustainable materials. A commonly available recycled material has been studied to extract its acoustic and non-acoustic properties and experimentally validating the numerical models.

8.1. IMPACT OF TEXTILE PROCESS ON NONWOVENS

In the previous chapters, the influence of key acoustic and non-acoustic parameters has been covered. Those properties were of direct significance to efficient modelling for acoustic outcome. However, few secondary parameters that arise because of the textile processes during or after the manufacturing have an impact on the acoustic behaviour of nonwoven materials. The impact of these parameters has been briefly discussed in this section.

Cross-sectional shape

Polyesters that have been majorly studied have a cylindrical shape. However, there are many materials that have fibres of varying shapes. In such case, the most common approach to examine their overall acoustic performance is by calculating an effective diameter as detailed in the single fibre cell description. Within the nonwoven variety, there are other materials besides polyesters. At the very beginning, it was informed that one of the main reasons in the selection of polyester for this study was owing to its nearly cylindrical shape. Typical cross-sectional shapes that have been studied include, Viscose (cloud shape) and 4 Deep Groove (4DG) samples as in Figure 8.1.

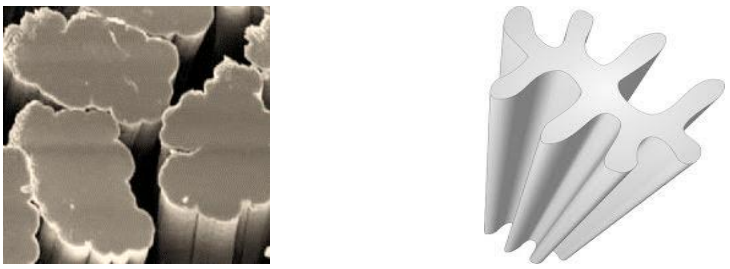

Figure 8.1.: a) SEM image of viscose fibres [109] b) Representation of 4DG fibre [110]

In the literature review, a note on effective diameter calculation has been provided to study such materials. For the non-circular shapes such as those shown above, the equivalent circular diameter can be calculated as per equation (8.1):

$$d_{fib} = \sqrt{4\frac{S_{fib}}{\pi}} = \sqrt{\frac{4t_{fib}}{\pi\rho_{fib}}} \tag{8.1}$$

where d_{fib} is the equivalent diameter to be calculated as defined in Table 2.1 earlier. Calculating thence leads to equivalent values as in Table 8.1.

Table 8.1.: Equivalent fibre diameter and material properties for its calculation

Property/Material	**Polyester**	**Viscose**	**4DG**
t_{fib} (dtex)	7	5.56	2
ρ_{fib} (kg/m^3)	1380	1530	1240
d_{fib} (μm)	25	21.5	15

When attempting to replicate the exact shape of these fibres, the numerical models come in handy as the material can be visually inspected for their expected performance. Ideally, these types of fibres would be blended along with their binder materials and thus the cluster model type would best suit for analysis. Study outcomes using both these types of materials is covered further.

The impact of shape on the acoustic characteristics has been justified through various studies presented in the literature review. Hence, it is important to have clarity of the type of fibres involved in the nonwoven blend.

Manufacturing processes

Samples modelled in the previous chapters were based on thermal bonding approach. However, mechanically bonded materials have been reviewed for their needle punching impact on the acoustics of nonwovens. Figure 8.2 compares the influence of bonding on sound absorption values of similar composed materials manufactured by thermal and needle punched bonding techniques.

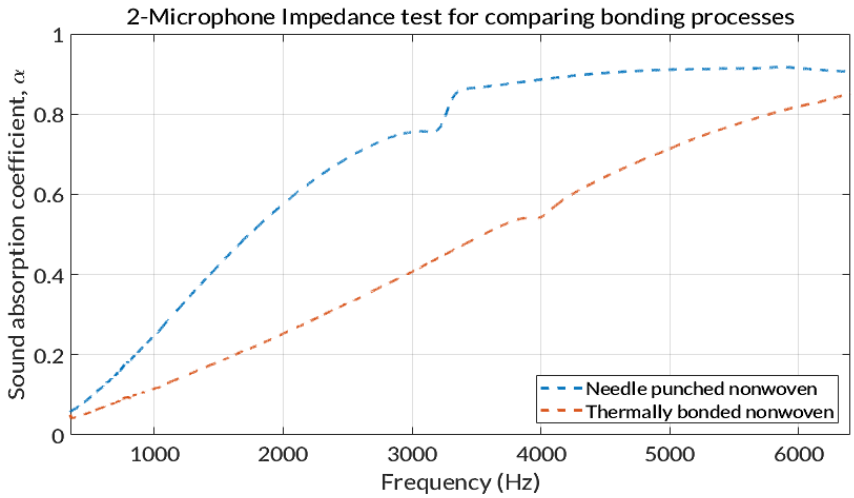

Figure 8.2.: Experimental comparison between nonwovens made from different bonding processes

8.2. LAYERED NONWOVENS AND MEMBRANES

Gradation in layers

When considering a multi-layer porous absorber, the first instinct is to look at the impact of gradation in physical property such as density amongst layers of materials having same chemical make. In the absence of gradation, the group of materials would typically represent a thicker block of the material under consideration. The analyses have been carried out to provide a comparison between the graded and the block unit of isotropic material. This comparison is not only beneficial from the acoustic aspects but also gives an insight into the material consumption for each case giving an idea of the cost effectiveness.

Two Layer Materials

As a special case to the multi-layer materials being visualised, special configurations have two layers have been explored further. Cases have been considered based on the thickness of the layers in consideration. The first set of studies has been in thick layers while the next bit focuses on membranes having thickness less than 1 mm.

Polyester and Viscose

While initial studies had been carried out with layers of varying densities of the same nonwoven material, in this part of application, review of systems comprising of a layer of two different materials having high thickness (thickness > 1 mm) has been the highlighted. Combination of polyester and viscose samples has been studied as layers here due to the interesting outcomes.

The striking differences between the two selected materials is as follows; Polyester has a larger fibre radius than viscose and is more cylindrical in shape than the cloudy viscose fibre. Also, the polyester fabric layer is 20 mm thick while the viscose is 25 mm thick. Hence when considering these materials for their individual performances, the viscose material will tend to have a higher acoustic performance than the polyester. This selection has been done with the intent of studying the impact viscose will have as an additional layer to the low performing polyester sample.

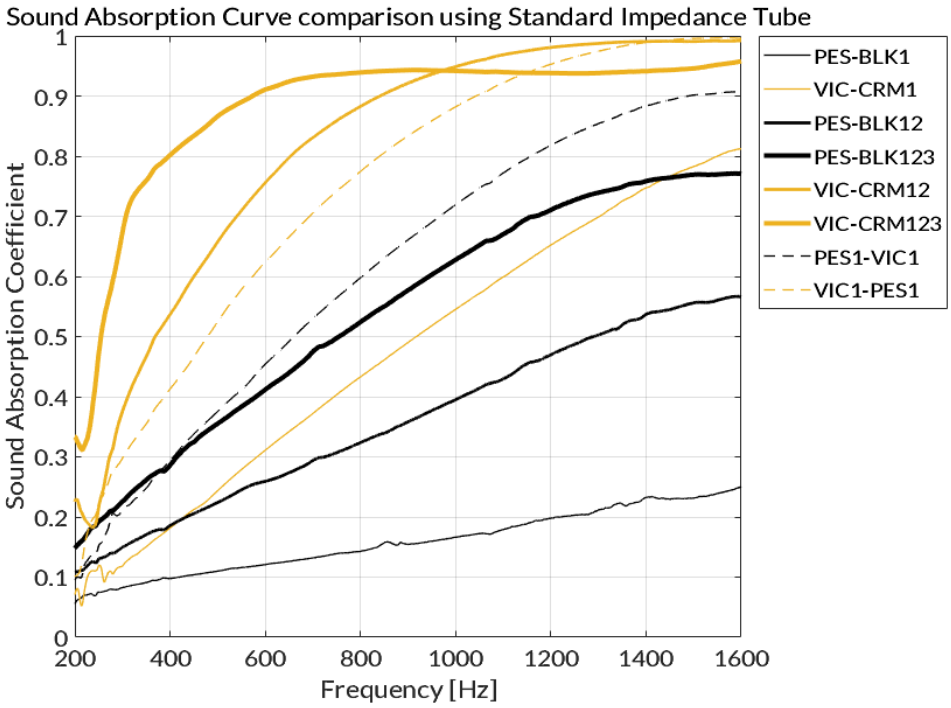

Figure 8.3.: Comparison of absorption coefficients between polyester and viscose

Figure 8.3. shows several trends produced with these layers. The black curves correspond to the polyester while cream for viscose. Solid lines show either polyester (PES) or viscose (VIC) being considered individually.

For polyester as the number of layers (same thickness) is increased, the absorption rises progressively. The viscose sample has finer fibres and thus the single layer performs comparable to the three layers of polyester. In addition, as the viscose layers increase, the performance begins to shift focus for the overall sound absorption to the low frequency specific absorption, also suggesting the amount of material that would be necessary for this shift.

Interesting observations have been made when using a single layer of polyester and viscose. When positioning them such that the viscose forms the upstream layer has a higher impact as compared to the polyester being upstream. This suggests that the normal incident sound waves within the impedance tube get better absorbed for a configuration with a better absorber in the upstream. In the reverse configuration, as expected the performance is lower, with only a slight boost to the trend of single layer of viscose. This experiment has validated the role of positioning of better performing side of a graded absorbing material.

Membrane facing polyester wadding

Finally, a system has been studied where a membrane (thickness < 1 mm) of either similar or chemically different material covers the general thick nonwoven fabric.

Two Microphone Impedance Tube tests for Sound Absorption

As per the Figure 8.5, the comparisons have been made between the performances of three different membranes. The plot shows results for PES, a high-density polyester-backing sample, curves for the membranes alone (solid lines) and curves for the layered configuration (dotted lines). Of the membrane (MEM) samples studied, MEM1 and MEM2 are similar products with MEM2 being denser than MEM1. The 4DG membrane is a different material altogether. These membranes have been experimentally characterised using the impedance tube setup.

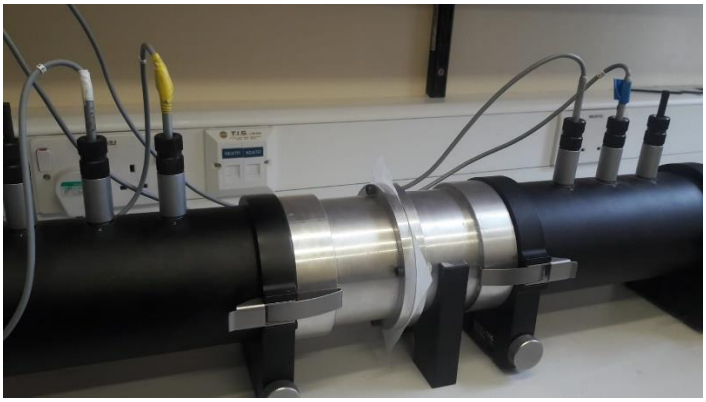

Figure 8.4.: Fine membrane tested for acoustic properties using 4- microphone impedance tube

The trends for the layered samples show unusual behaviour. The 4DG membrane seems to work much like the trends suggested throughout literature. However, the extent to which it boosts the absorption in the low frequency limits is brilliant. The curve begins to sharply drop as the frequency rises suggesting a narrow range of high performance of the configuration. On the other hand, the MEM1 and MEM2 provide a gradual drop at higher frequencies. These membranes could be much suited for a broader range of frequency applications. For a particular membrane, comparisons have also been carried out with the membrane being positioned as both facing and backing the polyester wadding.

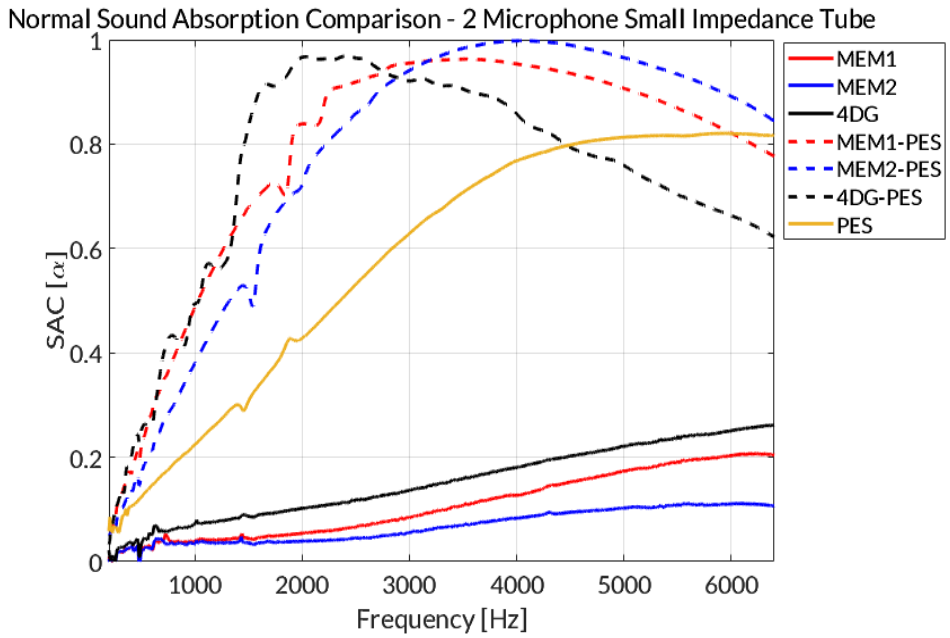

Figure 8.5.: Comparison of absorption coefficients for studying membranes

The Figure 8.6 shows interesting results that the presence of a thin membrane can have on an average polyester wadding. The black curve is the absorption coefficient for the membrane alone with the cyan curve is the polyester wadding. With the combination of the membrane situated behind the polyester, there is negligible impact on the absorption. However, on placing it as the upstream layer has a drastic boost in absorption capability. Considering the low frequency range as per the plot, the boost is nearly 50 – 70 % from 1k Hz – 1.6k Hz. Such a striking impact by a thin membrane has perhaps not been reported in literature.

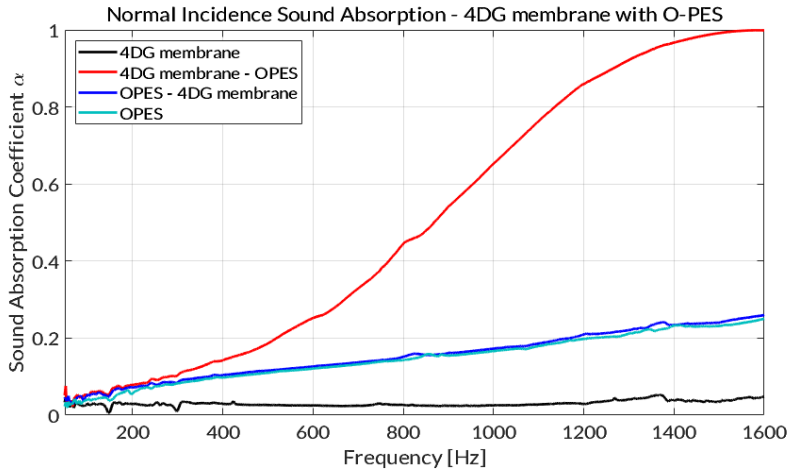

Figure 8.6.: Comparison of absorption coefficients for membrane positioning

8.3. OPTIMISATION FOR SUSTAINABLE MATERIALS

Materials that are said to meet the need of today and have the capability to keep providing in the future are classified as sustainable materials. Such materials can be classified into two categories:

1. Naturally resourced materials
2. Recycled materials

Many sustainable materials have been studied for their mechanical and acoustic properties. However, for this research section, a 50 mm of recycled natural-nonwoven blended material [REC] has been selected. This material had a blend ratio of 85:15 where in 85% of the staple product was recycled in nature. Effective properties of the material were not entirely disclosed by manufacturer, so these was extracted using the academic version of FOAM-X software [111] as in Table 8.2.

Table 8.2.: Recycled material properties obtained using FOAM-X software

Material	Density ρ (Kg/m^3)	Flow Resistivity (σ)	Open porosity (θ)	Tortuosity (α_∞)	Thermal length (Λ') m	Viscous Length (Λ) m
REC - 50	80.0	8.90E+03	0.99	1.00	1.58E-04	7.89E-05

Modelled results have been validated with experimentally obtained data as shown in Figure 8.7 for sound absorption using the Delany-Bazley-Miki model, demonstrating an excellent replication. Nonwovens, particularly the recycled or blended with natural fibres may have random variety of fibres that may be easily characterised, assessed, and optimised for better performances as shown.

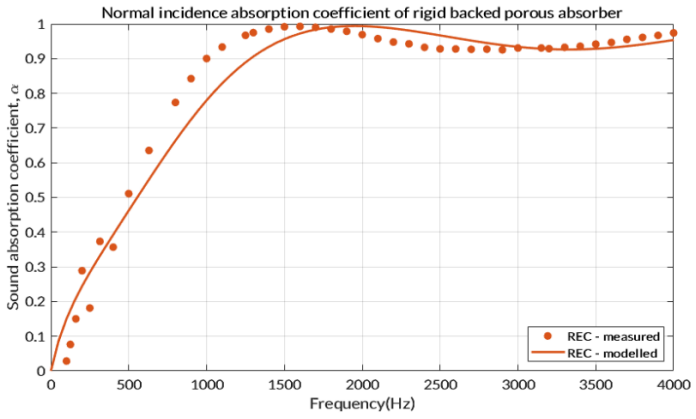

Figure 8.7.: Modelled sound absorption trend of recycled material compared with experimental data

Chapter 9

CONCLUSIONS AND FUTURE SCOPE

The acoustic behaviour of nonwoven materials has been rigorously investigated in this research work with a view to develop a robust technique that shall be suitable in effectively representing the material and further optimising it to bring out a novel range of applications. A detailed literature review has been carried out followed by physical material characterisation to evaluate the complexities of the nonwoven material. This visual assessment of the material has been developed from the textile frameworks to explore the fabrication induced parameters that usually may get left out when examining from an acoustic mindset.

Governing wave equations that form the theoretical basis for understanding the sound propagation around fibrous media have been formulated. The limitations of solving theoretical derivations without assumptions have been identified. Accordingly, the usual dynamic expressions have been simplified to static case and have been derived for a simplified single fibre case. Solutions based on such simplifications lead to obtaining the transport parameters that shall provide deeper understanding of the porous fibrous material when exploring the various models. Having established a theoretical background and its limitations owing to the complexity of the realistic material, popularly available models have been explored for their effectiveness.

The empirical models were a starting point although they are well-known to be applicable only to their specific groups of similar materials. They are mainly known to use mean diameters and bulk densities of the nonwoven to give the airflow resistivity parameter and have proposed constants that associate to the selected material type. These models have helped in identifying how such materials have been categorised based on which specific traits. This information is useful in terms of correlating the relevant parameters with the material features. These models have been reviewed

from both acoustic as well as textile perspectives, as both fraternities have their unique contributions that prove useful in shaping the desired model. The other set of empirical studies provide models that use this airflow resistivity parameter to obtain sound absorption characteristics of the overall material. This set of empirical models are handy and have been used often to get an estimate performance.

Having worked out how the empirical models function and identifying their respective domains, the next best set of models were of theoretical nature. These models have gradually introduced some key parameters such as porosity along with the fibre and fabric dimensions and densities. These models have been developed from general physics and treat fibres as ideal cylinders or tubes. They have improved the averaging of fibre diameter technique by introducing the idea that nonwoven have at least two types of fibres, i.e., the staple and the bicomponent variety. This factor also involves the consideration of weighted proportion of each fibre type. These models have led the curiosity to understand the solid domain as well rather than just the fluid domain. They have done this by presenting the porosity concept from a solidity perspective. The solidity is also the relative density which is a ratio of the fibre to the fabric density.

Yet another set of theoretical models have observed the sound propagation around fibres from various orientations thereby introducing further insight into their interaction. Both empirical and theoretical models have been redeveloped to suit a set of test samples whose material properties are well-known. Comparisons have pointed out that when both fibre components are accounted for then they represent the realistic materials better. These theoretical models form the basis to develop further analytical exploration of the nonwoven materials.

Analytical models have been initially developed for single fibre case where few inputs are required. These include the radius of the fibre, which can be either the main fibre or a weighted average value, porosity, and thickness of the test material. These models have been developed from first principles that have been elaborated in the theoretical background section. It has been validated that these models provide a good prediction of sound absorption of some of the realistic materials. However, since these models have very few inputs and many simplifications, they may not always represent correctly. The analytical understanding has extended to understand the visco-inertial and thermal effects that occur when sound along with the airflow intercepts a fibrous obstacle. This helps in gaining clarity on how such forces are dependent on the frequency range.

The growing complexity in models is important as the knowledge of how sound affects porous fibrous materials not just from a bulk reaction but also at the local scale is achieved. Concepts such as homogenisation of the porous media have introduced the correlations between the micro-scale and the macro-scale of a medium. Idealised material treatment has been transformed via the self-consistent method to study materials for their actual physical features by considering energy consistency between the two scales. The pressure velocity and vorticity effects for a representative unit have been expressed as estimating conditions to judge the materials more efficiently.

Having conceptualised a unit comprising of single fibre, whose study leads to acoustic features at bulk scale and vice-versa, it was imperative to visualise the interaction of propagating sound with this unit. Thu the numerical single fibre cell models has been developed for this study. The unit cell is also known as an REV – representative elementary volume or a PUC – periodic unit cell based on the periodicity that has been applied at the boundaries. The numerical version has transformed the approach to understanding the interactions as the velocity and pressure fields provide visual understanding and a pair of models for the low and high frequency limiting condition are sufficient to obtain transport parameters that lead to sound absorption characteristics.

This single fibre numerical model has broadened the scope of exploration as principles associated with sound waves can be quantifiable but not always visual, making it challenging to predict. With this fresh knowledge, the models have been modified to explore the role of two fibres. As it is empirically established that a nonwoven comprises of two types of fibres, rather than averaging it, this numerical model looks at dual fibre interaction. Various orientations and parametric influences have been studied using this setup. The main configurations include the tandem, side-by-side and the staggered arrangements. Now although these models visually consider the presence of two types of fibres, yet their proportion of blending is not well reflected from the overall super cell.

The quest to present the representative unit as the material is realistically fabricated, leads to advancing the dual cell approach to the fibre cluster approach. This proposed version of model is the novelty of the research work. Its development of the fibre cluster follows a mathematical simplification where in based on the type of the fibres and the least count of each type forming the blend is considered. This is related to the least common multiple case where for instance, a 75:25 blend implies 3 fibres of one type and one of the other. When nonwoven materials are inspected in a textile research laboratory, a similar procedure is followed but using microscopic techniques.

This concept has been adopted to develop the fibre cluster models. The results have shown that these models have shown excellent agreement with the experimental data for a variety of blends and combinations. Also, from all of the adaptations of the previous models it has been established that the consideration of the bicomponent or the biner material is critical. It is understood that a unique model would need to be created for a particular type of material, much like the empirical models, yet the amount of information that the numerical models can reveal are far more beneficial.

Future scope

These models have the desired amount of information and can be trained to help optimise and develop novel range of materials. The scope of these cluster models is vast as the numerical analyses conducted so far are in 2D and assumed that the fibrous material is rigid. The COMSOL software that has been used to develop these numerical models has the capability to visualise the cells in 3D and evaluating the fluid structure interaction by assigning mechanical properties to the solid domain of the cell components. These 2D representation can be used to study non-circular fibre shapes and inspect them as spherical media as well. The inclusions can be considered as additives or defects. The fluid domain which has been assumed as air can be substituted as resin saturated or any other fluid. When the problem can be easily visualised, the possibilities to explore become endless.

APPENDIX A

```
%CODE TO CALCULATE AIRFLOW RESISTIVITY OF A DOUBLE FIBRE SAMPLE
%NONWOVEN FIBRE PROPERTY DATA CONVERSION FROM TEXTILE UNITS

clc
clear all
close all

%sample details

%Know your material before calculating!!!
%sampleinfo = readtable('polyester7.txt');% polyester test info

%%
% Fibre density
rho_f1 = 1380;% density of bicomponent fibre in kg/m^3
rho_f2 = 1380;% density of main fibre in kg/m^3
% Viscose = 1530
% Polyester = 1380
% Polylacticacid = 1240
% Nylon 66 = 1140
% Polypropylene = 910
% Hytrel Elastomer = 705

%%
% Fibre fraction or fibre blend (for two component fabric blends!)

X1 = 0.2;% weight fraction of bicomponent fibre in fabric
X2 = 1-X1;% weight fraction of main fibre in fabric

%%
% If fineness value is in dtex
fin1_dtex = 4.8;% bicomponent fibre in dpf
fin2_dtex = 7;% main fibre in dpf
%fin2_dtex = table2array(sampleinfo(1:end,2));% main fibre in dpf

% dtex = dpf/0.9; conversion formula if not in dpf

fin1_dpf = fin1_dtex.*0.9;% fineness in dpf for bicomponent fibre
fin2_dpf = fin2_dtex.*0.9;% fineness in dpf for main fibre

% %If fineness value is in dpf (use directly!)
%
% fin1_dpf = 10;% fineness in dpf for bicomponent fibre
% fin2_dpf = 2;% fineness in dpf for main fibre
```

```
% Conversion in microns
% fin_micron = 11.89.*sqrt(dpf/rho_f);% fineness in dpf and fibre
density (rho_f) in g/cc

dia_micron1 = 11.89.*sqrt(fin1_dpf/rho_f1/1000);% diameter of
bicomponent fibre in micron
dia_micron2 = 11.89.*sqrt(fin2_dpf/rho_f2/1000);% diameter of
bicomponent fibre in micron

d1 = dia_micron1*10^-3;% diameter of bicomponent fibre in mm
d2 = dia_micron2*10^-3;% diameter of main fibre in mm

%%
% Bulk sample inputs

dia = 100;% diameter of bulk sample in mm
th = 30;% height of bulk sample in mm
%th = table2array(sampleinfo(1:end,3));% height
wt = 10.06;% weight of bulk sample in g
%wt = table2array(sampleinfo(1:end,4));% weight

%%
% Calculations

rho_b = wt./(3.14*(dia/2).^2*th)*10^6;% bulk density of fabric

C = (X1.*rho_b./(rho_f1))+(X2.*rho_b./(rho_f2));% Solidity

phi = 1 - C;% porosity

bsq =
((3.14.*(d1/2).^2*(d2/2).^2)./C).*((X1.*rho_f2)+(X2.*rho_f1))./...
    ((X1.*rho_f2.*(d2/2).^2)+(X2.*rho_f1.*(d1/2).^2));% mean spacing

%%%% For single fibre considering only the main fibre values
C1 = rho_b./rho_f2;
bsq1 = (3.14.*(d1/2).^2)./C1;
%%

eta = 1.8E-5;% dynamic viscosity of air

% Sigma calculations

% Tarnow Perpendicular Random model for AFR - double fibre
sig_tperp = 4*3.14*eta./bsq./((0.640.*log(1./C))+C-0.737);

% Tarnow Perpendicular Random model for AFR - single fibre
sig_tperp1 = 4*3.14*eta./bsq1./((0.640.*log(1./C1))+C1-0.737);

% Tranow Parallel Random model for AFR - double fibre
sig_tpara = 4*3.14.*eta./bsq./((1.28.*log(1./C))+2.*C-1.474);
```

```
% Tranow Parallel Random model for AFR - single fibre
sig_tpara1 = 4*3.14.*eta./bsq1./((1.28.*log(1./C1))+2.*C1-1.474);

% Pelegrini et al model - double fibre
sig_pel = 45*3.14*eta*C./bsq./((1-C).^3);

% Pelegrini et al model - single fibre
sig_pel1 = 45*3.14*eta*C1./bsq1./((1-C1).^3);

% BAL semi-empirical AFR model
sig_bal = 10^(-
5.7).*((rho_b).^1.61).*(((X1.^1.61)./((rho_f1.^1.61).*((d1/2).^2.25)))
+...
    ((X2.^1.61)./(rho_f2.^1.61).*((d2/2).^2.25)));

% Happel model
sig_hap = 8*3.14.*eta./bsq./(log(1/C)-((1-C.^2)./(1+C.^2)));

% Kuwabara model
sig_kuw = 8*3.14.*eta./bsq./(log(1/C)+2*C-((C.^2)/2)-1.5);

% FR tube - measured values
%sig_frt = table2array(sampleinfo(1:end,5));% sigma values from flow
resistivity tube

%%
% Result plotting

% plot(C,sig_bal,'rD')
% xlabel ('Solidity C')
% ylabel ('Flow Resistivity \sigma')
xlabel ('Flow Resistivity \sigma')
ylabel ('Porosity \phi')
title ('Flow Resistivity model Comparison for Polyester')
hold on
% plot(C,sig_hap,'co')
% plot(C,sig_kuw,'go')
plot(sig_pel,phi,'ko')
plot(sig_pel1,phi,'kD')
plot(sig_tpara,phi,'bo')
plot(sig_tpara1,phi,'bD')
plot(sig_tperp,phi,'mo')
plot(sig_tperp1,phi,'mD')
%plot(sig_frt,phi,'rP')
hold off
```

APPENDIX B

```
%CODE TO ANALYTICALLY CALCULATE SOUND ABSROPTION CHARATCERISTICS
%NONWOVEN FIBRES ALIGNED IN PERPENDICULAR OR PARALLEL ORIENTATION

clc
clear all
close all

%known parameter inputs

phi = 0.90;%porosity

a = 2.31e-3;%[m]fibre radius

th = 3e-2;%[m]thickness of sample

f = linspace(50,6400,100);

T=20;%[C] temperature

P0=101325;% [bar] Atmospheric pressure

R=287.05;% Universal constant
(http://en.wikipedia.org/wiki/Density_of_air)

T0=291.15;% Reference temperature for dynamic viscosity calculation

C=120;% Sutherland's constant for dynamic viscosity calculation

Eta0=18.27e-6;% Viscosity reference value for dynamic viscosity
calculation

adia=1.4;% specific heat ratio

%derived variables

rho=P0./(R*(T+273.15));% Density calculation

Eta=Eta0*((T0+C)./(T+273.15+C))*((T+273.15)/T0)^(3/2);% Dynamic
viscosity (Sutherland's law)

Cp=1e3*(1.0062+3.6028e-5*T-1.0855e-6*T^2+1.3791e-8*T^3);% Specific
heat at constant pressure
```

```
kappa=1.5207e-11*(T+273.15)^3-4.8574e-8*(T+273.15)^2+1.0184e-
4*(T+273.15) - 3.9333e-4;% Thermal conductivity

co=sqrt(adia*(R*(T+273.15)));% Speed of sound

Z0=rho.*co;% Characteristic Impedance of Air


%%%%%%%%%%%%%%%%%%%%%%%%%%%%%%%%%%%%%%%%%%%%%%%%%%%%%%%%%%%%%%%%%%%%%%%%

%NOTE BY DEFAULT THIS CODE CALCULATES THE PERPENDICULAR ORIENTATION

%Fibres perpendicular to wave propagation

k0v = (a^2*(-2*log(1-phi)-2*phi-phi^2)/(16*(1-phi)));%static viscous
permeability

k0t = (a^2*(-2*log(1-phi)-2*phi-phi^2)/(8*(1-phi)));%static thermal
permeability

sigma = Eta/k0v;%flow resistivity

alf_inf = 2-phi;%tortuosity

vcl = a*phi*(2-phi)/(2*(1-phi));%viscous characteristic length

tcl = a*phi/(1-phi);%thermal characteristic length


%%%%%%%%%%%%%%%%%%%%%%%%%%%%%%%%%%%%%%%%%%%%%%%%%%%%%%%%%%%%%%%%%%%%%%%%

%TO ACTIVATE PARALLEL ORIENTATION, UNCOMMENT THIS SECTION OF THE CODE

% % Fibres parallel to wave propagation
%
% k0t = (a^2*(-2*log(1-phi)-2*phi-phi^2)/(8*(1-phi)));%static thermal
permeability
%
% k0v = k0t;%static viscous permeability
%
% sigma = Eta/k0v;%flow resistivity
%
% alf_inf = 1;%tortuosity
%
% tcl = a*phi/(1-phi);%thermal characteristic length
%
% vcl = tcl;%viscous characteristic length


%%%%%%%%%%%%%%%%%%%%%%%%%%%%%%%%%%%%%%%%%%%%%%%%%%%%%%%%%%%%%%%%%%%%%%%%
```

```
w = 2*pi*f;

RW = (alf_inf.*rho./phi).*(1+(sigma.*phi./(-1i.*w.*rho.*alf_inf)).*...
    (1+(-
1i.*(4.*alf_inf^2.*Eta.*rho.*w./(sigma.^2.*vcl.^2.*phi^2)))).^0.5);%co
mplex dynamic density

BM = (adia.*P0./phi)./(adia-(adia-1).*((1-
1i.*(phi.*kappa./(k0t.*Cp.*rho.*w)).*...
    (1+1i.*(4.*k0t.^2.*Cp.*rho.*w)./(kappa.*tcl.^2.*rho.^2))).^-
0.5));%dynamic bulk modulus

kc = w.*(RW./BM).^0.5;

ZC = (RW.*BM).^0.5;

ZW = ZC.*coth(adia.*th);%Surface Impedance

R = (ZW-Z0)./(ZW+Z0); %Reflection Factor

anormal = 1-abs(R).^2;%Absorption Coefficient

%%%%%%%%%%%%%%%%%%%%%%%%%%%%%%%%%%%%%%%%%%%%%%%%%%%%%%%%%%%%%%%%%%%%%%%

%CREATING PLOTS OF SOUND CHARACTERISTICS

plot(f,real(RW),'r',f,-imag(RW),'g');
title('Dynamic Density')
xlabel('Frequency(Hz)')
ylabel('Dynamic Density RW')
legend('Real','Imaginary')

figure

plot(f,BM);
title('Bulk Modulus')
xlabel('Frequency(Hz)')
ylabel('Bulk Modulus BM')

figure

plot(f,kc);
title('Characteristic Wave Number')
xlabel('Frequency(Hz)')
ylabel('Characteristic Wave Number')

figure

plot(f,ZC);
title('Characteristic Impedance')
xlabel('Frequency(Hz)')
ylabel('Characteristic Impedance')
```

```
figure

plot(f,ZW);
title('Surface Impedance')
xlabel('Frequency(Hz)')
ylabel('Surface Impedance')

figure

plot(f,R);
title('Reflection Factor')
xlabel('Frequency(Hz)')
ylabel('Reflection Coefficient')

figure

plot(f,anormal);
title('Sound Absorption Coefficient')
xlabel('Frequency(Hz)')
ylabel('Alpha')
```

REFERENCES

[1] Mida, V. and Chavhan, M. V. (2012), *Nonwoven Sound Absorption Textiles* International Journal of Textile and Fashion.

[2] Puranik, P. R., Parmar, R. R. and Rana, P. P. (2014) *Nonwoven Acoustic Textiles – a Review*, International Journal of Advanced Research in Engineering and Technology, 5(3), pp. 976–6480.

[3] Rwawiire, S. et al. (2017) *Acoustic and thermal properties of a cellulose nonwoven natural fabric (barkcloth)*, Applied Acoustics. Elsevier Ltd, 116, pp. 177–183.

[4] Paul N. C. and Fred E. (1982) *Guide For Industrial Noise Control*, Ann Arbor, Mich.: Ann Arbor Science.

[5] Lewis H. Bell, (1994) *Industrial noise control, Fundamentals and applications*, 2nd edition, New York: M. Dekker.

[6] Kuczmarski, M. A. and Johnston, J. C. (2011) *Acoustic Absorption in Porous Materials*, Nasa/Tm—2011-216995, (March), pp. 1–20.

[7] Leclaire, P. et al. (2015) *Acoustical properties of air-saturated porous material with periodically distributed dead-end pores*, J. Acoust. Soc. Am., 137(4), pp. 1772–1782.

[8] British Standards Institution. (2014) BS 8233:2014 *Guidance on sound insulation and noise reduction for buildings*. BSI. [Online]

[9] Wright, M. (2005). *Lecture notes on the mathematics of acoustics*. 1st ed. London: Imperial College Press.

[10] Lee, Y. and Joo, C. (2003) *Sound absorption properties of recycled polyester fibrous assembly absorbers*, Autex Research Journal, 3(2), pp. 78–84.

[11] Gong, H. and Ozgen, B. (2018) *Fabric structures: Woven, knitted, or nonwoven, Engineering of High-Performance Textiles*. Elsevier Ltd.

[12] Tascan, M. et al. (2011) *Effects of total surface area and fabric density on the acoustical behavior of traditional thermal-bonded highloft nonwoven fabrics*, Journal of the Textile Institute, 102(9), pp. 746–751.

[13] What are nonwovens? EDANA Available at: *https://www.edana.org/nw-related-industry/what-are-nonwovens* [Accessed: 20 October 2017].

[14] What are Nonwovens INDA. Available at: *https://www.inda.org/about-nonwovens/* [Accessed: 20 October 2017].

[15] Russell, S. (2007). *Handbook of nonwovens*. Boca Raton, Fla.: CRC Press.

[16] fitfibers.com. (2019). *Cross Sections | fitfibers.com*. [online] Available at: http://fitfibers.com/cross-sections/ [Accessed 29 May 2019].

[17] Dent, R. (2001*). Inter-fiber Distances in Paper and Nonwovens.* Journal of the Textile Institute, 92(1), pp.63-74.

[18] Batra, S., Pourdeyhimi, B., Shiffler, D., (2004) TT 305 *Fibre Web and Nonwoven Production*, Desk Copy, North Carolina State University, USA.

[19] Neckar, B. and Das, D., (2011) *Theory of structure and mechanics of fibrous assemblies*, Woodhead Publishing India Ltd., New Delhi.

[20] Simmonds, G. E., Bomberger, J. D., Bryner, M. A., (2007) *Designing nonwovens to meet pore size specifications*, Journal of Engineered Fibres and Fabrics 2 (1), 1-15.

[21] Kallmes, O. and Corte, H., (1960) *TAPPI 43* (9), 737-752.

[22] Allampalayam Jayaraman, K. (2005). *Acoustical Absorptive Properties of Nonwovens*. *MS*. NC State.

[23] Hyde, N. (1959) *Wool-Fabric of History*, National geographic magazine. Available at: *https://archive.org/details/nationalgeograph173nati/page/n5/mode/2up* [Accessed 15 June 2020].

[24] Rouette, H. K. (2001), *Encyclopedia of textile finishing*, Vol 3, Springer, Germany.

[25] Shahani, F., Soltani, P. and Zarrebini, M. (2014) *The analysis of acoustic characteristics and sound absorption coefficient of needle punched nonwoven fabrics*, Journal of Engineered Fibers and Fabrics, 9(2), p. 155892501400900. doi:10.1177/155892501400900210.

[26] Luu, H. T., Panneton, R. and Perrot, C. (2017) *Effective fiber diameter for modeling the acoustic properties of polydisperse fiber networks*, J. Acoust. Soc. Am. 141.

[27] Schladitz, K., Peters, S., Reinel-Bitzer, D., Wiegmann, A. and Ohser, J. (2006) *Design of acoustic trim based on geometric modeling and flow simulation for non-woven*, Comp. Mat. Sci. 38, 56–66.

[28] Singha, K., Maity, S., Singha, M., Paul, P. and Gon, D. P.(2012) *Effects of fiber diameter distribution of nonwoven fabrics on its properties*, Int. J. Text. Sci. 11, 7–14.

[29] Peyrega, C. and Jeulin, D. (2013) *Estimation of acoustic properties and of the representative volume element of random fibrous media*, J. Appl. Phys. 113, 104901.

[30] Luu, H. T. (2016) *Multi-scale modeling of the sound dissipation in fabrics made of natural fibers*, Ph.D. dissertation, Universit**é** de Sherbrooke, Sherbrooke, Quebec, Canada, 2016, Chap. 3, pp. 29–52 (in English).

[31] Xue, Y., Bolton, J., Gerdes, R., Lee, S. and Herdtle, T. (2018). *Prediction of airflow resistivity of fibrous acoustical media having two fiber components and a distribution of fiber radii*. Applied Acoustics, 134, pp.145-153.

[32] Piégay, C., Glé, P., Gourlay, E., Gourdon, E. and Marceau S. (2018) *Acoustical model of vegetal wools including two types of fibers*, Appl. Acoust. 129 36–46.

[33] Piégay, C., Glé, P., Gourlay, E., Gourdon, E. and Marceau S. (2021) *A self-consistent approach for the acoustical modeling of Vegetal Wools*, Journal of Sound and Vibration, 495, p. 115911.

[34] Das, D., Ishtiaque, S. M, Das, S. (2005) *Influence of fiber cross-sectional shape on air permeability of nonwovens*. Fibers and Polymers.16:79-85.

[35] Allard, J. F. and Atalla, N. (2009) *Propagation of Sound in Porous Media*. John Wiley & Sons, Ltd.

[36] Lai, H. Y. (1997) *Modeling of acoustical properties of limp fibrous materials*, Ph.D. thesis, Purdue university.

[37] Brouard, B., Lafarge, D. and Allard, J. (1995). *A general method of modelling sound propagation in layered media*. Journal of Sound and Vibration, 183(1), pp.129-142.

[38] Tang, X. and Yan, X. (2018) *Airflow resistance of acoustical fibrous materials: Measurements, calculations and applications*, Journal of Industrial Textiles, 49(8), pp. 981–1010.

[39] Nichols, R.H. (1947) *Flow-resistance characteristics of fibrous acoustical materials*, The Journal of the Acoustical Society of America, 19(5), pp. 866–871.

[40] Bies, D. and Hansen, C. (1980). *Flow resistance information for acoustical design*. Applied Acoustics, 13(5), pp.357-391.

[41] Narang, P. P. (1995). *Material parameter selection in polyester fibre insulation for sound transmission and absorption.* Applied Acoustics, *45*(4), 335–358.

[42] Garai M., Pompoli F. (2005), *A simple empirical model of polyester fibre materials for acoustical applications*, Applied Acoustics, 66, 12, 1383–1398.

[43] Manning, J. and Panneton, R. (2013) *Acoustical model for shoddy-based fiber sound absorbers*, Textile Research Journal, 83(13), pp. 1356–1370.

[44] Yang, T., Mishra, R., Horoshenkov, K., Hurrell, A., Saati, F. and Xiong, X. (2018). *A study of some airflow resistivity models for multi-component polyester fiber assembly*. Applied Acoustics, 139, pp.75-81.

[45] Delany M. E. and Bazley E. N., (1970) *Acoustical properties of fibrous absorbent materials*, Applied Acoustics 3, pp. 105-116.

[46] Miki Y., (1990) *Acoustical properties of porous materials - Modifications of Delany-Bazley models*, J. Acoust. Soc. Jpn (E). 11(1), pp. 19-24.

[47] Komatsu, T. (2008) *Improvement of the Delany-Bazley and Miki models for fibrous sound-absorbing materials*, Acoustical Science and Technology, 29(2), pp. 121–129.

[48] Voronina, N. (1996) *Improved empirical model of sound propagation through a fibrous material*, Applied Acoustics, 48(2), pp. 121–132.

[49] Umnova, O., Tsiklauri, D. and Venegas, R. (2009) *Effect of boundary slip on the acoustical properties of microfibrous materials*, J. Acoust. Soc. Am., 126(4), p. 1850.

[50] Sutera SP, Richard S.(1993) *The history of Poiseuille's law*. Annu Rev Fluid Mech, 25:1–20.

[51] J. Kozeny (1927) *Über kapillare Leitung des Wasser sim Boden*; *Aufsteig, Versickerung und Anwendung auf die Bewässering*

[52] P.C. Carman (1937) *Fluid Flow through Granular Beds*, Trans. Instn Chem. Engrs., 15, S32-47

[53] Carman PC (1956) *Flow of gases through porous media*. New York: Academic Press.

[54] Davies CN (1953) *The separation of airborne dust and particles*. Proceedings of the institution of mechanical engineers, Part B: Management and engineering manufacture1:185–213.

[55] Lind-Nordgren E, Göransson P. (2010) *Optimising open porous foam for acoustical and vibrational performance*. J Sound Vib 329:753–67.

[56] Doutres O, Atalla N, Dong K. (2011) *Effect of the microstructure closed pore content on the acoustic behavior of polyurethane foams*. J Appl Phys 110:064901.

[57] Pelegrini, M.T., Horoshenkov, K. V., Burnett, A. (2016) *An application of Kozeny-Carman flow resistivity model to predict the acoustical properties of polyester fibre*.Appl Acoust.101:1–4.

[58] Tarnow, V. (1996) *Airflow resistivity of models of fibrous material*. J Acoust Soc Am ; 100(6):3706–13.

[59] Morse PM, Inga˚rd KU. (1968) *Theoretical Acoustics*. New York: McGraw-Hill.

[60] Hamet JF. (1992) *Mode´lisation Acoustique d'un enrobé Drainant.* Bron: Rapport INRETS. p. 159.

[61] Biot, M. (1956) *Theory of Propagation of Elastic Waves in a Fluid-Saturated Porous Solid*, J. Acoust. Soc. Am., 28(2), pp. 168–191.

[62] Yazaki, T., Tashiro, Y., & Biwa, T. (2007). *Measurements of Sound Propagation in Narrow Tubes*. Proceedings: Mathematical, Physical and Engineering Sciences, 463(2087), 2855–2862.

[63] C. Zwikker and C.W. Kosten, (1949) *Sound absorbing materials*, Elsevier. Amsterdam.

[64] Attenborough K. (1983) *Acoustical characteristics of rigid fibrous absorbent and granular materials*. J Acoust Soc Am 73(3):785–99.

[65] Allard JF. (1993) *Propagation of Sound in Porous Media*. London: Elsevier Applied Science.

[66] Johnson D. L., Koplik J. and Dashen R., (1987) *Theory of dynamic permeability and tortuosity in fluid-saturated porous media*, J. Fluid Mech. 176, pp. 379-402.

[67] Champoux Y. and Allard J.-F. (1991) *Dynamic tortuosity and bulk modulus in air-saturated porous media*, J. Appl. Phys. 70, pp. 1975-1979.

[68] Lafarge D., (1993) *Propagation du son dans les matériaux poreux à structure rigide saturés par un fluide viscothermique (Translation: Sound propagation in rigid porous media saturated by a viscothermal fluid).*, PhD thesis, Université du Maine (France).

[69] Horoshenkov, K. V., Hurrell, A., Groby, J.-P. (2020) *Erratum: A three-parameter analytical model for the acoustical properties of porous media* [J. Acoust. Soc. Am. 145(4), 2512–2517 (2019)], The Journal of the Acoustical Society of America 147 (1) 146–146.

[70] Kino, N. and Ueno, T. (2007) *Improvements to the Johnson–Allard model for rigid-framed fibrous materials*, Applied Acoustics, 68(11-12), pp. 1468–1484.

[71] Bensoussan, A., Lions, J.-L. and Papanicolaou, G. (1978) *Asymptotic Analysis for periodic structures*. Amsterdam: North Holland.

[72] Sanchez-Palencia, E. (1980). *Non-homogeneous media and vibration theory*. In Lectures Notes in Physics, Vol. 127., Berlin: Springer-Verlag.

[73] Zieliński, T.G. et al. (2020) *Benchmarks for microstructure-based modelling of sound absorbing rigid-frame porous media*, Journal of Sound and Vibration, 483, p. 115441.

[74] Berdichevsky, A.L. and Cai, Z. (1993) *Preform permeability predictions by self-consistent method and finite element simulation*, Polymer Composites, 14(2), pp. 132–143.

[75] Boutin, C. (2000) *Study of permeability by periodic and self-consistent homogenisation*, European Journal of Mechanics - A/Solids, 19(4), pp. 603–632.

[76] Umnova, O., Attenborough, K., and Ming Li, K. (2000) *Cell model calculations of dynamic drag parameters in packings of spheres*, J. Acoust. Soc. Am. 107 (6), 3113-3119.

[77] Boutin, C. and Geindreau, C. (2008) *Estimates and bounds of dynamic permeability of granular media*, The Journal of the Acoustical Society of America, 124(6), pp. 3576–3593.

[78] Leclaire, P. (2012) *Characterization of porous absorbent materials*, Proceedings of the Acoustics, 25-27 April, pp. 1883–1888.

[79] K. Wilson, (1993) *Relaxation-matched modeling of propagation through porous media*, including fractal pore structure, J. Acoust. Soc. Am. 94(2), pp. 1136-1145.

[80] Pride S. R., Morgan F. D. and Gangi A. F., (1993) *Drag forces of porous-medium acoustics*, Phys. Rev. B 47, pp. 4964-4978.

[81] Apmr.matelys.com. (2019). *Motionless skeleton models | APMR*. [online] Available at: *http://apmr.matelys.com/PropagationModels/MotionlessSkeleton/index.html* [Accessed 1 Aug. 2018].

[82] Auriault, J.-L., Boutin, C. and Geindreau, C. (2009) *Homogenization of coupled phenomena in Heterogenous Media*. London: ISTE.

[83] Cox, T. and D'Antonio, P. (2017). *Acoustic absorbers and diffusers*. Boca Raton: CRC Press, Taylor & Francis.

[84] Rockwool dual density insulation technology *ROCKWOOL Dual Density Insulation Technology*. Available at: *https://www.rockwool.com/uk/advice-and-inspiration/why-stone-wool/dual-density-technology/* (Accessed: 10 November 2019).

[85] Dunn, I. and Davern, W. (1986). *Calculation of acoustic impedance of multi-layer absorbers*. Applied Acoustics, 19(5), pp.321-334.

[86] Jiménez, N., Romero-García, V. and Groby, J. (2018). *Perfect Absorption of Sound by Rigidly-Backed High-Porous Materials*. Acta Acustica united with Acustica, 104(3), pp.396-409.

[87] Tang, X. and Yan, X. (2017). *Multi-layer fibrous structures for noise reduction*. The Journal of The Textile Institute, 108(12), pp.2096-2106.

[88] Tang, X., Zhang, X., Zhuang, X., Zhang, H. and Yan, X. (2018). *Sound absorption properties of nonwoven fabric based multi-layer composites*. Polymer Composites, 40(5), pp.2012-2018.

[89] Chevillotte, F. (2012). *Controlling sound absorption by an upstream resistive layer*. Applied Acoustics, 73(1), pp.56-60.

[90] British Standards Institution. (2003) BS EN ISO 354: 2003 *Acoustics- Measurement of Sound Absorption In A Reverberation Room*. BSI. [Online]

[91] British Standards Institution. (2001) BS EN ISO 10534: 2001 *Acoustics — Determination of sound absorption coefficient and impedance in impedance tubes: — Part 1: Method using standing wave ratio; — Part 2: Transfer-function method*. BSI. [Online]

[92] British Standards Institution. (1997) BS EN ISO 11654: 1997 *Acoustics - Sound absorbers for use in buildings - Rating of sound absorption*. BSI. [Online]

[93] Wolkesson, M. (2013) *Evaluation of impedance tube methods - A two microphone in-situ method for road surfaces and the three microphone transfer function method for porous materials*, p. 69.

[94] Smith, C. D. and Parrott, T. L. (1983) *Comparison of three methods for measuring acoustic properties of bulk materials*, J. Acoust. Soc. Am., 74(5), pp. 1577–1582

[95] Cosmotec: CHA Technologies Group (2015) *Cha Technologies Group | Nonwoven Fibers, Yarns and filters. Available at: https://www.chatechnologies.com/cosmotec/*

[96] Venegas, R. (2011) *Microstructure Influence on Acoustical Properties of Multi-Scale Porous Materials*, PhD Thesis, (May), p. 360.

[97] DiameterJ (no date) ImageJ. Available at: *https://imagej.net/imagej-wiki-static/DiameterJ* (Accessed: 23 October 2018).

[98] British Standards Institution. (2001) BS EN ISO 10534-2: *Acoustics. Determination of sound absorption coefficient and impedance in impedance tubes. Transfer-function method*. BSI. [Online]

[99] ASTM E1050-19 *Standard Test Method For Impedance And Absorption Of Acoustical Materials Using A Tube, Two Microphones And A Digital Frequency Analysis System*, ASTM

[100] Smith, C.D. and Parrott, T.L. (1983) *Comparison of three methods for measuring acoustic properties of bulk materials*, The Journal of the Acoustical Society of America, 74(5), pp. 1577–1582. doi:10.1121/1.390119.

[101] Salissou, Y., Panneton, R. And Doutres, O. (2011) *Three-Microphone Two-Cavity Method for Measuring Sound Transmission Loss in a Modified Impedance Tube*, Canadian Acoustics / Acoustique Canadienne, 39(3).

[102] ASTM E2611-17 *Standard Test Method For Normal Incidence Determination Of Porous Material Acoustical Properties Based On The Transfer Matrix Method*, ASTM

[103] Brüel&Kjær. (2007) *Measurement of transmission loss of materials using a standing wave* Sound&Vibration Measurement A/S Available at: *https://www.bksv.com/media/doc/bn0216.pdf*

[104] British Standards Institution. (2003) BS EN ISO 354:2003: *Acoustics. Measurement of sound absorption in a reverberation room*. BSI. [Online]

[105] British Standards Institution. (2003) BS EN ISO 11654:1997: *Acoustics. Sound absorbers for use in buildings. Rating of sound absorption*. BSI. [Online]

[106] Drábek, P., & Holubová, G. (2014). *Elements of partial differential equations* (Second, revised and extended edition.). Appendix B. *https://doi.org/10.1515/9783110316674.*

[107] Greenberg, M.D. (2012) *Ordinary differential equations*. Hoboken, N.J: Wiley.

[108] Polı͡anin, A.D. and Zaĭt͡sev, V.F. (2003) *Handbook of exact solutions for ordinary differential equations*. Boca Raton: Chapman & Hall/CRC.

[109] Röder, Thomas & Moosbauer, Johann & Wöss, K. & Schlader, S. & Kraft, Gregor. (2013). *Man-made cellulose fibers–a comparison based on morphology and mechanical properties*. Lenzing. Ber.. 91. 7-12.

[110] Clemson University Research Technology put to practice - fitfibers.com. Available at: *https://www.fitfibers.com/wp-content/uploads/2018/06.0/4dg-fibers.pdf*

[111] Foam-X (2020) Mecanum. Available at: *https://mecanum.com/software/foam-x/*